UNIVERSITÄT FÜR BODENKULTUR WIEN
University of Natural Resources
and Life Sciences, Vienna

Doctoral Dissertation

The fast track for production of biomolecules with insect cells in bioreactors

submitted by

DI (FH) Florian STROBL, MSc

in partial fulfilment of the requirements for the academic degree

Doktor der Bodenkultur (Dr.nat.techn.)

Vienna, May 2022

Supervisor:

Univ.Prof. Dipl.-Ing. Dr.rer.nat Gerald Striedner
Institute of Bioprocess Science and Engineering
Department of Biotechnology

Eidesstattliche Erklärung

Ich versichere an Eides statt, dass ich diese Dissertation selbstständig verfasst und keine anderen als die angegebenen Quellen und Hilfsmittel verwendet habe. Alle Gedanken, die im Wortlaut oder in grundlegenden Inhalten aus unveröffentlichten Texten oder aus veröffentlichter Literatur übernommen wurden, sind ordnungsgemäß gekennzeichnet, zitiert und mit genauer Quellenangabe versehen. Beiträge von Kolleg*innen habe ich ausdrücklich in der Autorenerklärung der veröffentlichten Publikationen angegeben.

Die vorliegende Arbeit wurde bisher weder ganz noch teilweise in gleicher oder ähnlicher Form an einer Bildungseinrichtung als Voraussetzung für den Erwerb eines akademischen Grades eingereicht. Sie entspricht vollumfänglich den Leitlinien der Wissenschaftlichen Integrität und den Richtlinien der Guten Wissenschaftlichen Praxis.

Ort, Datum	Florian Strobl

Danksagung

Mit dieser Arbeit endet ein weiterer Abschnitt in meinem Leben und es ist an der Zeit Danke zu sagen.

Beginnen möchte ich bei meinem Betreuer Gerald Striedner. Unser gemeinsamer Weg begann 2005 als ich die Möglichkeit bekam in der damaligen AG Bayer die Kunst des Fermentierens, unter seiner Obhut, zu erlernen. In den kommenden 15 Jahren begleitete er mich auch durch meine Ausbildung und ich konnte sehr viel von ihm und der gesamten AG lernen. Ich bin ihm sehr zu Dank verpflichtet, für das in mich gesteckte Vertrauen und die Möglichkeit Teil dieser Gemeinschaft gewesen zu sein.

Danke an die morgendliche, mittägige und nachmittägige Kaffeerunde, Luggi, Hiasi, FloW, FloM, Esther, Patrick, Sabine, Bernhard, Lukas und noch viele mehr, so manche Tiefs konnten hier, durch guten Zuspruch und Ratschläge, gelindert oder überwunden werden.

Ein weiterer Dank gebührt den „Downies“ und den „Baculos“, die mich auf meinem Weg begleiteten. Im speziellen auch Didi, Miriam und Shirin die mir die Kniffe der Zellkultur nähergebracht haben.

Danke an Nico und den Rest der Wappler Brew Crew für die gemeinsamen Sude und den regen Austausch.

Ich möchte mich bei meinen Eltern Elisabeth und Franz so wie meinen Geschwistern Kornelia und Lukas sowie deren Familien für ihre Förderung und Unterstützung bedanken.

Zum Schluss gebührt der größte Dank meiner Freundin Nicole, die mich, während dieser nicht einfachen Zeit begleitete, mich ermunterte, anspornte, und manchmal sogar antreiben musste. Ohne dich wäre das alles nicht möglich gewesen.

Zusammenfassung

Epidemien und Pandemien sind für die Menschheit, die Behörden und für die biopharmazeutische Industrie eine große Herausforderung. Auf lokale oder großflächige Ereignisse muss rasch und flexibel reagiert werden. Eine Herausforderung, die konträr zu den starren und unflexiblen Prozessabläufen steht, die der Industrie durch die Behörden auferlegt wurden, um die Qualität und die Sicherheit der Produkte zu gewährleisten.

Um rasch und flexibel reagieren zu können gibt es verschiedene Plattformtechnologien, eine davon basiert auf Insektenzellen. Es gibt verschiedene Möglichkeiten, um Produkte mit Insektenzellen zu produzieren, wobei die Infektion der Zellen mit genetisch modifizierten Baculoviren die derzeit am häufigsten verwendete Methode darstellt. Des Weiteren gibt es stabile produzierende Zelllinien sowie die Möglichkeit die Zellen mit DNA transient zu transfizieren. Die Basis für die Etablierung von Plattformprozessen und rationales Prozessdesign sind jedoch umfassende Kenntnisse über den zu kultivierenden Organismus sowie über die kritischen produkt- und prozessrelevanten Parameter.

Das Ziel dieser Dissertation war es einen Produktionsprozess für Insektenzellen aufzusetzen, der vom Mikrotitervolumen bis hin zum Produktionsreaktor skalierbar ist. Im Zuge dieser Arbeiten wurde eine Methode zur Bestimmung der Zellstabilität gegenüber Scherkräften entwickelt welche beim Scale-up eine große Rolle spielen. Weiters konnte ein Screeningverfahren zur Identifikation optimaler Bedingungen zur Infektion von Insektenzellen, mit Baculoviren erstellt und diese in Produktionsprozessen im Labormaßstab erfolgreich angewandt werden. Auch konnte eine Methode zur transienten Transfektion von Insektenzellen, eine Alternative zum herkömmlichen Produktionsschema im Reaktor, etabliert werden.

Abstract

Epidemics and pandemics are a major challenge for mankind, the authorities, and the biopharmaceutical industry. Local or widespread events need to be responded to quickly and flexibly, which contrasts with the rigid and inflexible processes imposed on the industry by the authorities to ensure the quality and safety of the products.

To be able to react quickly and flexibly, there are various platform technologies, one of which based on insect cells. There are various ways to produce products with insect cells, whereby the infection of the cells with a baculovirus is currently the most commonly used method. Furthermore, there are stable producing cell lines as well as the possibility to transiently transfect the cells with DNA. However, this requires basic knowledge about the organism to be cultured, the process control and the critical process parameters, respectively.

The aim of this dissertation was, on the one hand, to set up a production process for insect cells that is scalable from the microtiter volume to the production reactor scale and is also be compatible with various production methods. A method was developed to determine the cell stability to shear forces, which play a major role in scale-up. Furthermore, a screening method for infection with baculoviruses was developed and applied to production processes in the bioreactor. A method for the transient transfection of insect cells, an alternative to the conventional production scheme, was established in the bioreactor.

Table of Contents

Danksagung ..... **i**

Zusammenfassung ..... **ii**

Abstract ..... **iii**

Table of Contents **1**

1 Introduction **3**

1.1 Insect cell lines 3

1.2 Cultivation of insect cells 3

1.3 Critical process parameters for insect cell cultivations 4

1.3.1 Temperature 4

1.3.2 pH – control and influence of CO_2 4

1.3.3 Dissolved Oxygen (DO) Level 5

1.4 Shear force 5

1.5 Insect cell expression systems 6

1.5.1 Insect cell/Baculovirus expression vector system (BEVS) 6

1.5.2 Insect cells with transient transfection 8

1.6 Production strategies 10

2 Objectives **11**

3 Results and Discussion **12**

3.1 Publications 12

3.1.1 Publication I 12

3.1.2 Publication II 15

3.1.3 Publication III 18

4 Discussion and Conclusion 20

5 List of Publications 24

6 Contribution to publications 26

7 List of Figures 27

8 Abbreviations 28

9 References 29

10 Publications 42

1 Introduction

1.1 Insect cell lines

Experiments with insect cells date back to the early 20th century when Glaser [1] worked with insect blood cells cultured in hemolymph and simple salt solutions. Back then cells could hardly kept alive over a few days. In 1962 Grace et al. [2] established a stable insect cell line derived from pupal ovary tissue. From there on, over five hundred cell lines from more than hundred insect species were established [3]. Among these cell lines three are heavily and widely used for manufacturing and developing therapeutic proteins, which namely are: S2 derived from *Drosophila melanogaster, Sf9* from *Spodoptera frugiperda* and Tn5B1-4 (High Five) from *Trichoplusia ni* [4].

Initially, they were used as model eukaryotes in physiological and pathological research [5],[6], but eventually insect cells were also recognized for their potential as host cells in biopharmaceutical production processes. Insect cell lines currently account for 2.3% of all newly approved active pharmaceutical ingredients, the majority of which are virus-like particles (VLPs), a product class of high complexity and rapidly growing importance [7].

1.2 Cultivation of insect cells

Most insect cell lines are adapted for growth in suspension using serum free media, but they can also be grown adherend [8]–[10] and cultivation can be performed in biosafety level 1 environment [11]–[13].

A continuously stirred tank reactor (CSTR) is the preferred system when cultivating insect cells in suspension, even though different designs of bioreactors (packed-bed, airlift, or wave-bag) were evaluated for suitability and scale-up [14]. CSTRs used for mammalian cell culture can be either made of stainless steel with up to 25 m^3 working volume [15], [16], or single-use bioreactors with up to 2 m^3 working volume [17]. The major advantages that CSTRs offer come

from the extensive experience to operate and scale-up these systems, as well as the availability of such CSTRs from the milliliter to the cubic meter range for cultivation of insect cell lines. Such CSTRs, which are also used for cultivation of mammalian cell lines are different from bioreactors designed for micro-organisms especially with respect to the reactor geometry, the oxygen transfer coefficient (k_La) and the specific power input. Typical height to diameter (H/D) ratios for mammalian cell culture bioreactors are in the range of 1.5 - 2:1 [18] compared to microbial systems with H/D ratios between 2.5 and 3:1 or even higher. Standard k_La values for cell culture bioreactors range from 5 – 10 h^{-1} when using a macro-sparger this could be pushed to a maximum value of 80 h^{-1} [19]. In microbial cultivation systems k_La values are > 250 h^{-1} and can even exceed 1000 h^{-1} [19], [20]. With respect to specific power input a range from 5 to 300 W m^{-3} is covered in cell culture systems [21] for example an 8 m^3 bioreactor was operated at 11.5 W m^{-3}, whereas microbial bioreactor systems should have specific power inputs > 5 kW m^{-3} [22]–[24].

1.3 Critical process parameters for insect cell cultivations

1.3.1 Temperature

Insect cells achieve the highest specific growth rate and final cell density when growing at 27°C in comparison to mammalian cells which typical grow at 37°C. It has also been shown that insect cells can be grown at a temperature range of 25 – 30°C [25], [26] and a *Sf9* culture was even adapted to growth at 37°C, via long-term passaging [27].

1.3.2 pH – control and influence of CO_2

The optimal pH for cultivating insect cells vary from pH 6.0 to 6.4, depending on the cell line [28]–[31]. Commercially available insect cell media normally utilize a phosphate buffer rather than carbonate buffer like other cell culture media. CO_2 for incubation and cultivation of insect cells is not needed, as they do not require CO_2 to grow like mammalian and human cell lines

[32]. Using CO_2 for pH control can even lead to growth inhibition of insect cell cultures, as it was observed that already a CO_2 level 24mM inhibits growth of *Sf9* and *Tn-5* cells in a bioreactor [31].

1.3.3 Dissolved Oxygen (DO) Level

Experiments with *Sf9* cells showed that they can grow in a wide range of oxygen saturation, with the optimum ranging from 30 to 100% DO saturation [32], [33]. Insect cells have a rather high oxygen demand, for example *Sf9* has a four and High Five has a 13-time higher specific oxygen consumption rate than Chinese hamster ovary (CHO) cells. After infection, these rates increase by 30 to 40% [34]–[37]. The key process parameter, the oxygen transfer rate (OTR) can be influenced during the cultivation process by stirrer speed, air flow rate, oxygen partial pressure, head space pressure, temperature of the fermentation broth and by the composition of the used media [19], [38].

1.4 Shear force

The resulting challenge in insect cell cultivation is to overcome the interfering problems of high oxygen demand and high shear sensitivity, both becoming more pronounced in the production phase after infection of the cells. The task to be solved is to ensure efficient transfer of oxygen required for cell growth and product formation but simultaneously to keep shear rates low to prevent disruption of cells. However, stirring speed and air flow rate, which are the main process inputs to vary OTR, are also the main factors responsible for increased shear forces in the bioreactor. Consequently, the general practice in CSTRs and state of the art in insect cell culture is to reduce stirring speed to a level that fulfills mixing requirements and to manipulate oxygen transfer via flow rate and composition of the supplied gas. However, increased gas flow comes along with foam formation and increased shear forces caused by bursting air bubbles on the liquid surface, both contributing to destruction of cells and products produced such as VLPs [39]. Low stirring speeds and thus limited mixing efficiency amplify

the problem of zone and gradient formation [40] in larger scales which can cause additional stress in cells [41]. For insect cell lines harboring inherent retroviral information in their genome this can cause an increased risk of virus DNA reactivation and retro virus release.

The assumption that insect cells are susceptible to shear is widely accepted, although there is no solid scientific support for this theory. Some studies point in the direction that insect cells are not more pronounced to shear than mammalian cells [42], [43]. Due to the lack of methods to determine shear sensitivity, there is little or no objective data for insect cells available and existing knowledge is largely based on empirical data and experience generated with similar cell types.

1.5 Insect cell expression systems

1.5.1 Insect cell/Baculovirus expression vector system (BEVS)

Since its introduction in 1983 [44], BEVS has been used for a variety of applications, it is used for recombinant protein production, transient gene expression, tissue therapy, vaccine production, and the baculovirus is also used as biopesticide [45]–[48]. For these applications more than 400 cell lines have been modified [49].

The BEVS uses *Baculoviridae* which belong to the family of double-stranded DNA viruses that infect the larvae of Lepidoptera, Hymenoptera, and Diptera. The enveloped rod-shaped virus (30–60 × 250–300 nm) contains a circular DNA genome that has about 80-180 kilobase pairs [50], [51].

The most studied and commonly used baculovirus is the *Autographa califonica* multiple nucleopolyhedrovirus (AcMNPV), based on which several commercially available BEVS have been developed [52]. The system allows the insertion of large foreign DNA fragments (at least 38 kbp) [53]. The donor plasmid which inherits the gen of interest (GOI) is transformed into *E. coli* competent cells which contain the bacmid DNA. After expansion of the bacterial cells bacmid DNA is purified and then used for transfection of insect cells. Generated baculovirus

is released into the medium and then harvested by centrifugation (Figure 1). The BEVS enables multiple post-translational modifications and allows for multiple proteins to be produced with a single virus [56]. Insertion of a gene of interest under the p10 or polh promoter results in strong expression and the recombinant protein titers can reach milligram per liter scales [55], [56]. Parameters to consider when infecting cells with the BEVS are the cell concentration at the time of infection (CCI), the number of plaque-forming units per cell (PFU/cell), commonly referred to as the multiplicity of infection (MOI), and the time of harvesting [59].

There are also some down sides to this system, in a late phase of infection it comes to a baculovirus-mediated lysis of insect cells [60] which limits the BEVS production period. In addition, the baculovirus can be seen as an impurity - for example in the case of VLP production - and therefore needs to be removed. There are already commercial BEV-based products on the market for human and veterinary use, and many more are in the pipeline [61]. However, due to the ease and speed of the BEVS it is suitable for the production of vaccines against emerging viruses that are rapidly changing their antigens between each outbreak like the influenza virus [59] and it is probably the best expression system for VLP-based vaccine production [60] .

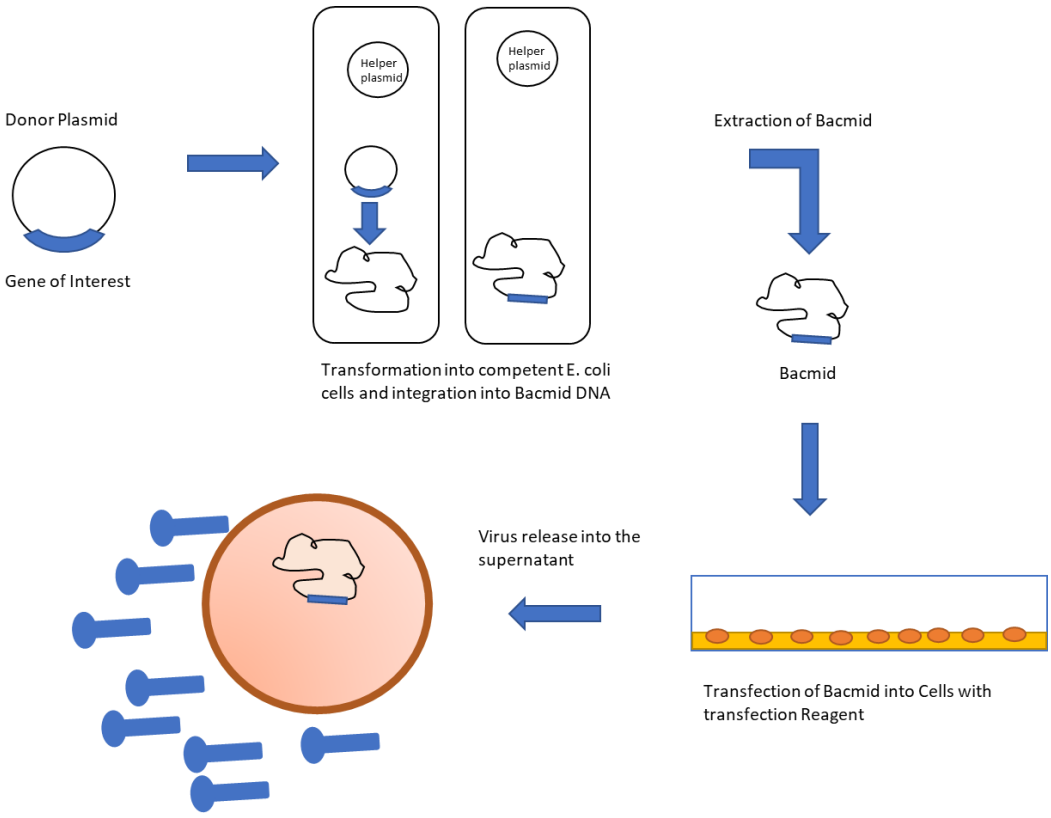

Figure 1: Scheme of baculovirus production.

1.5.2 Insect cells with transient transfection

An alternative to the BEVS is the plasmid DNA based transient gene expression (TGE) where the problem of cell lysis and baculovirus contamination of the product can be circumvented. TGE offers the ability of rapid protein production at levels sufficient to be used in pre-clinical and early clinical phase [64]. For VLPs as product it can give moderate to high product titres in a short period of time [65]. TGE plasmid DNA encoding the GOI is transferred into the cells using positively charged transfection agents such as Polyethyleneimine (PEI) which start to form complexes. After a defined time, the mixture is transferred to the cell solution. The polymer-plasmid complex enters the cell via endocytosis. After the vesicle is degraded the complex is dissolved and the polymer gets degraded as well. The plasmid is entering the nucleolus and transcription starts. Once the plasmid DNA is introduced into the cells it remains as an episomal element inside the cells without integrating into the genome

(Figure 2). However, this plasmid DNA is eventually lost over time due to cell division. [66]. Therefore, the production time is limited to 7-14 days post-transfection [67].

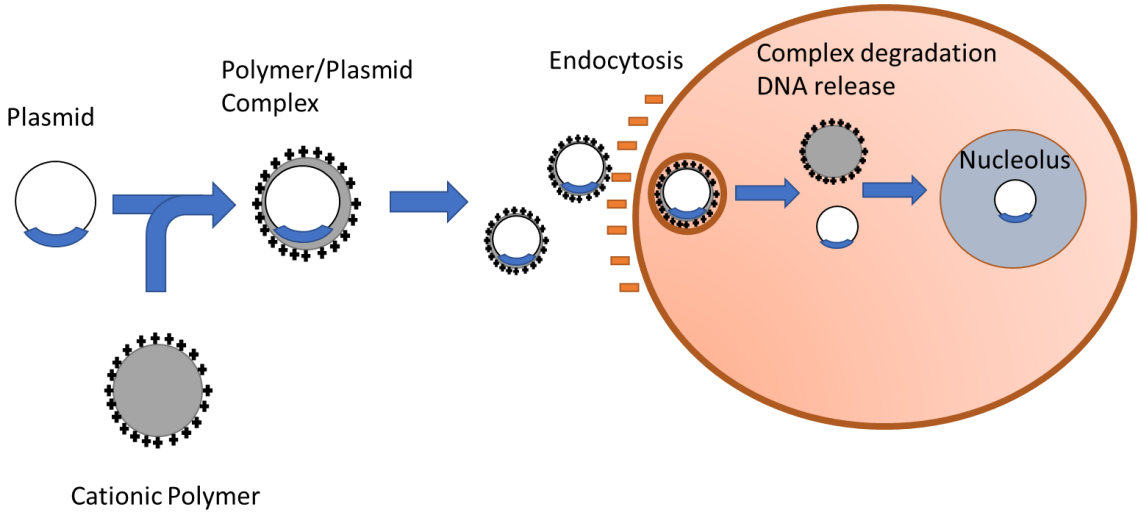

Figure 2: TGE - transfection scheme.

The first transfection techniques date back to 1973 where calcium phosphate precipitation method was used [65]. Over time alternative methods for transfection of insect cells using DNA-adsorptive reagents like DEAE-dextran, poly-L-lysine, polyornithine, and polybrene were established [66]. Also used for delivering DNA into cells are liposome-mediated transfection [67], [68] and electroporation [72], [73]. A cheaper alternative to commercially available reagents that is also more efficient when it comes to transfection is PEI. Production costs can be cut down by using PEI [74] which is important when transfecting on a production scale level.

Most of these techniques were initially developed for mammalian cells and unfortunately, their application with insect cells can be difficult due to toxicity of the transfection reagents, the complexity of the procedures the low transfection efficiency and the poor reproducibility of results [75].

However, several studies have shown that the production of reporter proteins [76]–[78], antibodies [79]–[81] or surface proteins [79] using suspension adapted High Five or *Sf9* cells in combination with plasmid mediated TGE is possible.

1.6 Production strategies

The mainly used cultivation type for insect cells is the batch process, it's a two-stage process [32]. In the first phase cells are expanded to a certain cell count, in the second phase the production is started, and cells get either infected (BEVS) or transfected (TGE). Using BEVS an optimization of multiplicity of infection (MOI) and cell density at infection (CDI) must be determined for each virus/host combination [83].

Efforts were made to set-up fed batch and perfusion processes where cell densities higher than 10^7 cells/mL could be reached for various cell lines [84]–[86]. However, the so called "cell density effect" resulted in unsuccessful infection at these high cell densities [87]. This early observed effect occurs when CDI exceeds a certain threshold and manifests as loss of specific productivity, or the ability to infect cells [88], [89].

2 Objectives

In this thesis, two main topics will be addressed. The first one deals with the verification of the hypothesis that high throughput titre plate cultivation with advanced monitoring provides results of equal or superior quality which are better transferable to larger scales than conventional shake flask screening methods.

- In a first step a high-throughput µ-bioreactor screening platform for insect cells shall be developed.
- In the second step the conventional shake flask cultivation screening platform with PEI mediated transiently transfected High Five cells producing different recombinant proteins and VLPs should be evaluated.

The transferability of screening results to standard benchtop cultivation systems for insect cells is defined as the selected test criterion. The MOI is defined as the process parameter to be varied.

The second topic is to verify the hypothesis that insect cells are much more robust to shear forces than generally described. For that purpose, three different insect cell lines and a baculovirus producing VLPs containing influenza virus hemagglutinin were selected as model systems. In this context the following main objectives were defined:

- Development of a method to evaluate the shear resistance of insect cells in suspension. A shear device that allows to apply defined shear stresses to cells should be used. By measuring the viability of the cell suspensions treated this way was selected as a measurement to determine the upper limit of shear that can be applied to the selected cell lines shall be determined.
- Development of an efficient and scalable bioreactor cultivation strategy for insect cells based on the results generated in the resistance study. A new strategy for insect cell cultivation in microbial bioreactor systems is proposed and should be developed and tested in different scales (1 – 14 L bioreactors).

3 Results and Discussion

3.1 Publications

In the course of this thesis three research papers have been published.

3.1.1 Publication I

Evaluation of screening platforms for virus-like particle production with the baculovirus expression vector system in insect cells. Strobl, F., Ghorbanpour, S.M., Palmberger, D. *et al. Sci Rep* 10**,** 1065 (2020). https://doi.org/10.1038/s41598-020-57761-w

The research focus of this work was to develop a protocol and characterize a high through put (HTP) µ-bioreactor system with advanced monitoring features as a screening platform for VLP production with insect cells using the BEVS. Furthermore, it was planned to compare the performance of this method to that of the conventional shake flask screening methodology. The transferability of the screening results to bioreactor cultures was defined and investigated as the main evaluation criterion.

The experiments were performed with *Tnms42* cell line (BTI, Gary W. Blissard), which is an alpha-nodavirus-free *Trichoplusia ni* - Tn5B1-4 derivative. The used baculovirus encoded the nucleic acid sequence for the hemagglutinin (HA) 1 protein of Influenza A/California/04/2009 (H1N1) and the matrix protein Gag of the type 1 human immunodeficiency virus. In addition, the virus harboured a yellow fluorescence protein (YFP) expression cassette, which was used as an infection marker to determine the infectivity of the virus stock.

The used µ-bioreactor can monitor pH, dissolved oxygen (DO) level and is equipped with sensors for fluorescence and scattered light measurements. In a first step the capability

of the µ-bioreactor to cultivate insect cells was tested and in parallel the extent to which the available online measurement systems can be used and what process information they provide was investigated. Subsequently, experiments covering a broad range of MOIs were conducted to identify MOIs suitable for efficient infection of insect cells in the µ-bioreactor. In the next step the cultivation and infection results generated in the µ-bioreactor were tested and compared to results from shaker flask and benchtop bioreactor cultivations. Therefore, three different MOI´s and a non-infected control were cultivated in triplicates and compared against bioreactor data (Figure 3).

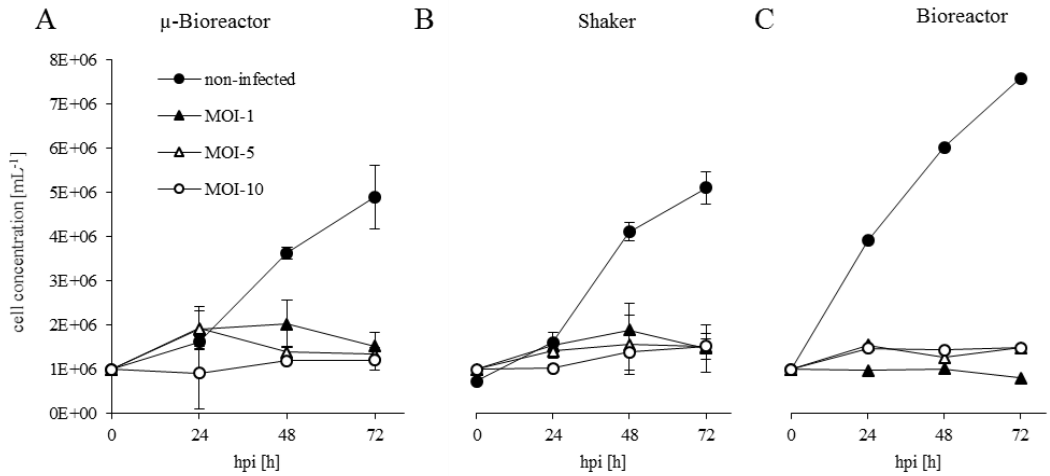

Figure 3: Course of the cell concentration of infected and non-infected Tnms42 cell cultures in A) µ-bioreactor cultivation, B) shake flask cultivation, and C) benchtop bioreactor cultivation. All experiments in A and B were conducted in triplicate. Error bars indicate the standard deviation. Taken from Strobl et.al. [59]

All used production platforms reached similar cell densities in the experiments where cells were infected with different MOIs. When comparing the growth curves of the non-infected controls the final cell concentrations in the bioreactor reached higher levels compared to the screening platforms (Figure 3). One major difference between those cultivation methods is the pH value of the suspension. While in the bioreactor the pH is maintained at 6.40 ± 0.05 the pH in the µ-bioreactor system increases from 6.45 to 6.65 and in the shakers, it reached the highest pH end-values of 6.8. Unfortunately, for the infected µ-

bioreactor experiments the pH value was not on-line available, due to interference of the YFP signal with the pH fluorescence measurement.

Also, product titers of the different screening systems, which were analyzed via ELISA, were compared and again in the bioreactor the highest titers could be found.

In summary it was clearly demonstrated that the µ-bioreactor could be used as a HTP screening tool with insect cells which could be a time-saving alternative to conventional shake flasks. However, to exploit the whole potential of online monitoring of the µ-bioreactor it is crucial to use fluorescence markers that do not interfere with the wavelength of the optodes. The results give an indication that the pH of the suspension has an impact of product formation and growth which should be further investigated. The transferability of the results from the µ-bioreactor to the benchtop bioreactor have identical rankings and are comparable to shaker flask cultivation.

3.1.2 Publication II

PEI-Mediated Transient Transfection of High Five Cells at Bioreactor Scale for HIV-1 VLP Production. Puente-Massaguer, E.; Strobl, F.; Grabherr, R.; Striedner, G.; Lecina, M.; Gòdia, F. *Nanomaterials* 2020, *10*, 1580.

The emerging virus outbreaks over the world must be countered with fast and safe vaccine production. A system of choice could be the TGE using insect cells. In this work, PEI-mediated TGE of High Five cells with plasmids was evaluated in shaker flasks using different recombinant products including VLPs. The VLP production protocol was then transferred to bench-top bioreactors and analysed.

The PEI-mediated TGE using High-Five which already was demonstrated [90], was used producing more complex products. For this purpose, three different classes of products were selected, enhanced green fluorescence protein (eGFP) expressed intracellular, human-secreted alkaline phosphatase (hSEAP) as secreted protein and a HIV-1 Gag-eGFP VLP as multimeric nanoparticle. All three products reached their maximum titre in shaker flask production after 72 hours post transfection (hpt). Intracellular eGFP reaching a volumetric concentration of 5.0 ± 0.4 mg/L and secreted hSEAP a titre of 4.2 ± 0.3 mg/L in the supernatant.

For the VLP concentrations measured with nanoparticle tracking analysis a titre of 3.6 ± 1.0 × 10^8 VLP/mL was observed. This product yield was 2-fold higher than that obtained with a stable VLP-producing High Five cell line but lower than that generated with the BEVS system [91], [92].

The TGE process for VLP production was then transferred to the bioreactor, after inoculation cells were transfected at a cell concentration of 1.5 × 10^6 cells/mL, in parallel the same preculture was used as positive control in shaker flasks. Samples were drawn in 24h interval, and no differences in terms of growth behavior were observed until the end of cultivation, where a higher cell concentration in the bioreactor could be reached. The

transfection efficiency in reactor and shake flask were comparable. The major difference was the production of VLPs which was 1.8-fold higher in the bioreactor compared to the control (Figure 4).

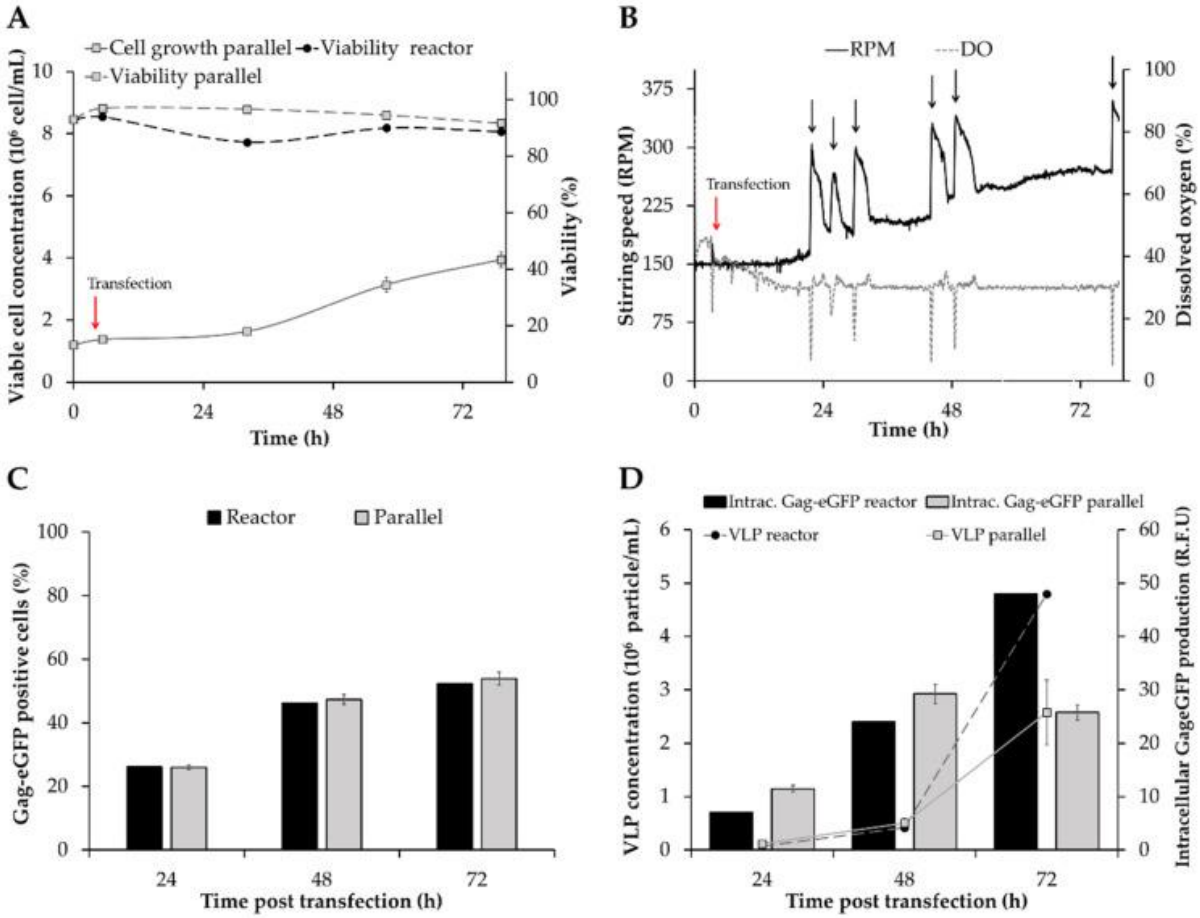

*Figure 4: Comparison of Gag-eGFP VLP production in a 2 L DASGIP® Bioblock glass bioreactor and 125 mL Erlenmeyer flasks (parallel). (**A**) Cell growth and viability profile of transfected cultures. The red arrow indicates the time of transfection. (**B**) Evolution of dissolved oxygen and stirring speed requirements of transfected High Five cells. Black arrows show the addition of Antifoam C. (**C**) Percentage of Gag-eGFP positive cells at different time points. (**D**) Analysis of VLP production and intracellular Gag-eGFP content by flow virometry and spectrofluorometry, respectively. Mean values ± standard deviation of triplicate experiments are represented. Taken from Puente-Massaguer et.al.* [93]

In this study for the first time, the successful production of VLPs using TGE at bioreactor scale could be demonstrated, with no differences in terms of transfection efficiency. Further a 1.8-fold increase in VLP titre in comparison to the control experiment

could be achieved. It could be shown that the TGE/insect system could be a valuable approach for the accelerated development of processes for production of biotechnological products.

3.1.3 Publication III

High shear resistance of insect cells: the basis for substantial improvements in cell culture process design. Strobl, F., Duerkop, M., Palmberger, D. *et al. Sci Rep* 11**,** 9413 (2021). https://doi.org/10.1038/s41598-021-88813-4

When it comes to cultivating cells in stirred tank bioreactors the shear applied to the cells is an essential variable. In this work we focused on characterization of shear sensitivity and shear resistance of insect cells. For this purpose, a shear device [83] was used which allowed to apply a defined shear to the cells. The experiments were performed using High-Five (BTI-TN-5B1-4) cell line and again the alpha-nodavirus-free *Tnms42* cell line (BTI, Gary W. Blissard), additionally CHO-K1 (ATCC CCL-61) cells were also included in this study.

The shear device was used to apply different shear rates to the cells, and viability of the cells after the treatment was determined. It was found that the cells could withstand a maximum and average shear rates of up to $8.73 \times 10^5\ s^{-1}$ and $5.82 \times 10^5\ s^{-1}$ (Figure 5)

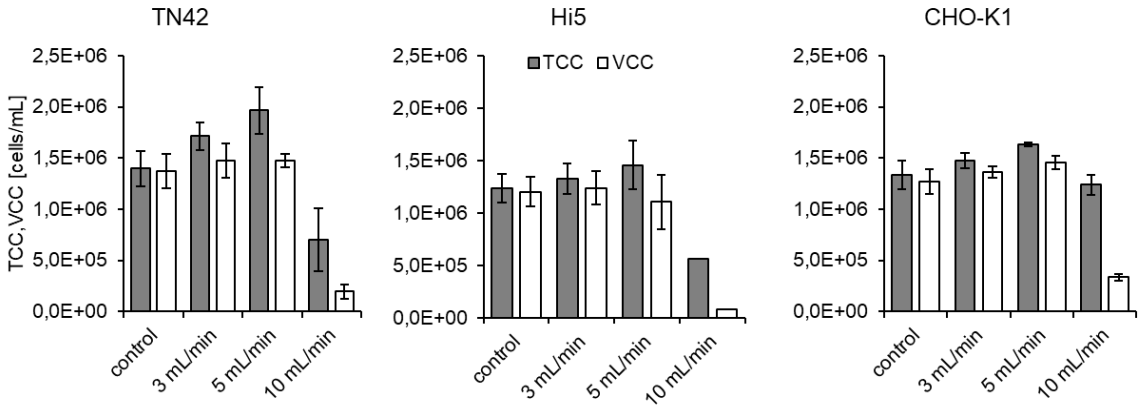

Figure 5: Total and viable cell counts after treatment with the shear device. Shear was measured at different flow rates for (left) TN42, (center) Hi5, and (right) CHO-K1 cells. Each run was performed in triplicate, except the Hi5 experiment (center) run at 10-mL/min. Taken from Strobl et.al. [95]

In literature equations were found which correlate the maximum and average shear rate to stirrer speeds of the bioreactor. The data gathered from the shear device experiments indicated that shear rates inside the bioreactor generated by stirring were not likely to damage cells regardless the used stirrer type.

To test these findings multiple bioreactor cultivations were conducted were cells get exposed to increased stirrer speeds, speeds up to 1000 rpm were tested and the viability of the cells were measured. In the cultivation with speeds of 1000 rpm the lack of baffles resulted in the formation of a fluid vortex that introduced air bubbles from the surface, causing cell damage due to the bursting of bubbles. The results from these cultivations were used to set-up an improved DO control strategy for insect cell cultivation which was tested for infected and non-infected cells. Similar findings could be gathered for the CHO cultivations.

In this work we could utilize the shear device as a simple and efficient tool to apply defined shear levels to characterize the shar sensitivity of different cell types. The investigated shear that cells could withstand enabled the design of a new DO control regime, based on high energy input through stirring, with applying typical Rushton-powered microbial bioreactor set-up. The introduced DO control regime has the benefit of improving the economic efficiency of the process. Due to the lower gas volumes foam formation and bubble rupture at the surface was reduced which positively affects cell viability, virus, and product quality.

4 Discussion and Conclusion

The validity of screening experiments performed in simpler process setups and their transferability to larger scale were key questions to be answered within this work. The hypothesis to be verified was that µ-bioreactor cultivations are comparable or better than the currently used standard procedure with shaker flasks.

For this purpose, a µ-bioreactor system was evaluated with respect to its suitability as insect cell cultivation platform. Initial experiments clearly showed that this system is well suited for this application. Consequently, a HTP screening protocol for fast and easy cultivation and infection of insect cells with the BEVS was established for this µ-bioreactor system. Experimental evaluation confirmed that (i) the results generated are in line with conventional used shaker flasks with identical rankings, (ii) the online measurement capabilities of the µ-bioreactor system give valuable information on the process during screening experiments and (iii) the transferability of the results generated with the µ-bioreactor to benchtop bioreactor setting is equal to that from shake flask screening cultivations. Based on the online measurements in the µ-bioreactor, this part of the work also revealed physiological differences between the used insect cell lines. However, in both screening methods the final product titers were significantly lower than in the benchtop bioreactor experiments which could be linked to the increasing pH in the screening platforms due to the missing pH control. One solution to overcome this problem would be to develop media for these screening processes that have better buffering capacity, as it was already shown for a different host using the µ-bioreactor [96]. Another option is to use the successor model of the tested µ-bioreactor, which enables feeding of media and addition of acid or base. This, however, would also implicate a reduced number of wells and consequently lower throughput. Experimental evaluation would be necessary if these drawbacks are justified.

In general, the used µ-bioreactor turned out to be a cost-effective, and time-saving alternative to conventional shake flask screenings. In view of the fact that the sampling volume

of the µ-bioreactor is limited to the well volume of the titer plate, parallel experiments have to be carried out if data for important process variables or information about the process course needs be generated. Taking this into account, the µ-bioreactor system is still more efficient and requires less space than the conventional shake flask approach. Furthermore, the user gains additional process knowledge delivered through the online measurements of cell number (scattered light signal), pH and dissolved oxygen levels (optodes) as well as product formation (fluorescence).

One disadvantage of the insect cell/BEVS is the co-expression of baculovirus together with the recombinant protein or VLP, which need to be separated them from the product [97]. Using the BEVS for large-scale production of pharmaceutical proteins, many reports indicated that the productivity is significantly decreased when the cell density during infection exceeds a certain threshold, which is often referred to as “the density effect” [98]. To overcome the problems related to the BEVS system TGE could be used as an alternative which was chosen as second model system in this work.

We selected a transient transfection method with different products on the one hand and a BEVS system with different insect cell lines producing VLPs on the other hand as model systems. A method for TGE of High-Five insect cells using PEI as transfection agent in shaker flasks was established to produce three classes of products: eGFP as an intracellular protein, hSEAP as secreted recombinant protein and HIV1-Gag VLPs. Moreover, the protocol for VLP production was transferred to bioreactor scale where the cells could be successfully transfected. Similar transfection efficiency but with 1.8-fold increase in VLP productivity compared to shake flask cultures was achieved. This again can be related to the controlled environment in the bioreactor where the DO and pH are kept at an optimum, compared to the shaker flask where these parameters cannot be controlled over time. TGE holds the possibility to express products in a baculovirus free environment, which simplifies the downstream processing significantly [93], even though the yields with TGE are lower compared to the BEVS [99]. Comparing the starting material that is necessary for TGE and BEVS, plasmid DNA is easy to store, and production can be performed in industrial scale [100], compared to

the baculovirus where the generation of high-quality stocks is time consuming and long-term storage of baculoviruses remains troublesome [101].

The second part of this work focused on characterization of physical properties of insect and mammalian cells, specifically in terms of their resistance/sensitivity to shear. Current doctrine assumes that eucaryotic cells can only withstand a low shear rate before they are damaged, which is why one relies on low stirrer speeds and higher gassing rates in bioreactor cultivation.

Commonly, screening protocols use different micro titre or well plates for adherent growing cells or shaker flask-based systems for cells grown in suspension. These systems are not stirred or heavily shaken, thus shear is either not present or very low in contrast to bioreactors [102]. To determine the maximum shear that can be applied to cells before they take damage an easy-to-use shear device was employed that can apply precisely defined shear forces. Our experiments showed that shear generated by stirring in bioreactors designed for mammalian cells, with a maximum shear of 1.32×10^4 s^{-1} at 1000 rpm in a bench-top bioreactor, cannot reach levels to harm insect or CHO cells which withstand maximum shear rate of 8.73×10^5 s^{-1}. The generated results are in full agreement with the publication of Nienow et al.[45] who demonstrated much higher robustness of different cell types to shear forces.

This finding also offers the possibility to use a bioreactor designed for microbial cultures for insect or mammalian cells and thus enabling the option for much higher energy transfer and OTR via stirring. Thereby the design of new DO process control regimes for insect cell cultures is facilitated. The main control variable to increase the DO during cultivation should be the stirrer rather than applying higher aeration rates and addition of pure oxygen, which is still the commonly used method in research and industry [103], [104]. Since most of the insect cell cultivations are still batch processes [104] there should be no longer the need for oxygen addition, which has the advantage to improve the economic efficiency of the process. Moreover, the lower gas volumes added to the suspension also reduce foam formation and

bubble rupture at the liquid surface which positively affects cell viability, virus, and product quality.

Based on this new process design, higher cell densities can be achieved, which in turn opens a variety of further process optimization possibilities, with enormous potential in media optimization, as already successfully demonstrated for CHO processes [105]. It can also be assumed that the intensified mixing will also lead to an improvement in transfection or infection efficiency in larger scales and at higher cell densities. Thus, the cell density effect described for BEVS can be overcome.

In summary, the presented work has fulfilled the predefined objectives and our research hypotheses were successfully verified.

- An HTP screening platform for infection of insect cells with baculovirus using a µ-bioreactor was developed, compared to a conventional screening platform, and successfully transferred to a bench-top bioreactor.
- A method for TGE in High five cells for shaker flasks was established and successfully transferred to bench-top bioreactor.
- A method with a simple to use shear device was established for critical shear force detection in different cell lines.
- The identified upper limits of shear rates for insect cell were used to redesign the cultivation process scheme yielding in a superior cultivation strategy that allows for higher biomass and product quality and quantity.

  The protocol established in this work for the new process design was already successfully implemented in other research projects [97], [106]–[109].

5 List of Publications

I. Strobl, F., Ghorbanpour, S.M., Palmberger, D. *et al.* Evaluation of screening platforms for virus-like particle production with the baculovirus expression vector system in insect cells. *Sci Rep* 10**,** 1065 (2020). https://doi.org/10.1038/s41598-020-57761-w

II. Puente-Massaguer, E.; Strobl, F.; Grabherr, R.; Striedner, G.; Lecina, M.; Gòdia, F. PEI-Mediated Transient Transfection of High Five Cells at Bioreactor Scale for HIV-1 VLP Production. *Nanomaterials* 2020, *10*, 1580.

III. Strobl, F., Duerkop, M., Palmberger, D. *et al.* High shear resistance of insect cells: the basis for substantial improvements in cell culture process design. *Sci Rep* 11**,** 9413 (2021). https://doi.org/10.1038/s41598-021-88813-4

Four additional papers where I contributed via collaboration, originated along the thesis:

IV. Miriam Klausberger, Irina A. Leneva, Andrey Egorov, Florian Strobl, Sahar M. Ghorbanpour, Irina N. Falynskova, Alexander V. Poddubikov, Nailya R. Makhmudova, Artem Krokhin, Oxana A. Svitich, Reingard Grabherr, Off-target effects of an insect cell-expressed influenza HA-pseudotyped Gag-VLP preparation in limiting postinfluenza Staphylococcus aureus infections, Vaccine, Volume 38, Issue 4, 2020, Pages 859-867, ISSN 0264-410X, https://doi.org/10.1016/j.vaccine.2019.10.083

V. Puente-Massaguer, E., Grau-Garcia, P., Strobl, F., Grabherr, R., Striedner, G., Lecina, M., & Gòdia, F. (2021). Accelerating HIV-1 VLP production using stable insect cell pools. Biotechnol J, 16, e2000391. https://doi.org/10.1002/biot.202000391

VI. Miriam Klausberger, Mark Duerkop, Helmuth Haslacher, Gordana Wozniak-Knopp, Monika Cserjan-Puschmann, Thomas Perkmann, Nico Lingg, Patricia Pereira Aguilar, Elisabeth Laurent, Jelle De Vos, Manuela Hofner, Barbara Holzer, Maria Stadler, Gabriele Manhart, Klemens Vierlinger, Margot Egger, Lisa Milchram, Elisabeth Gludovacz, Nicolas Marx, Christoph Köppl, Christopher Tauer, Jürgen Beck, Daniel Maresch, Clemens Grünwald-Gruber, Florian Strobl, Peter Satzer, Gerhard Stadlmayr, Ulrike Vavra, Jasmin Huber, Markus Wahrmann, Farsad Eskandary, Marie-Kathrin Breyer, Daniela Sieghart, Peter Quehenberger, Gerda Leitner, Robert Strassl, Alexander E. Egger, Christian Irsara, Andrea Griesmacher, Gregor Hoermann, Günter Weiss, Rosa Bellmann-Weiler, Judith Loeffler-Ragg, Nicole Borth, Richard Strasser, Alois Jungbauer, Rainer Hahn, Jürgen Mairhofer, Boris Hartmann, Nikolaus B. Binder, Gerald Striedner, Lukas Mach, Andreas Weinhäusel, Benjamin Dieplinger, Florian Grebien, Wilhelm Gerner, Christoph J. Binder, Reingard Grabherr,

A comprehensive antigen production and characterisation study for easy-to-implement, specific and quantitative SARS-CoV-2 serotests, EBioMedicine, Volume 67, 2021, 103348, ISSN 2352-3964, https://doi.org/10.1016/j.ebiom.2021.103348.

VII. Puente-Massaguer, E., Grau-Garcia, P., Strobl, F., Grabherr, R., Striedner, G., Lecina, M. and Gòdia, F. (2021), Stable Sf9 cell pools as a system for rapid HIV-1 virus-like particle production. J Chem Technol Biotechnol, 96: 3388-3397. https://doi.org/10.1002/jctb.6895

6 Contribution to publications

I. In Publication I, Florian Strobl designed the research, conducted the experiments, performed the data analyses and interpretation, as well as wrote the manuscript.

II. In Publication II, Florian Strobl designed and executed the bioreactor cultivation experiments, performed the data and software analyses of the cultivation data, and reviewed as well as edited the manuscript.

III. In Publication III Florian Strobl designed the research, conducted the experiments, performed the data analyses and interpretation, and drafted the manuscript.

7 List of Figures

Figure 1: Scheme of baculovirus production. 8

Figure 2: TGE - transfection scheme. 9

Figure 3: Course of the cell concentration of infected and non-infected Tnms42 cell cultures in A) µ-bioreactor cultivation, B) shake flask cultivation, and C) benchtop bioreactor cultivation. All experiments in A and B were conducted in triplicate. Error bars indicate the standard deviation. Taken from Strobl et.al. [59] 13

Figure 4: Comparison of Gag-eGFP VLP production in a 2 L DASGIP® Bioblock glass bioreactor and 125 mL Erlenmeyer flasks (parallel). (**A**) Cell growth and viability profile of transfected cultures. The red arrow indicates the time of transfection. (**B**) Evolution of dissolved oxygen and stirring speed requirements of transfected High Five cells. Black arrows show the addition of Antifoam C. (**C**) Percentage of Gag-eGFP positive cells at different time points. (**D**) Analysis of VLP production and intracellular Gag-eGFP content by flow virometry and spectrofluorometry, respectively. Mean values ± standard deviation of triplicate experiments are represented. Taken from Puente-Massaguer et.al. [93] 16

Figure 5: Total and viable cell counts after treatment with the shear device. Shear was measured at different flow rates for (left) TN42, (center) Hi5, and (right) CHO-K1 cells. Each run was performed in triplicate, except the Hi5 experiment (center) run at 10-mL/min. Taken from Strobl et.al. [95] 18

8 Abbreviations

AcMNPV ..... Autographa califonica multiple nucleopolyhedrovirus

BEVS ..... Baculovirus expression vector system

CDI ..... cell density at infection

CHO ..... chinese hamster ovary

CSTR ..... continuously stirred tank reactor

DEAE ..... Diethylaminoethylcellulose

DNA ..... *deoxyribonucleic acid*

DO ..... dissolved oxygen

eGFP ..... enhanced green fluorescence protein

ELISA ..... Enzyme-linked Immunosorbent Assay

H/D ..... height to diameter

HA ..... hemagglutinin

HIV ..... human immunodeficiency viruses

hpt ..... hours post transfection

hSEAP ..... human-secreted alkaline phosphatase

HTP ..... high through put

MOI ..... multiplicity of infection

OTR ..... oxygen transfer rate

PEI ..... Polyethyleneimine

PFU/cell ..... plaque-forming units per cell

rpm ..... round per minute

TGE ..... transient gene expression

VLP ..... virus like particle

YFP ..... yellow fluorescence protein

9 References

[1] R. W. Glaser, “The growth of insect blood cells in vitro,” *Psyche (Stuttg)*, vol. 24, pp. 1–6, 1917.

[2] T. D. C. Grace, “Establishment of four strains of cells from insect tissues grown in vitro,” *Nature*, vol. 195, no. 4843, pp. 788–789, 1962, doi: 10.1038/195788a0.

[3] D. E. Lynn, “Novel techniques to establish new insect cell lines,” *In Vitro Cellular & Developmental Biology - Animal*, vol. 37, no. 6, pp. 319–321, Jun. 2001, doi: 10.1007/bf02577564.

[4] C. M. Yee, A. J. Zak, B. D. Hill, and F. Wen, “The Coming Age of Insect Cells for Manufacturing and Development of Protein Therapeutics.,” *Ind Eng Chem Res*, vol. 57, no. 31, pp. 10061–10070, Aug. 2018, doi: 10.1021/acs.iecr.8b00985.

[5] D. E. Lynn, “Novel techniques to establish new insect cell lines,” in *In Vitro Cellular and Developmental Biology - Animal*, Jun. 2001, vol. 37, no. 6, pp. 319–321. doi: 10.1290/1071-2690(2001)037<0319:NTTENI>2.0.CO;2.

[6] G. Smagghe, C. L. Goodman, and D. Stanley, “Insect cell culture and applications to research and pest management,” *In Vitro Cellular and Developmental Biology - Animal*, vol. 45, no. 3–4. Springer New York LLC, pp. 93–105, Feb. 27, 2009. doi: 10.1007/s11626-009-9181-x.

[7] E. Langer and R. Rader, “Biopharmaceutical Manufacturing: Historical and Future Trends in Titers, Yields, and Efficiency in Commercial-Scale Bioprocessing,” *BioProcessing Journal*, vol. 13, no. 4, pp. 47–54, 2015, doi: 10.12665/J134.Langer.

[8] J. Archambault, J. Robert, and L. Tom, “Culture of immobilized insect cells,” *Bioprocess Engineering*, vol. 11, no. 5, pp. 189–197, 1994, doi: 10.1007/BF00369629.

[9] J. Wu, G. King, A. J. Daugulis, P. Faulkner, D. H. Bone, and M. F. A. Goosen, “Adaptation of insect cells to suspension culture,” *Journal of Fermentation and Bioengineering*, vol. 70, no. 2, pp. 90–93, Jan. 1990, doi: 10.1016/0922-338X(90)90277-4.

[10] M. M. van Oers, “Vaccines for Viral and Parasitic Diseases Produced with Baculovirus Vectors,” *Advances in Virus Research*, vol. 68, pp. 193–253, 2006, doi: 10.1016/S0065-3527(06)68006-8.

[11] L. Ikonomou, Y. J. Schneider, and S. N. Agathos, “Insect cell culture for industrial production of recombinant proteins,” *Applied Microbiology and Biotechnology*, vol. 62, no. 1, pp. 1–20, 2003.

[12] T. A. Kost, J. P. Condreay, and D. L. Jarvis, “Baculovirus as versatile vectors for protein expression in insect and mammalian cells,” *Nature Biotechnology*, vol. 23, no. 5. pp. 567–575, 2005. doi: 10.1038/nbt1095.

[13] K. J. Airenne *et al.*, “Baculovirus: An insect-derived vector for diverse gene transfer applications,” *Molecular Therapy*, vol. 21, no. 4. Nature Publishing Group, pp. 739–749, 2013. doi: 10.1038/mt.2012.286.

[14] S. N. Agathos, “Insect cell bioreactors,” *Cytotechnology*, vol. 20, no. 1–3. Kluwer Academic Publishers, pp. 173–189, 1996. doi: 10.1007/BF00350398.

[15] S. S. Farid, “Process economics of industrial monoclonal antibody manufacture,” *J Chromatogr B Analyt Technol Biomed Life Sci*, vol. 848, no. 1, pp. 8–18, 2007, doi: 10.1016/j.jchromb.2006.07.037.

[16] C. Sieblist, M. Jenzsch, and M. Pohlscheidt, “Equipment characterization to mitigate risks during transfers of cell culture manufacturing processes,” *Cytotechnology*, vol. 68, no. 4, pp. 1381–1401, Aug. 2016, doi: 10.1007/S10616-015-9899-0/TABLES/3.

[17] C. Löffelholz *et al.*, “Bioengineering Parameters for Single-Use Bioreactors: Overview and Evaluation of Suitable Methods,” *Chemie Ingenieur Technik*, vol. 85, no. 1-2, pp. 40–56, 2013, doi: 10.1002/cite.201200125.

[18] R. Godoy-Silva, C. Berdugo, and J. J. Chalmers, “Aeration, Mixing, and Hydrodynamics, Animal Cell Bioreactors,” *Encyclopedia of Industrial Biotechnology*, pp. 1–27, 2010, doi: doi:10.1002/9780470054581.eib010.

[19] P. Czermak, R. Pörtner, and A. Brix, “Special Engineering Aspects,” in *Cell and Tissue Reaction Engineering: With a Contribution by Martin Fussenegger and Wilfried Weber*,

R. Eibl, D. Eibl, R. Pörtner, G. Catapano, and P. Czermak, Eds. Berlin, Heidelberg: Springer Berlin Heidelberg, 2009, pp. 83–172. doi: 10.1007/978-3-540-68182-3_4.

[20] F. Garcia-Ochoa, E. Gomez, V. E. Santos, and J. C. Merchuk, “Oxygen uptake rate in microbial processes: An overview,” *Biochemical Engineering Journal*, vol. 49, no. 3, pp. 289–307, 2010, doi: https://doi.org/10.1016/j.bej.2010.01.011.

[21] D. Eisenkraetzer, “6.1 Bioreactors for Animal Cell Culture,” *Animal Cell BiotechnologyIn Biologics Production*. 2014. doi: 10.1515/9783110278965.389.

[22] C. Langheinrich *et al.*, “Oxygen Transfer in Stirred Bioreactors Under Animal Cell Culture Conditions,” *Food and Bioproducts Processing*, vol. 80, no. 1, pp. 39–44, 2002, doi: https://doi.org/10.1205/096030802753479098.

[23] V. Jossen, R. Eibl, R. Pörtner, M. Kraume, and D. Eibl, “7 - Stirred Bioreactors: Current State and Developments, With Special Emphasis on Biopharmaceutical Production Processes,” in *Current Developments in Biotechnology and Bioengineering*, C. Larroche, M. Á. Sanromán, G. Du, and A. Pandey, Eds. Elsevier, 2017, pp. 179–215. doi: https://doi.org/10.1016/B978-0-444-63663-8.00007-0.

[24] P. Sagmeister, M. Jazini, J. Klein, and C. Herwig, “Bacterial Suspension Cultures,” *Industrial Scale Suspension Culture of Living Cells*, pp. 40–93, 2014, doi: doi:10.1002/9783527683321.ch01.

[25] S. Reuveny, Y. J. Kim, C. W. Kemp, and J. Shiloach, “Production of recombinant proteins in high-density insect cell cultures,” *Biotechnology and Bioengineering*, vol. 42, no. 2. pp. 235–239, 1993. doi: 10.1002/bit.260420211.

[26] S. N. AGATHOS, Y. -H JEONG, and K. VENKAT, “Growth Kinetics of Free and Immobilized Insect Cell Cultures,” *Ann N Y Acad Sci*, vol. 589, no. 1, pp. 372–398, 1990, doi: 10.1111/j.1749-6632.1990.tb24259.x.

[27] M. GERBAL *et al.*, “ADAPTATION OF AN INSECT CELL LINE OF SPODOPTERA FRUGIPERDA TO GROW AT 37° C: CHARACTERIZATION OF AN ENDODIPLOID CLONE,” *In Vitro Cellular & Developmental Biology - Animal*, vol. 36, no. 2, p. 117, 2000, doi: 10.1290/1071-2690(2000)036<0117:aoaicl>2.0.co;2.

[28] W. Hensler, V. Singh, and S. N. Agathos, “Sf9 insect cell growth and β-galactosidase production in serum and serum-free media,” in *Annals of the New York Academy of Sciences*, 1994, vol. 745, pp. 149–166. doi: 10.1111/j.1749-6632.1994.tb44370.x.

[29] J. Zhang, N. Kalogerakis, and L. A. Behie, “Optimization of the physiochemical parameters for the culture of Bombyx mori insect cells used in recombinant protein production,” *Journal of Biotechnology*, vol. 33, no. 3, pp. 249–258, Apr. 1994, doi: 10.1016/0168-1656(94)90073-6.

[30] J.-C. Drugmand, Y.-J. Schneider, and S. N. Agathos, “Environmental Effects of Lactate on High-Five™ Insect Cell Metabolism,” in *Animal Cell Technology Meets Genomics*, Springer-Verlag, 2005, pp. 91–94. doi: 10.1007/1-4020-3103-3_14.

[31] W. F. Hink and E. M. Strauss, “Suspension culture of the cabbage looper (TN-368) cell line,” *TCA manual / Tissue Culture Association*, vol. 5, no. 1, pp. 1023–1025, 1979, doi: 10.1007/BF00919724.

[32] J. C. Drugmand, Y. J. Schneider, and S. N. Agathos, “Insect cells as factories for biomanufacturing,” *Biotechnology Advances*, vol. 30, no. 5. pp. 1140–1157, Sep. 2012. doi: 10.1016/j.biotechadv.2011.09.014.

[33] C. Mitchell-Logean and D. W. Murhammer, “Bioreactor headspace purging reduces dissolved carbon dioxide accumulation in insect cell cultures and enhances cell growth,” *Biotechnology Progress*, vol. 13, no. 6, pp. 875–877, Nov. 1997, doi: 10.1021/bp970078s.

[34] L. A. Palomares, S. López, and O. T. Ramírez, “Utilization of oxygen uptake rate to assess the role of glucose and glutamine in the metabolism of infected insect cell cultures,” *Biochemical Engineering Journal*, vol. 19, no. 1, pp. 87–93, Jul. 2004, doi: 10.1016/j.bej.2003.12.002.

[35] G. Schmid, “Insect cell cultivation: Growth and kinetics,” *Cytotechnology*, vol. 20, no. 1–3. Kluwer Academic Publishers, pp. 43–56, 1996. doi: 10.1007/BF00350388.

[36] B. A. Wagner, S. Venkataraman, and G. R. Buettner, “The rate of oxygen utilization by cells,” *Free Radic Biol Med*, vol. 51, no. 3, pp. 700–712, 2011, doi: 10.1016/j.freeradbiomed.2011.05.024.

[37] A. A. Kamen, R. L. Tom, A. W. Caron, C. Chavarie, B. Massie, and J. Archambault, “Culture of insect cells in helical ribbon impeller bioreactor,” *Biotechnology and Bioengineering*, vol. 38, no. 6, pp. 619–628, 1991, doi: 10.1002/bit.260380607.

[38] T. K. K. Wong, L. K. Nielsen, P. F. Greenfield, and S. Reid, “Relationship between oxygen uptake rate and time of infection of Sf9 insect cells infected with a recombinant baculovirus,” *Cytotechnology*, vol. 15, no. 1, pp. 157–167, 1994, doi: 10.1007/bf00762390.

[39] R. D. Guarino, L. E. Dike, T. A. Haq, J. A. Rowley, J. B. Pitner, and M. R. Timmins, “Method for determining oxygen consumption rates of static cultures from microplate measurements of pericellular dissolved oxygen concentration,” *Biotechnology and Bioengineering*, vol. 86, no. 7, pp. 775–787, 2004, doi: 10.1002/bit.20072.

[40] F. Garcia-Ochoa and E. Gomez, “Bioreactor scale-up and oxygen transfer rate in microbial processes: An overview,” *Biotechnology Advances*, vol. 27, no. 2, pp. 153–176, 2009, doi: https://doi.org/10.1016/j.biotechadv.2008.10.006.

[41] P. L. L. Walls, O. McRae, V. Natarajan, C. Johnson, C. Antoniou, and J. C. Bird, “Quantifying the potential for bursting bubbles to damage suspended cells,” *Scientific Reports*, vol. 7, no. 1, p. 15102, 2017, doi: 10.1038/s41598-017-14531-5.

[42] J. Tramper, “Oxygen gradients in animal-cell bioreactors,” *Cytotechnology*, vol. 18, no. 1, pp. 27–34, 1995, doi: 10.1007/BF00744317.

[43] K. Paul and C. Herwig, “Scale-down simulators for mammalian cell culture as tools to access the impact of inhomogeneities occurring in large-scale bioreactors,” *Engineering in Life Sciences*, vol. 20, no. 5–6, pp. 197–204, 2020, doi: 10.1002/elsc.201900162.

[44] N. Kioukia, A. W. Nienow, M. Al-Rubeai, and A. N. Emery, “Influence of agitation and sparging on the growth rate and infection of insect cells in bioreactors and a comparison

with hybridoma culture," *Biotechnology Progress*, vol. 12, no. 6, pp. 779–785, Nov. 1996, doi: 10.1021/bp9600703.

[45] A. W. Nienow, "Reactor engineering in large scale animal cell culture," *Cytotechnology*, vol. 50, no. 1–3. Springer, pp. 9–33, Mar. 20, 2006. doi: 10.1007/s10616-006-9005-8.

[46] G. E. Smith *et al.*, "Modification and secretion of human interleukin 2 produced in insect cells by a baculovirus expression vector," *Proc Natl Acad Sci U S A*, vol. 82, no. 24, pp. 8404–8408, 1985, doi: 10.1073/pnas.82.24.8404.

[47] T. A. Kost and J. P. Condreay, "Recombinant baculoviruses as expression vectors for insect and mammalian cells," *Current Opinion in Biotechnology*, vol. 10, no. 5. Current Biology Ltd, pp. 428–433, Oct. 01, 1999. doi: 10.1016/S0958-1669(99)00005-1.

[48] M. D. Summers, "Milestones Leading to the Genetic Engineering of Baculoviruses as Expression Vector Systems and Viral Pesticides," *Advances in Virus Research*, vol. 68. pp. 3–73, 2006. doi: 10.1016/S0065-3527(06)68001-9.

[49] K. J. Airenne *et al.*, "Baculovirus: An insect-derived vector for diverse gene transfer applications," *Molecular Therapy*, vol. 21, no. 4. Nature Publishing Group, pp. 739–749, 2013. doi: 10.1038/mt.2012.286.

[50] C. H. Tsai, S. C. Wei, H. R. Lo, and Y. C. Chao, "Baculovirus as versatile vectors for protein display and biotechnological applications," *Current Issues in Molecular Biology*, vol. 34, pp. 231–255, 2020, doi: 10.21775/CIMB.034.231.

[51] M. G. Aucoin, J. A. Mena, and A. A. Kamen, "Bioprocessing of baculovirus vectors: A review," *Current Gene Therapy*, vol. 10, no. 3, pp. 174–186, 2010.

[52] M. van Oers and J. Vlak, "Baculovirus Genomics," *Current Drug Targets*, vol. 8, no. 10, pp. 1051–1068, Oct. 2007, doi: 10.2174/138945007782151333.

[53] R. GF. et al. Theilmann DA, Blissard GW, Bonning B, Jehle J, O'Reilly DR, *Family Baculoviridae Fauquet CM, Mayo MA, Maniloff J, Desselberger U, Ball LA.eds.). Virus Taxonomy: Eight Report of the International Committee on Taxonomy of Viruses.* Elsevier: London, 2005.

[54] V. A. Luckow, S. C. Lee, G. F. Barry, and P. O. Olins, “Efficient generation of infectious recombinant baculoviruses by site-specific transposon-mediated insertion of foreign genes into a baculovirus genome propagated in Escherichia coli.,” *Journal of Virology*, vol. 67, no. 8, pp. 4566–4579, Aug. 1993, doi: 10.1128/jvi.67.8.4566-4579.1993.

[55] K. J. Airenne *et al.*, “Baculovirus: An insect-derived vector for diverse gene transfer applications,” *Molecular Therapy*, vol. 21, no. 4. Nature Publishing Group, pp. 739–749, 2013. doi: 10.1038/mt.2012.286.

[56] F. Fernandes, A. P. Teixeira, N. Carinhas, M. J. T. Carrondo, and P. M. Alves, “Insect cells as a production platform of complex virus-like particles,” *Expert Review of Vaccines*, vol. 12, no. 2. Taylor & Francis, pp. 225–236, Feb. 2013. doi: 10.1586/erv.12.153.

[57] L. Ikonomou, Y. J. Schneider, and S. N. Agathos, “Insect cell culture for industrial production of recombinant proteins,” *Applied Microbiology and Biotechnology*, vol. 62, no. 1, pp. 1–20, 2003.

[58] C. G. M. De Pinheiro, M. D. O. Pedrosa, N. C. Teixeira, A. P. D. Ano Bom, M. M. Van Oers, and G. G. D. S. Oliveira, “Optimization of canine interleukin-12 production using a baculovirus insect cell expression system Biotechnology,” *BMC Research Notes*, vol. 9, no. 1, Jan. 2016, doi: 10.1186/s13104-016-1843-7.

[59] F. Strobl, S. M. Ghorbanpour, D. Palmberger, and G. Striedner, “Evaluation of screening platforms for virus-like particle production with the baculovirus expression vector system in insect cells,” *Scientific Reports*, vol. 10, no. 1, Dec. 2020, doi: 10.1038/s41598-020-57761-w.

[60] Y. Ho, H. R. Lo, T. C. Lee, C. P. Y. Wu, and Y. C. Chao, “Enhancement of correct protein folding in vivo by a non-lytic baculovirus,” *Biochemical Journal*, vol. 382, no. 2, pp. 695–702, Sep. 2004, doi: 10.1042/BJ20040007.

[61] N. Kumar, D. Pandey, and A. Halder, “Preventive, diagnostic and therapeutic applications of baculovirus expression vector system,” in *Trends in Insect Molecular*

Biology and Biotechnology, Springer International Publishing, 2018, pp. 163–191. doi: 10.1007/978-3-319-61343-7_9.

[62] J. Fuenmayor, L. Cervera, F. Gòdia, and A. Kamen, “Extended gene expression for Gag VLP production achieved at bioreactor scale,” *Journal of Chemical Technology and Biotechnology*, vol. 94, no. 1, pp. 302–308, Jan. 2019, doi: 10.1002/jctb.5777.

[63] T. Vicente, A. Roldão, C. Peixoto, M. J. T. Carrondo, and P. M. Alves, “Large-scale production and purification of VLP-based vaccines,” *Journal of Invertebrate Pathology*, vol. 107, pp. S42–S48, 2011, doi: https://doi.org/10.1016/j.jip.2011.05.004.

[64] S. Gutiérrez-Granados, L. Cervera, A. A. Kamen, and F. Gòdia, “Advancements in mammalian cell transient gene expression (TGE) technology for accelerated production of biologics,” *Critical Reviews in Biotechnology*, vol. 38, no. 6. Taylor and Francis Ltd, pp. 918–940, Aug. 18, 2018. doi: 10.1080/07388551.2017.1419459.

[65] S. Geisse, “Reflections on more than 10 years of TGE approaches,” *Protein Expression and Purification*, vol. 64, no. 2. Protein Expr Purif, pp. 99–107, Apr. 2009. doi: 10.1016/j.pep.2008.10.017.

[66] F. Strobl *et al.*, “PEI-mediated transient transfection of high five cells at bioreactor scale for HIV-1 VLP production,” *Nanomaterials*, vol. 10, no. 8, pp. 1–16, Aug. 2020, doi: 10.3390/nano10081580.

[67] A. D. Bandaranayake and S. C. Almo, “Recent advances in mammalian protein production,” *FEBS Letters*, vol. 588, no. 2. John Wiley & Sons, Ltd, pp. 253–260, Jan. 21, 2014. doi: 10.1016/j.febslet.2013.11.035.

[68] F. L. Graham and A. J. van der Eb, “A new technique for the assay of infectivity of human adenovirus 5 DNA,” *Virology*, vol. 52, no. 2, pp. 456–467, Apr. 1973, doi: 10.1016/0042-6822(73)90341-3.

[69] V. W.-A. in cell culture and undefined 1989, “Gene transfer in insects,” *Elsevier*.

[70] A. D. Bangham, “Liposomes: Realizing their promise,” *Hospital Practice*, vol. 27, no. 12, 1992, doi: 10.1080/21548331.1992.11705537.

[71] X. Zhou and L. Huang, “DNA transfection mediated by cationic liposomes containing lipopolylysine: characterization and mechanism of action,” *BBA - Biomembranes*, vol. 1189, no. 2, pp. 195–203, Jan. 1994, doi: 10.1016/0005-2736(94)90066-3.

[72] K. Shigekawa, W. D.- Biotechniques, and undefined 1988, “Electroporation of eukaryo and prokaryotes: a general approach to the introduction of macromolecules into cells,” *pascal-francis.inist.fr*.

[73] G. Andreason, G. E.- Biotechniques, and undefined 1988, “Introduction and expression of DNA molecules in eukaryotic cells by electroporation.,” *europepmc.org*.

[74] S. Gutiérrez-Granados, L. Cervera, A. A. Kamen, and F. Gòdia, “Advancements in mammalian cell transient gene expression (TGE) technology for accelerated production of biologics,” *Critical Reviews in Biotechnology*, vol. 38, no. 6. Taylor and Francis Ltd, pp. 918–940, Aug. 18, 2018. doi: 10.1080/07388551.2017.1419459.

[75] I. D. Ogay, O. A. Lihoradova, S. S. Azimova, A. A. Abdukarimov, J. M. Slack, and D. E. Lynn, “Transfection of insect cell lines using polyethylenimine,” *Cytotechnology*, vol. 51, no. 2, pp. 89–98, Jun. 2006, doi: 10.1007/s10616-006-9022-7.

[76] E. Puente-Massaguer, M. Lecina, and F. Gòdia, “Nanoscale characterization coupled to multi-parametric optimization of Hi5 cell transient gene expression,” *Applied Microbiology and Biotechnology*, vol. 102, no. 24, pp. 10495–10510, 2018, doi: 10.1007/s00253-018-9423-5.

[77] M. Bleckmann *et al.*, “Genomic analysis and isolation of RNA polymerase II dependent promoters from Spodoptera frugiperda,” *PLoS ONE*, vol. 10, no. 8, Aug. 2015, doi: 10.1371/journal.pone.0132898.

[78] X. Shen, A. K. Pitol, V. Bachmann, D. L. Hacker, L. Baldi, and F. M. Wurm, “A simple plasmid-based transient gene expression method using High Five cells,” *Journal of Biotechnology*, vol. 216, pp. 67–75, Dec. 2015, doi: 10.1016/j.jbiotec.2015.10.007.

[79] X. Shen, D. L. Hacker, L. Baldi, and F. M. Wurm, “Virus-free transient protein production in Sf9 cells,” *Journal of Biotechnology*, vol. 171, no. 1, pp. 61–70, Dec. 2013, doi: 10.1016/j.jbiotec.2013.11.018.

[80] K. Mori, H. Hamada, T. Ogawa, Y. Ohmuro-Matsuyama, T. Katsuda, and H. Yamaji, “Efficient production of antibody Fab fragment by transient gene expression in insect cells,” *Journal of Bioscience and Bioengineering*, vol. 124, no. 2, pp. 221–226, Aug. 2017, doi: 10.1016/j.jbiosc.2017.03.007.

[81] Y. Mizote, K. Masumi-Koizumi, T. Katsuda, and H. Yamaji, “Production of an antibody Fab fragment using 2A peptide in insect cells,” *Journal of Bioscience and Bioengineering*, vol. 130, no. 2, pp. 205–211, Aug. 2020, doi: 10.1016/j.jbiosc.2020.03.009.

[82] M. Bleckmann *et al.*, “Identifying parameters to improve the reproducibility of transient gene expression in High Five cells,” *PLoS ONE*, vol. 14, no. 6, Jun. 2019, doi: 10.1371/journal.pone.0217878.

[83] N. Carinhas, V. Bernal, A. Y. Yokomizo, M. J. T. Carrondo, R. Oliveira, and P. M. Alves, “Baculovirus production for gene therapy: The role of cell density, multiplicity of infection and medium exchange,” *Applied Microbiology and Biotechnology*, vol. 81, no. 6, pp. 1041–1049, Jan. 2009, doi: 10.1007/S00253-008-1727-4.

[84] S. M. Deutschmann and V. Jäger, “Optimization of the growth conditions of Sf21 insect cells for high-density perfusion culture in stirred-tank bioreactors,” *Enzyme and Microbial Technology*, vol. 16, no. 6, pp. 506–512, Jun. 1994, doi: 10.1016/0141-0229(94)90022-1.

[85] C. CAVEGN, H. D. BLASEY, M. A. PAYTON, B. ALLET, J. LI, and A. R. BERNARD, “EXPRESSION OF RECOMBINANT PROTEINS IN HIGH DENSITY INSECT CELL CULTURES,” *Animal Cell Technology*, pp. 569–578, Jan. 1992, doi: 10.1016/B978-0-7506-0421-5.50126-4.

[86] C. Bédard, S. Perret, and A. A. Kamen, “Fed-batch culture of Sf-9 cells supports 3 3 10 7 cells per ml and improves baculovirus-expressed recombinant protein yields,” *Biotechnology Letters 1997 19:7*, vol. 19, no. 7, pp. 629–632, 1997, doi: 10.1023/A:1018378529299.

[87] J. C. Drugmand, Y. J. Schneider, and S. N. Agathos, “Insect cells as factories for biomanufacturing,” *Biotechnology Advances*, vol. 30, no. 5, pp. 1140–1157, Sep. 2012, doi: 10.1016/J.BIOTECHADV.2011.09.014.

[88] C. B. Elias, A. Zeiser, C. Bé, and A. A. Kamen, “Enhanced Growth of Sf-9 Cells to a Maximum Density of 5.2 × 10 7 Cells per mL and Production of-Galactosidase at High Cell Density by Fed Batch Culture,” *Biotechnol Bioeng*, vol. 68, pp. 381–388, 2000, doi: 10.1002/(SICI)1097-0290(20000520)68:4.

[89] A. W. Caron, J. Archambault, and B. Massie, “High-level recombinant protein production in bioreactors using the baculovirus–insect cell expression system,” *Biotechnology and Bioengineering*, vol. 36, no. 11, pp. 1133–1140, Dec. 1990, doi: 10.1002/BIT.260361108.

[90] E. Puente-Massaguer, M. Lecina, and F. Gòdia, “Nanoscale characterization coupled to multi-parametric optimization of Hi5 cell transient gene expression,” *Applied Microbiology and Biotechnology*, vol. 102, no. 24, pp. 10495–10510, Dec. 2018, doi: 10.1007/s00253-018-9423-5.

[91] E. Puente-Massaguer, M. Lecina, and F. Gòdia, “Application of advanced quantification techniques in nanoparticle-based vaccine development with the Sf9 cell baculovirus expression system,” *Vaccine*, vol. 38, no. 7, pp. 1849–1859, Feb. 2020, doi: 10.1016/j.vaccine.2019.11.087.

[92] B. Fernandes *et al.*, “Adaptive laboratory evolution of stable insect cell lines for improved HIV-Gag VLPs production,” *Journal of Biotechnology*, vol. 307, pp. 139–147, Jan. 2020, doi: 10.1016/j.jbiotec.2019.10.004.

[93] E. Puente-Massaguer, F. Strobl, R. Grabherr, G. Striedner, M. Lecina, and F. Gòdia, “PEI-mediated transient transfection of high five cells at bioreactor scale for HIV-1 VLP production,” *Nanomaterials*, vol. 10, no. 8, pp. 1–16, Aug. 2020, doi: 10.3390/nano10081580.

[94] M. Duerkop, E. Berger, A. Dürauer, and A. Jungbauer, “Influence of cavitation and high shear stress on HSA aggregation behavior,” *Engineering in Life Sciences*, vol. 18, no. 3, pp. 169–178, 2018, doi: 10.1002/elsc.201700079.

[95] F. Strobl, M. Duerkop, D. Palmberger, and G. Striedner, “High shear resistance of insect cells: the basis for substantial improvements in cell culture process design,” *Scientific Reports 2021 11:1*, vol. 11, no. 1, pp. 1–11, May 2021, doi: 10.1038/s41598-021-88813-4.

[96] M. Fink, M. Cserjan-Puschmann, D. Reinisch, and G. Striedner, “High-throughput microbioreactor provides a capable tool for early stage bioprocess development,” *Scientific Reports 2021 11:1*, vol. 11, no. 1, pp. 1–10, Jan. 2021, doi: 10.1038/s41598-021-81633-6.

[97] K. Reiter, P. Pereira Aguilar, D. Grammelhofer, J. Joseph, P. Steppert, and A. Jungbauer, “Separation of influenza virus-like particles from baculovirus by polymer-grafted anion exchanger,” *Journal of Separation Science*, vol. 43, no. 12, pp. 2270–2278, Jun. 2020, doi: 10.1002/jssc.201901215.

[98] W. Cao, H. Cao, X. Yi, and Y. Zhuang, “Development of a simple and high-yielding fed-batch process for the production of porcine circovirus type 2 virus-like particle subunit vaccine,” *AMB Express*, vol. 9, no. 1, p. 164, 2019, doi: 10.1186/s13568-019-0880-8.

[99] E. Puente-Massaguer, M. Lecina, and F. Gòdia, “Integrating nanoparticle quantification and statistical design of experiments for efficient HIV-1 virus-like particle production in High Five cells,” *Applied Microbiology and Biotechnology*, vol. 104, no. 4, pp. 1569–1582, Feb. 2020, doi: 10.1007/s00253-019-10319-x.

[100] J. Urthaler, H. Schuchnigg, P. Garidel, and H. Huber, “Industrial Manufacturing of Plasmid-DNA Products for Gene Vaccination and Therapy,” *Gene Vaccines*, vol. 9783709104392, pp. 311–330, Mar. 2012, doi: 10.1007/978-3-7091-0439-2_16.

[101] M. Bleckmann *et al.*, “Identifying parameters to improve the reproducibility of transient gene expression in High Five cells,” *PLOS ONE*, vol. 14, no. 6, p. e0217878, Jun. 2019, doi: 10.1371/JOURNAL.PONE.0217878.

[102] H. Giese *et al.*, “Effective shear rates in shake flasks,” *Chemical Engineering Science*, vol. 118, pp. 102–113, Oct. 2014, doi: 10.1016/J.CES.2014.07.037.

[103] L. Käßer, M. Rotter, L. Coletta, D. Salzig, and P. Czermak, “Process intensification for the continuous production of an antimicrobial peptide in stably-transformed Sf-9 insect cells,” *Scientific Reports 2022 12:1*, vol. 12, no. 1, pp. 1–10, Jan. 2022, doi: 10.1038/s41598-022-04931-7.

[104] B. Buckland *et al.*, “Technology transfer and scale-up of the Flublok® recombinant hemagglutinin (HA) influenza vaccine manufacturing process,” *Vaccine*, 2014, [Online]. Available: http://www.scopus.com/inward/record.url?eid=2-s2.0-84906015460&partnerID=40&md5=23383871eada628529d534d1d6f3110c

[105] F. v. Ritacco, Y. Wu, and A. Khetan, “Cell culture media for recombinant protein expression in Chinese hamster ovary (CHO) cells: History, key components, and optimization strategies,” *Biotechnology Progress*, vol. 34, no. 6, pp. 1407–1426, Nov. 2018, doi: 10.1002/BTPR.2706.

[106] E. Puente-Massaguer, F. Strobl, R. Grabherr, G. Striedner, M. Lecina, and F. Gòdia, “PEI-mediated transient transfection of high five cells at bioreactor scale for HIV-1 VLP production,” *Nanomaterials*, vol. 10, no. 8, pp. 1–16, Aug. 2020, doi: 10.3390/nano10081580.

[107] M. Klausberger *et al.*, “Off-target effects of an insect cell-expressed influenza HA-pseudotyped Gag-VLP preparation in limiting postinfluenza Staphylococcus aureus infections,” *Vaccine*, 2019, doi: https://doi.org/10.1016/j.vaccine.2019.10.083.

[108] E. Puente-Massaguer *et al.*, “Accelerating HIV-1 VLP production using stable High Five insect cell pools,” *Biotechnology Journal*, vol. 16, no. 4, p. 2000391, Apr. 2021, doi: https://doi.org/10.1002/biot.202000391.

[109] E. Puente-Massaguer *et al.*, “Stable Sf9 cell pools as a system for rapid HIV-1 virus-like particle production,” *Journal of Chemical Technology & Biotechnology*, vol. n/a, no. n/a, Aug. 2021, doi: https://doi.org/10.1002/jctb.6895.

10 Publications

I. Evaluation of screening platforms for virus-like particle production with the baculovirus expression vector system in insect cells.

II. PEI-Mediated Transient Transfection of High Five Cells at Bioreactor Scale for HIV-1 VLP Production.

III. High shear resistance of insect cells: the basis for substantial improvements in cell culture process design.

IV. Off-target effects of an insect cell-expressed influenza HA-pseudotyped Gag-VLP preparation in limiting postinfluenza Staphylococcus aureus infections.

V. Accelerating HIV-1 VLP production using stable insect cell pools.

VI. A comprehensive antigen production and characterisation study for easy-to-implement, specific and quantitative SARS-CoV-2 serotests.

VII. Stable Sf9 cell pools as a system for rapid HIV-1 virus-like particle production.

Publication I

SCIENTIFIC REPORTS
nature research

OPEN

Evaluation of screening platforms for virus-like particle production with the baculovirus expression vector system in insect cells

Florian Strobl[1,2], Sahar Masoumeh Ghorbanpour[1,2], Dieter Palmberger[1,2] & Gerald Striedner[2*]

Recombinant protein and virus-like particle (VLP) production based on the baculovirus expression vector system is fast, flexible, and offers high yields. Independent from the product, a multitude of parameters are screened during process development/optimisation. Early development acceleration is a key requirement for economic efficiency, and µ-scale bioreactor systems represent an attractive solution for high-throughput (HTP) experimentation. However, limited practical knowledge is available on the relevance and transferability of screening data to pilot scales and manufacturing. The main goal of the present study was to evaluate a HTP µ-bioreactor platform with respect to its aptitude as a screening platform mainly based on transferability of results to benchtop bioreactors representing the conventional production regime. Second question was to investigate to what extent the online sensors of the µ-bioreactor contribute to process understanding and development. We demonstrated that transferability of infection screening results from the HTP µ-bioreactor scale to the benchtop bioreactor was equal or better than that from shaker cultivation. However, both experimental setups turned out to be sub-optimal solutions that only allowed for a first and rough ranking with low relevance in the case of absolute numbers. Bioreactor yields were up to one order of magnitude higher than the results of screening experiments.

Over the last few decades, the baculovirus expression vector system (BEVS) has become a powerful tool for the production of a variety of recombinant proteins. More than 400 cell lines have since been modified to produce wild-type or recombinant baculovirus, recombinant proteins, virus-like particles (VLPs) or gene therapy vectors[1]. Parameters that have to be considered when infecting cells are the cell concentration at time of infection (CCI), the number of plaque-forming units per cell (PFU/cell) commonly described as multiplicity of infection (MOI), and the harvest time point. There are studies focused on development of mathematic models to calculate the best infection strategies including MOI, TOI, CCI and media depletion[2–4]. In these studies, *Sf9* cells expressing the same soluble secreted product were used. Over time insect cell lines from different species were established exhibiting growth, infection and production characteristics different from that of Sf9 cells. In several studies significant variation with respect to optimal MOI were observed, mostly stating that there are correlations between MOI levels and product formation or concentration. Recommended MOIs range from 1 to 20 plaque-forming units per cell[5].

The CCI is another important factor influencing the infection efficiency, and CCIs $>2 \times 10^6$ cells mL^{-1} for *Sf9* and High Five lead to significantly reduced specific productivities, and even non-infected cell populations have been observed[6,7]. Another point to consider is the stability of the virus stock during long-term storage at 4 °C, which can lead to a decrease in virus titre[8]. In general, the determination of virus titre is a critical and time-consuming step and, independent of the methods used, there is significant analytical error in the range of ± 1 log fold changes[9]. This is valid for both plaque assay and tissue culture infectious dose 50 (TCID50), two methods commonly used and accepted in academia and industry[10].

To identify the optimal CCI and MOI for high yield production of VLPs or proteins of interest, multiple costly and time-consuming cultivations have to be performed in small scale before transferring the process to a larger scale. In commonly used shake flasks or cell culture flasks, monitoring and control of key process parameters such

[1]acib GmbH, Petersgasse 14, 8010, Graz, Austria. [2]Department of Biotechnology, University of Natural Resources and Life Sciences, Vienna, Austria. *email: gerald.striedner@boku.ac.at

as OD, pH and dissolved oxygen (DO) is limited or simply not possible. An alternative to conventional shaker flasks or cell culture flasks is the Biolector® (m2p-labs GmbH, Baesweiler, Germany), a titre plate-based platform. This high-throughout (HTP) µ-bioreactor system enables online monitoring of cell density, fluorescence, DO level, and pH in a continuously shaken 2.5 mL volume and has already been described as being well-suited for *Sf*9 insect cells[11]. Continuous scattered light measurement offers the possibility of obtaining real-time information on cell growth during cultivation. Moreover, fluorescence measurements can provide direct or indirect information on product formation and infection kinetics when the baculovirus harbours a fluorescence marker or the product is able to emit fluorescence itself. Biolector® was already used as a tool for condition screening to identify the optimal MOI and CCI for *Sf*9 insect cells producing recombinant secreted alkaline phosphatase. Identical behaviour was observed in TubeSpin® Bioreactor 50 experiments and the results transferred to stirred tank and wave bioreactors[12]. Nevertheless, there are systems used for other organism which, combined with shaker platforms, offer non-invasive measurement of OD[13] and also pH and DO using shaker flasks[14]. For these systems special shaker flasks are needed and the incubator has to be adapted with a special platform which is connected to a control unit, with a limited number of shaker flasks per control unit (e.g. SFR vario (Presens).

However, for the BEVS, direct comparisons for transferability of results (cell growth, infection, and production) generated in screening experiments with the µ-bioreactor or shake flask to stirred tank bioreactor cultivations are missing. In this work, we summarise a benchmark study focused on the suitability and performance of the µ-bioreactor platform as a HTP screening tool for the early development and optimisation of BEVS. We varied the MOI in the µ-bioreactor, shake flask, and 1.5 L benchtop bioreactor cultivation scales and compared the results with respect to information content and transferability. We clearly demonstrate that the µ-bioreactor system is an efficient screening tool for baculovirus insect cell technology.

Results and Discussion

Process knowledge is a key factor in bioprocess scale-up. In early stages of development, real-time process data are limited and, for shakers and adherent culture, little to no online monitoring tools exist. To close this gap, the Biolector®, an HTP µ-bioreactor system, was benchmarked as an alternative to shaker flasks, as it is capable of monitoring different process-relevant parameters online. As discussed transferability of results from shake flask experiments to bioreactors is limited the main focus of this study was to investigate if the µ-bioreactor system can serve as an alternative screening platform and to what extent generated results are transferable to benchtop bioreactors. Consequently, we did not use standard shake flask experiments as benchmark for the µ-bioreactor online sensor evaluation.

Evaluation of online µ-bioreactor monitoring capabilities. In order to fully benefit from the online monitoring capabilities of the µ-bioreactor system, the output of each individual sensor during insect cell cultivation needs to be evaluated. The optodes for pH and DO measurement provide meaningful real-time information on the process state that can be used directly to describe and compare individual cultivations and to identify problems, such as DO limitations or critical pH values.

Calibration of the light scatter signal. In general, the light scatter signal correlates with the cell concentration in the culture. However, calibration experiments are essential to identify this correlation for a respective cell system and cultivation regimen. To establish the calibration curve centrifuged cells were resuspended in media and diluted to respective concentrations. With the recommended shaking speed of 700 rpm for high insect cell concentrations[11], we observed a high tendency of cells to settle and build up a layer on the bottom of the well. This led to a saturation of the scattered light signal, even at low cell densities, and consequently false cell count estimates. A previous study demonstrated that the scattered light signal directly correlates with a cell density of up to 3×10^6 cells mL^{-1} using this shaking speed[15]. As the µ-bioreactor was established[16] as a screening tool for bacterial cultivation with cell densities up to 10 g L^{-1}, cell densities in standard BEVS cultivations should not lead to saturation of the light scattering signal. By increasing the shaking speed to 800 rpm, cell settling was eliminated and a direct correlation between the light scatter signals and cell concentrations up to 1.2×10^7 cells mL^{-1} was demonstrated. However, the blank signal was quite high which can cause inaccurate estimates for low cell densities as the limit of detection is at least in the range of 1.0×10^6 cells mL^{-1} (Fig. 1A). In Fig. 1B, the cell count calibration was tested on datasets from µ-bioreactor experiments. For both, infected and non-infected cells the calculated cell concentrations based on the calibration curve differed significantly from offline measured cell concentrations. The on-line values were lower in the early phase and higher in the later stage of the process. Several factors could contribute to the observed differences. The cells used for the calibration were concentrated via centrifugation and diluted to the corresponding concentrations with fresh media. In contrast to that treatment samples from cultivation experiments were directly measured in suspension. The supernatant changes continuously along the process due to cell lysis, vesicle formation, release of product and consumption of media compounds. Consequently, the background signal from samples can significantly differ from the calibration background signal and may lead to an overestimation of the cell concentration. Another source of variation is caused by changes in cell size during cultivation which can which can add up to more than 20% even in non-infected cultivations[17]. Finally, cell viability which is decreased to 57% for infected cultures and to 93% for non-infected cultures can also significantly influence the light scatter signal as dead cells show different light scattering properties.

Evaluation of fluorescence for process monitoring. To evaluate the potential of the fluorescence measurements as a process-monitoring tool, a set of cultivations with different MOIs (0.001, 0.01, 0.1, 1, 3, 5, 7, and 10) were performed in the µ-bioreactor (Fig. 2A,C). For clarity of presentation, online data are displayed in 5-h intervals, though the measurement frequency was 15 min. The target product, H1Gag VLPs, was expressed using the same polyhedrin promoter as for yellow fluorescent protein (YFP), which was used as a marker of infection

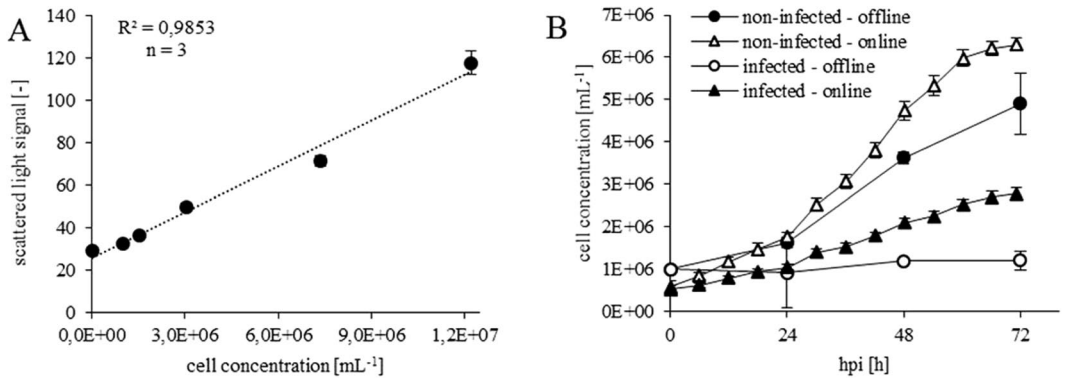

Figure 1. (**A**) Cell concentration calibration of the µ-bioreactor for Tnms42 cells. (**B**) Comparison of cell concentrations measured online and offline for non-infected and infected Tnms42 populations. The displayed mean values correspond to three different plate well titres (n = 3 and the error bars represent standard deviations). Online data recorded at a frequency of 15 minutes are displayed in 6 h interval to improve readability.

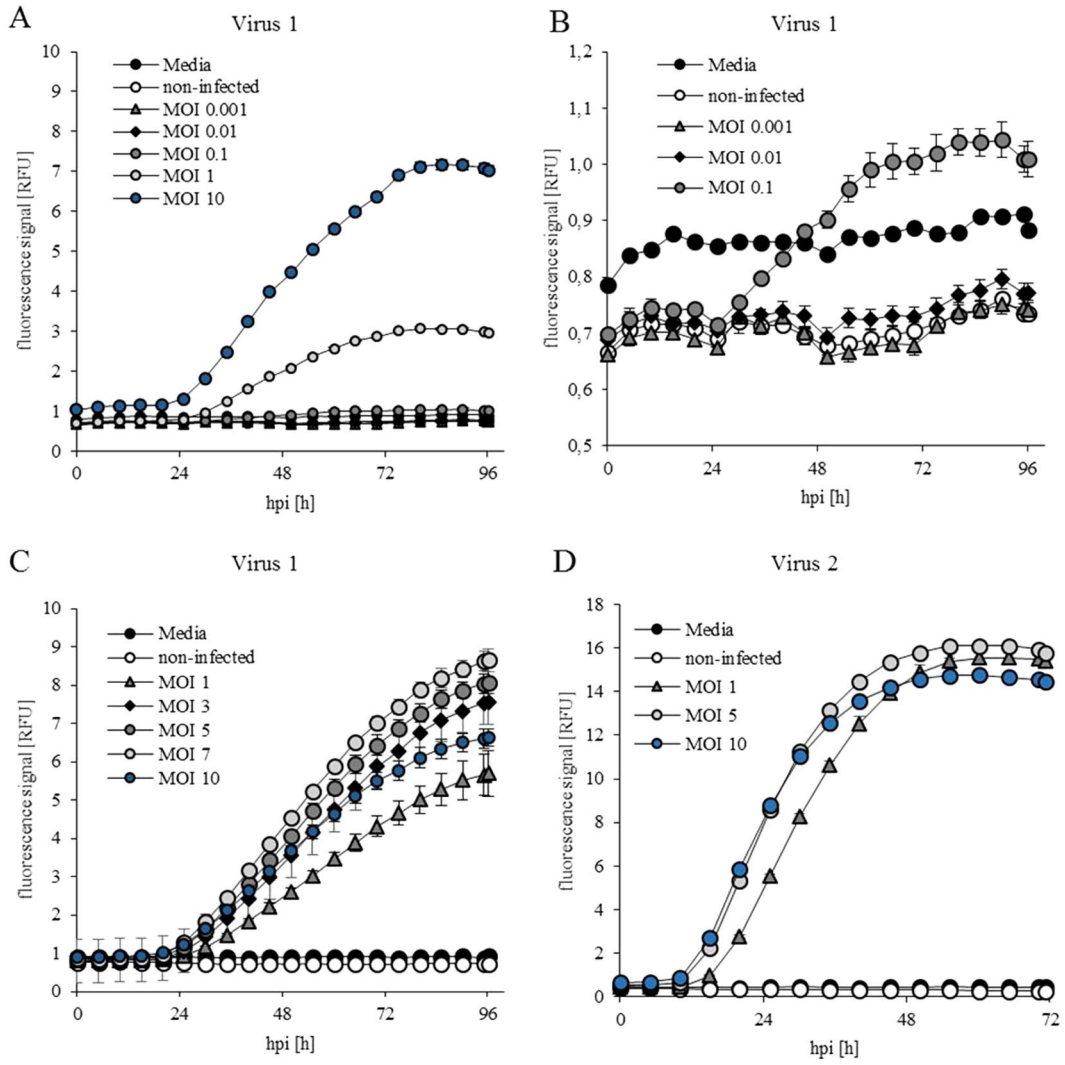

Figure 2. Fluorescence signals in non-infected and infected Tnms42 cultivations over time. (**A**) Experiment with Virus 1 with MOIs of 0.001 to 10 and (**B**) focused on MOIs ≤0.1 resulting in low fluorescence values. (**C**) Experiments with MOIs from 1 to 10. (**D**) Experiments with infection using Virus 2 using MOIs of 1 to 10. In each experiment, non-infected cells and media without cells were measured as references. All experiments were conducted in triplicate and the error bars represent standard deviations.

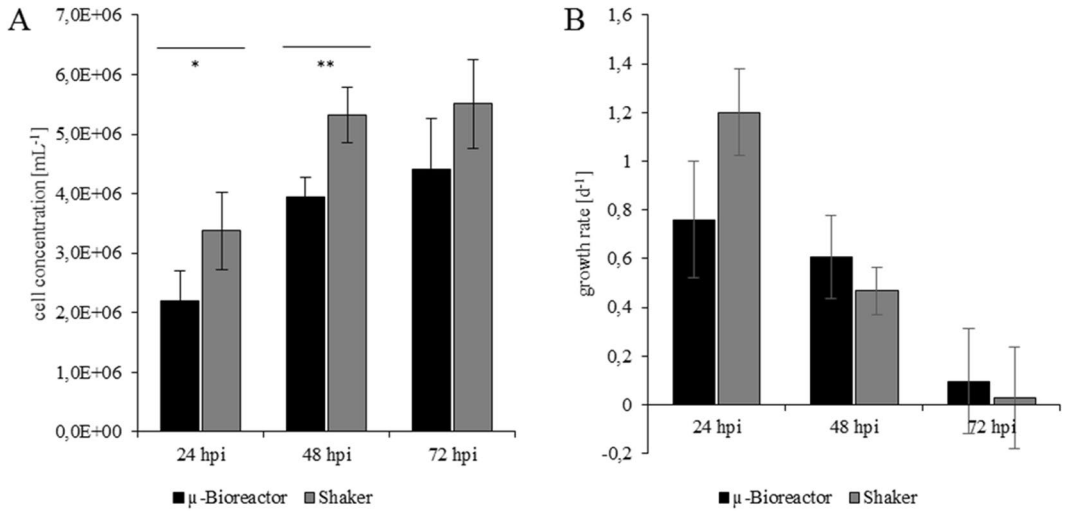

Figure 3. Comparison of Tnms42 cell cultivation in the µ-bioreactor (n = 5) and shake flasks (n = 4). (**A**) Cell densities and (**B**) growth rates per day displayed as mean with standard deviation. (**A**) Cell concentrations were analysed for normality by Shapiro-Wilk test and a t- test was performed, statistical significant differences are indicated (*P = 0.032, **P = 0.00258).

(Virus1). The process information delivered by the fluorescence signal measured online allowed for a first estimate of accurate MOI ranges and provided meaningful information on the starting point for protein production and infection efficiency. In experiments with MOIs <0.1, no YFP expression was observed (Fig. 2B) and an MOI of 0.1 resulted in an increase in the YFP signal after 24 hours. Within the MOI range of 0.1 to 7, the infection increase directly correlated with increased YFP signal and product formation. However, an MOI of 10 resulted in a reduced YFP signal (Fig. 2C).

The fluorescence curves provided additional information on infection and production kinetics. Production starts with a delay of approximately 18 hpi, independent of the applied MOI, and slopes are slightly steeper for higher MOIs. The information delivered by online fluorescence measurements represents a significant advantage of the µ-bioreactor over the shaker, with which fluorescence measurements are limited to offline samples.

Experiments with baculovirus in which YFP is under the control of the p6.9 promoter (Virus 2) showed that product formation had already started 11 hpi (Fig. 2D). This can be related to the p6.9 promoter, which starts production at an earlier stage than the polyhedron promoter and is described as a weaker promotor system[18].

Growth characteristics in the µ-bioreactor system and shake flask cultivation. To evaluate the growth behaviour of cells in the µ-bioreactor system, we performed comparative experiments in shaker flasks using different passages of *Tnms42* cells. Cells were seeded at a cell density of 1.0×10^6 cells mL^- and growth monitored via offline analysis (24 h sampling frequency) over 72 h without passaging or adding fresh media. The mean cell concentrations of four different shaker experiments and five different µ-bioreactor runs are given in Fig. 3A. The final *Tnms*42 cell concentrations in these experiments were comparable to literature values for *Tnms*42-related High Five cells grown under similar conditions[19,20]. The results in both cultivation regimens were comparable with regard to growth kinetics. However, cell growth in µ-bioreactor cultivations exhibited a delay that can be attributed to an initial phase of adaptation to µ-bioreactor conditions which was also seen when cells were transferred from shaker flasks into the benchtop bioreactor (see next section). There was a lower cell density and lower growth rate after 24 hours compared to shaker flask results (Fig. 3). At the end of cultivation, these significant differences were no longer present and similar growth kinetics observed with only 20% lower cell density in the µ-bioreactor system.

Transferability of screening results to production environment and benchtop bioreactor conditions. The key question in process development is the extent to which results generated in screening experiments can be transferred to larger scales and production conditions. Based on growth and infection screening experiments in shaker flasks and µ-bioreactor cultivations, three different MOIs (MOI of 1, 5, and 10) were selected for a direct and more detailed comparison of the µ-bioreactor, shake flask, and benchtop bioreactor cultivations. As bioreactor experiments in 1.5 L and 15 L scale showed comparable growth kinetics and product yields (data not shown) we concluded that the 1.5 L scale is suited to generate results transferable to pilot scale of 50–100 L. *Tnms*42 cells were infected with the baculovirus for VLP production expressing YFP under control of the p6.9 promoter. Cultures were inoculated at a cell density of 1×10^6 cells mL^{-1} with identical cell material from the same pre-culture. Shake flask and µ-bioreactor cultivations were infected at an MOI of 1, 5, and 10 using the same virus stock. The benchtop bioreactor cultivations were infected 24 hours after inoculation. In addition, non-infected control cultures were performed in each setting.

For non-infected cultures, the shaker and µ-bioreactor platforms achieved similar final cell concentrations of approximately 5×10^6 cells mL^{-1} the DO level for the non-infected cultures never dropped below 70% (supplemented data), which was significantly lower compared to the final cell concentration of 7.5×10^6 cells mL^{-1}

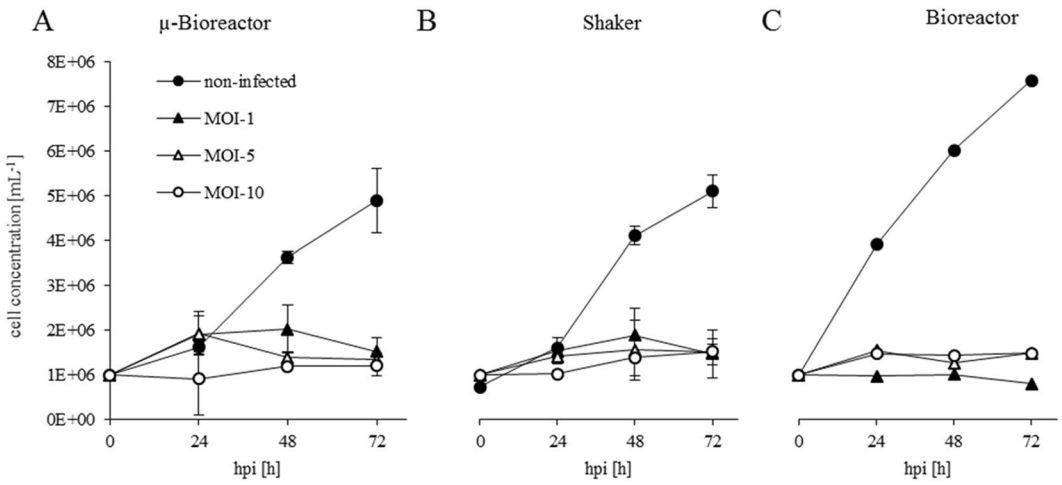

Figure 4. Course of the cell concentration of infected and non-infected Tnms42 cell cultures in (**A**) µ-bioreactor cultivation, (**B**) shake flask cultivation, and (**C**) benchtop bioreactor cultivation. All experiments in A and B were conducted in triplicate. Error bars indicate the standard deviation.

generated in the stirred bioreactor with controlled DO and pH (Fig. 4). The differences in the final cell density of non-infected *Tnms*42 cultivations can be attributed mainly to an unfavourable pH in the shaker and µ-bioreactor cultures as described in the literature[21,22]. In benchtop bioreactor experiments, the pH was maintained at 6.4 ± 0.05. In contrast, the online pH value in the µ-bioreactor system increased from 6.45 to 6.65 in the first 20 hours, and then decreased during cultivation to 5.9 for the non-infected cells. Offline measurement of the shakers showed an increase in pH. At the starting point, the media in all shakers had a pH of 6.4, increasing to 6.8 after 24 hours and finally 7.0 at the end of the cultivation. The observed pH conditions in the screening set-ups were most likely inappropriate for insect cell cultivation. The pH values in the µ-bioreactor system cannot be used in combination with YFP-expressing cells, as the fluorescence signal interferes with the pH and OD measurement. Moreover, to evaluate the impact of pH on the growth behaviour of the insect cells, a microfluidic µ-bioreactor offering pH control could be used[23].

For a more detailed characterisation of the infection status, offline samples were analysed using a flow cytometer, as each infected cell should produce YFP. The results clearly demonstrated that the infection efficiency was high in all settings with all MOIs (Fig. 5A–C). Independent from the MOI, all bioreactor and shaker cultivations were 100% infected after 24 hours. The µ-bioreactor performed similarly and reached the 100% infection level after 24 h in experiments with an MOI of 5 or 10. The major difference was observed for µ-bioreactor experiments with an MOI of 1, in which only 80% of the cells were infected after 24 hours. However, full infection was achieved after 48 hours in all cultivations with MOI = 1.

For identification of the optimal MOI and optimal length of production phase, HIV-p24-ELISA (Fig. 5D–F) and an influenza-HA-ELISA (Fig. 5G,H) were used to quantify VLP production over the course of the cultivations in the three platforms. Assuming a constant HIV-p24/HA ratio in produced VLPs, the two ELISAs resulted in identical rankings and characteristics with respect to product concentrations. This was the case for most of the samples except for the µ-bioreactor sample MOI 5/72 hpi and shaker flask sample MOI 5/24 hpi. As the variations in these samples cannot be attributed to analytical error, the two samples were not included in further interpretation of the results. With respect to the optimal length of the production phase, we observed increasing HIV-p24 and HA concentrations over time in all three platforms and throughout all infection levels (Fig. 5D–I). Consequently, 72 hpi has been shown to be the optimal production period for all cultivation setups under given infection and cultivation conditions. With respect to the MOI, the shake flask results yielded different rankings with an MOI of 1 as the preferred infection level.

Based on the assumption that a single VLP contains 5000 structural p24/GAG protein molecules[24,25], a maximum of 8.8×10^8 VLPs per 10^6 insect cells was produced in the bioreactor with an MOI of 10. Experiments in both screening platforms yielded significantly lower specific VLP concentrations, with 5.27×10^8 VLPs per 10^6 cells in the shaker and 2.97×10^8 VLPs per 10^6 cells in the µ-bioreactor. Again, variations in pH in screening cultivations could be an important source of variation in product formation.

Conclusion

In this work, the Biolector® µ-bioreactor system was evaluated as a platform for HTP insect cell culture cultivation and shown to be an attractive, cost-effective, and time-saving alternative to conventional shake flasks. With respect to provided online measurement capabilities the light scatter signal delivers information on cell growth but do not facilitate direct estimation of cell concentrations as there are inevitable error sources in real samples. The online fluorescence measurement delivers information on infection kinetics and efficiency if autofluorescent proteins like YFP are used as infection marker.The most important result was that the transferability of screening results from the µ-bioreactor to benchtop bioreactor, and that production conditions were acceptable with identical rankings and comparable to shaker flask cultivations. However, the use of both screening setups is limited regarding the estimation of final product titres because they are significantly lower than in benchtop bioreactor

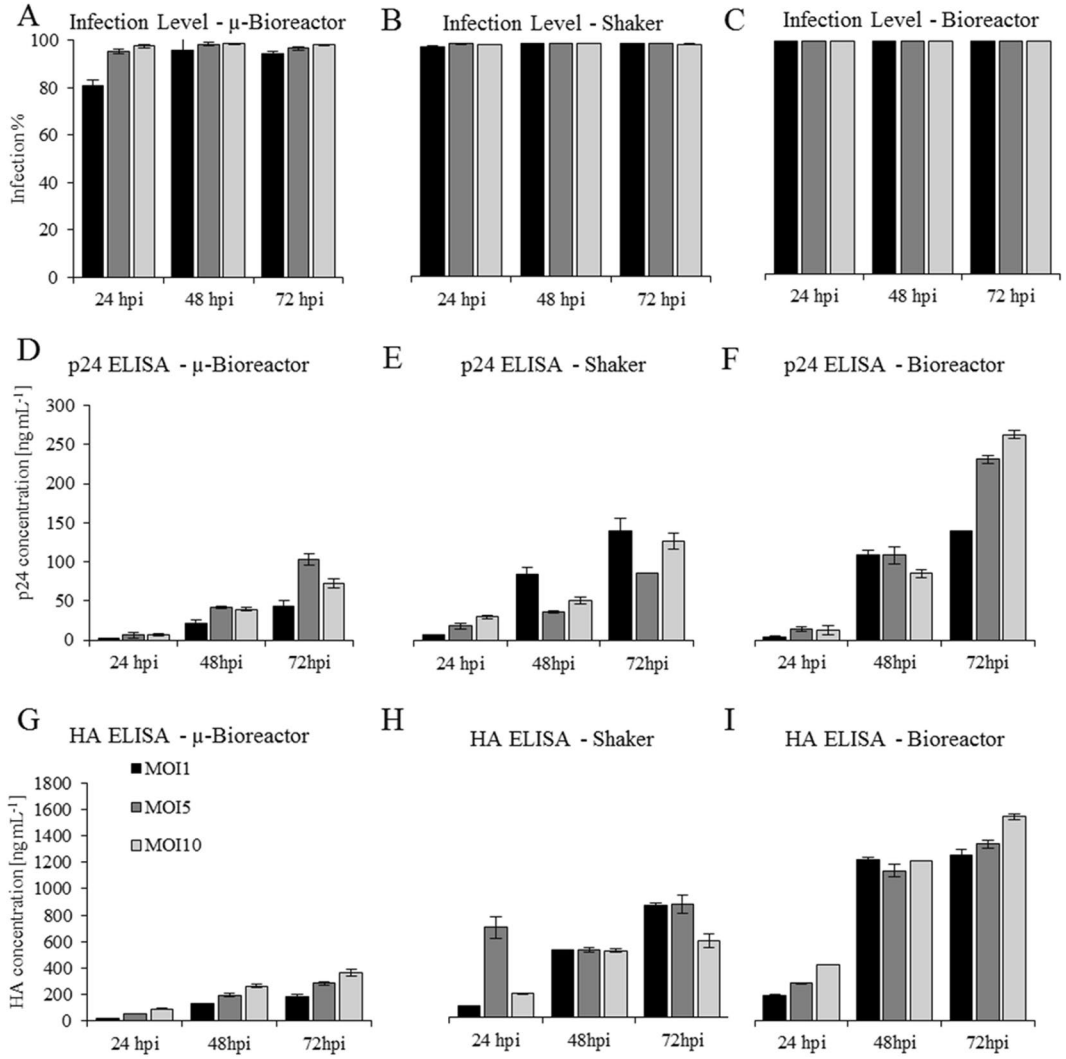

Figure 5. (**A**–**C**) The infection status of the three production systems over the course of the cultivations. (**D**–**F**) The hemagglutinin concentration. (**G**–**I**) The p24 concentrations measured with ELISA and standardised to 10^6 cells mL^{-1} for all three cultivation platforms. The error bars indicate the standard deviation (n = 3).

experiments. The experiments also revealed that *Trichoplusia ni* cell lines have a stronger influence on pH during cultivation than *Sf*9 cell lines, and that this variation may be a potential source of divergence in screening setups. In shake flasks, using medium with a stronger buffer system could be an option to improve the informative value of screening experiments, and the µ-bioreactor platform, a new system with microfluidics-based pH control, represents another possibility.

Methods

Insect cell lines. Spodoptera frugiperda 9 (*Sf*9) cells (ATCC CRL-1711) were used for the production of virus stock, and an alphanodavirus-free *Trichoplusia ni* - Tn5B1–4 (High Five) derivative, the *Tnms*42 cell line (BTI, Gary W. Blissard) for VLP production.

Cloning and generation of recombinant baculoviruses and virus stock generation. Two different baculovirus working stocks were generated for the experiments. Virus1 encoded the nucleic acid sequence for the hemagglutinin (HA) 1 protein of Influenza A/California/04/2009 (H1N1) (GenBank accession no. JF915184.1), whereas Virus2 encoded the HA protein of Influenza A/Puerto Rico/08/1934 (H1N1) (GenBank accession no. EF467821.1). Both viruses encoded the matrix protein Gag of the type 1 human immunodeficiency virus (GenBank accession no. K03455.1). All genes were codon-optimised for expression in *Trichoplusia ni* and chemically synthesised by IDT (Leuven, Belgium). After PCR amplification, the HA of A/California/04/2009 was inserted into the pACEBac-1 acceptor vector (EMBL, Grenoble), resulting in pACEBac-1-H1; the HA of A/Puerto Rico/08/1934 was cloned into the pACEBac-2 acceptor vector, resulting in pACEBac-2-HA; and the Gag fragment was cloned into the pIDC donor vector (EMBL, Grenoble), resulting in pIDC-Gag. Cre-LoxP recombination of the acceptor and donor vectors resulted in H1Gag acceptor-donor fusion plasmids. The H1-Gag fusion plasmids were transformed into either *E. coli* DH10EMBacY (EMBL, Grenoble) or DH10EMBacp6.9Y, which

	Virus1	Virus2
H1N1	polH	p10
Matrix Protein	polH	polH
Fluorescence Marker	polH	p6.9

Table 1. Promoters used for virus constructs.

harbour a YFP expression cassette under control of the polH or p6.9 promoter, respectively. Table 1 summarises the promoters used for gene expression in the two different viruses. The purified bacmid DNA was transfected into *Sf*9 cells using FuGene HD transfection reagent (Promega, Madison, Wisconsin, USA) according to the manufacturer's instructions. The titre of the amplified passage 3 stock was determined by 50% tissue culture infective dose ($TCID_{50}$).

Cultivation strategies. *Preculture.* For all experiments, the *Tnms*42 cells were kept in exponential growth phase at 27 °C in shaker flasks at 100 rpm. The cells were grown in serum-free medium (Hyclone SFM4Insect, GE Healthcare) supplemented with 0.1% Kolliphor P188 (Sigma-Aldrich). Viable cell counts were determined by trypan blue exclusion using an automated cell counter (TC20 Biorad). For each experiment, cells were taken from adherent culture, transferred to suspension with a starting cell density of 0.5×10^6 cells mL^{-1}, and grown to desired cell numbers. All pre-cultures with *Tnms*42 cells were supplemented with heparin (1:1000) to avoid cell clumping.

µ-Bioreactor cultivation. The m2p Labs Biolector® is a micro-cultivation system enabling continuous online monitoring of cell density, fluorescence, DO levels, and pH in a continuously shaken microtitre plate format. Up to 48 different cultures were performed in parallel in one experiment in deep well, round plates equipped with optodes for DO and pH measurement. The working volume was 1.7 mL, the shaking speed 800 rpm, the temperature 27 °C, and the humidity 85%. Plates were inoculated and infected simultaneously with an initial cell concentration of 1×10^6 cells mL^{-1} without any further passaging during the experiment. All experiments were performed in triplicate.

Shaker flask cultivation. Shaker flask cultivations were performed to generate an adequate reference data set following the conventional standard procedure. The cells were cultivated in triplicate in 200 mL shake flasks at a working volume of 20 mL. The cultures were inoculated with an initial cell density of 1×10^6 cells mL^{-1} and infection performed simultaneously with the inoculation. The temperature of the incubator was set at 27 °C and 100 rpm.

Benchtop bioreactor cultivations. Experiments were performed in a 1.5 L bioreactor (DASGIP SR1500 DLS, Eppendorf) equipped with three Rushton impellers. The temperature was set to 27 °C and the pH maintained at 6.4 ± 0.05 using 25% (v/v) phosphoric acid and 7.5% (w/v) sodium bicarbonate. The DO level was maintained at 30%. Cells were inoculated at a cell density of 1×10^6 cells mL^{-1} and cultivated in the bioreactor for 1 day prior to infection. Cell counts in the four bioreactors were determined, and each vessel was infected with the respective amount of virus and simultaneously diluted back to 1×10^6 cells mL^{-1}.

Infection strategy and sampling. Cells in all three cultivation platforms were infected at an MOI of 1, 5, and 10, and one culture of non-infected cells was grown in parallel. As the virus stock is stored at 4 °C and studies have shown that the titre decreases over time[8], a sample was analysed to determine the TCID50 of the virus stock. Sampling was performed over a period of 72 hours at 24-hour intervals.

Analytical methods. *Flow cytometry.* To evaluate the infection status on a single cell level, a CytoFlex flow cytometer (Beckman Coulter Life Sciences) was used to discriminate between infected and non-infected cells. A total of 1 mL of cell suspension was centrifuged for 5 minutes at 300 × g, the supernatant frozen at -20 °C for further testing, and the pellet washed once in 1x phosphate-buffered saline (PBS). They cytometer was equipped with a 488 nm laser, enabling excitation of YFP. We recorded 10000 events per sample and used Kaluza software (Beckman Coulter version 2.1) for the data analysis.

Tissue culture infectious dose 50 (TCID50) assay. The titre of virus stocks was determined using TCID50[26] based on the detection of YFP fluorescence. *Sf*9 cells were infected with serial dilutions of virus stock or supernatant samples of the different cultivations in a 96-well culture plate (Corning Incorporated, USA) and incubated at 27 °C without agitation. After 4 days, the wells were inspected for fluorescence using a fluorescence microscope (Leica DMIL-LED).

Enzyme-linked immunosorbent assay (ELISA). The HA content in the expression supernatant was determined using the Influenza A H1N1 (A/Puerto Rico/8/1934) Hemagglutinin/HA ELISA pair set (Sino Biological, Wayne, USA) according to the manufacturer's recommendations. For solubilisation of VLP-incorporated HA surface glycoproteins, samples were pre-treated with 1% zwitterionic detergent 1% (w/v) (Zwittergent 3–14, Calbiochem, San Diego, CA) for 30 minutes at room temperature[27]. A soluble trimeric insect cell expressing HA protein served as the calibration standard[28].

The HIV-Gag polyprotein was indirectly quantified by measuring the concentration of p24, the major viral core structural protein generated by viral protease cleavage of Gag. Free soluble HIV-1 p24 and total HIV-1 p24 concentration, including VLP-incorporated p24, in the expression supernatant were determined by the HIV-1 p24 capsid protein p24 ELISA Kit (Sino Biological, Wayne, USA). For measurement of the total p24 concentration, VLPs were disrupted by incubation with SNCR buffer for 10 min at 70 °C, followed by an incubation step in 0.5% (v/v) Triton X-100 for 10 min at 99 °C[29].

The influenza HA and HIV-1 p24 ELISAs were both developed with 100 µL of SIGMAFAST™ OPD substrate (Sigma Aldrich, St. Louis, MO, USA), and the reaction was stopped by the addition of 50 µL 3 N H2SO4 solution. The absorbance was measured at 492 nm and 620 nm (reference wavelength) using a Tecan Infinite 200 Pro (Tecan, Männedorf, CH) and data fitted to a 4th degree polynomial equation of a duplicate calibration curve.

Statistical analysis. SigmaPlot 13 software was used for statistical analysis. Shapiro-Wilk test was used for normality distribution and t-test was used for comparison of differences between groups. The calculated probability (p) values were two-tailed, differences were considered as statistically significant if the p-value was lower than 0.05.

Received: 5 September 2019; Accepted: 3 January 2020;
Published online: 23 January 2020

References

1. Aucoin, M. G., Mena, J. A. & Kamen, A. A. Bioprocessing of baculovirus vectors: A review. *Current Gene Therapy* **10**, 174–186 (2010).
2. Licari, P. & Bailey, J. E. Modeling the population dynamics of baculovirus-infected insect cells: Optimizing infection strategies for enhanced recombinant protein yields. *Biotechnology and Bioengineering* **39**, 432–441, https://doi.org/10.1002/bit.260390409 (1992).
3. Wong, K., Peter, C., Greenfield, P., Reid, S. & Nielsen, L. Low multiplicity infection of insect cells with a recombinant baculovirus: The cell yield concept. *Biotechnology and Bioengineering* **49**, 659–666, 10.1002/(sici)1097-0290(19960320)49:6<659::aid-bit7>3.0.co;2-n (2000).
4. Power, J. F., Reid, S., Radford, K. M., Greenfield, P. F. & Nielsen, L. K. Modeling and optimization of the baculovirus expression vector system in batch suspension culture. *Biotechnology and Bioengineering* **44**, 710–719, https://doi.org/10.1002/bit.260440607 (1994).
5. Lee, S. & Park, T. Two - phase cultivation of insect cells for production of recombinant protein. *Biotechnol Tech.* **9**, 719–724, https://doi.org/10.1007/bf00159236 (1995).
6. Bernal, V., Carinhas, N., Yokomizo, A. Y., Carrondo, M. J. T. & Alves, P. M. Cell density effect in the baculovirus-insect cells system: A quantitative analysis of energetic metabolism. *Biotechnology and Bioengineering* **104**, 162–180, https://doi.org/10.1002/bit.22364 (2009).
7. Sequeira, D. P. *et al*. Combining stable insect cell lines with baculovirus-mediated expression for multi-HA influenza VLP production. *Vaccine* **36**, 3112–3123, https://doi.org/10.1016/j.vaccine.2017.02.043 (2018).
8. Jorio, H., Tran, R. & Kamen, A. Stability of Serum-Free and Purified Baculovirus Stocks under Various Storage Conditions. *Biotechnology Progress* **22**, 319–325, https://doi.org/10.1021/bp050218v (2006).
9. Rossi, A. C. *et al*. Evaluation of ViroCyt® Virus Counter for Rapid Filovirus Quantitation. *Viruses* **7**, https://doi.org/10.3390/v7030857 (2015).
10. A. King, L. & Possee, R. *The Baculovirus Expression System*. (1992).
11. Bleckmann, M. *et al*. Identification of Essential Genetic Baculoviral Elements for Recombinant Protein Expression by Transactivation in Sf21 Insect Cells. *PLoS ONE* **11**, e0149424, https://doi.org/10.1371/journal.pone.0149424 (2016).
12. Imseng, N. *et al*. Single-use wave-mixed versus stirred bioreactors for insect-cell/BEVS-based protein expression at benchtop scale. *Engineering in Life Sciences* **14**, 264–271 (2014).
13. Bruder, S., Reifenrath, M., Thomik, T., Boles, E. & Herzog, K. Parallelised online biomass monitoring in shake flasks enables efficient strain and carbon source dependent growth characterisation of Saccharomyces cerevisiae. *Microb Cell Fact* **15**, 127–127, https://doi.org/10.1186/s12934-016-0526-3 (2016).
14. Tsai, W.-L., Autsen, J., Ma, J., Hudson, T. & Luo, J. Noninvasive Optical Sensor Technology in Shake Flasks. *BioProcess International* **10**, 50–56 (2012).
15. Bleckmann, M., Schmelz, S., Schinkowski, C., Scrima, A. & van den Heuvel, J. Fast plasmid based protein expression analysis in insect cells using an automated SplitGFP screen. *Biotechnology and Bioengineering* **113**, 1975–1983, https://doi.org/10.1002/bit.25956 (2016).
16. Toeroek, C., Cserjan-Puschmann, M., Bayer, K. & Striedner, G. Fed-batch like cultivation in a micro-bioreactor: screening conditions relevant for Escherichia coli based production processes. *SpringerPlus* **4**, 490, https://doi.org/10.1186/s40064-015-1313-z (2015).
17. Huynh, H. T., Tran, T. T. B., Chan, L. C. L., Nielsen, L. K. & Reid, S. Effect of the peak cell density of recombinant AcMNPV-infected Hi5 cells on baculovirus yields. *Applied Microbiology and Biotechnology* **99**, 1687–1700, https://doi.org/10.1007/s00253-014-6260-z (2015).
18. Yang, S. & Miller, L. K. Control of Baculovirus Polyhedrin Gene Expression by Very Late Factor 1. *Virology* **248**, 131–138, https://doi.org/10.1006/viro.1998.9272 (1998).
19. Sander, L. & Harrysson, A. Using cell size kinetics to determine optimal harvest time for Spodoptera frugiperda and Trichoplusia ni BTI-TN-5B1-4 cells infected with a baculovirus expression vector system expressing enhanced green fluorescent protein. *Cytotechnology* **54**, 35–48, https://doi.org/10.1007/s10616-007-9064-5 (2007).
20. Puente-Massaguer, E., Lecina, M. & Gòdia, F. Nanoscale characterization coupled to multi-parametric optimization of Hi5 cell transient gene expression. *Applied Microbiology and Biotechnology* **102**, 10495–10510, https://doi.org/10.1007/s00253-018-9423-5 (2018).
21. Yang, T. T., Cheng, L. & Kain, S. R. Optimized codon usage and chromophore mutations provide enhanced sensitivity with the green fluorescent protein. *Nucleic acids research* **24**, 4592–4593, https://doi.org/10.1093/nar/24.22.4592 (1996).
22. Rhiel, M., Mitchell-Logean, C. M. & Murhammer, D. W. Comparison of Trichoplusia ni BTI-Tn-5b1-4 (high five(TM) and Spodoptera frugiperda Sf-9 insect cell line metabolism in suspension cultures. *Biotechnology and Bioengineering* **55**, 909–920 (1997).
23. Blesken, C., Olfers, T., Grimm, A. & Frische, N. The microfluidic bioreactor for a new era of bioprocess development. *Engineering in Life Sciences* **16**, 190–193, https://doi.org/10.1002/elsc.201500026 (2016).
24. Briggs, J. A. G. *et al*. The stoichiometry of Gag protein in HIV-1. *Nature Structural & Molecular Biology* **11**, 672–675, https://doi.org/10.1038/nsmb785 (2004).
25. Chua, A. J. S. *et al*. A novel platform for virus-like particle-display of flaviviral envelope domain III: induction of Dengue and West Nile virus neutralizing antibodies. *Virol J* **10**, 129–129, https://doi.org/10.1186/1743-422x-10-129 (2013).

26. Smither, S. J. *et al.* Comparison of the plaque assay and 50% tissue culture infectious dose assay as methods for measuring filovirus infectivity. *Journal of Virological Methods* **193**, 565–571, https://doi.org/10.1016/j.jviromet.2013.05.015 (2013).
27. Rajendran, M. *et al.* An immuno-assay to quantify influenza virus hemagglutinin with correctly folded stalk domains in vaccine preparations. *PLoS ONE* **13**, e0194830, https://doi.org/10.1371/journal.pone.0194830 (2018).
28. Klausberger, M. *et al.* Globular Head-Displayed Conserved Influenza H1 Hemagglutinin Stalk Epitopes Confer Protection against Heterologous H1N1 Virus. *PLoS One* **11**, e0153579, https://doi.org/10.1371/journal.pone.0153579 (2016).
29. Schupbach, J. Ultrasensitive quantitative HIV-1 p24 antigen assay adapted to dried plasma spots to improve treatment monitoring in low-resource settings. (2006).

Acknowledgements

This work has been supported by the Federal Ministry for Digital and Economic Affairs (bmwd), the Federal Ministry for Transport, Innovation and Technology (bmvit), the Styrian Business Promotion Agency SFG, the Standortagentur Tirol, Government of Lower Austria and ZIT - Technology Agency of the City of Vienna through the COMET-Funding Program managed by the Austrian Research Promotion Agency FFG. The funding agencies had no influence on the conduct of this research.

Author contributions

F.S., D.P. and G.S. designed the research; F.S. and S.M.G. performed the experiments and did the data analysis and interpretation; F.S. and G.S. wrote the manuscript with the contribution of the other authors.

Competing interests

The authors declare no competing interests.

Additional information

Supplementary information is available for this paper at https://doi.org/10.1038/s41598-020-57761-w.

Correspondence and requests for materials should be addressed to G.S.

Reprints and permissions information is available at www.nature.com/reprints.

Publisher's note Springer Nature remains neutral with regard to jurisdictional claims in published maps and institutional affiliations.

Evaluation of screening platforms for virus-like particle production with the baculovirus expression vector system in insect cells

Florian Strobl [ab], *Sahar Masoumeh Ghorbanpour* [ab] *Dieter Palmberger* [ab] *and Gerald Striedner*[b*]

[a] *acib GmbH, Petersgasse 14, 8010 Graz*

[b] *Dep. of Biotechnology, University of Natural Resources and Life Sciences, Vienna, Austria*

* Correspondence to [gerald.striedner@boku.ac.at]

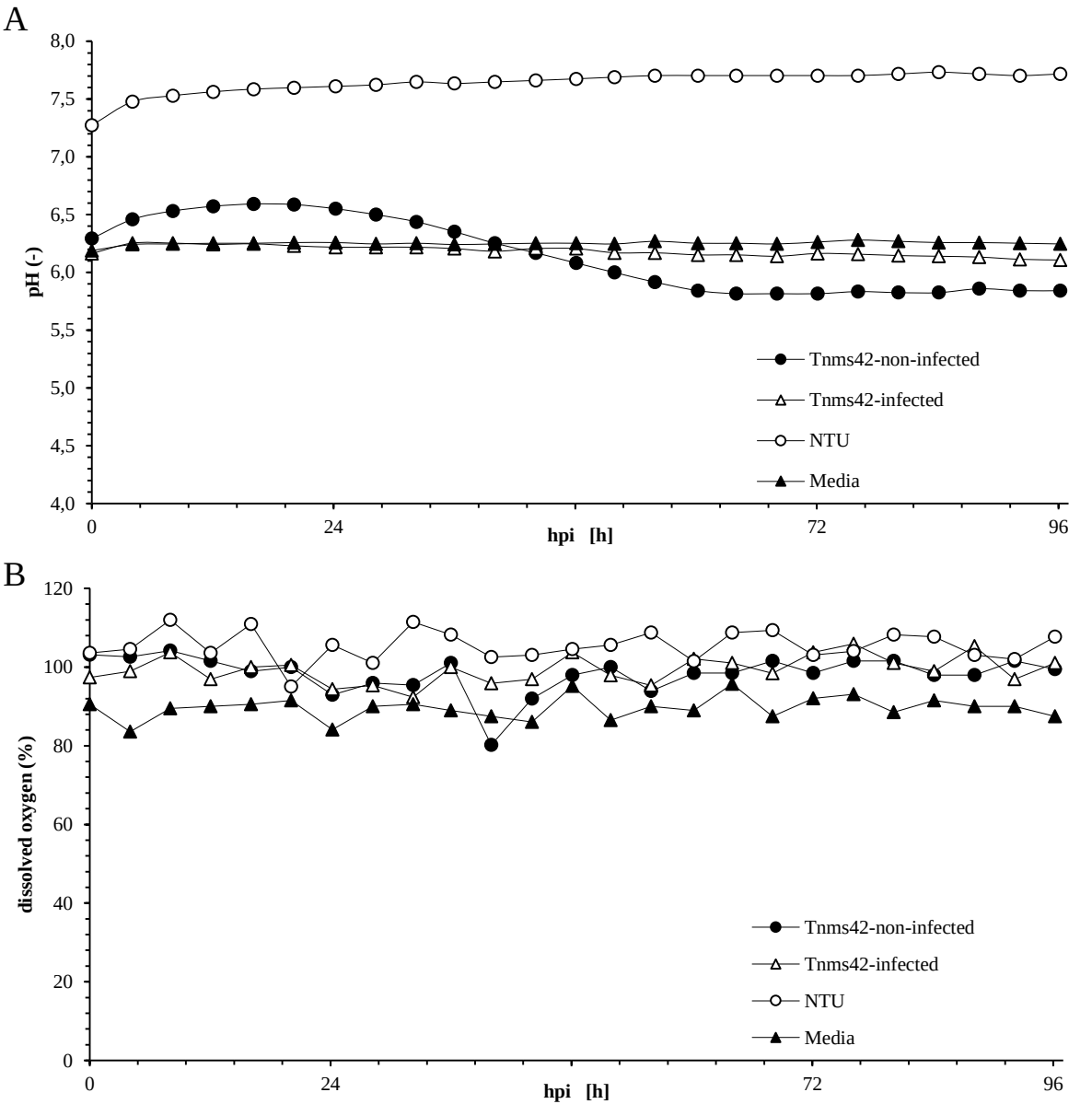
A
8,0
7,5
7,0
6,5
6,0
5,5
5,0
4,5
4,0
pH (-)
0
24
72
96
hpi [h]
Tnms42-non-infected
Tnms42-infected
NTU
Media
B
120
100
80
60
40
20
0
dissolved oxygen (%)
0
24
72
96
hpi [h]
Tnms42-non-infected
Tnms42-infected
NTU
Media

Figure 6: pH (**A**) and DO (**B**) time courses of infected non-infected Tnms42 cells, media and NTU200 standard are displayed. A virus without a fluorescence marker was used to demonstrate the pH and DO behavior over time.

Publication II

nanomaterials

MDPI

Article

PEI-Mediated Transient Transfection of High Five Cells at Bioreactor Scale for HIV-1 VLP Production

Eduard Puente-Massaguer [1,*], Florian Strobl [2,3], Reingard Grabherr [3], Gerald Striedner [3], Martí Lecina [4] and Francesc Gòdia [1]

1 Departament d'Enginyeria Química, Biològica i Ambiental, Universitat Autònoma de Barcelona, 08193 Barcelona, Spain; francesc.godia@uab.cat
2 Austrian Centre of Industrial Biotechnology (acib GmbH), 1010 Vienna, Austria; florian.strobl@boku.ac.at
3 Department of Biotechnology, University of Natural Resources and Life Sciences, 1190 Vienna, Austria; reingard.grabherr@boku.ac.at (R.G.); gerald.striedner@boku.ac.at (G.S.)
4 IQS School of Engineering, Universitat Ramón Llull, 08017 Barcelona, Spain; marti.lecina@iqs.url.edu
* Correspondence: eduard.puente@uab.cat

Received: 22 June 2020; Accepted: 7 August 2020; Published: 12 August 2020

Abstract: High Five cells are an excellent host for the production of virus-like particles (VLPs) with the baculovirus expression vector system (BEVS). However, the concurrent production of high titers of baculovirus hinder the purification of these nanoparticles due to similarities in their physicochemical properties. In this study, first a transient gene expression (TGE) method based on the transfection reagent polyethylenimine (PEI) is optimized for the production of HIV-1 VLPs at shake flask level. Furthermore, VLP production by TGE in High Five cells is successfully demonstrated at bioreactor scale, resulting in a higher maximum viable cell concentration (5.1×10^6 cell/mL), the same transfection efficiency and a 1.8-fold increase in Gag-eGFP VLP production compared to shake flasks. Metabolism analysis of High Five cells indicates a reduction in the consumption of the main metabolites with respect to non-transfected cell cultures, and an increase in the uptake rate of several amino acids when asparagine is depleted. Quality assessment by nanoparticle tracking analysis and flow virometry of the VLPs produced shows an average size of 100–200 nm, in agreement with immature HIV-1 viruses reported in the literature. Overall, this work demonstrates that the High Five/TGE system is a suitable approach for the production of VLP-based vaccine candidates and other recombinant proteins.

Keywords: High Five cells; transient gene expression; polyethylenimine; virus-like particle; bioreactor

1. Introduction

Insect cell lines are a well-established platform for the production of a wide variety of recombinant products, including antibodies [1], enzymes [2], hormones [3] and more complex biologicals such as different types of nanoparticles [4,5]. The production strategy typically consists of infecting insect cells with a modified baculovirus (BV) encoding for the gene of interest (GOI). The insect cell/baculovirus expression vector system (BEVS) has proven to be very useful for the production of virus-like particles (VLPs), generally achieving higher nanoparticle yields in comparison to mammalian cell lines [6]. VLPs mimic a virus structure but do not harbor genetic material of the wild-type virus, being exclusively formed by the structured and repetitive self-assembly of one or more virus-derived proteins [7]. Enveloped VLPs are a subclass of these nanoparticles that offer the possibility to display different types of epitopes in their lipid membrane, making them very attractive in cancer immunotherapy [8] and vaccine development [9]. Among them, Gag-based VLPs have received special attention since they can be produced at high levels with the insect cell/BEVS [10]. Nevertheless, several limitations are associated with this system and are principally related to the lytic nature of the

BV infection. Disadvantages comprise the early appearance of cell death and consequent release of host-derived proteases, and the need to amplify, maintain and titrate the BV working stock. As for Gag VLPs, the co-production of BV particles that share similar physicochemical properties with VLPs hinders the purification of these nanoparticles. Despite recent advancements have been made in this direction [11,12], difficulties are still encountered to achieve a complete separation between specimens.

Plasmid DNA-based transient gene expression (TGE) has become a powerful alternative to the BEVS given that moderate to high VLP titers can be obtained in a short time frame [13]. TGE consists of the introduction of foreign DNA encoding for a GOI into cells, which is usually achieved by means of positively charged transfection reagents. Once the DNA is introduced, it remains as an episomal element inside cells unless selection pressure, typically an antibiotic, is added to the culture [14]. Therefore, the expression of the GOI is lost over time after cell division. In recent years, several studies have shown that suspension-adapted High Five and Sf9 cells are ideal hosts for the production of reporter proteins [15–17], antibodies [18–20] and surface proteins [21] in this BV-free environment. Still, the assessment of the insect cell/TGE system to produce more complex products such as VLPs remains to be investigated.

Polyethylenimine (PEI) has gained progressive relevance as transfection carrier for insect cell/TGE approaches, since transfection efficiencies are high, it is cheaper than the majority of commercial reagents and the overall cost of the bioprocess is reduced [22]. This is of great importance for the production at larger scales in order to meet the increasing demand of therapeutic and diagnostic products. Despite the recent advancements reported for this system, most of the studies dealing with TGE scale-up have been conducted in mammalian cell lines, and there is little information about PEI-mediated insect cell/TGE at this level. Current knowledge about recombinant protein production in insect cells at bioreactor scale is related to the BEVS, with results reported in stirred tank [4,23,24] and wave bioreactors [25,26], and high-volume shake flasks [27]. Therefore, considering the advances reported for TGE in insect cells at small scale, there is a need to evaluate the feasibility of this system at bioreactor scale.

In this work, PEI-mediated TGE of High Five cells is evaluated as a strategy to produce several recombinant products with different complexities, including the intracellular enhanced green fluorescent protein (eGFP) [16], the human secreted alkaline phosphatase (hSEAP) and human immunodeficiency virus type 1 (HIV-1) Gag VLPs. Toward facilitating bioprocess characterization and discriminating VLPs from other nanoparticles, the Gag-eGFP fusion protein is used. VLP production is successfully achieved in a 0.5 L stirred-tank bioreactor, with a detailed study of the metabolism of transfected High Five cells. In an attempt to gain insight into the quantity and quality of the nanoparticles produced, flow virometry and nanoparticle tracking analysis are applied to monitor the High Five/TGE system.

2. Materials and Methods

2.1. Cell Culture Conditions

The suspension-adapted *Trichoplusia ni* BTI-TN-5B1-4 cell line (High Five, cat. num. B85502, Thermo Fisher Scientific, Grand Island, NY, USA) was grown in the low-hydrolysate animal origin-free Sf900III medium (Thermo Fisher Scientific). Cells were subcultured three times a week at a density of 2–4 $\times$ 10^5 cells/mL in 125 mL disposable polycarbonate Erlenmeyer flasks (Corning, Steuben, NY, USA), as previously described [16]. All cultures were grown in an orbital shaker at 130 rpm (Stuart, Stone, UK) and maintained at 27 °C. Cell count and viability were measured with the Nucleocounter NC-3000 (Chemometec, Allerød, Denmark) using acridine orange for cell detection and 4',6-diamidino-2-phenylindole (DAPI) (Chemometec) to quantify non-viable cells.

2.2. Construction of Plasmid DNA

The plasmid vector used in this work was pIZTV5 (cat. num. V801001, Thermo Fisher Scientific), which harbors the immediate–early *OP*IE2 promoter. The genes encoding for the

intracellular enhanced green fluorescent protein (eGFP), the truncated form of the human placental secreted alkaline phosphatase (hSEAP) and the HIV-1 Gag fused in frame to the eGFP were cloned into this vector using standard cloning procedures. Briefly, the hSEAP gene was amplified by PCR from the pUNO1-hSEAP plasmid (Invivogen, San Diego, CA, USA) with the following specific primers: fwd 5′-CGTAGGTACCTCATGATTCTGGGGCCCTGC-3′, rev 5′-CGTAGCGGCCGCGTCCAAACTCATCAATGTATC-3′. The amplified fragment was digested with *Kpn*I and *Not*I and ligated, resulting in the pIZTV5-hSEAP. The Gag-eGFP gene was obtained by digesting the pGag-eGFP plasmid (NIH AIDS Reagent Program, cat. num. 11468) [28] with *Kpn*I and *Not*I obtaining the pIZTV5-Gag-eGFP plasmid after ligation. The pIZTV5-eGFP plasmid was developed as previously described [16]. Plasmid DNA concentration was measured using a Nanodrop 1000 spectrophotometer (Thermo Fisher Scientific).

2.3. Transient Gene Expression in Erlenmeyer Flask

High Five cells were transiently transfected with different DNA plasmids using 25 kDa linear polyethylenimine (PEI, PolySciences, Warrington, PA, USA) according to an optimized protocol reported in a previous work [16]. Briefly, exponentially growing cells were centrifuged at 300× *g* for 5 min and resuspended to 1.5×10^6 cell/mL in 15 mL of pre-warmed Sf900III medium. DNA and PEI polyplex formation was performed in 150 mM NaCl at a final volume of 1 mL with DNA at 2.1 µg/mL added first and vortexed for 10 s. Afterwards, PEI at 9.3 µg/mL (DNA:PEI mass ratio of 1:4.4) was added to DNA, vortexed for 3 s three times and added to the cell culture.

2.4. Transient Gene Expression in Bioreactor

A 2 L DASGIP® Bioblock glass bioreactor (Eppendorf, Hamburg, Germany) equipped with three Rushton impellers was used for High Five cell cultivation in 0.5 L working volume. Aeration was performed through the sparger by air pulses to maintain the dissolved oxygen (DO) at 30% oxygen of air saturation. The air flow rate was set at 1 L/h and temperature at 27 °C. Initial agitation conditions were set at 150 rpm and were automatically adjusted by the DASware control software (Eppendorf) to maintain the DO setpoint at 30% oxygen of air saturation. The pH was fixed at 6.4 and controlled with 20% *w/w* H_3PO_4 and 7.5% *w/w* $NaHCO_3$. Antifoam C (Sigma Aldrich, Saint Louis, MO, USA) was added to the cell culture by pulses to prevent foam formation.

High Five cells were grown in the incubator to 1×10^6 cell/mL. Prior to inoculation, the medium was exchanged by centrifugation at 300× *g* for 5 min, cells were resuspended in 0.5 L of fresh Sf900III medium and transferred to the bioreactor. Cells were transfected when they reached 1.5×10^6 cell/mL using the standard procedure for DNA:PEI polyplex formation detailed in the previous section. pH control was started the day after transfection in order to avoid interferences with positively charged DNA:PEI polyplexes.

2.5. Flow Cytometry

The percentage of eGFP and Gag-eGFP-expressing cells was assessed using a BD FACS Canto II flow cytometer equipped with a 488 and 635 nm laser configuration (BD Biosciences, San Jose, CA, USA). The number of eGFP and Gag-eGFP positive cells was determined in the FITC-A PMT detector. Briefly, 2×10^4 cells were analyzed per sample at a flow rate of 60 µL/min. Single cells were gated according to side scatter (SSC-H) vs. forward scatter (FSC-A) dot plots and GFP positive cells in comparison to a non-transfected control depending on their mean FITC-A fluorescence intensity. Data acquisition and analysis was performed with the BD FACSDIVA software v.5.0 (BD Biosciences).

2.6. Fluorescence Confocal Microscopy

eGFP and Gag-eGFP transfected cells were visualized using a TCS SP5 confocal microscope (Leica, Wetzlar, Germany). To do this, cells were stained with 0.1% *v/v* of CellMask™ and 0.1% *v/v* of Hoechst (Thermo Fisher Scientific) to visualize the lipid membrane and cell nucleus, respectively.

A washing step was performed to remove excess dye by centrifugation at 300× *g* for 5 min, and the cells were resuspended in fresh Dulbecco's phosphate-buffered saline (DPBS, Thermo Fisher Scientific). Samples were placed in 35 mm glass-bottom Petri dishes with a 14 mm microwell (MatTek Corporation, Ashland, MA, USA) for visualization.

2.7. HPLC Analyses

Glucose, lactate and phosphate concentrations were measured with an ion-exclusion liquid chromatographic method using a sulfonated polystyrene divinyl benzene column (Aminex HPX-87H, Bio-Rad, Hercules, CA, USA) in an Agilent 1200 series HPLC system (Agilent, Santa Clara, CA, USA). A 0.01 N H_2SO_4 solution was used as the mobile phase with a flow rate of 0.45 mL/min [29]. All measurements were performed with an AZURA UV/VIS detector (Knauer, Berlin, Germany) with a refractive index detector temperature of 35 °C. The standard deviation of the technique was determined as 0.31% for glucose, 0.26% for lactate and 1.01% for phosphate measurement. Phosphate uptake rate was calculated taking into consideration the amount of phosphate present in the medium and also the volume of H_3PO_4 added for pH control.

Amino acid concentrations were determined by HPLC after derivatization in a reversed-phase Eclipse Plus C18 column (Agilent) at 40 °C according to manufacturer's instructions (Agilent). The flow rate was adjusted to 0.64 mL/min and two solvents (solution A and B) were used in the mobile phase. Solution A consisted of 10 mM K_2HPO_4 and 10 mM $K_2B_4O_7$ and solution B of a 45/45/10% *v*/*v*/*v* mix of acetonitrile, methanol and water, respectively [29]. Amino acids were detected at 266/305 nm for fluorenylmethoxycarbonyl derivates and at 450 nm for o-phthalaldehyde derivates. The final amino acid concentration was quantified using an internal standard calibration. The standard deviation associated with the measurement of amino acid concentration was 4 ± 1%.

2.8. Analysis of Nanoparticle Production

2.8.1. Nanoparticle Tracking Analysis

Gag-eGFP VLP and total nanoparticle concentration in crude supernatants was measured by nanoparticle tracking analysis (NTA) using a NanoSight NS300 (Malvern Panalytical, Malvern, UK) equipped with a 488 nm filter module for fluorescent nanoparticle detection. Samples from harvested supernatants at 3000× *g* for 5 min were diluted in 0.22 µm-filtered DPBS and continuously injected into the device chamber through a syringe pump at an average concentration of 10^8 particles/mL (20–60 particles/frame). Videos of 60 s from independent triplicate measurements were analyzed with the NanoSight NTA 3.2 software (Malvern Panalytical).

2.8.2. Flow Virometry

The Gag-eGFP VLP and total nanoparticle production process was followed by flow cytometry using a CytoFlex LX (Beckman Coulter, Brea, CA, USA) equipped with a 488 nm blue laser for fluorescent particle detection and a 405 nm laser/violet side scatter configuration to improve nanoparticle size resolution. Gating of the different populations was made according to SSC-A vs. FITC-A dot plots and using fresh DPBS and Sf900III medium samples as negative controls. Samples from supernatants harvested at 3000× *g* for 5 min were diluted in 0.22 µm-filtered DPBS and triplicate measurements from independent samples were analyzed with the CytExpert 2.3 software (Beckman Coulter).

2.9. eGFP/Gag-eGFP Measurement by Spectrofluorometry

The supernatants of eGFP and Gag-eGFP transfected cells were sampled once a day by centrifugation at 3000× *g* for 5 min. Pelleted cells were then subjected to three freeze-thaw cycles for intracellular eGFP and Gag-eGFP quantification. Briefly, cell pellets were maintained at −20 °C for 2.5 h, thawed at 37 °C during 0.5 h and vortexed for 5 s three times between cycles. Green fluorescence levels were measured in a Cary Eclipse fluorescence spectrophotometer (Agilent Technologies, Santa Clara,

CA, USA) at room temperature as follows: λ_{ex} = 488 nm (5 nm slit), λ_{em} = 500–530 nm (10 nm slit). Relative fluorescence units (R.F.U.) were calculated by subtracting fluorescence unit values of non-transfected cultures. eGFP concentrations were determined using a standard curve developed in a previous study [30]. The equation used to convert R.F.U. to eGFP concentration values is:

$$\text{eGFP (mg/L)} = (\text{R.F.U.} - 6.7221)/59.144 \quad (1)$$

where eGFP is the estimated concentration of eGFP protein and R.F.U. is the measured eGFP fluorescence intensity in the samples.

VLP quantification was also performed by an indirect quantification technique [31]:

$$\text{Gag-eGFP (ng/mL)} = (3.254 \times \text{R.F.U.} - 1.6833) \times 36 \quad (2)$$

where Gag-eGFP is the estimated concentration of Gag-eGFP polyprotein and R.F.U. is the measured Gag-eGFP fluorescence intensity in the samples. Conversion of the Gag-eGFP concentration to VLP was performed by assuming that one VLP contains 2500 Gag-eGFP monomers of 87.7 kDa per monomer.

The Sf900III medium and a 0.1 mg/mL quinine sulphate solution were used as control patterns to normalize R.F.U. values between experiments.

2.10. hSEAP Quantification

High Five cells transfected with the pIZTV5-hSEAP plasmid were harvested by centrifugation at 3000× *g* for 5 min and cell pellets were disrupted as reported in the previous section. The QUANTI-Blue system (Invivogen), which is based on a colorimetric enzyme reaction, was used to evaluate the alkaline phosphatase activity. To do this, 20 µL of sample were added to 200 µL of pre-warmed QUANTI-Blue solution and incubated at 37 °C for 1 h. The absorbance was measured in a Victor^3 spectrophotometer (PerkinElmer, Waltham, MA, USA) at a wavelength of 620 nm. Relative activity units (R.A.U.) were calculated by subtracting the absorbance of non-transfected cultures. hSEAP concentrations were determined using a calibration curve based on a linear correlation of known hSEAP (Invivogen) concentrations and the corresponding activity units in R.A.U.:

$$\text{hSEAP (mg/L)} = (\text{R.A.U.} + 0.0098)/0.2772 \quad (3)$$

where hSEAP is the estimated concentration of the hSEAP protein and R.A.U. is the measured hSEAP activity units in the samples (Figure S1).

2.11. Gag-eGFP Quantification using p24 Enzyme-Linked ImmunoSorbent Assay (ELISA)

The intracellular concentration of Gag-eGFP in transfected High Five cells and in culture supernatants was determined with an HIV-1 p24 ELISA Kit (Sino Biological, Wayne, NJ, USA). Supernatants were harvested by centrifugation at 3000× *g* for 5 min and cell pellets were disrupted as described in the previous section. Samples were incubated in SNCR buffer for 10 min at 70 °C and in 1.5% Triton X-100 for 10 min at 100 °C to disrupt nanoparticles. The substrate solution was prepared by dissolving a SIGMA*FAST* OPD substrate tablet and one urea hydrogen peroxide tablet (Sigma Aldrich) in deionized water at a final concentration of 0.4 mg/mL. An HIV-1 p24 standard of known concentration was also included for Gag-eGFP determination. The reaction was stopped by adding a 625 mM H_2SO_4 solution. The absorbance was measured at 492 nm with a reference wavelength at 630 nm in a Tecan Infinite 200 Pro reader (Tecan, Männedorf, Switzerland) [32]. p24 concentration values were corrected according to the Gag-eGFP molecular weight.

2.12. Analytical Ultracentrifugation

The supernatant of Gag-eGFP transfected High Five cells at 72 hpt was sublayered with 5 mL of 25% and 8 mL of 45% (*w*/*v*) sucrose (Sigma) solution prepared in DPBS or Dulbecco's modified eagle

medium (DMEM, Thermo Fisher Scientific), respectively. An amount of 10 mL of supernatant was loaded in ultracentrifuge tubes (Beckman Coulter), filled to the top with sterile DPBS, and centrifuged at 4 °C for 2.5 h in a Beckman Optima L100XP equipped with a SW-32Ti rotor set at 31,000 rpm. Samples were taken from each ultracentrifugation fraction and pellets were resuspended in 100 µL of sterile DPBS at 4 °C overnight. All samples were maintained at 4 °C until analysis.

2.13. Statistical Analyses

Multiple comparative analyses between different conditions and the control were conducted with the Dunnett's method. The unpaired Student's *t*-test was used to compare two separate independent samples. Nanoparticle quantification values from triplicate experiments represent the mean and standard deviations of the average of individual analyses. All statistical analyses were performed with SigmaPlot v.12.0 (Systat Software, San Jose, CA, USA).

3. Results and Discussion

3.1. Production of Different Recombinant Products

The use of High Five cells as a platform to produce simple intracellular recombinant proteins by polyethylenimine (PEI)-mediated transient gene expression (TGE) has been previously demonstrated [16]. The objective in this work is to widen the applicability of the High Five/TGE system for the production of more complex recombinant products, including secreted proteins and multimeric nanoparticles. For this purpose, human-secreted alkaline phosphatase (hSEAP) and HIV-1 Gag-eGFP virus-like particles (VLPs) were selected and compared to the production of intracellular enhanced green fluorescent protein (eGFP). Upon transfection, maximum viable cell concentration was reduced in all cases when compared to the non-transfected condition (Figure 1A), which is probably related to the overexpression of a heterologous product as previously reported for transfected Sf9 cells [30]. The complexity associated with the production of VLPs could be causing the pronounced deceleration of cell growth observed in that case, with cells peaking at 72 hpt instead of the 48 hpt, as observed for the rest of products. In these conditions, a maximum transfection yield of 50–60% was measured for pIZTV5-Gag-eGFP and pIZTV5-eGFP transfected cells at 48 hpt (Figure 1B). Confocal microscopy analysis of pIZTV5-eGFP transfected cells showed that eGFP was intracellularly retained (Figure 1C), while fluorescent nanoparticles (VLPs) could be visualized as green dots (white arrows) in the membrane of pIZTV5-Gag-eGFP transfected cells (Figure 1D, upper right). The latter indicated that transfected High Five cells are capable of correctly processing Gag-eGFP in the form of VLPs, as observed in baculovirus infected insect cells [33,34] and mammalian cell lines [35,36].

Maximum eGFP and hSEAP production was achieved at 72 hpt, with the majority of the eGFP produced intracellularly (5.0 ± 0.4 mg/L) and hSEAP secreted to the supernatant (4.2 ± 0.3 mg/L), as expected (Figure 2A). In the same line, the production of Gag-eGFP continuously increased, attaining its maximum concentration at 72 hpt. Notably, analysis of intracellular Gag-eGFP content by spectrofluorometry revealed that a significant amount of the Gag-eGFP produced remained inside the cells and was not being released to the supernatant, thus highlighting the inherent complexity in processing these nanoparticles. Similar results have been recently reported in Sf9 [30] and HEK 293 cells [37], showing a potential bottleneck in processing all the Gag polyprotein produced into VLPs. This evidence possibly indicates that the limiting step in producing these nanoparticles is not cell line but rather product-dependent. Despite Gag-eGFP concentration achieved a plateau at 72 hpt, a 4-fold increase in Gag-eGFP production was measured in the supernatant at 96 over 72 hpt. A significant drop in cell viability was measured in this period, which could explain the increase in Gag-eGFP fluorescence in the supernatant due to leakage from dead cells (Figure 1A). Therefore, the time of harvest was defined as 72 hpt in order to maintain a cell viability at harvest >80% and minimize the amount of non-assembled Gag-eGFP monomer released to the supernatant. In these conditions, the quantity of Gag-eGFP secreted to the supernatant assembled as VLPs accounted for the

60% (Figure 2B). The Gag-eGFP VLP assembly was in the range of that reported for HEK 293 cells by TGE [31] and 4.5-fold higher in comparison to Gag-eGFP VLP production by baculovirus infection in High Five cells [34].

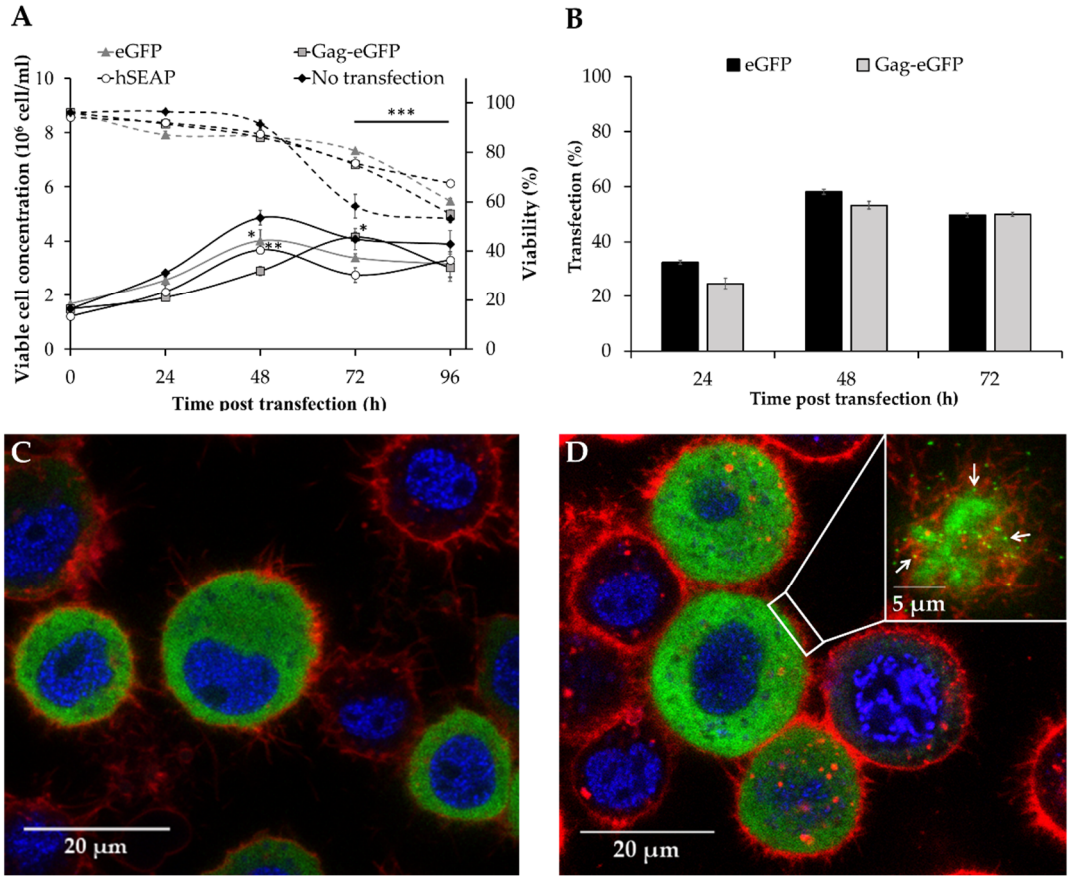

Figure 1. Transient gene expression of eGFP, hSEAP and HIV-1 Gag-eGFP VLPs in High Five cells cultured in shake flasks. (**A**) Cell growth (solid lines) and viability (dashed lines) profiles. (**B**) Transfection efficiencies measured by flow cytometry. (**C**–**D**) Fluorescence microscopy images of transfected High Five cells producing eGFP (**C**) and Gag-eGFP VLPs (**D**). Cell membranes were stained in red with CellMask^{TM} and cell nucleus in blue with Hoechst 33342. VLPs can be observed as green dots (white arrows) budding from cells. Cell nucleus was stained with Hoechst 33342 (blue) and membrane was stained with CellMask^{TM} (red). Mean values ± standard deviation of triplicate experiments are represented. A Dunnett's test analysis was used to compare the peak of viable cell concentration of the different conditions with the control (no transfection), while a Student *t*-test was performed to evaluate the drop in cell viability between 72 and 96 hpt. * *p*-value < 0.05, ** *p*-value < 0.01, *** *p*-value < 0.001.

Assessment of the VLP production process by flow virometry was in agreement with spectrofluorometry results during the 0–72 hpt period (Figure 2C). VLP production increased up to 72 hpt, attaining a maximum concentration of 2.9 ± 0.7 × 10^6 VLP/mL (Table 1). Interestingly, a higher VLP yield of 3.6 ± 1.0 × 10^8 VLP/mL was quantified by nanoparticle tracking analysis (NTA) at the same time, a 2-fold increase in VLP production in comparison to stable Gag VLP producing High Five cell lines [38]. Despite that higher VLP titers were achieved with the baculovirus expression vector system (BEVS) [34], the possibility of producing these nanoparticles in a BV-free environment significantly simplifies the downstream processing, which represents an interesting asset for VLP production.

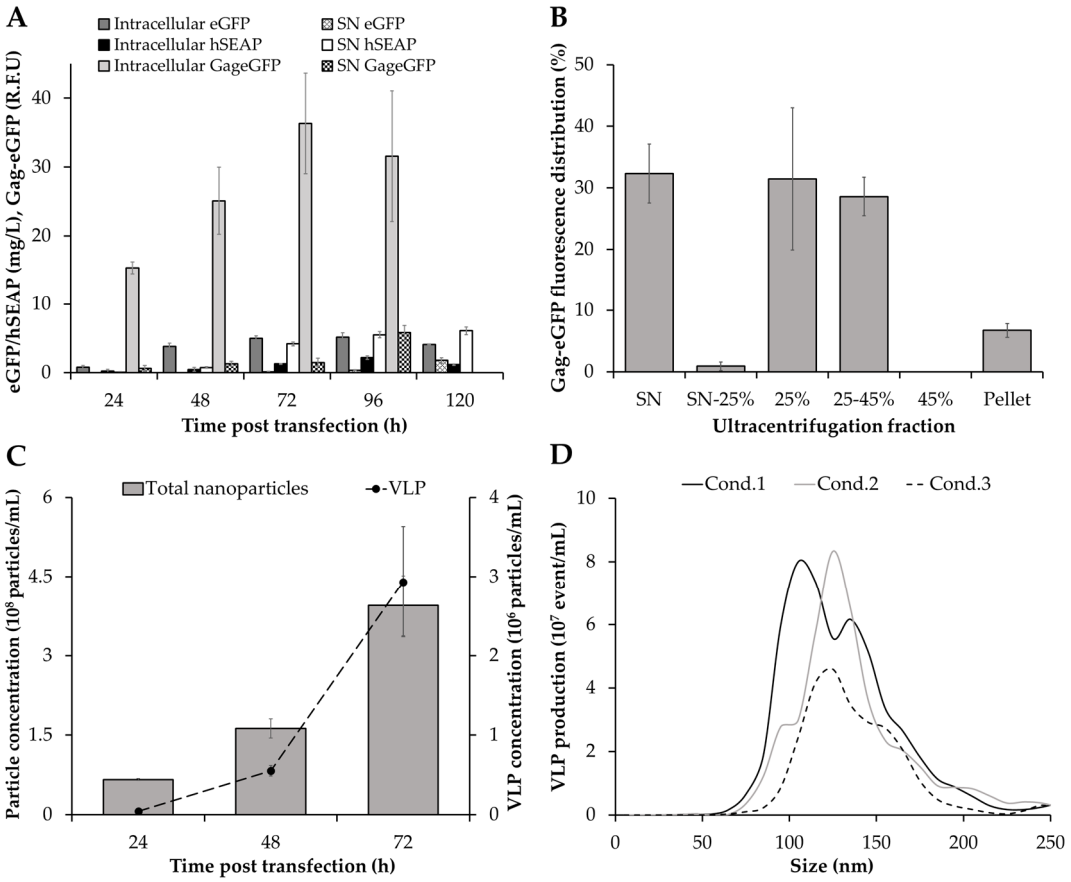

Figure 2. Recombinant protein production in transfected High Five cells cultured in shake flasks. (**A**) Intra- and extracellular production of eGFP, hSEAP and Gag-eGFP. (**B**) Fluorescence distribution of Gag-eGFP by spectrofluorometry in supernatants harvested at 72 hpt after double sucrose cushion ultracentrifugation. (**C**) Analysis of the nanoparticle production process by flow virometry. (**D**) Assessment of VLP size distribution by nanoparticle tracking analysis at 72 hpt. The average values of triplicate experiments are represented.

Table 1. Gag-eGFP production in shake flasks at 72 hpt using different quantification methodologies.

Quantification Method	Fluorescent Particles/mL	Total Particles/mL	Supernatant	Intracellular
NTA (particles/mL)	$3.6 \pm 1.0 \cdot 10^{8}$	$2.4 \pm 0.3 \cdot 10^{11}$	-	-
Flow virometry (particles/mL)	$2.9 \pm 0.7 \cdot 10^{6}$	$4.0 \pm 0.6 \cdot 10^{8}$	-	-
ELISA (ng/mL)	-	-	17.1	238.4
Fluorometry (R.F.U.)	$1.4 \pm 0.6 \cdot 10^{8}$[a]	-	1.5 ± 0.6	36.3 ± 7.3

[a] This is the resulting value of correlating R.F.U. to VLP concentration with Equation (2).

The difference in terms of VLP quantification between NTA and flow virometry has also been reported previously [33]. Several studies indicate that the lower nanoparticle levels measured by flow virometry could be the consequence of detecting several nanoparticles as a single larger particle, a phenomenon known as swarm effect [39]. However, it is not clear whether these differences can be fully attributed to this event or to the non-detection of nanoparticles that are below the flow cytometer detection threshold [40].

The presence of extracellular vesicles (EVs) was also observed in supernatants (Figure 2C), confirming that these nanoparticles are concurrently produced with VLPs in High Five cells by TGE.

EVs were recently observed in VLP production studies with the BEVS in insect cells [33,34], showing that they are not an exclusive matter of mammalian cell lines [41,42]. Analysis of the average VLP size by NTA resulted in 157.2 ± 8.5 nm (Figure 2D), in agreement with Gag-eGFP VLPs produced in insect cells with the BEVS [43]. EVs displayed a similar mean size of 152.4 ± 15.9 nm than VLPs (p-value > 0.05), which raises the need to develop methodologies enabling their separation. Despite recent advancements have been reported by means of chromatographic methods [32,44], difficulties are still encountered in achieving a complete separation between both nanoparticle populations. Furthermore, additional research is required to understand their role and impact in insect cell-based bioprocesses.

3.2. Transferability of VLP Production to Bioreactor

A relevant issue in a new bioprocess is the capacity to translate the results to a bigger scale. In this sense, it is essential to prove that the optimal conditions achieved in Erlenmeyer flasks are reproduced at larger scale in a bioreactor. This is highly important for meeting the demands of large amounts of recombinant product for structural or functional studies and pre-clinical testing [45]. High Five cells were inoculated at 1×10^6 cell/mL after medium replacement and transfected with the Gag-eGFP encoding DNA plasmid for VLP production when the viable cell concentration reached 1.5×10^6 cell/mL [16]. In parallel, the same pre-culture was also used in shake flasks as a positive control. No differences were observed in High Five cell growth between bioreactor and shake flask conditions until 48 hpt (Figure 3A). From this point until the end of transfection, cells cultured in the bioreactor attained 5.1×10^6 cell/mL while the shake flask condition achieved a maximum viable cell concentration of 3.9×10^6 cell/mL. These differences in final viable cell concentration could be due to the uncontrolled pH and aeration conditions in shake flasks, resulting in a more unfavorable environment for cell growth [46]. A slight drop in cell viability was measured in the bioreactor at 24 hpt, possibly suggesting that the toxic effect of PEI increased in these conditions. Indeed, shear stress at bioreactor scale can induce a certain degree of cell membrane damage [47], and this could make cultured cells in the bioreactor more susceptible to the toxic effect of PEI. However, cell viability was maintained at >80% in all cases, indicating that High Five cells successfully adapted to the additional stress caused by stirring. Moreover, no deleterious effect on cell viability was observed due to the increasing stirring speeds to maintain the DO level at 30% oxygen of air saturation, highlighting the robustness of this cell line for recombinant protein production in stirred-tank bioreactors.

High Five cell culture in suspension conditions often requires the addition of anti-clumping agents to decrease the formation of cell aggregates that could impact recombinant product expression [48]. In this study, cell culture in Sf900III medium without the addition of anti-clumping agents resulted in a low level of aggregation, which became more evident in shake flasks at the end of the production phase. As for the bioreactor, no cell clumping was observed, but antifoam addition by pulses was periodically required to prevent foam formation and oxygen limitation (Figure 3B, black arrow).

Analysis of transfected cells by flow cytometry was conducted every 24 h and resulted in similar transfection efficiencies between both cultivation strategies (Figure 3C). In terms of production, higher concentrations of Gag-eGFP VLPs were quantified by flow virometry in the bioreactor (4.8×10^6 VLP/mL) in comparison to the shake flask condition ($2.6 \pm 0.6 \times 10^6$ VLP/mL) at harvest (Figure 3D). Calculation of the specific productivity in each system yielded a 1.5-fold improvement in VLP (6×10^6 VLP/10^6 transfected cell·day) but also in intracellular Gag-eGFP production in the bioreactor. This indicates that the larger amount of VLPs achieved in the bioreactor is not only a consequence of a higher viable cell concentration, but the culture conditions are better suited to produce these nanoparticles. These results are in agreement with the VLP productivity increase observed in HEK 293 cells when cultured in bioreactor [49]. An increase of 1.7-fold in VLP production by baculovirus infection of *Tnms*42 insect cells in bioreactor culture conditions has also been reported [50].

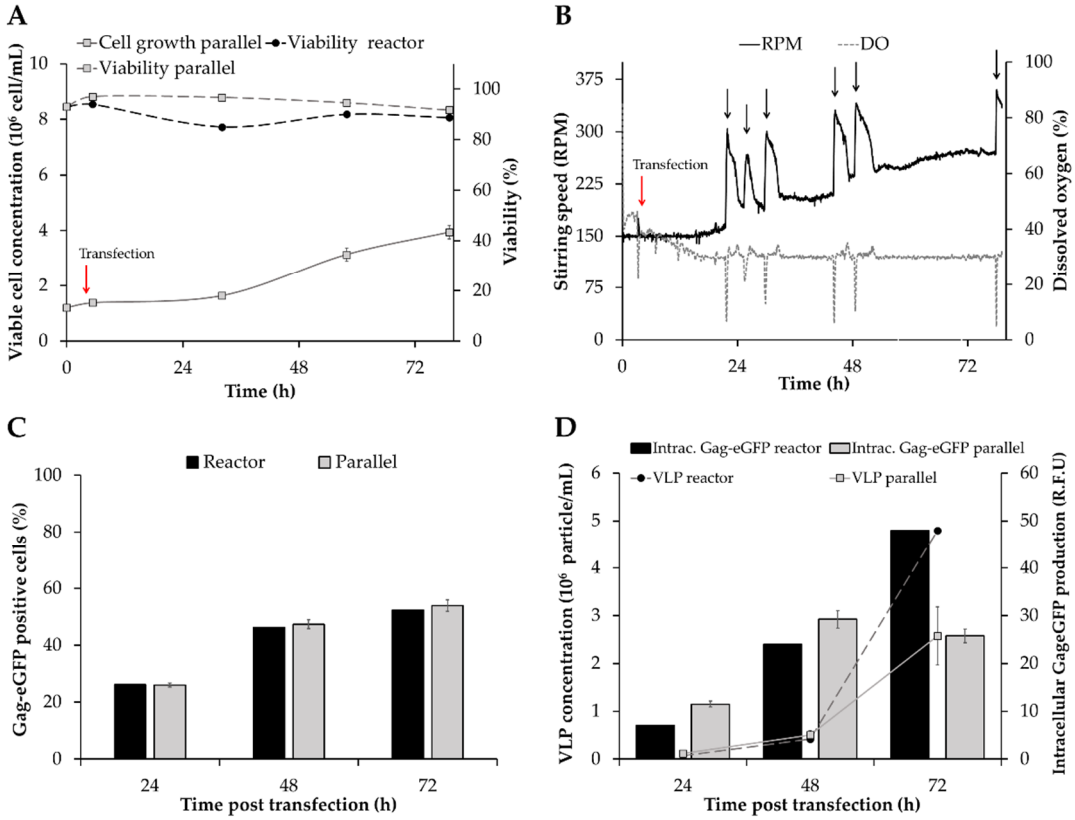

Figure 3. Comparison of Gag-eGFP VLP production in a 2 L DASGIP® Bioblock glass bioreactor and 125 mL Erlenmeyer flasks (parallel). (**A**) Cell growth and viability profile of transfected cultures. The red arrow indicates the time of transfection. (**B**) Evolution of dissolved oxygen and stirring speed requirements of transfected High Five cells. Black arrows show the addition of Antifoam C. (**C**) Percentage of Gag-eGFP positive cells at different time points. (**D**) Analysis of VLP production and intracellular Gag-eGFP content by flow virometry and spectrofluorometry, respectively. Mean values ± standard deviation of triplicate experiments are represented.

Eventually, the quality of VLPs produced in the bioreactor was evaluated by NTA at 72 hpt. In this context, an average VLP size of 163.1 ± 12.7 nm was measured, which is in the range of that observed for shake flask-produced VLPs (p-value > 0.05). Likewise, the concomitant production of EVs with a mean size of 160.7 ± 5.8 nm was also detected.

3.3. Analysis of Metabolites

The metabolic profile of High Five cells was analyzed in order to determine the effect of TGE on these cells during VLP production at bioreactor scale and to compare it to parental cells under the same culture conditions. Glucose and glutamine were consumed at high rates (Figure 4), with glucose being preferred over glutamine by 2- to 3-fold in the TGE condition (Table 2), and by 3- to 5-fold in the non-transfected culture (Table S1). None of them was completely exhausted during the bioreactor culture, but the specific glucose consumption rate decreased by 16 and 53% at the end of TGE and in the non-transfected cell culture, respectively, while a similar glutamine consumption level was maintained throughout the experiment. Both metabolites are important energy sources for animal cells via their incorporation into the Krebs cycle through glucose-derived acetyl-coA and glutamine-derived 2-oxoglutarate. Glucose and glutamine consumption rates are lower than those observed in non-transfected cells (Table S1), as well as compared to data reported for baculovirus infected cells [51] and stable insect cell lines [38] in similar culture conditions. The presence of glucose-containing disaccharides, maltose and sucrose, was also detected in the Sf900III medium, but they were consumed at significantly lower rates compared

to glucose (data not shown). The consumption of significant amounts of phosphate was also measured during transfection and could be a consequence of the need for lipid biosynthesis for cell growth and VLP production [52].

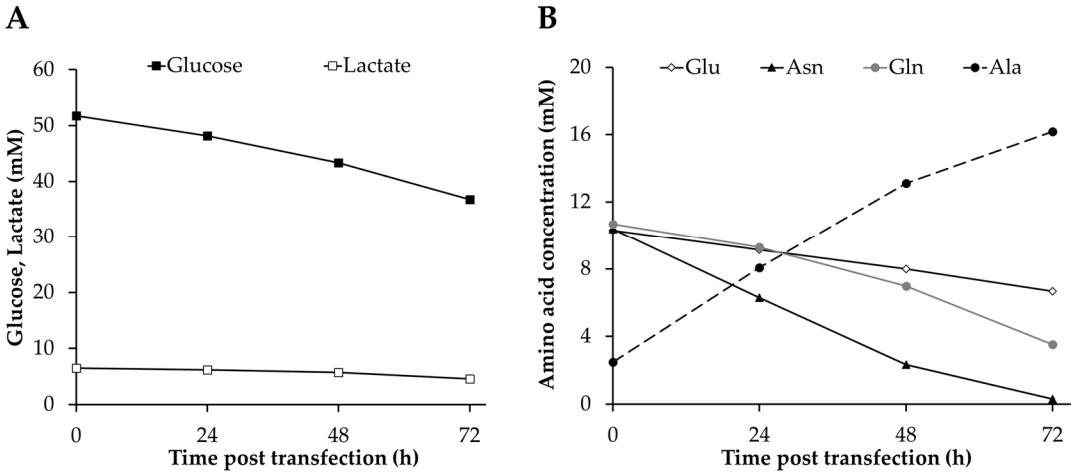

Figure 4. Consumption and production of different metabolites in transfected High Five cells at bioreactor scale. (**A**,**B**) Profiles of glucose and lactate (**A**) and main amino acids produced/consumed (**B**). Glu: glutamic acid; Asn: asparagine; Gln: glutamine; Ala: alanine.

Table 2. Uptake and production rates of the main metabolites in High Five cells transfected at bioreactor scale for Gag-eGFP VLP production. Rates are expressed in nmol/(10^6 cell·h) and negative values indicate consumption.

Metabolite	Time Post Transfection (h)		
	0–24	**24–48**	**48–72**
Glucose	−90.3	−83.0	−75.6
Lactate	−8.4	−7.8	−13.1
Phosphate	−48.5	−53.2	−17.6
Aspartic acid	25.8	7.1	−5.3
Glutamic acid	−29.0	−19.9	−15.0
Asparagine	−103.8	−68.0	−23.4
Serine	30.0	−0.3	1.8
Glutamine	−35.4	−39.8	−39.8
Histidine	−1.1	−2.2	−2.0
Glycine	−6.2	−7.8	−2.8
Threonine	1.5	−0.8	−2.0
Arginine	−0.7	−5.1	−1.7
Alanine	140.7	86.9	35.3
Tyrosine	0.3	−1.7	−3.0
Valine	0.2	−4.5	−5.7
Methionine	−5.6	−6.2	−5.2
Tryptophan	−0.1	−1.4	−0.9
Phenylalanine	−2.0	−3.7	−3.6
Isoleucine	−1.2	−4.8	−4.4
Leucine	−0.9	−6.1	−5.9
Lysine	−8.0	−17.9	−5.9
Proline	−2.6	−5.1	−4.6

Asparagine was the amino acid consumed at the highest rate (Table 2) and was completely exhausted by the end of the experiment (Figure 4B). Asparagine was consumed more rapidly in the non-transfected cell culture, probably due to the faster cell growth kinetics of parental High Five cells (Figure 1A). The high level consumption of this amino acid in High Five cells for energy generation

via oxaloacetate incorporation into the Krebs cycle is well-known and explains the lower glutamine consumption, but the dependence on this amino acid seems to be more pronounced in transfected High Five cells in comparison to baculovirus-infected cells, which tend to consume higher amounts of glucose [46]. Serine biosynthesis was detected at the beginning of transfection when the main carbon and nitrogen sources were not limiting. Likewise, aspartate was initially synthesized by High Five cells, but started to be metabolized at a late stage of transfection, when asparagine became limiting. Interestingly, this behavior of initial biosynthesis of both amino acids was not observed in baculovirus-infected High Five cells [53]. On the other hand, glutamic acid consumption decreased over time, which could be associated with the reduction in asparagine uptake rate as previously reported [54]. The rest of amino acids were consumed to a lesser extent and in the case of tyrosine, proline and the essential amino acids threonine, valine, isoleucine, leucine and phenylalanine the consumption rate increased at the end of transfection. Despite the lower consumption rates, these amino acids have proven to be fundamental for High Five cell maintenance and growth [52]. Alanine was the main by-product generated during cell culture, since this metabolite acts as a nitrogen acceptor under glucose excess conditions [55]. Interestingly, its production rate decreased in parallel to the reduction of asparagine consumption (Table 2 and Table S1) and the concentrations achieved were higher than those observed for baculovirus-infected High Five cells [53], which could be the consequence of a higher asparagine uptake rate. However, no lactate production was detected which differs from previous studies conducted in High Five cells that report substantial accumulation of this by-product [56]. In fact, lactate consumption was measured albeit maintained at low level until the end of the experiment. Similar results were reported in the bioreactor cultivation of Sf9 cells under no oxygen limitation conditions [57]. In general terms, it is possible to observe that metabolite consumption rates are lower for TGE with respect to parental cells, but a re-direction of the energetic sources occurs by the end of transfection to counterbalance the depletion of asparagine, since an increase in the uptake rate of several amino acids is detected.

4. Conclusions

The versatility of the High Five/TGE system for producing recombinant proteins with different complexities is proven in this study. For the first time, the successful production of VLPs using this strategy at bioreactor scale was demonstrated, with no differences in terms of transfection efficiency and a 1.8-fold increase in VLP titer at 72 hpt in comparison to the optimized conditions in shake flasks. The size of Gag-eGFP VLPs obtained corresponds to that observed in VLPs produced with the reference system based on the BEVS. In all cases, the co-expression of EVs with similar sizes to VLPs is observed, which underscores the need to develop efficient separation strategies. Metabolic analysis of transfected High Five cells shows a reduction in the consumption of the principal energy sources in comparison to parental cells and an increase in the uptake rate of several amino acids when asparagine becomes limiting. All in all, the High Five/TGE system provides a valuable approach for accelerating the manufacture of biotechnological products. Moreover, the good performance of this system at bioreactor scale opens the possibility of extending the production phase and increasing the final product yields through the tailored design of perfusion cultivation and re-transfection strategies.

Supplementary Materials: The following are available online at http://www.mdpi.com/2079-4991/10/8/1580/s1, Figure S1: Linear relation between relative activity units (arbitrary units) and hSEAP concentrations (mg/L), Table S1: Uptake and production rates of the main metabolites in parental High Five cells cultured at bioreactor scale.

Author Contributions: Conceptualization, E.P.-M.; methodology, E.P.-M. and F.S.; software, E.P.-M. and F.S.; investigation and data analysis, E.P.-M.; resources, F.G., R.G. and G.S.; writing—original draft preparation, E.P.-M; writing—review and editing, E.P.-M., F.G., M.L., F.S., R.G. and G.S.; supervision, F.G. and M.L.; funding acquisition, F.G., R.G. and G.S. All authors have read and agreed to the published version of the manuscript.

Funding: This research received no external funding.

Acknowledgments: The authors thank Paula Alves (Instituto de Biologia Experimental e Tecnológica, Oeiras, Portugal) for providing the High Five cell line and pIZTV5 plasmid, and Julià Blanco (IrsiCaixa, Badalona, Spain) for the pGag-eGFP plasmid. We also appreciate the support of Sahar Masoumeh Ghorbanpour (University

of Natural Resources and Life Sciences, Vienna, Austria) with ELISA quantification, Núria Barba (Servei de Microscòpia, Universitat Autònoma de Barcelona) in confocal microscopy, Manuela Costa (Servei de Cultius Cel·lulars, Producció d'Anticossos i Citometria, Universitat Autònoma de Barcelona) with flow cytometry, and Jorge Fomaro and Ángel Calvache (Beckman Coulter) for facilitating the access to CytoFlex LX. Eduard Puente-Massaguer is a recipient of an FPU grant from Ministerio de Educación, Cultura y Deporte of Spain (FPU15/03577). The research group is recognized as 2017 SGR 898 by Generalitat de Catalunya.

Conflicts of Interest: The authors declare no conflict of interest.

References

1. Guttieri, M.C.; Liang, M. Human antibody production using insect-cell expression systems. In *Methods in Molecular Biology*; Humana Press: Totowa, NJ, USA, 2004; Volume 248, pp. 269–299.
2. Brank, A.S.; Van Bemmel, D.M.; Christman, J.K. Optimization of Baculovirus-Mediated Expression and Purification of Hexahistidine-Tagged Murine DNA (Cytosine-C5)-Methyltransferase-1 in Spodoptera frugiperda 9 Cells. *Protein Expr. Purif.* **2002**, *25*, 31–40. [CrossRef] [PubMed]
3. Sarafanov, A.G.; Makogonenko, E.M.; Pechik, I.V.; Radtke, K.-P.; Khrenov, A.V.; Ananyeva, N.M.; Strickland, D.K.; Saenko, E.L. Identification of Coagulation Factor VIII A2 Domain Residues Forming the Binding Epitope for Low-Density Lipoprotein Receptor-Related Protein. *Biochemistry* **2006**, *45*, 1829–1840. [CrossRef] [PubMed]
4. Cruz, P.E.; Cunha, A.; Peixoto, C.C.; Clemente, J.; Moreira, J.L.; Carrondo, M.J.T. Optimization of the production of virus-like particles in insect cells. *Biotechnol. Bioeng.* **1998**, *60*, 408–418. [CrossRef]
5. Gheysen, D.; Jacobs, E.; de Foresta, F.; Thiriart, C.; Francotte, M.; Thines, D.; De Wilde, M. Assembly and release of HIV-1 precursor Pr55gag virus-like particles from recombinant baculovirus-infected insect cells. *Cell* **1989**, *59*, 103–112. [CrossRef]
6. Mena, J.A.; Kamen, A.A. Insect cell technology is a versatile and robust vaccine manufacturing platform. *Expert Rev. Vaccines* **2011**, *10*, 1063–1081. [CrossRef]
7. Roldão, A.; Mellado, M.C.M.; Castilho, L.R.; Carrondo, M.J.T.; Alves, P.M. Virus-like particles in vaccine development. *Expert Rev. Vaccines* **2010**, *9*, 1149–1176. [CrossRef]
8. Nika, L.; Cuadrado-Castano, S.; Arunkumar, G.A.; Grünwald-Gruber, C.; McMahon, M.; Koczka, K.; García-Sastre, A.; Krammer, F.; Grabherr, R. An HER2-displaying virus-like particle vaccine protects from challenge with mammary carcinoma cells in a mouse model. *Vaccines* **2019**, *7*, 41. [CrossRef]
9. Lua, L.H.L.; Connors, N.K.; Sainsbury, F.; Chuan, Y.P.; Wibowo, N.; Middelberg, A.P.J. Bioengineering virus-like particles as vaccines. *Biotechnol. Bioeng.* **2014**, *111*, 425–440. [CrossRef]
10. Buonaguro, L.; Buonaguro, F.M.; Tornesello, M.L.; Mantas, D.; Beth-Giraldo, E.; Wagner, R.; Michelson, S.; Prevost, M.C.; Wolf, H.; Giraldo, G. High efficient production of Pr55gag virus-like particles expressing multiple HIV-1 epitopes, including a gp120 protein derived from an Ugandan HIV-1 isolate of subtype A. *Antivir. Res.* **2001**, *49*, 35–47. [CrossRef]
11. Reiter, K.; Aguilar, P.P.; Grammelhofer, D.; Joseph, J.; Steppert, P.; Jungbauer, A. Separation of influenza virus-like particles from baculovirus by polymer grafted anion-exchanger. *J. Sep. Sci.* **2020**, *43*, 2270–2278. [CrossRef]
12. Moleirinho, M.G.; Fernandes, R.P.; Carvalho, S.B.; Bezemer, S.; Detmers, F.; Hermans, P.; Silva, R.J.S.; Alves, P.M.; Carrondo, M.J.T.; Peixoto, C. Baculovirus affinity removal in viral-based bioprocesses. *Sep. Purif. Technol.* **2020**, *241*, 116693. [CrossRef]
13. Geisse, S. Reflections on more than 10 years of TGE approaches. *Protein Expr. Purif.* **2009**, *64*, 99–107. [CrossRef] [PubMed]
14. Fernandes, F.; Vidigal, J.; Dias, M.M.; Prather, K.L.J.; Coroadinha, A.S.; Teixeira, A.P.; Alves, P.M. Flipase-mediated cassette exchange in Sf9 insect cells for stable gene expression. *Biotechnol. Bioeng.* **2012**, *109*, 2836–2844. [CrossRef] [PubMed]
15. Shen, X.; Pitol, A.K.; Bachmann, V.; Hacker, D.L.; Baldi, L.; Wurm, F.M. A simple plasmid-based transient gene expression method using High Five cells. *J. Biotechnol.* **2015**, *216*, 67–75. [CrossRef] [PubMed]
16. Puente-Massaguer, E.; Lecina, M.; Gòdia, F. Nanoscale characterization coupled to multi-parametric optimization of Hi5 cell transient gene expression. *Appl. Microbiol. Biotechnol.* **2018**, *102*, 10495–10510. [CrossRef] [PubMed]

17. Bleckmann, M.; Fritz, M.H.Y.; Bhuju, S.; Jarek, M.; Schürig, M.; Geffers, R.; Benes, V.; Besir, H.; Van Den Heuvel, J.; Li, Y. Genomic analysis and isolation of RNA polymerase II dependent promoters from Spodoptera frugiperda. *PLoS ONE* **2015**, *10*, e0132898. [CrossRef] [PubMed]
18. Shen, X.; Hacker, D.L.; Baldi, L.; Wurm, F.M. Virus-free transient protein production in Sf9 cells. *J. Biotechnol.* **2013**, *171*, 61–70. [CrossRef]
19. Mori, K.; Hamada, H.; Ogawa, T.; Ohmuro-Matsuyama, Y.; Katsuda, T.; Yamaji, H. Efficient production of antibody Fab fragment by transient gene expression in insect cells. *J. Biosci. Bioeng.* **2017**, *124*, 221–226. [CrossRef]
20. Mizote, Y.; Masumi-Koizumi, K.; Katsuda, T.; Yamaji, H. Production of an antibody Fab fragment using 2A peptide in insect cells. *J. Biosci. Bioeng.* **2020**, *130*, 205–211. [CrossRef]
21. Bleckmann, M.; Schürig, M.; Endres, M.; Samuels, A.; Gebauer, D.; Konisch, N.; van den Heuvel, J. Identifying parameters to improve the reproducibility of transient gene expression in High Five cells. *PLoS ONE* **2019**, *14*, e0217878. [CrossRef]
22. Gutiérrez-Granados, S.; Cervera, L.; Kamen, A.A.; Gòdia, F. Advancements in mammalian cell transient gene expression (TGE) technology for accelerated production of biologics. *Crit. Rev. Biotechnol.* **2018**, *38*, 918–940. [CrossRef] [PubMed]
23. Agathos, S.N. Insect cell bioreactors. *Cytotechnology* **1996**, *20*, 173–189. [CrossRef]
24. Elias, C.B.; Jardin, B.; Kamen, A. Recombinant Protein Production in Large-Scale Agitated Bioreactors Using the Baculovirus Expression Vector System. In *Baculovirus and Insect Cell Expression Protocols*; Humana Press: Totowa, NJ, USA, 2007; pp. 225–245.
25. Ghasemi, A.; Bozorg, A.; Rahmati, F.; Mirhassani, R.; Hosseininasab, S. Comprehensive study on Wave bioreactor system to scale up the cultivation of and recombinant protein expression in baculovirus-infected insect cells. *Biochem. Eng. J.* **2019**, *143*, 121–130. [CrossRef]
26. Weber, W.; Weber, E.; Geisse, S.; Memmert, K. Optimisation of protein expression and establishment of the Wave Bioreactor for Baculovirus/insect cell culture. *Cytotechnology* **2002**, *38*, 77–85. [CrossRef] [PubMed]
27. Cronin, C.N. High-volume shake flask cultures as an alternative to cellbag technology for recombinant protein production in the baculovirus expression vector system (BEVS). *Protein Expr. Purif.* **2020**, *165*, 105496. [CrossRef] [PubMed]
28. Hermida-Matsumoto, L.; Resh, M.D. Localization of Human Immunodeficiency Virus Type 1 Gag and Env at the Plasma Membrane by Confocal Imaging. *J. Virol.* **2000**, *74*, 8670–8679. [CrossRef] [PubMed]
29. Pappenreiter, M.; Sissolak, B.; Sommeregger, W.; Striedner, G. Oxygen uptake rate soft-sensing via dynamic kl a computation: Cell volume and metabolic transition prediction in mammalian bioprocesses. *Front. Bioeng. Biotechnol.* **2019**, *7*, 195. [CrossRef] [PubMed]
30. Puente-Massaguer, E.; Gòdia, F.; Lecina, M. Development of a non-viral platform for rapid virus-like particle production in Sf9 cells. *J. Biotechnol.* **2020**, *322*, 43–53. [CrossRef]
31. Gutiérrez-Granados, S.; Cervera, L.; Gòdia, F.; Carrillo, J.; Segura, M.M. Development and validation of a quantitation assay for fluorescently tagged HIV-1 virus-like particles. *J. Virol. Methods* **2013**, *193*, 85–95. [CrossRef]
32. Reiter, K.; Aguilar, P.P.; Wetter, V.; Steppert, P.; Tover, A.; Jungbauer, A. Separation of virus-like particles and extracellular vesicles by flow-through and heparin affinity chromatography. *J. Chromatogr. A* **2019**, *1588*, 77–84. [CrossRef]
33. Puente-Massaguer, E.; Lecina, M.; Gòdia, F. Application of advanced quantification techniques in nanoparticle-based vaccine development with the Sf9 cell baculovirus expression system. *Vaccine* **2020**, *38*, 1849–1859. [CrossRef] [PubMed]
34. Puente-Massaguer, E.; Lecina, M.; Gòdia, F. Integrating nanoparticle quantification and statistical design of experiments for efficient HIV-1 virus-like particle production in High Five cells. *Appl. Microbiol. Biotechnol.* **2020**, *104*, 1569–1582. [CrossRef] [PubMed]
35. Cervera, L.; Gutiérrez-Granados, S.; Martínez, M.; Blanco, J.; Gòdia, F.; Segura, M.M. Generation of HIV-1 Gag VLPs by transient transfection of HEK 293 suspension cell cultures using an optimized animal-derived component free medium. *J. Biotechnol.* **2013**, *166*, 152–165. [CrossRef] [PubMed]

36. Gutiérrez-Granados, S.; Cervera, L.; Segura, M.d.l.M.; Wölfel, J.; Gòdia, F. Optimized production of HIV-1 virus-like particles by transient transfection in CAP-T cells. *Appl. Microbiol. Biotechnol.* **2016**, *100*, 3935–3947. [CrossRef] [PubMed]
37. Cervera, L.; González-Domínguez, I.; Segura, M.M.; Gòdia, F. Intracellular characterization of Gag VLP production by transient transfection of HEK 293 cells. *Biotechnol. Bioeng.* **2017**, *114*, 2507–2517. [CrossRef] [PubMed]
38. Fernandes, B.; Vidigal, J.; Correia, R.; Carrondo, M.J.T.; Alves, P.M.; Teixeira, A.P.; Roldão, A. Adaptive laboratory evolution of stable insect cell lines for improved HIV-Gag VLPs production. *J. Biotechnol.* **2020**, *307*, 139–147. [CrossRef]
39. Van Der Pol, E.; Van Gemert, M.J.C.; Sturk, A.; Nieuwland, R.; Van Leeuwen, T.G. Single vs. swarm detection of microparticles and exosomes by flow cytometry. *J. Thromb. Haemost.* **2012**, *10*, 919–930. [CrossRef]
40. González-Domínguez, I.; Puente-Massaguer, E.; Cervera, L.; Gòdia, F. Quality Assessment of Virus-Like Particles at Single Particle Level: A Comparative Study. *Viruses* **2020**, *12*, 223. [CrossRef]
41. Théry, C.; Zitvogel, L.; Amigorena, S. Exosomes: Composition, biogenesis and function. *Nat. Rev. Immunol.* **2002**, *2*, 569–579. [CrossRef]
42. Li, J.; Chen, X.; Yi, J.; Liu, Y.; Li, D.; Wang, J.; Hou, D.; Jiang, X.; Zhang, J.; Wang, J.; et al. Identification and characterization of 293t cell-derived exosomes by profiling the protein, mRNA and microrna components. *PLoS ONE* **2016**, *11*, e0163043. [CrossRef]
43. Puente-Massaguer, E.; Saccardo, P.; Ferrer-Miralles, N.; Lecina, M.; Gòdia, F.; Ferrer-Miralles, N. Coupling Microscopy and Flow Cytometry for a Comprehensive Characterization of Nanoparticle Production in Insect Cells. *Cytom. Part A* **2020**. [CrossRef] [PubMed]
44. Steppert, P.; Burgstaller, D.; Klausberger, M.; Berger, E.; Aguilar, P.P.; Schneider, T.A.; Kramberger, P.; Tover, A.; Nöbauer, K.; Razzazi-Fazeli, E.; et al. Purification of HIV-1 gag virus-like particles and separation of other extracellular particles. *J. Chromatogr. A* **2016**, *1455*, 93–101. [CrossRef] [PubMed]
45. Pham, P.L.; Kamen, A.; Durocher, Y. Large-scale transfection of mammalian cells for the fast production of recombinant protein. *Mol. Biotechnol.* **2006**, *34*, 225–237. [CrossRef]
46. Rhiel, M.; Mitchell-Logean, C.M.; Murhammer, D.W. Comparison of Trichoplusia ni BTI-Tn-5b1-4 (high five(TM) and Spodoptera frugiperda Sf-9 insect cell line metabolism in suspension cultures. *Biotechnol. Bioeng.* **1997**, *55*, 909–920. [CrossRef]
47. Weidner, T.; Druzinec, D.; Mühlmann, M.; Buchholz, R.; Czermak, P. The components of shear stress affecting insect cells used with the baculovirus expression vector system. *Z. Naturforsch. C* **2017**, *72*, 429–439. [CrossRef] [PubMed]
48. Wickham, T.J.; Nemerow, G.R. Optimization of Growth Methods and Recombinant Protein Production in BTI-Tn-5B1-4 Insect Cells Using the Baculovirus Expression System. *Biotechnol. Prog.* **1993**, *9*, 25–30. [CrossRef]
49. Fuenmayor, J.; Cervera, L.; Gòdia, F.; Kamen, A. Extended gene expression for Gag VLP production achieved at bioreactor scale. *J. Chem. Technol. Biotechnol.* **2019**, *94*, 302–308. [CrossRef]
50. Strobl, F.; Ghorbanpour, S.M.; Palmberger, D.; Striedner, G. Evaluation of screening platforms for virus-like particle production with the baculovirus expression vector system in insect cells. *Sci. Rep.* **2020**, *10*, 1065. [CrossRef] [PubMed]
51. Monteiro, F.; Bernal, V.; Saelens, X.; Lozano, A.B.; Bernal, C.; Sevilla, A.; Carrondo, M.J.T.; Alves, P.M. Metabolic profiling of insect cell lines: Unveiling cell line determinants behind system's productivity. *Biotechnol. Bioeng.* **2014**, *111*, 816–828. [CrossRef]
52. Drugmand, J.C.; Schneider, Y.J.; Agathos, S.N. Insect cells as factories for biomanufacturing. *Biotechnol. Adv.* **2012**, *30*, 1140–1157. [CrossRef]
53. Monteiro, F.; Bernal, V.; Alves, P.M. The role of host cell physiology in the productivity of the baculovirus-insect cell system: Fluxome analysis of Trichoplusia ni and Spodoptera frugiperda cell lines. *Biotechnol. Bioeng.* **2017**, *114*, 674–684. [CrossRef] [PubMed]
54. Elias, C.B.; Carpentier, E.; Durocher, Y.; Bisson, L.; Wagner, R.; Kamen, A. Improving glucose and glutamine metabolism of human HEK 293 and Trichoplusia ni insect cells engineered to express a cytosolic pyruvate carboxylase enzyme. *Biotechnol. Prog.* **2003**, *19*, 90–97. [CrossRef]

55. Benslimane, C.; Elias, C.B.; Hawari, J.; Kamen, A. Insights into the central metabolism of Spodoptera frugiperda (Sf-9) and Trichoplusia ni BTI-Tn-5B1-4 (Tn-5) insect cells by radiolabeling studies. *Biotechnol. Prog.* **2005**, *21*, 78–86. [CrossRef] [PubMed]
56. Sugiura, T.; Amann, E. Properties of two insect cell lines useful for the baculovirus expression system in serum-free culture. *Biotechnol. Bioeng.* **2000**, *51*, 494–499. [CrossRef]
57. Drews, M.; Paalme, T.; Vilu, R. The growth and nutrient utilization of the insect cell line Spodoptera frugiperda Sf9 in batch and continuous culture. *J. Biotechnol.* **1995**, *40*, 187–198. [CrossRef]

Article

PEI-Mediated Transient Transfection of High Five Cells at Bioreactor Scale for HIV-1 VLP Production

Eduard Puente-Massaguer, Florian Strobl, Reingard Grabherr, Gerald Striedner, Martí Lecina and Francesc Gòdia

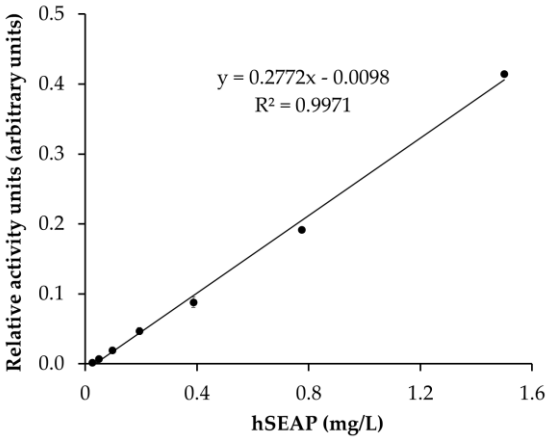

Figure S1. Linear relation between relative activity units (arbitrary units) and hSEAP concentrations (mg/L).

Table S1. Uptake and production rates of the main metabolites in parental High Five cells cultured at bioreactor scale. Cells were seeded at 1 x 10^6 cell/mL and cultured in 0.5 L of bioreactor volume. Rates are expressed in nmol/(10^6 cell·h).

Metabolite	Time (h)		
	0 – 24	**24 – 48**	**48 – 72**
Glucose	-118.5	-95.3	-55.4
Lactate	-17.8	-8.5	0.7
Aspartic acid	14.1	-17.3	-7.1
Glutamic acid	-37.0	-23.1	-7.6
Asparagine	-117.7	-19.7	-
Glutamine	-23.7	-30.0	-19.8
Alanine	161.6	86.9	41.3

Publication III

scientific reports

Check for updates

OPEN

High shear resistance of insect cells: the basis for substantial improvements in cell culture process design

Florian Strobl[1], Mark Duerkop[2,3], Dieter Palmberger[1] & Gerald Striedner[1,2,3]✉

Multicellular organisms cultivated in continuous stirred tank reactors (CSTRs) are more sensitive to environmental conditions in the suspension culture than microbial cells. The hypothesis, that stirring induced shear stress is the main problem, persists, although it has been shown that these cells are not so sensitive to shear. As these results are largely based on Chinese Hamster Ovary (CHO) cell experiments the question remains if similar behavior is valid for insect cells with a higher specific oxygen demand. The requirement of higher oxygen transfer rates is associated with higher shear forces in the process. Consequently, we focused on the shear resistance of insect cells, using CHO cells as reference system. We applied a microfluidic device that allowed defined variations in shear rates. Both cell lines displayed high resistance to shear rates up to $8.73 \times 10^5\ s^{-1}$. Based on these results we used microbial CSTRs, operated at high revolution speeds and low aeration rates and found no negative impact on cell viability. Further, this cultivation approach led to substantially reduced gas flow rates, gas bubble and foam formation, while addition of pure oxygen was no longer necessary. Therefore, this study contributes to the development of more robust insect cell culture processes.

In the biopharmaceutical industry, products are mainly produced by cultivating organisms in suspension. A rather small share (only 2.3%) of all newly approved active pharmaceutical ingredients (APIs) are produced with insect cells as host. Insect cells produce recombinant proteins and virus-like particles (VLPs), a highly complex product class that is rapidly gaining importance[1]. In contrast, Chinese hamster ovary cells are the main workhorse in biopharmaceutical production; they produced 51% of all newly approved APIs from 2014 to 2018[2]. Based on fermentation technologies and operating strategies developed for CHOs, a broad portfolio of methodologies is available, which can be transferred to insect cell processes with only minor modifications. The system of choice for cultivating insect cells in suspension is the CSTR. These bioreactors can be either stainless steel, multi-use systems, with up to 25 m^3 of working volume[3], or a single-use bioreactor with up to 2 m^3 of working volume[4].

If the aim is to transfer methods and approaches developed with CHO to insect cell culture, the significant differences in oxygen demand between these cell types must not be neglected. *Spodoptera frugiperda* (*Sf9*) cells show four and *Trichupulsia Ni* (*Hi5*) even 13 times higher specific oxygen consumption rates than CHO cells, even though for CHO the literature values vary about one order of magnitude[5,6] and these numbers even increase by 30–40% after the culture is infected[7,8]. The high oxygen demand of insect cells can cause severe problems in the cell culture process especially if the frequently postulated shear sensitivity for insect cells is really true.

The theory that mammalian or insect cells are highly sensitive to shear is widespread and persistent, although there is no sound scientific base supporting this hypothesis. On the contrary, there are studies, especially on CHO cell culture, which show that the influence of shear forces on the viability of CHO cells has been greatly overestimated. It has also been shown that cell damage will not occur as long as the size of a biological entity is less than the Kolmogorov scale of turbulence[9]. Different methods for quantifying the effect of hydrodynamic forces on mainly animal cells, are found in literature. They range from flow chambers containing a nozzle, rheological instruments, capillary tubes to specially designed flow devices where the applied shear is simulated via computational fluid dynamic (CFD)[10–15] For insect cell lines little or no objective data are available. Goldblum et al. made attempts to determine the sensitivity under laminar shear conditions using a modified Weissenberg rheogoniometer[16] and Ma et al. determined the sensitivity of Sf9-cells against hydrodynamic forces in

[1]ACIB GmbH, Vienna, Austria. [2]Institute of Bioprocess Science and Engineering, University of Natural Resources and Life Sciences, Vienna, Austria. [3]Novasign GmbH, Vienna, Austria. ✉email: gerald.striedner@boku.ac.at

a microfluidic channel[10]. Consequently, existing knowledge and concepts for insect cells are largely based on historical, empirical data, "rule of thumb"[17], and experience with similar cell types.

The state-of-the-art approach in insect cell culture, is still based on the hypothesis of insect cells high shear sensitivity and consequently CSTRs used for cultivation are designed to maintain low shear forces caused by stirring. Their typical height to diameter (H/D) ratios are in the range of 1.5–2:1[18]; the standard gas transfer coefficient, k_La, ranges from 5 to 10 h^{-1}; and the specific power input ranges from 5 to 300 W m^{-3}[19]. These bioreactors are additionally operated at low stirring speeds that just meet the requirements for mixing. The oxygen transfer, on the other hand, is exclusively manipulated via the flow rate and the composition of the supplied gas. However, this type of process operation leads to a number of problems. High gas flow rates create more gas bubbles in the system, which in turn lead to increased foaming and shear due to the bursting of air bubbles on the liquid surface[20,21]. Low stirring speeds, in turn, can lead to mixing problems and thus increase the formation of zones and gradients—a problem that is particularly relevant in scale-up[22]. With limited mixing, the addition of pure oxygen to the aeration gas can cause oxidative stress in the cells, which in turn can affect process efficiency[23–27].

In summary, the problems described in insect cell culture processes can all be linked to the assumption that these cells are very sensitive to shear stress. However, based on the published data on the shear sensitivity of mammalian cells, there is reason to question the extent to which there are any limitations in the field of insect cell culture process design related to shear sensitivity. Previous studies have shown that insect cells are not necessarily more shear sensitive than mammalian cells and since they are about the same size, the Kolmogorov approach would also point in this direction[28,29]. In this study, focused on the TN42 cell line, a cell line not yet well characterized yet, we decided to take a closer look on shear sensitivity. As a reference, we used CHO cells and SF9 cells, which are much better characterized. We applied a microfluidic shear device[30] that could quantify the shear resistances of cells under controlled conditions without the need of CFD modeling. We applied different shear rates to insect and CHO cells to determine the tolerable range of shear for these cell types and we observed high shear resistance for all cells tested. Based on these results, the cultivation strategy for insect cells was completely redesigned. We applied high stirring speeds to ensure efficient oxygen transfer, in combination with low aeration rates to reduce shear forces triggered by bubble rupture and foam formation. We used microbial CSTRs, which differ dramatically from cell culture reactors, in terms of reactor geometry (H/D ratios: 2.5–3:1 or more), oxygen transfer capacity ($k_La > 250\ h^{-1}$, and may exceed 1000 h^{-1}[31,32]), and specific power input (˃ 5 kW m^{-3}[33–35]). The new process design based on the knowledge that insect cells can withstand quite high shear forces, eliminates many problems identified with previous insect cell culture processes and allows for high flexibility and better scalability.

Materials and methods

Cell lines. We purchased two High Five (ThermoFisher) insect cell lines: the BTI-TN-5B1-4 cell line and the Tnms42 (TN42) cell line (BTI, Gary W. Blissard), which is alpha-nodavirus-free, TN-5B1-4 derivative[36]. In addition, we acquired a host cell variant of CHO-K1 (ATCC CCL-61) that was adapted to serum-free medium[37] (Antibody Lab GmbH, Vienna, Austria). The stable CHO-K1/D1 clonal cell line produced an IgG1 antibody that specifically recognized tumor necrosis factor alpha.

Cloning and generating recombinant baculoviruses and the virus stock. We used a baculovirus that encoded the hemagglutinin (HA) protein of Influenza virus A/California/04/2009 (H1N1) (GenBank accession no. JF915184.1) and the matrix protein for the Gag-polyprotein (Gag) of type 1 human immunodeficiency virus (GenBank accession no. K03455.1). These recombinant genes were codon-optimized for expression in *Trichoplusia ni* (IDTdna, Leuven, Belgium). After PCR amplification, the HA of H1N1 was inserted into the pACEBac-1 acceptor vector (EMBL, Grenoble), which resulted in pACEBac-1-H1. Similarly, the Gag fragment was cloned into the pIDC donor vector (EMBL, Grenoble), which resulted in pIDC-Gag. A Cre-LoxP recombination of the acceptor and donor vectors resulted in H1-Gag acceptor–donor fusion plasmids. The H1-Gag fusion plasmid was transformed into either *E. coli* DH10EMBacY (EMBL, Grenoble) or DH10EMBacp6.9Y cells, which harbored a yellow fluorescent protein (YFP) expression cassette under the control of the polH or p6.9 promoter, respectively. The purified bacmid DNA was transfected into *Sf*9 cells with the FuGene HD transfection reagent (Promega, Madison, Wisconsin, USA) according to the manufacturer's instructions. Viral titers were raised by subsequent passaging, and the titer of the passage 3 stock was determined by measuring the half-maximal tissue culture infective dose ($TCID_{50}$).

Shear experiments. The shear sensitivity and resistance of cells in suspension were tested with a shear device developed by Duerkop et al.[38]. This device was a T-4-SS micro-orifice (O´Keefe Control Co., Monroe, CT, USA) with a 15-fold reduction in diameter (from 1/16″ to 99 µm on a total length of 330 µm). It previously generated shear rates up to $10^8\ s^{-1}$ when used to evaluate the shear sensitivity of proteins[38]. We modified the described method by using a Nemesys XL syringe pump (Cetoni GmbH, Korbussen, Germany), instead of an ÄKTA P100 piston pump, to reduce pump induced cell stress. Figure 1 illustrates the experimental setup. With a two-way valve (3), the cells could either be hoovered from the sample reservoir (1) into the syringe pump (2) or, when the valve was switched, cells were pumped from the syringe pump (2) through an orifice (4), and into the sample collector (5).

Cells were pumped through the orifice at different volume flow rates. By increasing the volumetric flow rate, the shear rate was increased. We calculated the average and maximum shear rates (γ), as follows:

$$\gamma_{average} = \frac{16v}{3d} \quad (1)$$

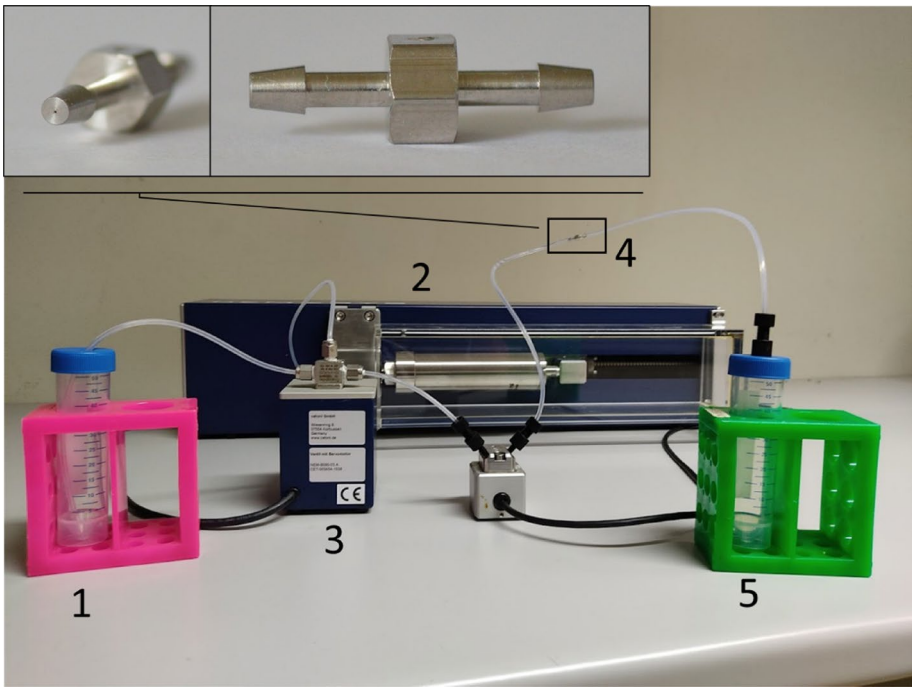

Figure 1. Illustration of the cell-stressing setup. (1) Sample reservoir, (2) syringe pump, (3) 2-way valve, (4) orifice, (5) sample collector. In the top left corner, the two insets display magnifications of the orifice (4).

$$\gamma_{max} = \frac{8v}{d} \tag{2}$$

where v is the velocity (m/s), and d is the diameter of the orifice (m). Equations (1) and (2) are valid in laminar flow conditions, which were applied in these experiments. To investigate the effect of the device, the collected cells were counted, and viability was determined. A control experiment without the device was used to estimate the impact of the system setup itself.

Shake flask cultivations. *Insect cell cultivation.* For each experiment, cells from adherent cultures were transferred to suspension at a starting concentration of 0.5×10^6 cells/mL. Cells were then expanded to the required cell concentrations. For all experiments, the cells were maintained in the exponential growth phase at 27 °C in shaker flasks, agitated at 100 rpm, and passaged until they reached a cell concentration of 4×10^6 cells/mL. Then, cells were grown in serum-free medium which contains poloxamer 188 (Hyclone SFM4Insect, GE Healthcare). Viable cell counts (VCC) were determined with the trypan blue stain method in an automated cell counter (TC20 Biorad).

CHO cell cultivation. To acquire the seed culture, cells were thawed from a working cell bank and cultured in Dynamis AGT Medium (A26175-01, Thermo Fisher Scientific, USA), supplemented with 8 mM L-Glutamine (25030081, Sigma-Aldrich, USA), 1:1000 Anti-Clumping Agent (01-0057AE, Thermo Fisher Scientific) and 0.7 mg/L G418 (108321-42-2, Thermo Fisher Scientific). For pre-cultures, cells were sub-cultured in Dynamis AGT Medium with 8 mM L-Glutamine every 3–4 days at 37 °C, in a humidified incubator (Heracell v10S 160, Thermo Fisher Scientific) with 5% v/v CO_2 and agitated at 200 rpm on an orbital shaker (88881102, Thermo Fisher Scientific). Cells were diluted to a total cell count (TCC) of 1.5×10^6 cells/mL in Dynamis AGT Medium before the shear stress tests.

Bioreactor cultivation and setup. Experiments were performed in 1 L (BioFlo320 1L, Eppendorf) and 1.5 L (DASGIP SR1500 DLS, Eppendorf) bioreactors. No additional baffles were deployed in the bioreactors used. The only obstacles to the free swirling motion of the fluid phase in the vessel are described below.

The BioFlo320 bioreactor system ($d_i = 12$ cm, $h = 23.9$ cm) was equipped with one pitched-blade impeller (3 blades; 45°, $d = 6$ cm, $h = 4$ cm) sitting on the end of the stirrer shaft. It was further equipped with a pH and a DO sensor ($d = 1.2$ cm, $h = 20$ cm and 22 cm), a ring sparger ($d = 6$ mm), a harvesting and a sample taking pipe ($d = 6$ mm) and a thermowell ($d = 7.8$ mm).

The DASGIP bioreactor system ($d_i = 10$ cm, $h = 30$ cm) was equipped with a six-blade Rushton impeller ($d = 4.5$ cm) sitting on the end of the stirrer shaft. It was further also equipped with a pH and a DO sensor ($d = 1.2$ cm, $h = 32.5$ cm), an L-sparger ($d = 6$ mm), a harvesting and a sample taking pipe ($d = 4$ mm) and a thermowell ($d = 6$ mm).

The specific power input of the DASGIP bioreactor was as follows:

Stirrer speed (rpm)	Tip speed (m/s)	Specific power input (W/kg)
100	0.24	0.01
200	0.48	0.07
300	0.72	0.23
600	1.45	1.85
800	1.93	4.37
1000	2.41	8.54

Table 1. Stirrer speeds with corresponding tip speeds and calculated specific power input.

Flow rate (mL/min)	Reynolds number	Max shear rate (s^{-1})	Average shear rate (s^{-1})	Dimensionless shear
3	613.47	5.24E + 05	3.49E + 05	17.93
5	1022.45	8.73E + 05	5.82E + 05	17.93
10	2044.89	1.75E + 06	1.16E + 06	17.93

Table 2. Flow rates inside the shear device, with corresponding Reynolds number, maximum and average shear rates, and the dimensionless shear.

$$\frac{P}{M} = \frac{Np \times \rho \times N^3 \times d^5}{M}, \tag{3}$$

where Np is the power number, ρ = 1050 kg/L, N is the corresponding stirrer speed in rounds per second, d is the impeller outer diameter (m) and M the mass of the culture broth. The Np values were experimentally determined using a torque meter[39], in a setup of no gas flow. The specific power inputs were calculated using Eq. (3) and are summarized in Table 1.

The BioFlo320 system maintained the dissolved oxygen level at 30%, and pure oxygen was supplemented when needed. The temperature was maintained at 27 °C, and the pH was monitored. This setup was chosen, because it was described previously[7,40]. The 1.5 L DASGIP bioreactor maintained the pH at 6.4 ± 0.05 with 25% phosphoric acid and 7.5% sodium bicarbonate.

Bioreactor infection strategy. Cells were grown in the bioreactor in batch mode, until they reached a cell density of about 2×10^6 cells/mL. Next, they were infected with the generated baculovirus stock, at a multiplicity of infection (MOI) of 1 and diluted with fresh media to a final density of 1×10^6 cells/mL.

Analytical methods: tissue culture infectious dose assay. The titer of virus stocks was determined by measuring the TCID50[41], based on the detection of YFP fluorescence. Briefly, *Sf*9 cells were infected with serial dilutions of virus stock or supernatant samples of the different cultivations in a 96-well culture plate (Corning Incorporated, USA). Plates were incubated at 27 °C without agitation. After 4 days, the wells were inspected with a fluorescence microscope (Leica DMIL-LED).

Results and discussion

Shear resistance of cell-lines: shear device experiments. To evaluate the influence of shear on insect and CHO cell lines, we set up controlled shear conditions with a micro-fluid shear device. In the first step, we conducted a control experiment to test the influence of the syringe pump and tubing on cell viability. We filled the syringe pump with the cell suspension and pumped it through the flow path without the nozzle. These experiments were performed at maximum pump speed (45 mL/min), which was the speed used to fill the syringe pump with the cell suspension. We evaluated cell viability before and after this treatment.

Next, directly before each experiment, we prepared 50-mL batches of cell suspensions at cell concentrations of 1.5×10^6 cells/mL. We used an untreated cell suspension with a defined cell concentration and viability as the reference sample (control). Then, a 20-mL aliquot of suspended cells was drawn into the syringe pump each passage and pumped through the device. The first 10-mL fraction of cells was discarded to exclude potential impurities from a former run. The fraction from 10 to 15 mL was used to evaluate cell viability. Each volume flow rate was measured in triplicate, if not otherwise indicated, and the system was flushed with media between volume flow rate changes. We selected three different volume flow rates (3, 5, and 10 mL/min) for shear rate determinations (Table 2). For all the tested flow conditions, a laminar flow profile was present inside the shear device; thus, we used Eqs. (1) and (2) for shear determinations. We also calculated the dimensionless shear, which was the product of the average shear rate and the incubation time. For proteins, it was assumed that, when the dimensionless shear exceeded 10^4, the proteins would irreversibly aggregate[42]. Although this theory was previously shown to be false for a large set of proteins[30], the result could be true for cells.

Furthermore, we showed that dimensionless shear-associated aggregation did not apply to these cells. The product of incubation time and shear rate was constant inside the shear device, because at higher flow rates,

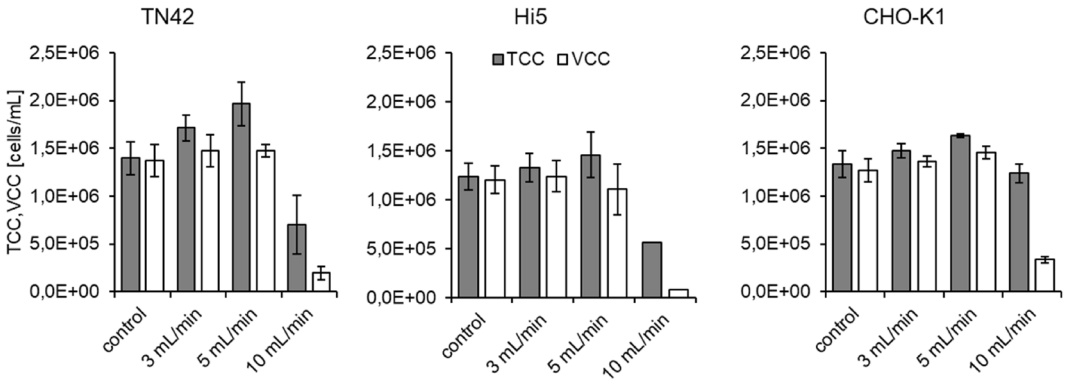

Figure 2. Total and viable cell counts after treatment with the shear device. Shear was measured at different flow rates for (left) TN42, (center) Hi5, and (right) CHO-K1 cells. Each run was performed in triplicate, except the Hi5 experiment (center) run at 10 mL/min.

the incubation time was reduced by the same amount as the shear rate was increased. Hence, the dimensionless shear was constant, as long as the flow conditions remained laminar. However, at higher flow rates, the viability decreased. This decrease indicated that cell damage occurred when the shear rate exceeded the threshold that maintained a constant dimensionless shear.

Our experiments, conducted under controlled shear conditions, indicated that all three cell lines could withstand much higher shear rates than expected, based on the literature[43]. Figure 2 shows that all cell lines could withstand flow rates up to 5 mL/min, which imposed maximum and average shear rates of up to 8.73×10^5 s^{-1} and 5.82×10^5 s^{-1}, respectively (Table 2). The increase in the TCC at flow rates of 3 and 5 mL/min could be attributed to the dispersion of cell clumps when passing through the orifice of the shear device. However, the shear imposed by 10-mL/min flow rates reduced the TCC and VCC. In addition, we observed a sharp increase in the VCC/TCC ratio. However, at lower shear rates, the shear had a positive effect, due to the dispersion of cell clumps[44]; clump dispersion also occurs when cells are filtered[45].

Bioreactor shear characterization. In a theoretical analysis, Sánchez Pérez, Rodríguez Porcel[46] established the connection between the average shear rate (γ_{av}) and the rotational speed of the impeller in turbulent flow. Below, Eq. (4) is based on a simplified assumption correlated to empirical data. In Eq. (5), the maximum shear stress (γ_{max}) also took into account the media and type of impeller used.

The relationship between the stirring speed (N) in a CSTR and the average shear rate (γ_{av})[46], for an A315 axial flow hydrofoil impeller, was:

$$\gamma_{av} = 33.1 \times N^{1.4}. \tag{4}$$

The relationship between the stirring speed (N) in a CSTR and the maximum shear stress (γ_{max})[47] was:

$$\gamma_{max} = 3.3xN^{1.5}xd_i\left(\frac{\rho}{\mu}\right)^{0.5}, \tag{5}$$

where $\mu = 1.1$ mPas, $\rho = 1050$ kg/m^3 are related to the used media, and $di = 0.06$ m of the used pitched-blade impeller.

The calculated average and maximum shears, based on Eqs. (4) and (5) are shown in Table 3 for reasonable stirrer speeds that are typically used in bench-top bioreactors. According to these numbers, any stirring speed currently used in bioreactors would be below the critical value for the cell lines tested with the shear device. Consequently, shear generated in a bioreactor equipped with a stirrer using a pitched-blade impeller or a Rushton should never exceed the critical limit for insect cells.

Furthermore, when a cell cultivation lasts 96 h, the dimensionless shear would be up to 8 orders of magnitude above the shear observed in the shear device. that the concept of dimensionless shear was introduced around 1970[42] and assumes, if proteins are incubated for a very long time, they will be harmed even by medium shear rates. If we assume that cells behaved like proteins, then cells incubated for long times should experience viability problems, even at rather low stirring speeds. We found that the maximum shear rate for short periods of time damaged cells, but an average shear rate for an extended period of time did not damage cells. Our findings indicate that cells can withstand high shear rates and that dimensionless shear should not be considered as critical. To reach the critical shear of 8.73×10^5 s^{-1} the corresponding theoretical speeds for the used stirrer blades would be 16,380 rpm for the pitched blade and 19,850 rpm for the Rushton impeller. The microbial bench-top bioreactors used within this study have only a maximum stirrer speed of 1600 rpm. Hence, calculated maximum shear rates cannot be reached with this setup. Further, before cells would sense impeller-induced shear damage the effect of vortex generation, air entrapment, bubble collapse and cavitation at elevated impeller revolutions would be the main drivers for cell death and might incorrectly be attributed to impeller shear.

Speed (rpm)	γ_{av} (s^{-1})[a]	γ_{max} (s^{-1})	Dimensionless shear
100	6.77E + 01	4.16E + 02	2.34E + 07
200	1.79E + 02	1.18E + 03	6.17E + 07
500	6.44E + 02	4.65E + 03	2.23E + 08
800	1.24E + 03	9.42E + 03	4.30E + 08
1000	1.70E + 03	1.32E + 04	5.87E + 08
1500	3.00E + 03	2.42E + 04	1.04E + 09

Table 3. Stirring speeds and corresponding average (γ_{av}) and maximum (γ_{max}) shear rates for a 1 L bioreactor equipped with one pitched-blade impeller. [a]The average shear values were generated by Sánchez Pérez, Rodríguez Porcel[46] with Eq. (5), for an A315 axial flow hydrofoil impeller (LIGHTNIN Mixers, Rochester, NY), which is similar to a pitched-blade stirrer.

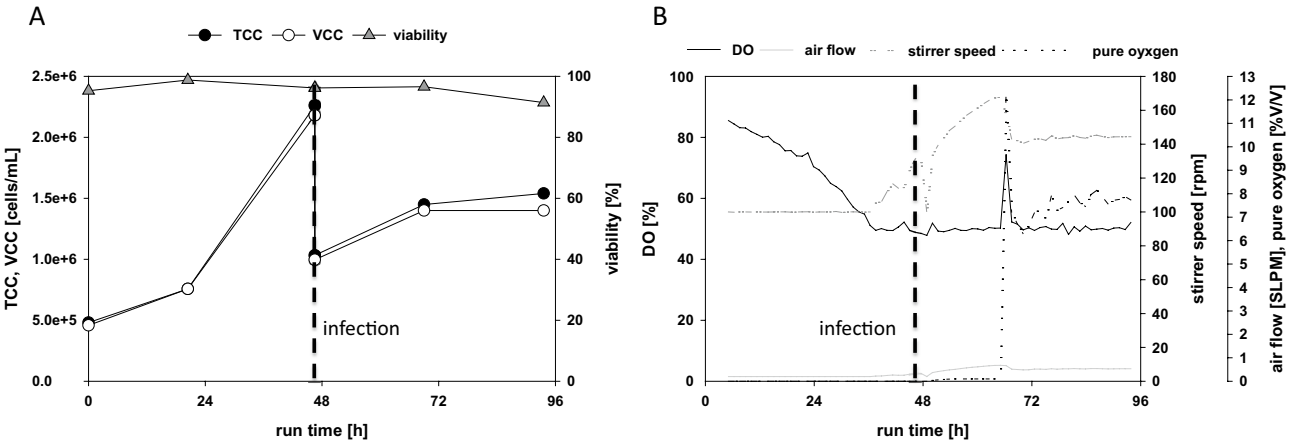

Figure 3. Reference process with TN42 insect cells. (**A**) Counts of total cells (TCC, filled symbols) and viable cells (VCC, open symbols), before and after infection (dashed line), and cell viability (triangles) over the course of the cultivation. (**B**) Trends are shown for the dissolved oxygen (DO)-level, the airflow, the stirrer speed, and the percentage of pure oxygen in the airflow. The time point of infection is indicated by the vertical bold dashed line.

Bioreactor shear experiments. The experiments with the shear device and the estimation of shear rates inside the bioreactor led to our conclusion that shear generated by stirring was not likely to damage insect cells. Because both insect cell lines showed similar behavior, we selected the TN42 cell line for the next series of experiments, which focused on verification of the shear device results.

In the first step, we conducted a TN42 reference cultivation run under standard operation conditions, in a 1 L BioFlo320 System (Eppendorf) equipped with one pitched-blade impeller. This experiment generated reference process data (Fig. 3).

In this reference experiment, cells were seeded at 0.5×10^6 cells/mL and grown in batch mode until they reached 2×10^6 cells/mL. At this point, the cells were infected with the baculovirus working virus stock at a MOI of 1, and they were diluted with fresh medium to 1.0×10^6 cells/mL (Fig. 3A). The stirring speed ranged from 100 to 160 rpm corresponding to a maximum shear rate of 416 s^{-1} and 842 s^{-1}, and the aeration rate ranged from 0.2 to 0.5 standard liter per minute (SLPM). The results showed that, even at a cell concentration of 1.5×10^6 cells/mL, after infection, it was necessary to add pure oxygen to maintain the dissolved oxygen level at 30% and avoid high stirring rates. Infection caused a decline in the cell growth rate, and at 48 h post infection, cell viability was reduced to 91.4% (Fig. 3A).

According to Table 3, the shear in the reference setting was more than two orders of magnitude below the critical values determined in the microfluidic shear device experiments. Therefore, to introduce higher shear rates with stirring, we switched to a microbial bioreactor (SR1500DLS, Eppendorf DASGIP System) equipped with one Rushton impeller. Cells were grown in a 500 mL batch volume and the stirring speed was set to 200 rpm (883 s^{-1}), as a starting value which corresponds to a calculated specific power input of 0.07 W/kg. The air flow was maintained at a constant 0.016 SLPM. Cells were seeded at 0.5×10^6 cells/mL and grown in batch mode for 72 h without the addition of fresh media. The cell viability increased during the batch run, and the cell density reached 4.5×10^6 cells/mL (Fig. 4A). Cell viability was not impacted by the shear rates generated with a Rushton impeller, even running at speeds up to 270 rpm (1385 s^{-1}, 0.17 W/kg).

The next batch cultivation (Fig. 4C) was started at 400 rpm (2497 s^{-1}, 0.55 W/kg), and a step increase to 800 rpm (7064 s^{-1}, 4.37 W/kg) was applied after 48 h of cultivation. The aeration rate was set to 0.016 SPLM to minimize bubbles and foam formation, because no antifoam was used in this experiment. Although the

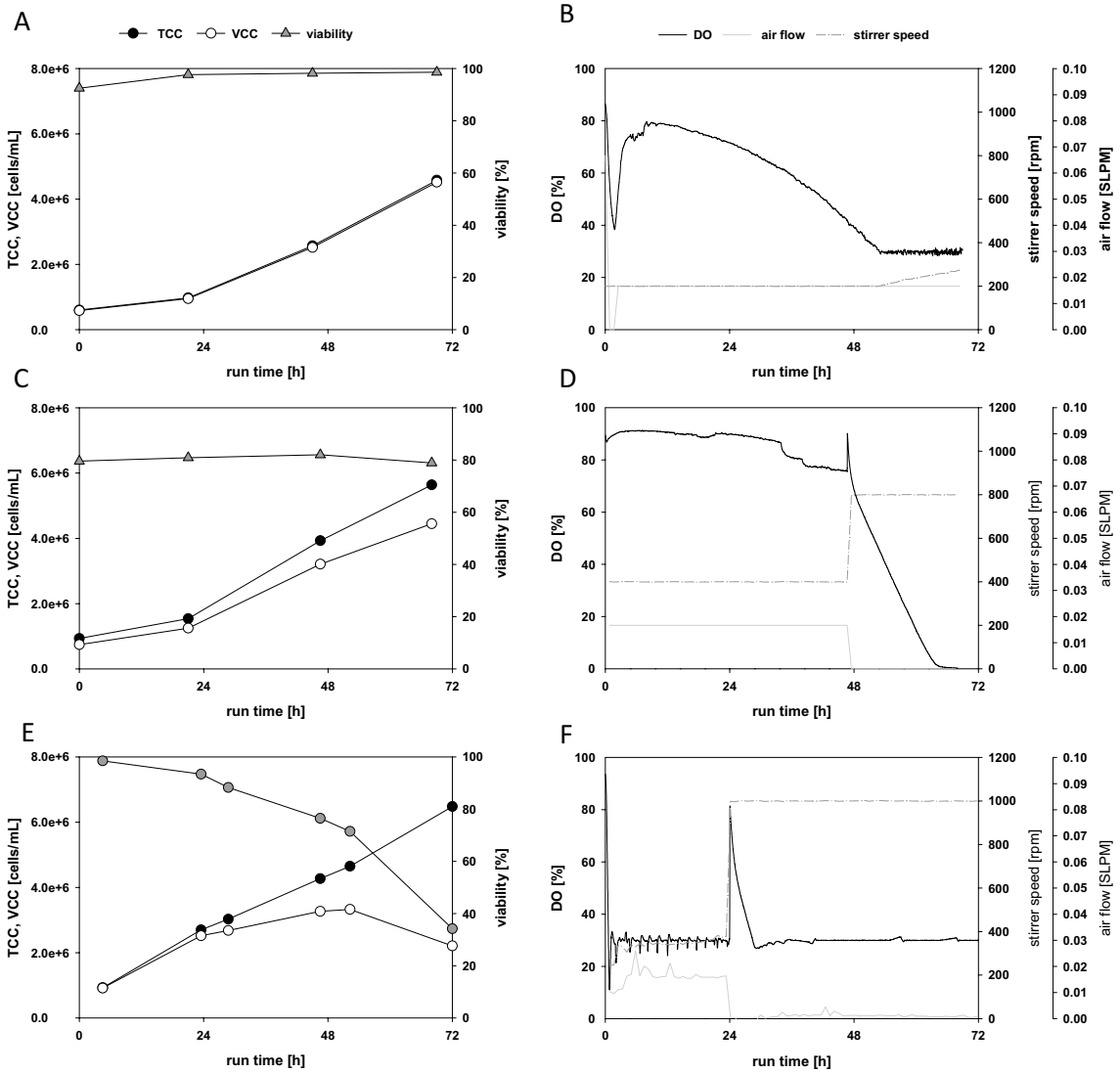

Figure 4. Batch fermentation of TN42 insect cells in a microbial bioreactor, at high stirring speeds. Bioreactors were equipped with either one Rushton impeller (**A**,**D**) or 3 levels of impellers (**E**,**F**). (Left column) Viability (triangles), and counts of total cells (TCC, filled circles) and viable cells (VCC, open circles) in the batch cultivation; (right column) the corresponding dissolved oxygen (DO, black solid line), stirring speed (dotted line), and air flow (grey solid line). Stirring speeds were (**A**,**B**) 200 rpm, incrementally increased to 270 rpm; (**C**,**D**) 400 rpm, stepped to 800 rpm at 48 h; (**E**,**F**) 400 rpm, stepped to 1000 rpm at 24 h.

inoculated cells showed low viability compared to the other batches (Fig. 4A), their viability increased in the first 48 h, from 79.6 to 82%. This increase in viability was also observed in the previous experiment (Fig. 4A), which led to the conclusion that a bioreactor powered by a Rushton turbine at 400 rpm would not impact the viability of insect cells. At the initial 400 rpm stirring rate and the low aeration rate, the DO level slowly decreased from 100 to 65% over the initial 48 h, and the culture reached a cell density of 4.0×10^6 cells/mL during this time. At 48 h, the stirring speed was increased to 800 rpm, and unintentionally, the aeration rate was set to 0 SPLM for the last 24 h of the batch run. Consequently, the DO steadily decreased to 0% for the last couple of hours of the experiment, and cells started to die, due to limited oxygen.

Another cultivation was performed at a working volume of 1 L, but the reactor was equipped with three Rushton blades which was the setup we use for microbial cultivation. The initial stirring speed of 400 rpm was stepped to 1000 rpm (9872 s^{-1}, 8.54 W/kg) after 24 h (Fig. 4E,F). At 24 h after this change, the viability initially decreased by about 5%; but at 48 h after the step to 1000 rpm, the viability dropped by 71.5%. This observation can be explained by the high stirring speed, which led to the formation of a liquid vortex, because no baffles were installed in the bioreactor. As a result, additional air was introduced into the suspension via the vortex surface, and the air was split into small bubbles by the Rushton elements. Thus, the air associated cell damage increased, due to bubbles bursting. The cells could not withstand these harsh conditions. Similar observations were previously described by Murhammer David and Goochee Charles[48] and by Maranga et al.[49].

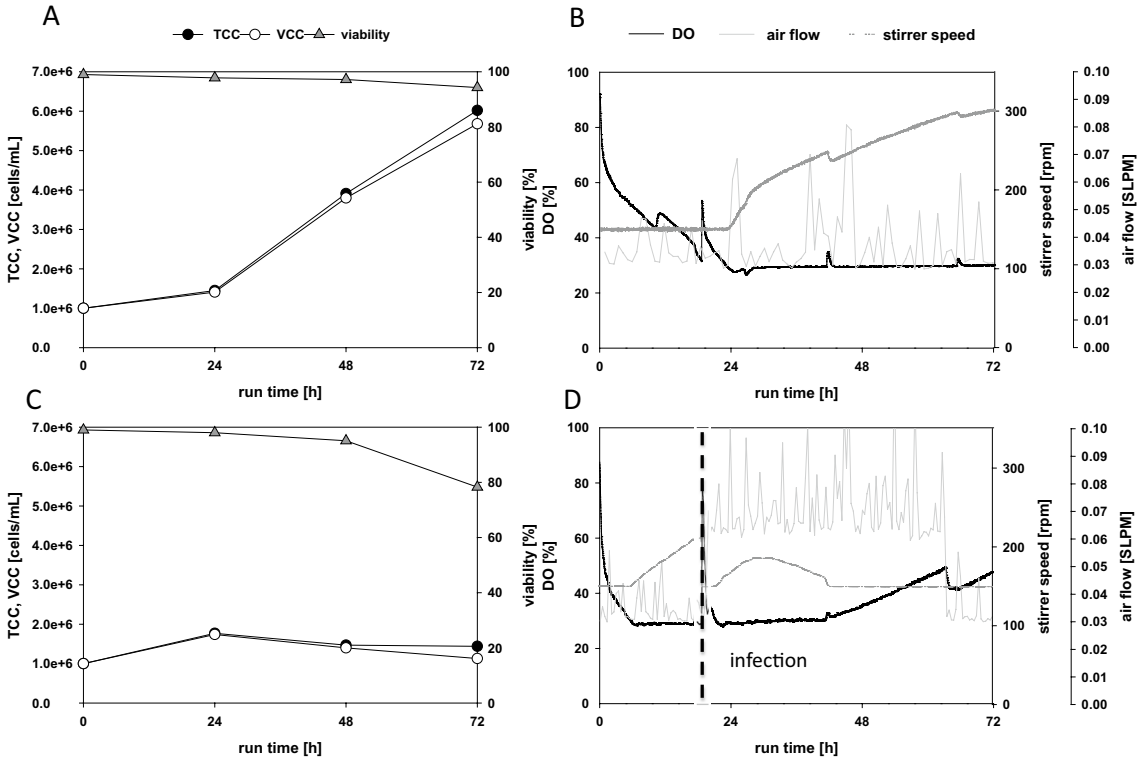

Figure 5. Testing a new control strategy on two cultivations of TN42 insect cells. The controller was tested on (**A**,**B**) an uninfected batch cultivation, and (**C**,**D**) an infected batch process. In both cases, the starting stirring speeds were 150 rpm, and the controller increased or decreased the speed to maintain the DO at 30%. (**A**,**C**) Counts of total (TCC, filled circles) and viable (VCC, open circles) cells, and cell viability (triangles) over the course of the batch cultivation. (**B**,**D**) Dissolved oxygen (DO, solid black line), air flow (solid grey line), and agitation speed (dotted line). The vertical line in Figure (**D**) indicates the time of infection.

New control strategy for insect cell cultivation processes. With the information generated in the preceding experiments, we set up a modified DO control strategy in the microbial bioreactor. The goal was to maintain the gas flow rate as low as possible to minimize foam formation and bubble-associated shear/stress. The PID control strategy for maintaining the DO was adapted by linking the stirring speed, which was the main parameter, to the airflow rate. In the initial phase, the impeller speed was set to the minimum (150 rpm, 574 s^{-1}, 0.03 W/kg). Then, when the DO level reached the set point of 30%, the controller was set to increase the stirring speed, incrementally, up to a maximum of 800 rpm. The stirrer was equipped with a Rushton impeller, and an L-sparger was used to distribute the aeration gas. During the cultivation of uninfected cells, the stirring speed increased to 300 rpm (1622 s^{-1}, 0.23 W/kg), and at the end of the exponential growth phase, the TCC was 6×10^6 cells/mL (Fig. 5A). The gas flow rate was set to the minimum of 0.03 SLPM, but unfortunately, the controller could not maintain this precise rate (Fig. 5B,D).

In parallel, the same process control strategy was tested in a batch that received a virus infection at 24 h. Due to the infection and VLP production, cell growth stopped (Fig. 5C), but oxygen consumption continued to increase (Fig. 5D). Additionally, at the timepoint of infection, the aeration rate increased to 0.06 SLPM. Compared to the reference process for the infected batch (Fig. 3), in this setup, there was no need to add pure oxygen, because increasing the stirring speed provided efficient oxygen transfer. The results of these batch cultivations are in line with Kioukia et al., where infected Sf9 cells were cultivated at 400 rpm with a similar stirrer without an influence in production[28].

CHO cultivations. To determine the impact of high shear due to increased stirring speeds, we performed a direct comparison between two CHO batches cultivated at different stirring speeds in a 1.5 L microbial CSTR bioreactor (SR1500DLS, Eppendorf) with a working volume of 500 mL. One bioreactor (Fig. 6A,B) was operated at a low stirring speed, starting at 100 rpm, and the aeration rate was set to 0.03 SLPM. The DO was maintained at 30% by incrementally increasing the stirring speed, which mimicked a standard CHO batch cultivation. The second bioreactor was operated at an increased stirring speed. After a short adjustment phase at 200 rpm, the stirring was maintained at 300 rpm with an aeration rate of 0.03 SLPM. Then, after 48 h, the stirring was increased to 600 rpm, and the aeration rate was lowered to 0.016 SLPM (Fig. 6D). In both reactors, the sparger supplemented the medium with carbon dioxide to control the pH.

We found that cell growth rates behaved nearly the same at the low and high stirring settings (Fig. 6A,C). Moreover, viability was not influenced by the high stirrer speed during exponential growth, which ended at around 96 h after inoculation. At the high stirring speed, the DO never dropped below 80% throughout the

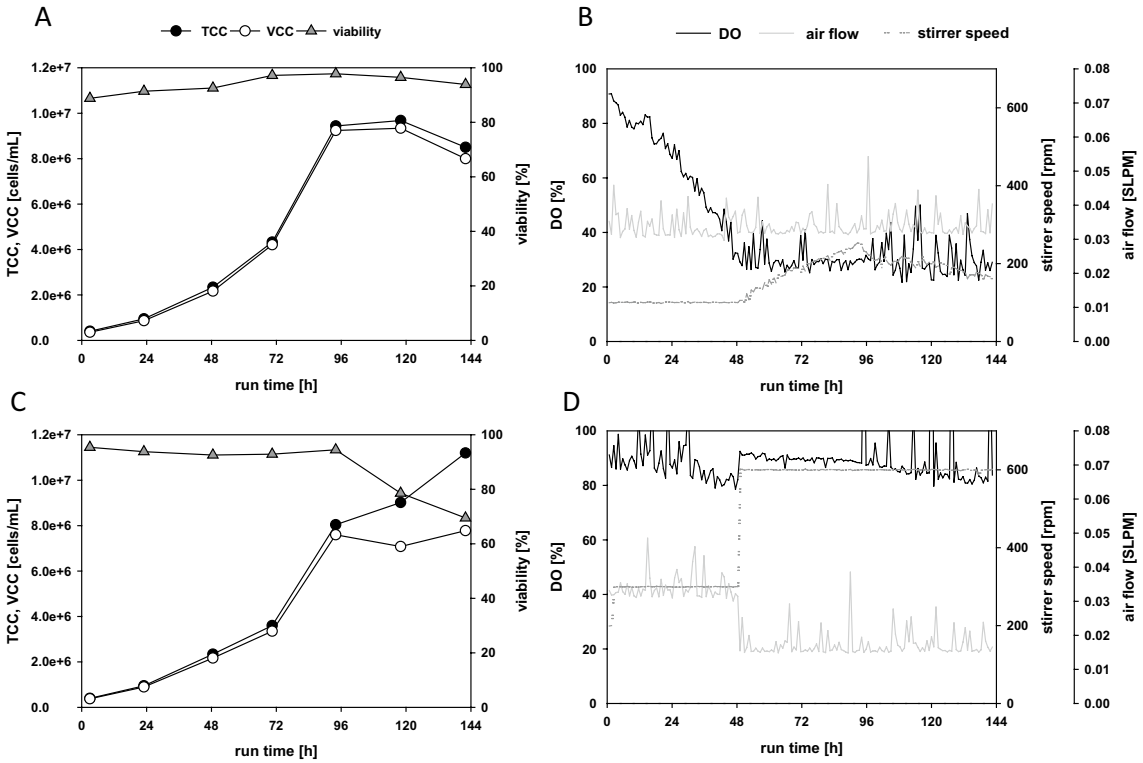

Figure 6. The impact of a high stirring speed tested by comparing two cultivations of CHO cells in microbial bioreactors, at different stirring speeds. (**A**,**B**) A standard batch cultivation with a low stirring speed (100 rpm); (**C**,**D**) a batch process with a high stirring speed (300 stepped to 600 rpm). (Left column) Viability (triangles), and counts of total cells (TCC, filled circles) and viable cells (VCC, open circles) in the batch cultivation; (right column) the corresponding dissolved oxygen (DO, black solid line), stirring speed (dotted line), and air flow (solid grey line).

entire process (Fig. 6D). However, we observed a difference in viability during the stationary phase; the viability decreased more rapidly in the bioreactor with the faster stirring speed (Fig. 6C,D) than in the bioreactor with the slower speed (Fig. 6A,B). This could possibly be due to the high DO levels during the batch cultivation. It has been reported that high DO levels during a cultivation can lead to oxidative stress and also to reduced protein yields[23–26].

Overall, our results showed that CHO cells could be cultivated with a Rushton impeller which was also shown by Ref.[27] but at higher stirring speeds, without damaging the cells. Additionally, aeration rates could be maintained at a minimum, and it was not necessary to add pure oxygen throughout the process. With the higher stirring rate and the lower aeration rate, foaming was nearly eliminated during the batch cultivations; thus, no antifoam had to be added. Applying this modified DO control strategy could enable CHO cell cultivations to achieve higher cell concentrations.

Conclusion

The shear device described in this study was an efficient and simple tool to apply defined levels of shear directly to cells to characterize their shear sensitivity. In this study, we used the shear device with insect and CHO cells, but it can also be used for other cell lines, viruses, or VLPs to determine critical shear stress.

We found that with the shear device methodology both insect cell lines High Five and the Tnms42 as well as the CHO-K1 cell line could withstand maximum and average shears of $8.73 \times 10^5\ s^{-1}$ and $5.82 \times 10^5\ s^{-1}$, respectively. These results are in full agreement with the finding of a much higher robustness of different cell types to shear forces published by Nienow et al.[29]. From our point of view, it is time to dispel the myth about the high shear sensitivity of cells, as this leads to massive and unnecessary limitations in process control.

Knowledge of the critical shear for the cell types investigated facilitated the design of a new DO process control regime, based on high energy input through stirring, with applying typical Rushton-powered microbial bioreactor setup. With this setup, the oxygen transfer rate could be significantly increased, even at very low gas flow rates. As expected from the micro-fluidic experiments, high stirring speeds did not harm neither the insect cells nor the CHO cells, as long as the gas flow rate and bubble introduction were maintained at low levels. In addition, low aeration rates provided significantly reduced foam formation, which was beneficial for both the process and the cells. The cell densities achieved in this study required maximum stirring speeds of 300 rpm ($1622\ s^{-1}$, 0.23 W/kg) for insect cells and 220 rpm ($1019\ s^{-1}$, 0.09 W/kg) for CHO cells. These stirrer speeds introduced shear rates that were far below the previously described critical values. The reduced cell viability observed in the experiment with stirring at 1000 rpm was most likely caused by vortex formation, which can,

to a certain extend be prevented by introducing baffles. Our results showed that the oxygen transfer rates that we achieved with relatively high stirring with Rushton-powered reactor design at low aeration rates produced much higher cell densities than the conventional operational mode. Further, our setup significantly reduced gas flow rates and avoided the application of pure oxygen.

Our control regime has the advantage of improving the economic efficiency of the process, but more importantly, the lower gas volumes in the suspension also reduces foam formation and bubble rupture at the liquid surface. This phenomenon can positively affect cell viability, virus quality, and products, like for instance, VLPs.

Received: 4 December 2020; Accepted: 13 April 2021
Published online: 03 May 2021

References

1. Langer, E. & Rader, R. Biopharmaceutical manufacturing: Historical and future trends in titers, yields, and efficiency in commercial-scale bioprocessing. *Bioprocess. J.* **13**(4), 47–54 (2015).
2. Walsh, G. Biopharmaceutical benchmarks 2018. *Nat. Biotechnol.* **36**(12), 1136–1145 (2018).
3. Farid, S. S. Process economics of industrial monoclonal antibody manufacture. *J. Chromatogr. B Anal. Technol. Biomed. Life Sci.* **848**(1), 8–18 (2007).
4. Löffelholz, C. *et al.* Bioengineering Parameters for Single-Use Bioreactors: Overview and Evaluation of Suitable Methods. *Chem. Ing. Tec.* **85**(1–2), 40–56 (2013).
5. Wagner, B. A., Venkataraman, S. & Buettner, G. R. The rate of oxygen utilization by cells. *Free Radic. Biol. Med.* **51**(3), 700–712 (2011).
6. Guarino, R. D. *et al.* Method for determining oxygen consumption rates of static cultures from microplate measurements of pericellular dissolved oxygen concentration. *Biotechnol. Bioeng.* **86**(7), 775–787 (2004).
7. Kamen, A. A. *et al.* Culture of insect cells in helical ribbon impeller bioreactor. *Biotechnol. Bioeng.* **38**(6), 619–628 (1991).
8. Wong, T. K. K. *et al.* Relationship between oxygen uptake rate and time of infection of Sf9 insect cells infected with a recombinant baculovirus. *Cytotechnology* **15**(1), 157–167 (1994).
9. Nienow, A. W. The impact of fluid dynamic stress in stirred bioreactors—The scale of the biological entity: A personal view. *Chem. Ing. Tech.* **93**(1–2), 17–30 (2021).
10. Ma, N., Koelling, K. W. & Chalmers, J. J. Fabrication and use of a transient contractional flow device to quantify the sensitivity of mammalian and insect cells to hydrodynamic forces. *Biotechnol Bioeng* **80**(4), 428–437 (2002).
11. McQueen, A. & Bailey, J. E. Influence of serum level, cell line, flow type and viscosity on flow-induced lysis of suspended mammalian cells. *Biotechnol. Lett.* **11**(8), 531–536 (1989).
12. Neunstoecklin, B. *et al.* Determination of the maximum operating range of hydrodynamic stress in mammalian cell culture. *J. Biotechnol.* **194**, 100–109 (2015).
13. Thomas, C. R., Al-Rubeai, M. & Zhang, Z. Prediction of mechanical damage to animal cells in turbulence. *Cytotechnology* **15**(1), 329–335 (1994).
14. Sieck, J. B. *et al.* Development of a Scale-Down Model of hydrodynamic stress to study the performance of an industrial CHO cell line under simulated production scale bioreactor conditions. *J. Biotechnol.* **164**(1), 41–49 (2013).
15. Nienow, A. W. *et al.* Scale-down studies for assessing the impact of different stress parameters on growth and product quality during animal cell culture. *Chem. Eng. Res. Des.* **91**(11), 2265–2274 (2013).
16. Goldblum, S. *et al.* Protective effect of methylcellulose and other polymers on insect cells subjected to laminar shear stress. *Biotechnol. Prog.* **6**(5), 383–390 (1990).
17. Chalmers, J. J. Mixing, aeration and cell damage, 30+ years later: What we learned, how it affected the cell culture industry and what we would like to know more about. *Curr. Opin. Chem. Eng.* **10**, 94–102 (2015).
18. Godoy-Silva, R., C. Berdugo, and J.J. Chalmers, Aeration, Mixing, and Hydrodynamics, Animal Cell Bioreactors. *Encyclopedia of Industrial Biotechnology*, 1–27 (2010).
19. Eisenkraetzer, D. 6.1 Bioreactors for animal cell culture. In *Animal Cell BiotechnologyIn Biologics Production.* https://doi.org/10.1515/9783110278965.389 (2014).
20. Walls, P. L. L. *et al.* Quantifying the potential for bursting bubbles to damage suspended cells. *Sci. Rep.* **7**(1), 15102–15102 (2017).
21. Puente-Massaguer, E. *et al.* PEI-mediated transient transfection of high five cells at bioreactor scale for HIV-1 VLP production. *Nanomaterials (Basel, Switzerland)* **10**(8), 1580 (2020).
22. Tramper, J. Oxygen gradients in animal-cell bioreactors. *Cytotechnology* **18**(1), 27–34 (1995).
23. Meilhoc, E., Wittrup, K. D. & Bailey, J. E. Influence of dissolved oxygen concentration on growth, mitochondrial function and antibody production of hybridoma cells in batch culture. *Bioprocess. Eng.* **5**(6), 263–274 (1990).
24. Heidemann, R. *et al.* Effects of dissolved oxygen levels and the role of extra- and intracellular amino acid concentrations upon the metabolism of mammalian cell lines during batch and continuous cultures. *Cytotechnology* **26**(3), 185–197 (1998).
25. Handlogten, M. W., Zhu, M. & Ahuja, S. Intracellular response of CHO cells to oxidative stress and its influence on metabolism and antibody production. *Biochem. Eng. J.* **133**, 12–20 (2018).
26. Siddiquee, K. *et al.* Cell-culture growth conditions resulting in the oxidation of a recombinant antigen-binding fragment. *Bioresour. Bioprocess.* **6**(1), 34 (2019).
27. Sandadi, S. *et al.* A comprehensive comparison of mixing, mass transfer, Chinese hamster ovary cell growth, and antibody production using Rushton turbine and marine impellers. *Bioprocess Biosyst. Eng.* **34**(7), 819 (2011).
28. Kioukia, N. *et al.* Influence of agitation and sparging on the growth rate and infection of insect cells in bioreactors and a comparison with hybridoma culture. *Biotechnol. Prog.* **12**(6), 779–785 (1996).
29. Nienow, A. W. Reactor engineering in large scale animal cell culture. *Cytotechnology* **50**(1–3), 9–33 (2006).
30. Duerkop, M. *et al.* Influence of cavitation and high shear stress on HSA aggregation behavior. *Eng. Life Sci.* **18**(3), 169–178 (2018).
31. Czermak, P., Pörtner, R., & Brix, A. Special engineering aspects. In *Cell and Tissue Reaction Engineering: With a Contribution by Martin Fussenegger and Wilfried Weber* (eds. Eibl, R. *et al.*) 83–172 (Springer, 2009).
32. Garcia-Ochoa, F. *et al.* Oxygen uptake rate in microbial processes: An overview. *Biochem. Eng. J.* **49**(3), 289–307 (2010).
33. Langheinrich, C. *et al.* Oxygen transfer in stirred bioreactors under animal cell culture conditions. *Food Bioprod. Process.* **80**(1), 39–44 (2002).
34. Sagmeister, P. *et al.* Bacterial suspension cultures. *Industrial Scale Suspension Culture of Living Cells.* 40–93 (2014).
35. Jossen, V. *et al.* 7—stirred bioreactors: current state and developments, with special emphasis on biopharmaceutical production processes. In *Current Developments in Biotechnology and Bioengineering* (eds. Larroche, C., *et al.*) 179–215 (Elsevier, 2017).
36. Granados, R., Blissard, G. & Debbie, P. Cell lines that are free of viral infection and methods for their production. Google patents. Google Scholar (2016).
37. Zboray, K. *et al.* Heterologous protein production using euchromatin-containing expression vectors in mammalian cells. *Nucleic Acids Res.* **43**(16), e102–e102 (2015).

38. Duerkop, M. *et al.* Impact of cavitation, high shear stress and air/liquid interfaces on protein aggregation. *Biotechnol. J.* **13**, 1800062 (2018).
39. Li, B. & Sha, M. *Scale-Up of Escherichia coli Fermentation from Small Scale to Pilot Scale Using Eppendorf Fermentation Systems.* Eppendorf Application Note no.306 (2016).
40. Zeiser, A. *et al.* On-line monitoring of physiological parameters of insect cell cultures during the growth and infection process. *Biotechnol. Prog.* **16**(5), 803–808 (2000).
41. Smither, S. J. *et al.* Comparison of the plaque assay and 50% tissue culture infectious dose assay as methods for measuring filovirus infectivity. *J. Virol. Methods* **193**(2), 565–571 (2013).
42. Charm, S. E. & Wong, B. L. Enzyme inactivation with shearing. *Biotechnol. Bioeng.* **12**(6), 1103–1109 (1970).
43. Tramper, J. *et al.* Shear sensitivity of insect cells in suspension. *Enzyme Microb. Technol.* **8**(1), 33–36 (1986).
44. Renner, W. A. *et al.* Cell–cell adhesion and aggregation: Influence on the growth behavior of CHO cells. *Biotechnol. Bioeng.* **41**(2), 188–193 (1993).
45. Vickroy, B., Lorenz, K. & Kelly, W. Modeling shear damage to suspended CHO cells during cross-flow filtration. *Biotechnol. Prog.* **23**(1), 194–199 (2007).
46. Sánchez Pérez, J. A. *et al.* Shear rate in stirred tank and bubble column bioreactors. *Chem. Eng. J.* **124**(1), 1–5 (2006).
47. Robertson, B. & Ulbrecht, J. J. *Measurement of Shear Rate on an Agitator in a Fermentation Broth. Biotechnology Processes, 1987 Scale-Up and Mixing* 72–81 (American Institute of Chemical Engineers, 1987).
48. Murhammer David, W. & Goochee Charles, F. Sparged animal cell bioreactors: Mechanism of cell damage and Pluronic F-68 protection. *Biotechnol. Prog.* **6**(5), 391–397 (1990).
49. Maranga, L. *et al.* Scale-up of virus-like particles production: effects of sparging, agitation and bioreactor scale on cell growth, infection kinetics and productivity. *J. Biotechnol.* **107**(1), 55–64 (2004).

Author contributions

F.S., M.D, D.P. and G.S. designed the research; F.S. performed the experiments F.S. and M.D. did the data analysis and interpretation; F.S. and G.S. wrote the manuscript with the contribution of the other authors.

Competing interests

The authors declare no competing interests.

Additional information

Correspondence and requests for materials should be addressed to G.S.

Reprints and permissions information is available at www.nature.com/reprints.

Publisher's note Springer Nature remains neutral with regard to jurisdictional claims in published maps and institutional affiliations.

Publication IV

Vaccine 38 (2020) 859–867

Contents lists available at ScienceDirect

Vaccine

journal homepage: www.elsevier.com/locate/vaccine

Off-target effects of an insect cell-expressed influenza HA-pseudotyped Gag-VLP preparation in limiting postinfluenza *Staphylococcus aureus* infections

Miriam Klausberger [a,*], Irina A. Leneva [b], Andrey Egorov [b,c], Florian Strobl [d], Sahar M. Ghorbanpour [d], Irina N. Falynskova [b], Alexander V. Poddubikov [e], Nailya R. Makhmudova [b], Artem Krokhin [a], Oxana A. Svitich [b], Reingard Grabherr [a]

[a] Department of Biotechnology, University of Natural Resources and Life Sciences (BOKU), Vienna, Austria
[b] Department of Virology, I. Mechnikov Research Institute for Vaccines and Sera, Moscow, Russia
[c] Smorodintsev Research Institute of Influenza, Saint-Petersburg, Russia
[d] Austrian Centre of Industrial Biotechnology (ACIB), Vienna, Austria
[e] Department of Microbiology, I. Mechnikov Research Institute for Vaccines and Sera, Moscow, Russia

ARTICLE INFO

Article history:
Received 28 June 2019
Received in revised form 21 October 2019
Accepted 26 October 2019
Available online 9 November 2019

Keywords:
Influenza
Staphylococcus aureus
Secondary bacterial infection
Vaccine off-target effects
VLP vaccine

ABSTRACT

Clinical and historical data underscore the ability of influenza viruses to ally with *Staphylococcus aureus* and predispose the host for secondary bacterial pneumonia, which is a leading cause of influenza-associated mortality. This is fundamental because no vaccine for *S. aureus* is available and the number of antibiotic-resistant strains is alarmingly rising. Hence, this leaves influenza vaccination the only strategy to prevent postinfluenza staphylococcal infections. In the present work, we assessed the off-target effects of a *Tnms*42 insect cell-expressed BEI-treated Gag-VLP preparation expressing the HA of A/Puerto Rico/8/1934 (H1N1) in preventing *S. aureus* superinfection in mice pre-infected with a homologous or heterologous H1N1 viral challenge strain. Our results demonstrate that matched anti-hemagglutinin immunity elicited by a VLP preparation may suffice to prevent morbidity and mortality caused by lethal secondary bacterial infection. This effect was observed even when employing a single low antigen dose of 50 ng HA per animal. However, induction of anti-hemagglutinin immunity alone was not helpful in inhibiting heterologous viral replication and subsequent bacterial infection. Our results indicate the potential of the VLP vaccine approach in terms of immunogenicity but suggest that anti-HA immunity should not be considered as the sole preventive method for combatting influenza and postinfluenza bacterial infections.

1. Introduction

Influenza virus infections are frequently complicated by bacterial superinfections during seasonal influenza outbreaks and particularly during influenza pandemics. Bacterial infections may occur concurrent or shortly after viral infection of the host; in either case manifesting as more severe illness with higher mortality rates as compared to infection with the viral or bacterial pathogen alone [1–5]. In fact, lung tissue autopsies of fatal cases uncovered bacterial secondary pneumonia as major cause of influenza-associated mortality during the influenza pandemics of the last century, as reviewed by Metersky et al. [4]. *Staphylococcus aureus* (*S. aureus*) is among the bacteria that had been most frequently isolated from postmortem lung specimens during the 1957 and 1968 influenza pandemics [1,2]. Also recently, *S. aureus* hit the headlines because of the high numbers of childhood fatalities in the context of postinfluenza secondary bacterial infections (SBIs) [3]. *S. aureus* is a gram-positive bacterium and a potentially lethal opportunistic pathogen. It is a common resident of the human nasal flora with 70–80% of the healthy adult population

Abbreviations: AcMNPV, Autographa californica multiple nuclear polyhedrosis virus; BEI, binary ethylenimine; CFU, colony-forming units; EID50, egg infectious dose 50; HA, hemagglutinin; HI, hemagglutination-inhibition; IFN, interferon; IIV, inactivated influenza vaccine; LAIV, live-attenuated influenza vaccine; MOI, multiplicity of infection; NA, neuraminidase; PR8, influenza H1N1 strain A/Puerto Rico/8/1934; rBV, recombinant baculovirus; *S. aureus*, *Staphylococcus aureus*; SBI, secondary bacterial infection; *Sf*9, *Spodoptera frugiperda* 9; TCID50, tissue culture infectious dose 50; TFF, tangential flow filtration; *T.ni*, *Trichoplusia ni*; VLP, virus-like particle.

* Corresponding author at: Department of Biotechnology, University of Natural Resources and Life Sciences (BOKU), Muthgasse 18, 1190 Vienna, Austria.
E-mail address: Miriam.klausberger@boku.ac.at (M. Klausberger).

https://doi.org/10.1016/j.vaccine.2019.10.083
0264-410X/

carrying the strain persistently or intermittently. Colonization is asymptomatic in most cases but is a risk factor and potential reservoir for acquiring invasive infection, particularly in the presence of influenza [6]. Preceding influenza virus infection was shown to predispose the host for secondary bacterial infection and complication. *In vivo* studies revealed mechanisms involved in this lethal synergism, which include virus-mediated modifications of the physical host cell barrier and complex interplays between host, viral and bacterial factors that ultimately impair the host immune response to the secondary invader and interfere with pathogen clearance [7–9]. Despite numerous efforts to develop *S. aureus* vaccines and immunotherapeutics, neither strategy has proven effective in preventing staphylococcal infections in humans as reviewed by Fowler and Proctor [10]. Much of the difficulty in developing an effective prophylaxis stems from the fact that correlates for protective staphylococcus immunity are not yet completely understood and that the bacterium possesses multiple virulence factors and causes a broad range of diseases [10]. Moreover, results from a phase III human trial on the efficacy of preoperative vaccination with a *S. aureus* vaccine candidate (V710, Merck) on reducing post-operative bacteremia raised safety concerns due to the higher mortality rates in vaccine recipients than in placebo subjects [11]. In addition to the fact that there is no licensed *S. aureus* vaccine, treatment options are severely limited by the rapid spread of clinically significant resistance among *S. aureus* (MRSA-strains); among them the highly virulent Panton-Valentine leukocidin toxin-producing strains [3,12]. This leaves the control of influenza virus infection as only measure to prevent secondary staphylococcal complications. Yet, influenza vaccine assessments have barely considered the effects of vaccine-elicited influenza immunity on secondary bacterial invaders.

In the current study, we investigated the efficacy of a recombinant influenza preparation in protecting from postinfluenza secondary bacterial complications in BALB/c mice, using a clinical *S. aureus* strain. The immunogen was a virus-like particle (VLP) preparation consisting of retroviral Gag-VLPs pseudo-typed with the influenza hemagglutinin (HA) as exclusive influenza virus antigen and was expressed using the novel *Trichoplusia ni* (*T.ni*)-derived insect cell line *Tnms*42 [13,14]. In light of current influenza vaccines exclusively focusing on establishing immunity toward the influenza HA we were particularly interested to assess the sole contribution of anti-HA immunity in limiting postinfluenza bacterial infection, morbidity and mortality in a situation of a vaccine match and mismatch.

2. Materials and methods

2.1. Ethics statements

All experimental procedures with animals were carried out in strict accordance with the "Rules for laboratory practice in the Russian Federation" of the Ministry of Health of Russia (23.08.2010 No. 708н) and according to an approved protocol (IACUC 03.09.2018 N11) from the Animal Care and Use Committee of the I. Mechnikov Research Institute for Vaccines and Sera, Moscow Russia. Animals were had free access to food and water *ad libitum* and were kept on a 12-h light/dark cycle.

2.2. Molecular cloning and recombinant baculovirus generation

The nucleic acid sequence of the influenza HA from A/Puerto Rico/8/1934 (PR8, H1N1) (GenBank: EF467821.1) was codon-optimized for the expression in *Trichoplusia ni* and was synthesized as gBlock Gene Fragment by IDT (Coralville, IA). The gene was PCR-amplified and cloned into the pACEBac2 vector (Geneva Biotech, Geneva, CH) under control of the *AcMNPV* p10 promoter. The pIDC-Gag vector was a gift from Lisa Nika (Department of Biotechnology, BOKU, Vienna) and harbors a HIV-1 Gag expression cassette driven by the *AcMNPV* pH promoter generated as described previously [15]. The two vectors were fused using Cre recombination and transformed into NEB® 5-alpha competent *E. coli* (New England Biolabs, Ipswich, UK). Sequence identity was confirmed by sequencing. A recombinant baculovirus (rBV) was generated in *Sf*9 cells using the Fugene® HD Transfection reagent (Promega, Madison, WI) and a modified MultiBac genome. There, an *AcMNPV* p6.9 promoter-driven YFP expression cassette was integrated into the loxP site of the MultiBac genome (Geneva Biotech) to monitor infection. A passage two working stock was generated in *Sf*9 cells and was titrated by $TCID_{50}$.

2.3. Production and purification of influenza HA-Gag VLPs

HA-Gag VLPs (termed PR8-Gag VLPs hereinafter) were expressed in *Tnms*42 cells in Hyclone SFM4 Insect cell culture medium (GE Life Sciences, Marlborough, MA) supplemented with 0.1% (w/v) Pluronic F-68 (Sigma, St. Louis, MO) in a 1L BioFlo320 glass bioreactor (Eppendorf, Hamburg, D) equipped with a pitched blade impeller. The temperature was set to 27 °C, pH was maintained at pH 6.4 using 25% (v/v) phosphoric acid and 7.5% (w/v) sodium bicarbonate and the dissolved oxygen level was maintained at 30%. A *Tnms*42 suspension pre-culture (4×10^6/mL, viability: 99%) cultivated in Fernbach flasks was inoculated into the bioreactor and diluted to a cell density of 1×10^6 cells per mL. After one round of cell division (24 h) cells were infected with recombinant baculoviruses at a MOI of about five and simultaneously were back-diluted with fresh medium to a final cell concentration of 1×10^6 cells per mL. Cell count and viability, volumetric HA and Gag yield as well as total protein content and hemagglutination activity in the supernatant were monitored daily. The expression supernatant was harvested three days post infection, when viability dropped below 50% and was clarified from cells and cellular debris by centrifugation at 1.000 rpm, 10 min, 4 °C and 5.500 rpm, 30 min, 4 °C using a JLA-9.1000 rotor (Beckman Coulter Brea, CA). For live baculovirus inactivation, a 0.1 M binary ethylenimine (BEI) solution was freshly prepared by cyclization of 0.1 M 1-bromoethylamine hydrobromide (Sigma, St. Louis, MO) in 0.175 M NaOH at 37 °C for about one hour under continuous stirring. A drop in pH to 8.5 due to the formation of binary ethylenimine indicated the completion of the reaction. The solution was utilized at the day of preparation. Eight hundred mL expression supernatant was treated with 4% (v/v) BEI at 37 °C for 48 h on a shaking incubator set at 30 rpm. After live BV inactivation, residual BEI was neutralized by the addition of equimolar amounts of $Na_2S_2O_3$ (33 mL of a 0.1 M $Na_2S_2O_3$ solution). A clarification step (5.000 rpm, 4 °C, 30 min, JLA-9.1000 rotor) followed by a pre-filtration step of the inactivated supernatant using a 0.65 μM mPES MidiKros (0.75 mm 275 cm^2) tangential-flow filtration (TFF) membrane (Spectrum Labs, now Repligen, Waltham, MA) and a MasterFlex L peristaltic pump (Masterflex, Gelsenkirchen, DE) were employed to remove precipitates formed during BV inactivation. The microfiltrated supernatant was about 5-fold concentrated, diafiltered against four diavolumes of 0.2x PBS and further concentrated about 3-fold using a 500 kDa mPES MidiKros (1 mm, 245 cm^2) membrane (Spectrum Labs, now Repligen, Waltham, MA) and a semi-automated ÄktaFlux cross-flow filtration system (GE Life Sciences, Marlborough, MA). Samples were stored at 4 °C until further use.

2.4. Bioprocess monitoring and product characterization

The HA content in the expression supernatant and the purified VLP preparation was determined with the Influenza A H1N1 (A/

Puerto Rico/8/1934) Hemagglutinin/HA ELISA pair set (Sino Biological, Wayne, PA) as per the manufacturer's protocol with minor modifications. For the solubilization of VLP-incorporated HA surface glycoproteins, samples were pre-treated with the zwitterionic detergent Zwittergent 3–14 (1%, w/v) (Calbiochem, San Diego, CA) for 30 min at room temperature [16]. A soluble trimeric insect-cell expressed HA from PR8 protein served as calibration standard [17].

The retroviral Gag precursor polyprotein was indirectly quantified by measuring the concentration of p24, the major viral core structural protein generated by viral protease cleavage of Gag [18]. The concentration of soluble HIV-1 p24 and total HIV-1 p24 (including VLP-incorporated p24) in the expression supernatant and purified VLP preparation was determined by the HIV-1 p24 capsid protein p24 ELISA Kit (Sino Biological, Wayne, PA) as in [19]. Briefly, for the measurement of the total p24 concentration, VLPs were disrupted by incubation with SNCR buffer (containing denaturating and non-denaturating detergents) for 10 min at 70 °C followed by an incubation step with 0.5% (v/v) Triton X-100 for 10 min at 99 °C. Free soluble p24 protein was measured without treatment. The influenza HA and HIV-1 p24 ELISAs were both developed with 100 μL of the SIGMAFAST™ OPD substrate (Sigma Aldrich, St. Louis, MO) and the reaction was stopped by the addition of 25 μL 3 N H_2SO_4 solution. Absorbances were measured at 492 nm and 620 nm (reference wavelength) using a Tecan Infinite 200 Pro microplate reader (Tecan, Männedorf, CH) and data were fitted to a 4-PL model of a duplicate calibration curve. HA activity and total protein concentration were measured by Hemagglutination and Bradford Assay, respectively, as previously described [19,20].

2.5. Infectious agents and cells

For viral challenge, influenza virus A/Puerto Rico/8/34 (PR8, H1N1) and NIBRG-121xp, a 6:2 re-assortant containing the internal proteins of PR8 and surface glycoproteins HA and neuraminidase (NA) from influenza virus A/California/7/09 (H1N1), were used. The viruses were obtained from the WHO Collaborating Center for Reference and Research of Influenza (St. Petersburg, Russia) and were propagated in 9-day-old embryonated hens' eggs at 37 °C. For bacterial challenge, *Staphylococcus aureus* No.884, a human isolate from a patient who died from pneumonia, was obtained from the Collective Usage Center "Collection of I. Mechnikov Research Institute for Vaccines and Sera (Moscow, Russia) and was propagated on Staphylococcus Agar No. 110 (Himedia Laboratories, Mumbai, IO). To prepare bacteria for bacterial challenge, a freshly inoculated culture was grown to an OD_{600} of 0.6 in Nutient Broth No. M002 (Himedia Laboratories, Mumbai, IO) and was diluted in PBS to a concentration 2×10^{10} CFU/ml prior to use. *Sf*9 (ATCC # CRL-1711) and *Tnms*42 insect cells (a gift from G. Blissard, Boyce Thompson Institute, NY) were maintained as adherent cultures at 27 °C in Hyclone SFM4 Insect cell culture medium (GE Life Sciences, Marlborough, MA) supplemented with 0.1% (w/v) Pluronic F-68 (Sigma, St. Louis, MO) and were expanded in suspension for rBV propagation or recombinant protein production.

2.6. Immunization and infection schedule

Four-to-six-week old female BALB/c mice were purchased from the Research Centre for Biomedical Technology (Andreevka, Moscow) and were assigned into groups of 7–19 mice. Vaccine groups (n = 19) received either one or two intraperitoneal (IP) immunizations (100 μL) with BV-inactivated influenza HA-Gag VLPs (termed 1x PR8-Gag VLPs, 2x PR8-Gag VLPs) at a dose of 0.05 μg HA per mouse 21 days apart or vector control (PBS). The non-vaccinated reference groups (n = 13–14) (termed PR8 + *S. aureus* or NIBRG-121xp + *S. aureus*) and virus-only and bacteria-only control groups (n = 7–9, termed PR8-only, NIBRG-121xp-only or *S. aureus*-only) were administered PBS on the respective days (Fig. 2A and B).

Prior to the delivery of infectious agents, mice were lightly anesthetized and were held in an upright position for intranasal viral (30 μL/nostril) or bacterial (50 μL/nostril) infection. Twenty-one days after the last immunization, vaccine groups and non-vaccinated reference groups were infected with 100 $TCID_{50}$ of PR8 (vaccine match) or 1000 $TCID_{50}$ of NIBRG-121xp (homosubtypic vaccine mismatch). Five days post viral infection, mice were inoculated with 2×10^9 CFU of *S. aureus* №884 for bacterial secondary infection. Control groups challenged with a single pathogen received PBS on the respective days of infection. Body weight was recorded every other day for a period of 18 days after viral infection. Animals that lost 30% or more or their initial body weight were scored dead and humanely euthanized.

2.7. Immunological assays

Pre-challenge sera were collected 21 days after the last immunization for the analysis of influenza virus-specific hemagglutination-inhibition antibodies. Six mice per vaccine group were humanely killed and individual pre-challenge sera were collected and treated with three volumes of receptor-destroying enzyme (RDE, Denka Seiken, Tokyo, JP) overnight at 37 °C followed by enzyme inactivation at 56 °C for 30 min. Sera were further diluted with physiological saline to yield a 1:10 dilution of the original serum sample. Sera were serially two-fold diluted with PBS (50 μL) in U-bottom microwell plates and were incubated with viruses PR8 or NIBRG-121xp, standardized at 8 HAU/50 μL. The mixtures were pre-incubated for 60 min at room temperature and were mixed with 100 μL of 1% (v/v) chicken red blood cells for another 60 min at room temperature. The hemagglutination-inhibition (HI)-titer was calculated from the reciprocal of the highest dilution that completely inhibited hemagglutination of red blood cells and geometric mean titers (GMTs) were calculated. Individual negative results were scored a value of five for the calculation of GMTs.

2.8. Measurement of viral and bacterial pulmonary titers

Viral pulmonary titers were measured two days before and after bacterial secondary infection (n = 3 per group, except control group receiving bacteria only), whereas bacterial load was determined two days after bacterial infection only (n = 3 per group). Whole lungs of mice were harvested at the given time points, thoroughly rinsed with sterile PBS, homogenized and resuspended in one mL of cold, sterile PBS. For the determination of bacterial titers, each lung homogenate was serially diluted (1:10) in PBS and aliquots of the homogenate and diluted samples were plated on tryptic soy agar plates supplemented with 3% (v/v) sheep erythrocytes. Plates were incubated at 37 °C, 5% (v/v) CO_2 and bacterial colonies counted after 18–24 h. For the determination of viral titers, lung homogenates were cleared of cellular debris by centrifugation at 2000g for 10 min. One hundred microliter of the supernatants were injected into the allantoic cavity of 9-day-old embryonated hens' eggs to determine the 50% egg infectious dose (EID_{50}). Viral and bacterial titers in mouse lungs were calculated as the mean $\log_{10}$ EID_{50}/mL or $\log_{10}$CFU/mL ± SE, respectively.

2.9. Statistical analyses

Pre-challenge serum HI-titers and pulmonary viral and bacterial titers were either analyzed using the unpaired Student *t* test or One-Way ANOVA followed by a post hoc Tukey's test for multiple comparisons. Weight loss curves were compared by multiple *t*

tests and the Holm-Sidak method to determine statistical significance at each time point of the weight curve. Survival curves were analyzed using the Mantel-Cox and Gehan-Breslow-Wilcoxon-Test. Statistical analyses were performed using the GraphPad Prism 8 software (GraphPad, San Diego, CA)

3. Results

3.1. Production and characterization of influenza A HA-Gag VLPs expressed in Tnms42 insect cells

A recombinant influenza VLP preparation was produced in *Tnms*42 insect cells by infection with a recombinant baculovirus expressing the HA of influenza A/Puerto Rico/8/34 (H1N1) and the HIV-1 Gag protein under the *AcMNPV* p10 and pH promoter respectively. Using a synchronous cell infection strategy (MOI 5), cell growth was immediately arrested after infection and cell viability began to decline (Fig. 1A). We decided for a non-influenza viral capsid protein with robust particle budding properties to exclusively evaluate anti-HA immunity in a postinfluenza superinfection model [21]. The HA and p24 antigens accumulated in the supernatant, predominantly within the first 48 h of baculovirus infection, and there already accounted for 100% and 91.6% of the final titers at harvesting time respectively (Fig. 1B and C). P10 promoter-driven HA expression reached a plateau earlier in the infection cycle than pH promoter-driven Gag expression, which is in accordance with earlier maximum synthesis rates of the p10 promoter [22]. The ratio of particle-incorporated to total p24 titer in the supernatant was highest in the early stage of infection and decreased with declining cell viability and the concomitant liberation of Gag protein from the cytoplasm due to cell lysis (Fig. 1C, 24 h post infection (hpi): 86% versus 72 hpi: 68%). The dramatic increase in total protein in the supernatant within the first 24 h post infection (Fig. 1D) is assumed to be linked to rBV accumulation by virus budding, starting at about 20 h post infection [23]. The supernatant was harvested 72 h post infection and contained biologically active HA protein (5.12×10^6 HAU/L) at a volumetric HA yield of 2.67 mg/L, which accounted for 1.4% of the total protein present in the harvest. The total p24-concentration in the supernatant (after VLP disruption) was 0.0192 mg/L; 58.5% of which was available as particle-incorporated p24 protein. BEI-treatment for the inactivation of live baculovirus in the supernatant resulted in a 4-fold drop in HA activity to 64 HAU/50 μL (data not shown). BEI-inactivation was accompanied by a slight alkalization of the culture medium (~pH 7.7) and the formation of inorganic salt precipitates, which may have been partially responsible for some quantitative loss of protein by co-precipitation. Despite earlier beliefs, several DNA alkylating agents were shown to chemically modify amino acids and thereby account for altered antigenic properties [24,25]. BEI has not yet been extensively investigated in this context and we therefore cannot exclude BEI-mediated protein modifications at the erythrocyte binding site as cause for the qualitative loss of erythrocyte binding in our assay [26]. Different BEI concentrations (1–20%, v/v) and inactivation temperatures (RT, 30 °C and 37°) had been tested in a preliminary screening and 4% (v/v) BEI at 37 °C was identified as condition with acceptable loss of biological activity and incubation time (data not shown). A 500 kDa tangential-flow filtration was employed to purify higher-molecular-weight particles from soluble proteins, which was confirmed by the absence of soluble free p24-protein (<0.1 ng/mL) in the final preparation. The vaccine dose contained 0.05 μg HA with an activity of 128 HAU and 0.001 μg VLP-incorporated p24 protein (Fig. 1E). The absence of live baculovirus in the final VLP preparation was proven by the inoculation of one mL (20 vaccine

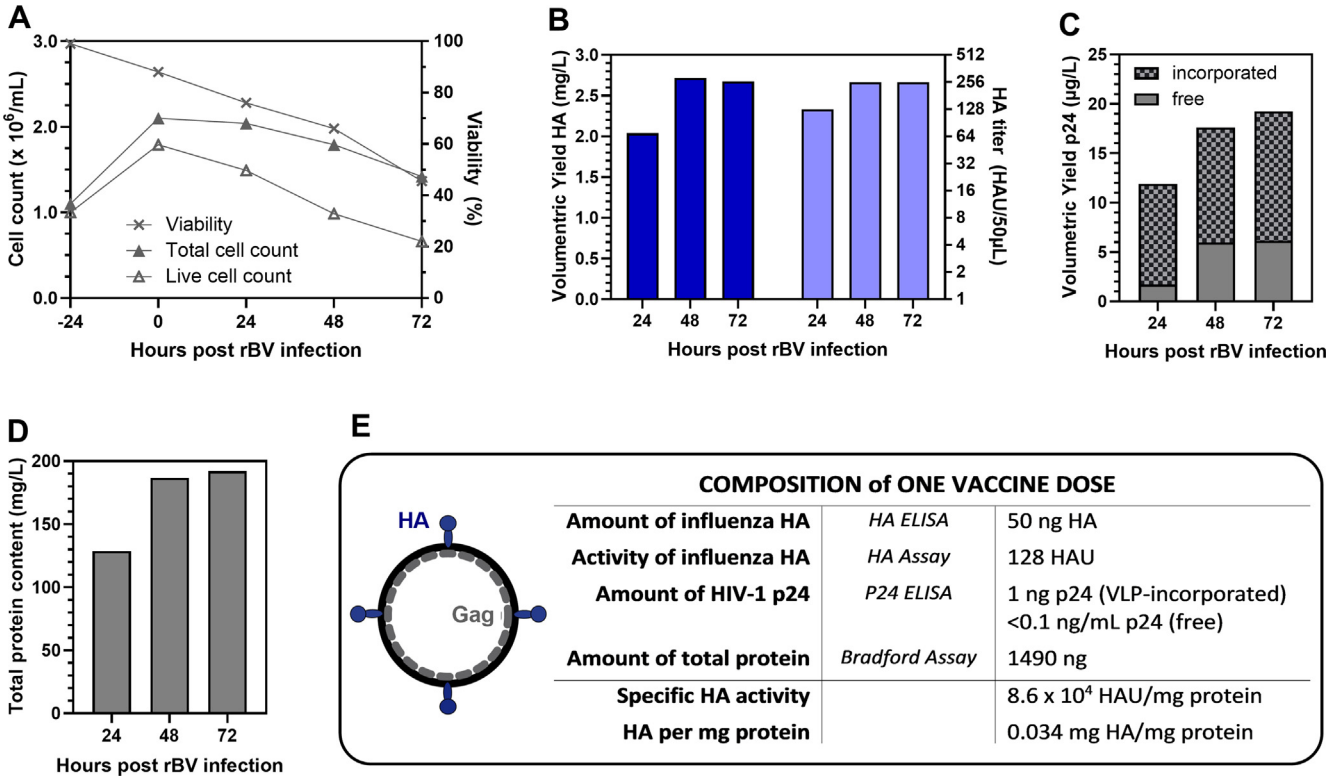

Fig. 1. Production of influenza HA-Gag VLPs. Over the course of the production process, **(A)** *Tnms*42 cell growth and viability, **(B)** volumetric HA yield and HA activity, **(C)** volumetric p24 protein yield and **(D)** total protein content in the expression supernatant was followed on a daily basis. The fraction of soluble free Gag versus VLP-incorporated Gag was determined by a p24-ELISA, whereby the latter has been assayed after treatment with buffer and detergent under heat to disrupt enveloped VLPs for the release of incorporated Gag protein. **(E)** The composition of a single vaccine dose and the respective analytical assays employed for quantification are given.

doses) to an adherent *Sf*9 cell culture, which did not result in YFP-expression of cells within five days of cultivation, as monitored by fluorescence microscopy (data not shown).

3.2. Matched anti-HA immunity potently protects mice from postinfluenza S. aureus infection, morbidity and mortality

We first aimed to assess the off-target effects of matched anti-HA immunity conferred by a recombinant influenza vaccine in a murine postinfluenza *S. aureus* model (Fig. 2A and B). BALB/c mice received one or two IP-immunizations with HA-Gag VLPs at a dose of 0.05 μg HA and three weeks later mice were sequentially infected with homologous influenza PR8 and five days later with *S. aureus*. This time point was demonstrated to render mice highly susceptibility to bacterial invasion after influenza infection [9]. In fact, with our superinfection model we could confirm that non-vaccinated superinfected mice displayed a well-described phenomenon of mutual enhancement of virus and bacterial replication (Fig. 3B and C) [9,27]. In contrast to the viral mono-infection group, where virus was detected in the lungs three days post infection (mean titer: 4.7 ± 0.3 $\log_{10}EID_{50}$/mL) and cleared by day seven, superinfected animals were not able to restrain virus replication in the lungs on day 7 (Fig. 3B). Superinfected mice even showed a rebound in viral titers manifest as a significant 3-log increase from day three to day 7 (day 7: 7.7 ± 1.5 $\log_{10}EID_{50}$/mL, adjusted p-value = 0.013). In addition to this increase in viral titers, superinfected mice displayed a defect in bacterial clearance in contrast to the bacterial mono-infected group (Fig. 3C).

The VLP preparation appeared to be highly immunogenic, inducing HI-antibodies with a geometric mean titer of 35.6 after single immunization, which could be significantly increased to a level of 71.3 ($p = 0.0017$) after booster immunization (Fig. 3A). Induced HI-titers were predictive of vaccine efficacy against influenza challenge and a single vaccine dose was sufficient to prevent homologous virus replication in the lungs (Fig. 3B). A single VLP vaccine dose also supported earlier clearance of the bacterial pathogen, demonstrated by no detectable *S. aureus* load in the lungs by day two post bacterial challenge in contrast to non-vaccinated mice (Fig. 3C, $p_{adjusted} = 0.0031$). Mice in both vaccine groups displayed no significant weight loss during the observation period (Fig. 3D, range 1.8–4.2%). In contrast to non-vaccinated mice (14.3% survival) matching anti-HA immunity elicited by a single low VLP dose conferred 100% protection from mortality associated with lethal postinfluenza *S. aureus* superinfection (Fig. 3D, $p = 0.0013$ Mantel-Cox test; $p = 0.0019$ Gehan-Breslow-Wilcoxon test).

3.3. Mismatched anti-HA immunity fails to protect from secondary bacterial infection

Seasonal influenza vaccines are not always matching the invading viral strains. This is why vaccine effectiveness is generally moderate and has not been exceeding 40% on average during the last 15 influenza seasons in the US, as described by observational studies conducted by the Centers for Disease control and Prevention (CDC) (https://www.cdc.gov/flu/vaccines-work/effectiveness-studies.htm). In this respect, we aimed to evaluate the efficacy of mismatched anti-HA immunity on limiting postinfluenza *S. aureus* replication and lethality using a divergent H1N1 challenge strain (NIBRG-121xp). Mice were immunized and infected according to the schedule in Fig. 2A. Since PR8-specific antibodies were not capable of suppressing HA activity of the heterologous challenge strain, (Fig. 4A), viral infection could not be restrained by single or double immunization (GMT range day 4: 4.0–4.3 $\log_{10}EID_{50}$/mL). In these groups, viral replication was significantly enhanced by staphylococcal infection (Fig. 4B, range 7.0–7.3 $\log_{10}EID_{50}$/mL, $p < 0.001$), similarly to non-vaccinated superinfected mice. In contrast, mice challenged with virus only were able to clear the infection by day 7 (Fig. 4B). A single immunization showed no effect in terms of limiting viral and bacterial replication (Fig. 4B and C). Interestingly, two immunizations with the non-matching vaccine could provide significant protection from weight loss on day three (Fig. 4D, $p_{adjusted} = 0.037$) and we saw some trend in protection from mortality in contrast to non-vaccinated animals (Fig. 4E, 57% vs 25% survival). This latter effect, however, was not significant ($p = 0.5121$ Mantel-Cox test; $p = 0.7547$ Gehan-Breslow-Wilcoxon test).

A

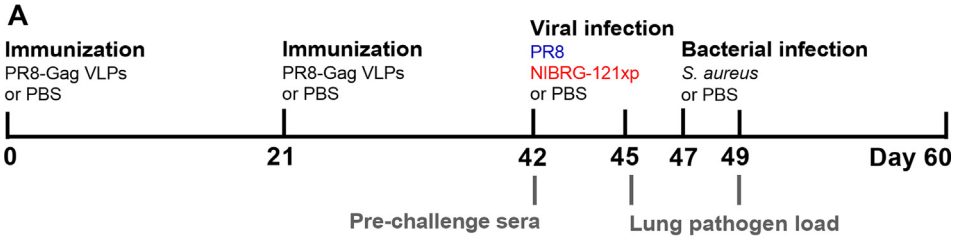

B

Groups		N	Primary pathogen	Secondary pathogen		N
1x PR8-Gag VLPs	*Vaccinated mice*	19	100 $TCID_{50}$ PR8	2x10^9 CFU *S.aureus*	*Mice monitored for body weight & survival*	7
2x PR8-Gag VLPs		19				7
Non-vaccinated		13				7
1x PR8-Gag VLPs		19	1000 $TCID_{50}$ NIBRG-121xp	2x10^9 CFU *S.aureus*		7
2x PR8-Gag VLPs		19				7
Non-vaccinated		14				7
S.aureus - only		7	PBS	2x10^9 CFU *S.aureus*		4
PR8 - only		8	100 $TCID_{50}$ PR8	PBS		5
NIBRG-121xp-only		9	1000 $TCID_{50}$ NIBRG-121xp	PBS		6

Fig. 2. Study schedule (A) and study groups (B). The VLP preparation was evaluated in a murine BALB/c postinfluenza superinfection model using parenteral prime-only and prime-boost immunization regimens followed by sequential infection with homologous influenza PR8 or heterologous NIBRG-121xp virus and *S. aureus* infection five days apart. Non-vaccinated reference groups and virus/bacteria-only control groups were mock-vaccinated (PBS) or mock-infected (PBS) on the respective other days. Mice were sacrificed for the determination of pre-challenge serum HI titers (n = 6, vaccine groups only) and lung pathogen loads (n = 3).

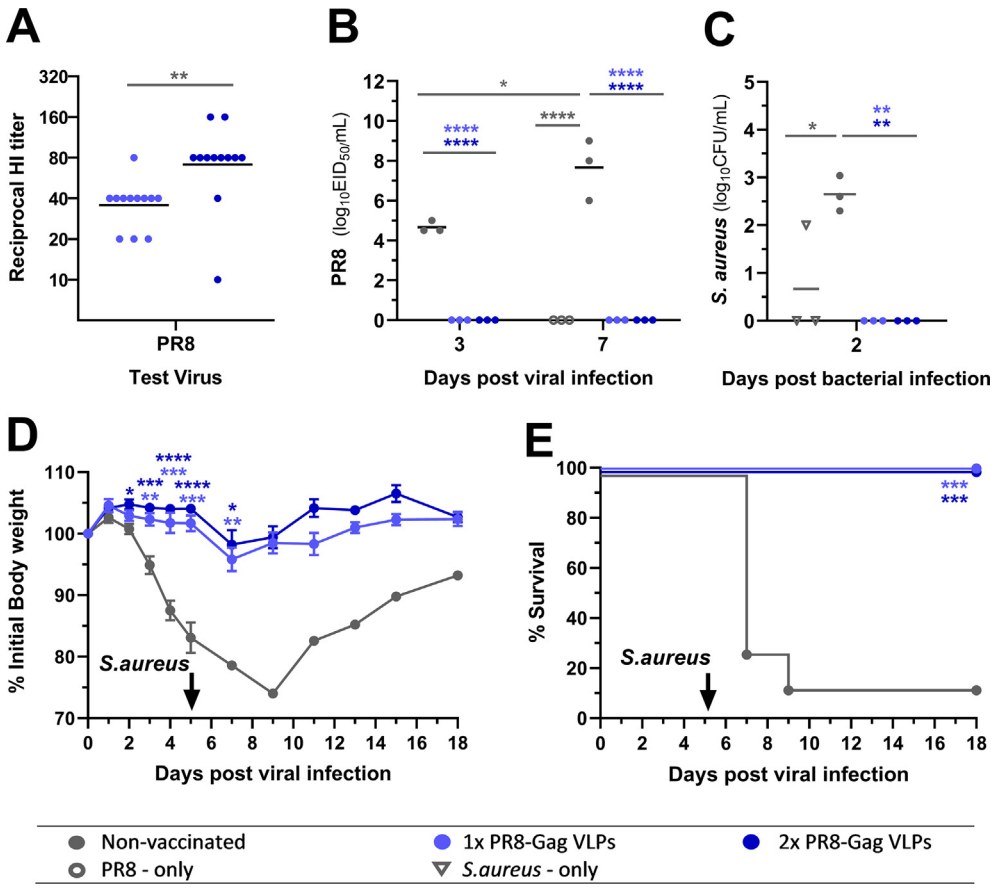

Fig. 3. Matched anti-HA immunity potently protects mice from secondary *S. aureus* infection. BALB/c mice received a single ot two IP-immunizations with VLPs at a dose of 0.05 μg HA per mouse 21 days apart or were mock-vaccinated with PBS. Three weeks after the last immunization, mice were infected with homologous influenza virus PR8 and *S. aureus* five days later. **(A)** On the day of viral infection six mice from all vaccine groups (undergoing homologous and heterologous viral challenge) were sacrificed for the determination of HI-antibodies against the homologous influenza strain. An unpaired two-tailed *t*-test was used to compare geometric mean titers of neutralizing antibodies. **(B)** Viral and **(C)** bacterial burden in the lungs of mice (n = 3) were measured two days before and after bacterial challenge and were analyzed by One-way-ANOVA and the Tukey's multiple comparison test. **(D)** Weight loss curves were analyzed by multiple *t* tests and the Holm-Sidak method. Error bars give the standard error of the mean. **(E)** Survival curves of the vaccine and control groups were compared using the Mantel-Cox (log-Rank)-test and the Gehan-Breslow-Wilcoxon test respectively. (*p < 0.05, **p < 0.01, ***p < 0.001, ****p < 0.0001).

4. Discussion

Since there is no *Staphylococcus aureus* prophylaxis available and the number of strains refractory to antibiotic treatment are rising influenza vaccination currently appears to be the only strategy to mitigate postinfluenza *S. aureus* infections and associated pathology [2–5,12]. In the present work, we investigated the vaccine off-target effects of a recombinant influenza VLP preparation on limiting postinfluenza *S. aureus* complications in BALB/c mice. In light of current influenza vaccines exclusively being standardized on basis of the hemagglutinin content it was our particular interest to assess whether anti-HA immunity alone was sufficient to limit secondary bacterial complications in the context of an influenza vaccine match and mismatch [28].

The immunogen we employed was a retroviral Gag-VLP preparation pseudo-typed with the HA of PR8 as exclusive influenza antigen. VLPs were produced using the novel *Trichoplusia ni* insect cell line *Tnms*42, an *Alphanodavirus*-free derivative of the High Five™ (BTI-TN-5NI-4) cell line [13,14]. Earlier reports of our group described *T.ni*-derived cell lines as being superior to *Sf*9 cells in terms of secretory capacity and influenza VLP yield [29,30]. Without any prior bioprocess development efforts, we readily obtained high levels of biologically active protein (5.12×10^6 HAU/L) at a volumetric yield of 2.67 mg HA/L in the harvest three days post infection (Fig. 1B). This is in agreement with what has been previously reported for High Five™ cells expressing influenza HA-M1 VLPs (3 mg HA/L), suggesting that *Tnms*42 cells may be equally well suited for the expression of recombinant secreted proteins [30]. The target antigen content in the TFF-purified VLP preparation was 0.034 mg HA per mg total protein. This antigen content is slightly lower but in the range of what other groups have described for insect cell-derived influenza VLP preparations (5–10% HA of total protein) purified by methods aiming at the purification/concentration of particulate structures, such as VLPs and baculoviruses [31,32]. As studies demonstrated that live rBV impurities in insect cell-derived VLP preparations may trigger innate immunity we decided to inactivate recombinant baculovirus by BEI-treatment to prevent any rBV-mediated adjuvant effects from biasing our assessment [21].

Owing to their repetitive surface geometry and particulate nature, VLPs per se exhibit two important features of traditional live-attenuated influenza vaccines (LAIVs) or inactivated influenza vaccines (IIVs) that support vaccine immunogenicity. Indeed, VLP one-dose regimens were often sufficient to elicit effective anti-influenza immunity in humans and mice, demonstrating the feasibility of the VLP-approach for expanding supplies of influenza vaccines [20,33–35]. The *Tnms*42-derived VLP preparation was highly immunogenic inducing HI-antibody titers of ≥40 in 9 out of 12 mice at a dose of 50 ng HA after single immunization (Fig. 3A). Using the influenza – *S. aureus* superinfection model we could

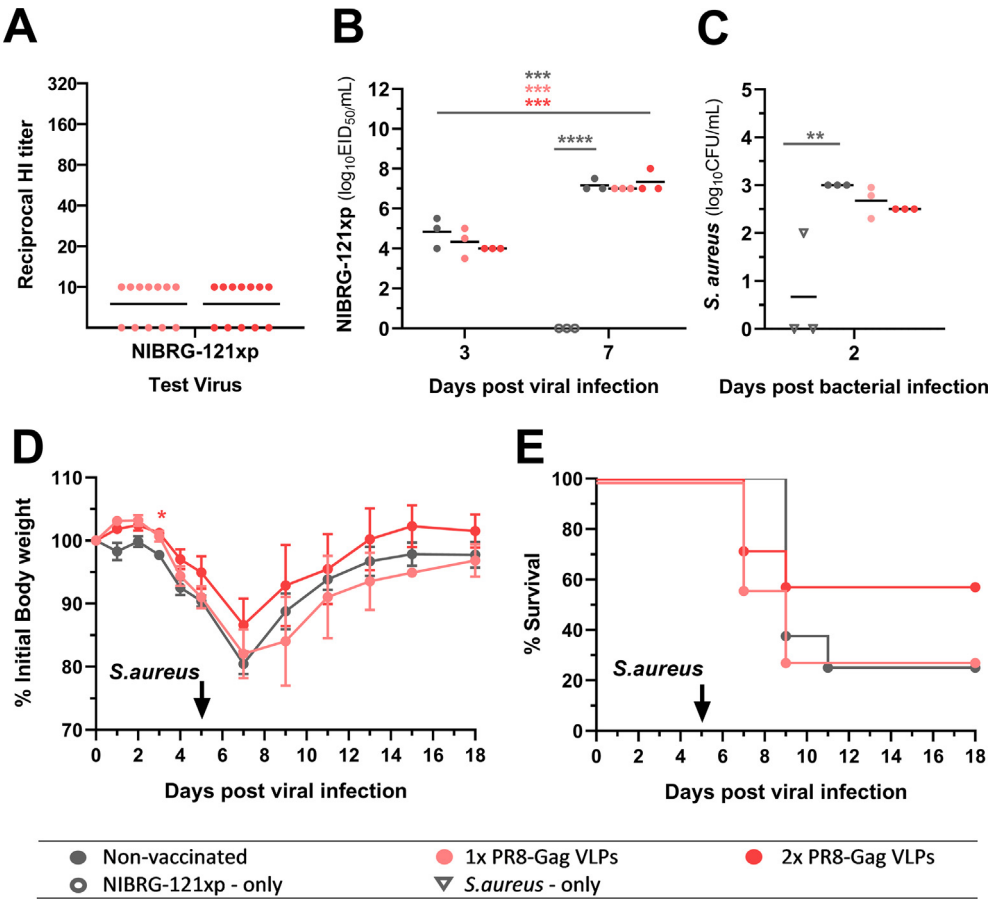

Fig. 4. Mismatched anti-HA immunity fails to protect mice from secondary bacterial infection and associated morbidity and mortality. BALB/c mice received one or two IP-immunizations with VLPs at a dose of 0.05 μg HA 21 days apart or were mock-vaccinated with PBS. Three weeks after the last immunization, mice were infected with heterologous influenza virus NIBRG-121xp (a PR8:CAL09(6:2)-re-assortant) and *S. aureus* five days later. **(A)** HI-assay with pre-challenge sera from immunized mice (n = 6 per vaccine group) using NIBRG-121xp as test virus. An unpaired two-tailed *t*-test was used to compare the geometric mean HI-antibody titers **(B)** Viral and **(C)** bacterial burden in the lungs of mice (n = 3) two days before and after bacterial challenge were analyzed by One-way-ANOVA and the Tukey's multiple comparison test. **(D)** Weight loss and **(E)** survival curves of immunized and non-vaccinated mice were analyzed by a multiple *t* test and the Holm-Sidak method as well as the Mantel-Cox (log-Rank)-test and the Gehan-Breslow-Wilcoxon test respectively (*p < 0.05, **p < 0.01, ***p < 0.001, ****p < 0,0001). Error bars in the weight loss curves indicate the SEM.

demonstrate that anti-HA immunity elicited by this low antigen dose was sufficient to prevent influenza replication and secondary bacterial complications, which was in first line reflected by a full protection from lethality (Fig. 3E, $p < 0.005$). A single immunization inhibited primary viral infection (Fig. 3B, $p < 0.0001$), which in turn allowed for full clearance of the bacterial density by day two post bacterial inoculation, in contrast to non-vaccinated mice (Fig. 3C, $p < 0.0001$). By comparison, a study by Chaussee and co-workers, demonstrated incomplete protection from secondary *Streptococcus pyogenes* infection after two immunizations with a matched IVV (3 μg HA per mouse) or LAIV using an equally lethal superinfection model [36]. However, this comparison is not indicative of the efficacy of certain types of vaccines, as bacterial strains/species differ in their potential to cause secondary bacterial pneumonia [37].

Overcoming strain-specificity of traditional influenza vaccines has until today been a major challenge in influenza vaccinology. In this respect, studies have appreciated VLPs as attractive platform capable of eliciting broader or more balanced immune responses in contrast to conventional vaccines in mice [38,34]. In our study, anti-HA immunity was not sufficient to protect immunized mice from secondary bacterial infection in the context of a preceding viral challenge with an antigenically divergent (81.7% sequence identity) H1N1 influenza strain. There, we observed an already described phenomenon of mutual enhancement of virus and bacterial replication, similarly to what we have seen for non-vaccinated mice (Fig. 4B and C) [9]. In contrast to our results, Zurli *et al*, were able to demonstrate significant protection from secondary *S. aureus* infection after a heterologous CAL09 virus infection when using an influenza PR8 subunit vaccine [39]. However, their vaccine contained an additional influenza antigen (the NA) and adjuvant. In fact, with testing different adjuvant supplements they were able to bias T-helper cell profiles in a way to exert different degrees of by-stander effects in the context of mismatched influenza immunity and secondary *S. aureus* infection [39]. In this respect, it would be of interest to what extent our VLP preparation is able to elicit influenza-specific T-cell immunity and whether the inclusion of the NA antigen into the VLP formulation would improve its cross-protection potential. Apart from HA-based-immunity, anti-NA immunity has already been demonstrated to limit SBI severity and mortality in a *S. pneumoniae* superinfection model by Huber and co-workers, while the inhibition of neuraminidase activity has been proven helpful in the treatment of postinfluenza bacterial pneumonia [40,41]. We observed significant protection from morbidity on day three post viral infection (Fig. 4D, $p = 0.0034$) as well as a trend in providing protection from mortality (Fig. 4E, 57% versus 25% survival). This latter effect, however, was not significant and may be due to non-neutralizing HA-specific humoral or cell-mediated responses (Fig. 4A), which we did not investigate.

In conclusion, our results confirm that apart from preventing influenza disease, influenza vaccination provides off-target bene-

fits on limiting secondary staphylococcal infections. We could demonstrate that postinfluenza *S. aureus* infections and complications can be mitigated by adequate anti-HA immunity elicited by a highly immunogenic insect cell-expressed HA-Gag VLP preparation. Our results further suggest that anti-HA immunity should not be considered as the sole preventive method for limiting influenza, as we thereby may not exploit the full beneficial impact of influenza vaccination on on-target and potential off-target pathogens.

Declaration of Competing Interest

The authors declare that they have no known competing financial interests or personal relationships that could have appeared to influence the work reported in this paper.

Acknowledgements

We would like to thank Nune O. Vartanova (Department of Microbiology, I. Mechnikov Research Institute for Vaccines and Sera), Nadezhda P. Kartashova and Ekaterina A. Glubokova (Department of Virology, I. Mechnikov Research Institute for Vaccines and Sera) and Petra Steppert (Department of Biotechnology, BOKU) for technical support.

This bilateral joint-project is funded by the Austrian Science Fund (FWF grant I 3490-B30) and the Russian Science Foundation (RSF grant 18-45-05002). FS and SG were funded by the Competence Centre ACIB in the framework of the Austrian FFG-COMET-Funding Program supported by the Federal Ministry for Transport, Innovation and Technology (bmvit), the Federal Ministry for Digital and Economic Affairs (bmwd) the Styrian Business Promotion Agency SFG, Standortagentur Tirol, the Government of Lower Austria and ZIT—the Technology Agency of the City of Vienna. The funding agencies had no influence on the conduct of this research.

Author's contributions

Conceived and designed the experiments: MK, IL, AE, RG; performed the experiments: MK, FS, SG, AK, IF, AP, NM, OS; analyzed and interpreted the data: MK, AE; administrated the project: MK, IL; wrote the paper: MK, AE; all authors contributed to the final manuscript.

References

[1] Robertson L, Caley JP, Moore J. Importance of staphylococcus aureus in pneumonia in the 1957 epidemic of influenza A. Lancet 1958;272:233–6. https://doi.org/10.1016/S0140-6736(58)90060-6.

[2] Morens DM, Taubenberger JK, Fauci AS. Predominant role of bacterial pneumonia as a cause of death in pandemic influenza: implications for pandemic influenza preparedness. J Infect Dis 2008;198:962–70. https://doi.org/10.1086/591708.

[3] Finelli L, Fiore A, Dhara R, Brammer L, Shay DK, Kamimoto L, et al. Influenza-associated pediatric mortality in the United States: increase of Staphylococcus aureus coinfection. Pediatrics 2008;122:805–11. https://doi.org/10.1542/peds.2008-1336.

[4] Metersky ML, Masterton RG, Lode H, File TM, Babinchak T. Epidemiology, microbiology, and treatment considerations for bacterial pneumonia complicating influenza. Int J Infect Diseases 2012;16:e321–31. https://doi.org/10.1016/j.ijid.2012.01.003.

[5] Nguyen T, Kyle UG, Jaimon N, Tcharmtchi MH, Coss-Bu JA, Lam F, et al. Coinfection with Staphylococcus aureus increases risk of severe coagulopathy in critically ill children with influenza A (H1N1) virus infection. Crit Care Med 2012;40:3246–50. https://doi.org/10.1097/CCM.0b013e318260c7f8.

[6] Wertheim HFL, Melles DC, Vos MC, van Leeuwen W, van Belkum A, Verbrugh HA, et al. The role of nasal carriage in Staphylococcus aureus infections. Lancet Infect Dis 2005;5:751–62. https://doi.org/10.1016/S1473-3099(05)70295-4.

[7] Nita-Lazar M, Banerjee A, Feng C, Amin MN, Frieman MB, Chen WH, et al. Desialylation of airway epithelial cells during influenza virus infection enhances pneumococcal adhesion via galectin binding. Mol Immunol 2015;65:1–16. https://doi.org/10.1016/j.molimm.2014.12.010.

[8] Shepardson KM, Larson K, Morton RV, Prigge JR, Schmidt EE, Huber VC, et al. Differential Type I interferon signaling is a master regulator of susceptibility to postinfluenza bacterial superinfection. MBio 2016;7:e00506–e516. https://doi.org/10.1128/mBio.00506-16.

[9] Rynda-Apple A, Harmsen A, Erickson AS, Larson K, Morton RV, Richert LE, et al. Regulation of IFN-γ by IL-13 dictates susceptibility to secondary postinfluenza MRSA pneumonia. Eur J Immunol 2014;44:3263–72. https://doi.org/10.1002/eji.201444582.

[10] Fowler VG, Proctor RA. Where does a Staphylococcus aureus vaccine stand?. Clin Microbiol Infect 2014;20:66–75. https://doi.org/10.1111/1469-0691.12570.

[11] McNeely TB, Shah NA, Fridman A, Joshi A, Hartzel JS, Keshari RS, et al. Mortality among recipients of the Merck V710 Staphylococcus aureus vaccine after postoperative S. aureus infections: an analysis of possible contributing host factors. Hum Vaccin Immunother 2014;10:3513–6. https://doi.org/10.4161/hv.34407.

[12] Redi D, Raffaelli CS, Rossetti B, De Luca A, Montagnani F. Staphylococcus aureus vaccine preclinical and clinical development: current state of the art. New Microbiol 2018;41:208–13.

[13] Shrestha A, Bao K, Chen Y-R, Chen W, Wang P, Fei Z, et al. Global analysis of baculovirus autographa californica multiple nucleopolyhedrovirus gene expression in the midgut of the lepidopteran host Trichoplusia ni. J Virol 2018;92. https://doi.org/10.1128/JVI.01277-18.

[14] Koczka K, Peters P, Ernst W, Himmelbauer H, Nika L, Grabherr R. Comparative transcriptome analysis of a Trichoplusia ni cell line reveals distinct host responses to intracellular and secreted protein products expressed by recombinant baculoviruses. J Biotechnol 2018;270:61–9. https://doi.org/10.1016/j.jbiotec.2018.02.001.

[15] Nika L, Wallner J, Palmberger D, Koczka K, Vorauer-Uhl K, Grabherr R. Expression of full-length HER2 protein in Sf9 insect cells and its presentation on the surface of budded virus-like particles. Protein Expr Purif 2017;136:27–38. https://doi.org/10.1016/j.pep.2017.06.005.

[16] Rajendran M, Sun W, Comella P, Nachbagauer R, Wohlbold TJ, Amanat F, et al. An immuno-assay to quantify influenza virus hemagglutinin with correctly folded stalk domains in vaccine preparations. PLoS ONE 2018;13. https://doi.org/10.1371/journal.pone.0194830.

[17] Klausberger M, Tscheliessnig R, Neff S, Nachbagauer R, Wohlbold TJ, Wilde M, et al. Globular head-displayed conserved influenza H1 hemagglutinin stalk epitopes confer protection against heterologous H1N1 virus. PLoS ONE 2016;11:. https://doi.org/10.1371/journal.pone.0153579e0153579.

[18] Peng C, Ho BK, Chang TW, Chang NT. Role of human immunodeficiency virus type 1-specific protease in core protein maturation and viral infectivity. J Virol 1989;63:2550–6.

[19] Reiter K, Aguilar PP, Wetter V, Steppert P, Tover A, Jungbauer A. Separation of virus-like particles and extracellular vesicles by flow-through and heparin affinity chromatography. J Chromatogr A 2019;1588:77–84. https://doi.org/10.1016/j.chroma.2018.12.035.

[20] Klausberger M, Wilde M, Palmberger D, Hai R, Albrecht RA, Margine I, et al. One-shot vaccination with an insect cell-derived low-dose influenza A H7 virus-like particle preparation protects mice against H7N9 challenge. Vaccine 2014;32:355–62. https://doi.org/10.1016/j.vaccine.2013.11.036.

[21] Margine I, Martinez-Gil L, Chou Y, Krammer F. Residual baculovirus in insect cell-derived influenza virus-like particle preparations enhances immunogenicity. PLoS One 2012;7. https://doi.org/10.1371/journal.pone.0051559.

[22] Roelvink PW, van Meer MM, de Kort CA, Possee RD, Hammock BD, Vlak JM. Dissimilar expression of Autographa californica multiple nucleocapsid nuclear polyhedrosis virus polyhedrin and p10 genes. J Gen Virol 1992;73(Pt 6):1481–9. https://doi.org/10.1099/0022-1317-73-6-1481.

[23] Rohrmann GF. The baculovirus replication cycle: Effects on cells and insects. National Center for Biotechnology Information (US) 2013.

[24] Käsermann F, Wyss K, Kempf C. Virus inactivation and protein modifications by ethyleneimines. Antiviral Res 2001;52:33–41. https://doi.org/10.1016/S0166-3542(01)00157-7.

[25] She Y-M, Cheng K, Farnsworth A, Li X, Cyr TD. Surface modifications of influenza proteins upon virus inactivation by β-propiolactone. Proteomics 2013;13:3537–47. https://doi.org/10.1002/pmic.201300096.

[26] Bradley KC, Galloway SE, Lasanajak Y, Song X, Heimburg-Molinaro J, Yu H, et al. Analysis of influenza virus hemagglutinin receptor binding mutants with limited receptor recognition properties and conditional replication characteristics. J Virol 2011;85:12387–98. https://doi.org/10.1128/JVI.05570-11.

[27] Warnking K, Klemm C, Löffler B, Niemann S, van Krüchten A, Peters G, et al. Super-infection with Staphylococcus aureus inhibits influenza virus-induced type I IFN signalling through impaired STAT1-STAT2 dimerization. Cell Microbiol 2015;17:303–17. https://doi.org/10.1111/cmi.12375.

[28] Wong S-S, Webby RJ. Traditional and New Influenza Vaccines. Clin Microbiol Rev 2013;26:476–92. https://doi.org/10.1128/CMR.00097-12.

[29] Krammer F, Schinko T, Palmberger D, Tauer C, Messner P, Grabherr R. Trichoplusia ni cells (High Five) are highly efficient for the production of influenza A virus-like particles: a comparison of two insect cell lines as production platforms for influenza vaccines. Mol Biotechnol 2010;45:226–34. https://doi.org/10.1007/s12033-010-9268-3.

[30] Krammer F, Nakowitsch S, Messner P, Palmberger D, Ferko B, Grabherr R. Swine-origin pandemic H1N1 influenza virus-like particles produced in insect cells induce hemagglutination inhibiting antibodies in BALB/c mice. Biotechnol J 2010;5:17–23. https://doi.org/10.1002/biot.200900267.

[31] Quan F-S, Huang C, Compans RW, Kang S-M. Virus-like particle vaccine induces protective immunity against homologous and heterologous strains of influenza virus. J Virol 2007;81:3514–24. https://doi.org/10.1128/JVI.02052-06.
[32] Quan FS, Yoo D-G, Song J-M, Clements JD, Compans RW, Kang S-M. Kinetics of immune responses to influenza virus-like particles and dose-dependence of protection with a single vaccination. J Virol 2009;83:4489–97. https://doi.org/10.1128/JVI.02035-08.
[33] Pillet S, Aubin É, Trépanier S, Bussière D, Dargis M, Poulin J-F, et al. A plant-derived quadrivalent virus like particle influenza vaccine induces cross-reactive antibody and T cell response in healthy adults. Clin Immunol 2016;168:72–87. https://doi.org/10.1016/j.clim.2016.03.008.
[34] Hodgins B, Yam KK, Winter K, Pillet S, Landry N, Ward BJ. A Single intramuscular dose of a plant-made virus-like particle vaccine elicits a balanced humoral and cellular response and protects young and aged mice from influenza H1N1 virus challenge despite a modest/absent humoral response. Clin Vaccine Immunol 2017;24. https://doi.org/10.1128/CVI.00273-17.
[35] Lee G-J, Quan F-S. Protection induced by early stage vaccination with pandemic influenza virus-like particles. Vaccine 2016;34:3764–72. https://doi.org/10.1016/j.vaccine.2016.06.011.
[36] Chaussee MS, Sandbulte HR, Schuneman MJ, DePaula FP, Addengast LA, Schlenker EH, et al. Inactivated and live, attenuated influenza vaccines protect mice against influenza: streptococcus pyogenes super-infections. Vaccine 2011;29:3773–81. https://doi.org/10.1016/j.vaccine.2011.03.031.
[37] Iverson AR, Boyd KL, McAuley JL, Plano LR, Hart ME, McCullers JA. Influenza virus primes mice for pneumonia from staphylococcus aureus. J Infect Dis 2011;203:880–8. https://doi.org/10.1093/infdis/jiq113.
[38] Bright RA, Carter DM, Daniluk S, Toapanta FR, Ahmad A, Gavrilov V, et al. Influenza virus-like particles elicit broader immune responses than whole virion inactivated influenza virus or recombinant hemagglutinin. Vaccine 2007;25:3871–8. https://doi.org/10.1016/j.vaccine.2007.01.106.
[39] Zurli V, Gallotta M, Taccone M, Chiarot E, Brazzoli M, Corrente F, et al. Positive contribution of adjuvanted influenza vaccines to the resolution of bacterial superinfections. J Infect Dis 2016;213:1876–85. https://doi.org/10.1093/infdis/jiw048.
[40] Huber VC, Peltola V, Iverson AR, McCullers JA. Contribution of vaccine-induced immunity toward either the HA or the NA component of influenza viruses limits secondary bacterial complications. J Virol 2010;84:4105–8. https://doi.org/10.1128/JVI.02621-09.
[41] McCullers JA. Effect of antiviral treatment on the outcome of secondary bacterial pneumonia after influenza. J Infect Dis 2004;190:519–26. https://doi.org/10.1086/421525.

Publication V

Received: 18 August 2020 | Revised: 21 October 2020

DOI: 10.1002/biot.202000391

Biotechnology Journal

RESEARCH ARTICLE

Accelerating HIV-1 VLP production using stable High Five insect cell pools

Eduard Puente-Massaguer[1] | **Paula Grau-Garcia**[1] | **Florian Strobl**[2,3] | **Reingard Grabherr**[3] | **Gerald Striedner**[3] | **Martí Lecina**[4] | **Francesc Gòdia**[1]

[1] Departament d'Enginyeria Química, Biològica i Ambiental, Universitat Autònoma de Barcelona, Cerdanyola del Vallès, Barcelona 08193, Spain

[2] Austrian Centre of Industrial Biotechnology (acib GmbH), Vienna 1010, Austria

[3] Department of Biotechnology, University of Natural Resources and Life Sciences, Vienna 1190, Austria

[4] IQS School of Engineering, Universitat Ramón Llull, Barcelona 08017, Spain

Correspondence
Dr. Eduard Puente-Massaguer, Departament d'Enginyeria Química, Biològica i Ambiental, Universitat Autònoma de Barcelona, carrer de les Sitges, 08193 Cerdanyola del Vallès, Barcelona, Spain.
Email: eduard.puente-massaguer@mssm.edu

Abstract

Stable cell pools are receiving a renewed interest as a potential alternative system to clonal cell lines. The shorter development timelines and the capacity to achieve high product yields make them an interesting approach for recombinant protein production. In this study, stable High Five cell pools are assessed for the production of a simple protein, mCherry, and the more complex HIV-1 Gag-eGFP virus-like particles (VLPs). Random integration coupled to fluorescence-activated cell sorting (FACS) in suspension conditions is applied to accelerate the stable cell pool generation process and enrich it with high producer cells. This methodology is successfully transferred to a bioreactor for VLP production, resulting in a 2-fold increase in VLP yields with respect to shake flask cultures. In these conditions, maximum viable cell concentration improves by 1.5-fold, and by-product formation is significantly reduced. Remarkably, a global increase in the uptake of amino acids in the Gag-eGFP stable cell pool is observed when compared with parental High Five cells, reflecting the additional metabolic burden associated with VLP production. These results suggest that stable High Five cell pools are a robust and powerful approach to produce VLPs and other recombinant proteins, and put the basis for future studies aiming to scale up this system.

KEYWORDS
bioreactor, fluorescence-activated cell sorting, High Five cells, metabolism, stable cell pool, virus-like particle

1 | INTRODUCTION

Recombinant protein production with the insect cell (IC)/baculovirus expression vector system (BEVS) is nowadays an extended platform.[1] The IC/BEVS enables to obtain high protein yields in a reduced time and proof of that is the myriad of products that have been produced with it.[2] Among them, the production of virus-like particles (VLPs) has proven very successful with the IC/BEVS, generally achieving superior yields to those obtained in other eukaryotic expression systems.[3] However, well-known limitations of using insect cells in combination with the BEVS include cell lysis and protease release due to the baculovirus (BV) infection process, incorporation of BV-derived proteins in the product, and difficulties in the downstream processing of complex nanoparticles. Plasmid-based transient gene expression (TGE) approaches are commonly used to circumvent some of these drawbacks.[4] TGE enables the rapid production of moderate to high amounts of recombinant products for diagnostic or therapeutic applications in the early phases of drug development. Nonetheless, the production of high amounts of plasmid DNA limits its use in large bioreactor volumes and introduces an additional step in operation due to the need to supply the DNA in combination with a transfection reagent, which impacts the reproducibility of the process. Also, issues related to media incompatibility with cell transfection reagents

Abbreviations: eGFP, enhanced green fluorescent protein; EV, extracellular vesicle; FACS, fluorescence-activated cell sorting; FBS, fetal bovine serum; GOI, gene of interest; HIV, human immunodeficiency virus; VLP, virus-like particle

are not easily solved when transferring the process to bioreactor scale.

Stable gene expression (SGE) is the most generally adopted option for large-scale manufacturing and remarkable efforts have been devoted to improving this system over the last decades.[5] Cell lines with a clonal origin are the preferred SGE strategy to ensure bioprocess robustness and product consistency, as requested by regulatory agencies. Clonal selection is focused on the screening of a high number of clones, whenever possible using high-throughput technologies, to identify cells with high cell growth and productivity profiles. On top, different molecular biology approaches such as CRISPR/Cas9[6] or recombinase-mediated cassette exchange (RMCE)[7] are used to this end since it is possible to direct the gene of interest (GOI) to genome loci with high transcription rates and low gene silencing.[8,9] Nevertheless, the development of efficient stable cell lines encompassing rapid cell growth rates, high cell concentrations, large recombinant protein yields, and product stability can be a very time-consuming and labor-intensive process that can take several months.[10] On the other hand, several studies have brought into debate the relevance of clonality by reporting the appearance of differentiated expression patterns during the culture of cells derived from a clonal cell line.[11,12] Cell-to-cell differences have even been detected in master cell banks of CHO cells, but this heterogeneous cell population performed consistently in terms of product quality.[13] In the same line, the development of a clonal CHO cell line did not provide an improved homogeneity of future cell progeny.[14] Therefore, it could be argued whether the efforts needed to develop a stable cell line are sufficiently justified.

Attention has recently been directed to the development of stable cell pools for recombinant protein production.[15] In this case, the timeline from transfection to production is substantially shortened and titers can equal those obtained with clonal cell lines.[16,17] As for VLPs, insect cells are a highly productive system with successful results reported by SGE using clonal cell lines.[18,19] However, alternative stable production strategies allowing bioprocess acceleration remain to be investigated. The transfectability[20,21] and capacity of High Five cells to produce large VLP yields[22,23] make them an interesting system for this purpose.

In this work, the generation of stable High Five cell pools for the production of HIV-1 Gag virus-like particles and the mCherry protein is investigated. Random integration of the GOI in combination with fluorescence-activated cell sorting (FACS) is employed to develop stable cell pools and enrich each pool with high producer cells. The stability of expression in this system is evaluated during a month in cell culture and its transferability to bioreactor is assessed and compared with parental High Five cells. Flow virometry is applied for nanoparticle quantification in native conditions with the *gag* gene fused in-frame to *eGFP* to ease VLP quantification and differentiation from other particles co-produced. Eventually, a detailed analysis of the metabolism between the VLP expressing pool and parental cells at different production scales, shake flask or bioreactor, is also conducted to gain insight into the specific nutritional requirements of this system.

2 | MATERIALS AND METHODS

2.1 | Cell line and culture conditions

BTI-TN-5B1-4 cells (High Five, cat. num. B85502, Thermo Fisher Scientific, Grand Island, NY, USA) were grown in the low hydrolysate and animal component-free Sf900III medium (Thermo Fisher Scientific) and subcultured in 125 mL disposable polycarbonate Erlenmeyer flasks (Corning, Steuben, NY, USA) three times a week at a density of 2–4 $\times$ 10^5 cell per mL. All cultures were grown in 15 mL of Sf900III medium at 130 rpm (Stuart, Stone, UK) in an incubator at 27°C (Memmert, Schwabach, Germany).

For cell selection, the medium was supplemented with the antibiotic zeocin (InvivoGen, San Diego, CA, USA) at a concentration of 300 µg mL^{-1} based on toxicity assays (Figure S1). Zeocin selection pressure was kept until the viability of the culture was completely recovered, but a minimum of 4 weeks of zeocin addition to the culture was maintained to ensure that the expression of the recombinant product of interest was not episomal but from stable gene integration.

Cell count and viability were measured with an automated cell counter Nucleocounter NC-3000 (Chemometec, Allerød, Denmark). Stable cell pools were also visualized under a TCS SP5 confocal microscope (Leica, Wetzlar, Germany) for qualitative analysis of mCherry and Gag-eGFP expression. Cell nuclei were stained with 0.1% v/v of Hoechst (Thermo Fisher Scientific). Dye excess was removed by mild centrifugation at 300 x *g* for 5 min and cells were then resuspended in fresh Sf900III medium. Afterward, samples were placed in 35 mm glass-bottom Petri dishes with a 14 mm microwell (MatTek Corporation, Ashland, MA, USA) for visualization. Image analysis and processing were performed with the LAS X software (Leica).

2.2 | Plasmid construction and transfection

The pIZTV5-Gag-eGFP plasmid encoding a Rev-independent HIV-1 Gag fused in frame to the enhanced green fluorescent protein eGFP (NIH AIDS Reagent Program, cat. num. 11468)[24] was constructed as previously described.[25] The pIZTV5-mCherry plasmid encoding the intracellular fluorescent mCherry protein was generated by PCR cloning of the *mCherry* gene from the pPEU3 plasmid[26] with the following primer pair: forward 5'-CGTAAAGCTTATTTACAATCAAAGGAGATATACCA-3' and reverse 5'-CGTAGCGGCCGCCTACTTGTACAGCTCGTCCATGC-3'. The amplified fragment and the pIZTV5-his plasmid (Thermo Fisher Scientific) were digested with *Hin*dIII and *Not*I and ligated, resulting in the pIZTV5-mCherry plasmid. Both plasmid DNAs encode the bleomycin resistance protein that confers resistance to zeocin, which is under the control of the *Op*IE1 (*Orgia pseudotsugata* immediate-early 1) promoter. The mCherry and Gag-eGFP proteins are under the control of the stronger *Op*IE2 promoter.[27]

High Five cells were transfected with the cationic lipid reagent Cellfectin II (Thermo Fisher Scientific) as previously reported.[18] Briefly, 0.3 µg 10^{-6} cells of linearized pIZTV5-mCherry or pIZTV5-Gag-eGFP

plasmid and 0.8 μg 10^{-6} cells of Cellfectin II were separately added to 500 μL of non-supplemented Grace's insect medium (Thermo Fisher Scientific), vortexed for 5 s, and added to the culture. Digestion with *Pci*I was used for plasmid DNA linearization.

The percentage of mCherry or Gag-eGFP positive cells was evaluated in a BD FACS Canto II flow cytometer and analyzed with the BD FACSDIVA software (BD Biosciences, San Jose, CA, USA). The number of mCherry and Gag-eGFP positive cells was determined in the PerCP-Cy5-A and FITC-A PMT detectors, respectively.

2.3 | Fluorescence-activated cell sorting

Stable cell pool enrichment with high producer cells was performed by three rounds of fluorescence-activated cell sorting (FACS) in a BD FACSJazz cell sorter (BD Biosciences) equipped with two lasers (488 and 635 nm). The threshold was set to select 30% of most fluorescent cells during the first two rounds of FACS, and the final round was used to remove the 10% of the lowest fluorescent cells. The initial conditions of FACS were optimized as reported elsewhere.[28] Shortly, the mCherry and Gag-eGFP stable cell pools were grown to 2×10^6 cell per mL before sorting. 1% v/v of Pluronic F-68 100*X* and a 1:100 diluted (1*X*) antibiotic-antimycotic solution (Thermo Fisher Scientific) were added to the cell culture to minimize the effect of shear stress and avoid contamination, respectively. The sheath fluid used was DPBS (Thermo Fisher Scientific), which was injected at a constant pressure of 27 psi and at a sorting rate maintained in the range of 500 to 2000 cell/s. 2×10^6 cell were collected in fresh Sf900III medium supplemented with 2% FBS (Sigma Aldrich, St. Louis, MO, USA) and 1*X* of antibiotic-antimycotic. After sorting, cells were centrifuged at 300 x *g* for 5 min to remove the sheath fluid and resuspended at a final concentration of 1×10^6 cell per mL in a 6-well plate (Nunc, Thermo Fisher Scientific) with fresh Sf900III medium containing 5% FBS, zeocin and 1*X* of antibiotic-antimycotic. Afterward, cells were maintained at 150 rpm in the incubator for 1 week. Zeocin, FBS, and the antibiotic-antimycotic solution were removed from cell culture after the different rounds of FACS were completed.

2.4 | VLP production at bioreactor scale

The production of Gag-eGFP VLPs in stable High Five cell pools was evaluated in a stirred tank bioreactor (DASGIP Parallel Bioreactor System, Eppendorf, Hamburg, Germany) equipped with three Rushton impellers. In parallel, parental High Five cells were cultured in the same conditions for comparison. Briefly, 1×10^6 cell per mL of exponentially growing cells were inoculated in the bioreactor at a final volume of 0.5 L. Dissolved oxygen (DO) was controlled by aeration through a sparger and set at 30% of air saturation with 1 L h^{-1} air flow rate and temperature at 27°C. Initial stirring conditions were set at 150 rpm and were automatically adjusted by the DASware control software (Eppendorf) to maintain the desired DO setpoint. The pH was fixed at 6.4 and controlled with 20% w/w H_3PO_4 and 7.5% w/w $NaHCO_3$ addition.

2.5 | Spectrofluorometry

Intracellular Gag-eGFP and mCherry production was evaluated based on the fluorescence levels from stable cell pools. Cell pellets were recovered by centrifugation at 3000 x *g* for 5 min and disrupted using three freeze-thaw cycles (2.5 h at −20°C and 0.5 h at 37°C), and vortexed 5 s three times between cycles. Lysed pellets were then resuspended in TMS buffer (50 mM Tris-HCl, 150 mM NaCl, 2 mM $MgCl_2$, pH 8.0) and centrifuged at 13,700 x *g* for 20 min. Gag-eGFP fluorescence was measured in a Cary Eclipse spectrophotometer (Agilent Technologies, Santa Clara, CA, USA) at RT as follows: $\lambda_{ex} = 488$ nm (slit = 5), $\lambda_{em} = 500–530$ nm (slit = 10). For mCherry fluorescence measurement, the equipment settings were set as: $\lambda_{ex} = 587$ nm (slit = 5), $\lambda_{em} = 600–630$ nm (slit = 10). Relative fluorescence units (R.F.U.) were calculated by measuring the difference in fluorescence levels between stable cell pools and parental cells (negative control). The mCherry concentration was determined using a standard curve based on the linear correlation between known mCherry concentrations (BioVision, Milpitas, CA, USA) and their associated fluorescence (R.F.U.):

$$\text{mCherry (mg/L)} = (\text{R.F.U} - 55.008)/9.0401 \quad (1)$$

The Sf900III medium and a 0.1 mg mL^{-1} quinine sulfate solution were used as internal controls to normalize R.F.U. between experiments.

2.6 | Nanoparticle quantification

The concentration of Gag-eGFP VLPs and extracellular vesicles was assessed by flow virometry in a CytoFlex LX (Beckman Coulter, Brea, CA, USA) equipped with a 488 nm blue laser for fluorescent particle detection and a 405 nm laser/violet side scatter configuration for improved nanoparticle size resolution. Samples were diluted 1:50 in 0.22 μm-filtered DPBS and analyzed with the CytExpert v.2.3 software. A sample of fresh Sf900III medium was also analyzed as a control.

An HIV-1 p24 enzyme-linked immunosorbent assay (ELISA) (Sino Biological, Wayne, NJ, USA) was used to quantify the concentration of Gag-eGFP polyprotein in the supernatant.[25] The p24 concentration values were corrected based on the Gag-eGFP molecular weight (87.7 kDa).

2.7 | Analysis of metabolites

The main metabolites consumed and produced by parental High Five cells and stable cell pools were determined by HPLC. An ion-exclusion liquid chromatography (Aminex HPX-87H, Bio-Rad, Hercules, CA, USA) in an Agilent 1200 series HPLC system (Agilent, Santa Clara, CA, USA) was used to measure the concentration of glucose, maltose, phosphate, and lactate. Using this protocol, co-elution of maltose and sucrose was detected but maltose consumption was only

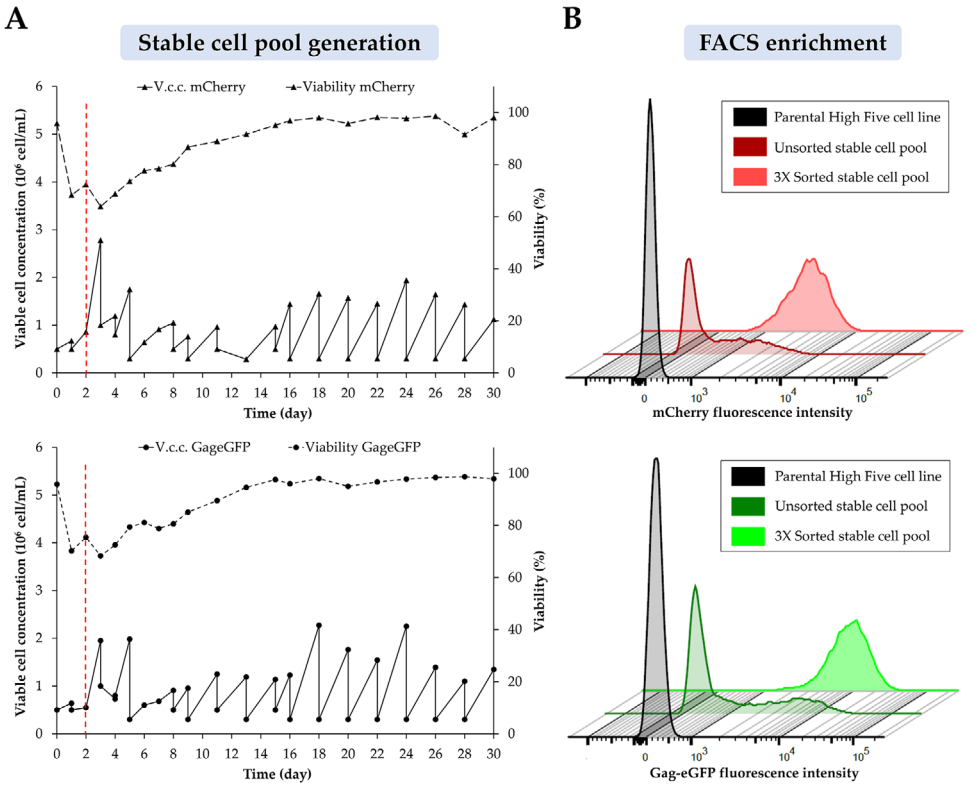

FIGURE 1 Stable cell pool development process for the continuous production of intracellular mCherry protein and Gag-eGFP VLPs. (A) Timeline of Gag-eGFP and mCherry stable cell pool generation from the time of transfection. The dashed red line indicates the moment of zeocin addition at 300 μg mL^{-1} and this concentration was maintained in every subculture. (B) Histograms comparing the average fluorescence intensity from the parental High Five cell line, unsorted stable cell pools, and stable cell pools after three rounds of sorting. The upper histogram (red) shows the FACS enrichment process for stable mCherry cell pools while the lower (green) refers to stable Gag-eGFP production. Average mCherry fluorescence intensity was measured in the PerCP detector of the flow cytometer whereas Gag-eGFP fluorescence was evaluated in the FITC detector. V.c.c: viable cell concentration

considered since sucrose is not metabolized at detectable levels in High Five cells.[29] The phosphate uptake rate was calculated taking into consideration the amount of phosphate in the medium and the volume of H_3PO_4 added for pH control. Amino acid concentrations were quantified by HPLC in a reversed-phase Eclipse Plus C18 column (Agilent) using a post-column derivatization method according to manufacturer's instructions (Agilent). After derivatization, amino acids were detected at a wavelength of 266/305 and 450 nm.

3 | RESULTS AND DISCUSSION

3.1 | Stable cell pool generation

Two recombinant products with different complexities, intracellular mCherry and enveloped Gag-eGFP VLPs, were selected to appraise the capacity of High Five cell pools as a system for rapid and stable recombinant protein production. Different zeocin concentrations were initially tested to define the antibiotic concentration used to generate stable cell pools. The concentration range was defined as 50 and 500 μg mL^{-1} according to preliminary experiments conducted with these cells (Figure S1). Zeocin activity arrested cell growth but viability was only partially affected, indicating that not having the resistance gene would cause the replacement of cells over time by cells that express it. Addition of 300 μg mL^{-1} of zeocin was selected as the condition for stable cell pool generation considering that higher antibiotic concentrations did not show a significant difference.

Cell transfection with the pIZTV5-mCherry and pIZTV5-Gag-eGFP plasmids was performed with Cellfectin II,[18] and cells were grown until 48 hpt before the antibiotic zeocin was added to the culture (red line, Figure 1A). The initial drop in cell viability was caused by the transfection process itself, while subsequent declines in cell viability were produced by the addition of zeocin. During the development process of stable cell pools, no relevant differences were observed for the time required to achieve the stable expression of mCherry and Gag-eGFP (Figure 1A). Cells exhibited an initial decline in cell viability to 70% that lasted one week and followed by a progressive recovery. Cell pool stability was achieved two times faster when compared with reported data for the development of CHO[30] and Sf9 cell pools,[31] likely due to the higher cell growth rate of High Five cells.[22] It took approximately 2 weeks of culture to completely recover cell viability, but cells were maintained for 2 additional weeks under selective pressure to ensure stable plasmid DNA integration into the cell genome, resulting in a total of 16 cell passages for stable cell pool generation.

TABLE 1 Average fluorescence intensity values for mCherry and Gag-eGFP unsorted stable cell pools and after three rounds of FACS

Condition	mCherry	Gag-eGFP
Unsorted cell pool	62	200
3× sorted cell pool	255	894
Fold sorted/unsorted	4.1	4.5

Values are expressed in arbitrary units.

3.2 | Stable cell pool enrichment by FACS

The initial stable cell pools (unsorted) were a heterogeneous cell population, probably including cells that had integrated one or several copies of the plasmid DNA to cells that had only integrated the resistance gene but lacking the gene of interest (GOI). At the end of the generation of each stable cell pool, the percentage of cells expressing the GOI was 47.8% for mCherry and 45.6% for Gag-eGFP, according to flow cytometry. This could indicate that several cells had only integrated a complete copy/s of the resistance gene or that some of them were experiencing silencing of the GOI, a phenomenon that has been previously reported in CHO cell lines and which is believed to occur due to epigenetic regulation of the expression of non-essential genes.[32] Little information is available for insect cells, but the principal causes of these changes in CHO cells are related to promoter methylation[33] and variations in the condensation of DNA owing to histone modifications.[34] Here, a similar behavior for zeocin resistant cells not expressing the GOI under control of the *Op*IE2 promoter is observed.

FACS was used to select cells exhibiting a phenotype of high mCherry/Gag-eGFP expression during the zeocin selection process and remove non-producing cells (Figure 1B). Cell enrichment by FACS has been successfully applied for the generation of stable CHO cells[35] and insect cell lines[28] to produce a variety of recombinant products, including monoclonal antibodies and fluorescent proteins. In this work, the process was directly conducted in agitated 6-well plates in order to eliminate the adaptation phase of adherent to suspension culture and speed-up the transition to shake flask cultivation. Three rounds of FACS enrichment for each stable cell pool were performed to maximize the number of high producing cells in each pool. After three rounds of cell sorting, the average fluorescence intensity of each cell pool was significantly improved, with a 4.1 and 4.5-fold increase for mCherry and Gag-eGFP, respectively. In these conditions, the 12.7 and 8.6% high producing cells of the unsorted mCherry and Gag-eGFP cell pools comprised the enriched cell pools (Table 1).

3.3 | Characterization of stable cell pools in shake flasks

Cell growth and recombinant protein production were evaluated in the enriched stable cell pools (Figure 2). Maximum viable cell concentration decreased in the mCherry and Gag-eGFP stable cell pools compared with parental High Five cells. Such a decline in the maximum viable cell concentration of stable cell lines with respect to parental cells has also been reported.[18] Similarly, a comparison of the different conditions showed an increase in the doubling times of stable cell pools in contrast to parental cells, possibly indicating that the constitutive production of a heterologous protein has an impact on cell growth (Figure 2A). The percentage of fluorescent cells was maintained up to 96 h in both cases and then started to decrease, especially in the mCherry cell pool (Figure 2B). Analysis of cell viability denoted that the decline in the number of fluorescent cells coincided with the decrease in cell viability, which was more pronounced for the mCherry than the Gag-eGFP cell pool. Visualization of stable cell pools by confocal microscopy enabled the detection of mCherry (magenta) and Gag-eGFP (green) expression (Figure 2C–D). Different fluorescence intensities could be observed within the same stable cell pool, indicating heterogeneity in the production levels of the individual cells comprising the pool.

Intracellular mCherry production levels steadily increased up to 120 h (Figure 2E), with a reduced amount of mCherry protein measured in the supernatant, which could be attributed to protein leakage from dead cells. In these conditions, a maximum of 187.5 ± 4.8 R.F.U. was obtained, corresponding to 26.8 ± 0.5 mg L^{-1} according to Equation 1, and a specific productivity of 0.9 ± 0.1 μg 10^{-6} cell·day. The mCherry production levels achieved in this work are 4.6-fold higher compared with eGFP production by transient gene expression (TGE) in High Five cells,[20] and in the range of titers obtained in stable insect cell lines[7] and with the baculovirus expression vector system (BEVS).[36] As regards the production of VLPs, intracellular Gag-eGFP fluorescence levels increased until 120 h, as observed for the mCherry stable cell pool, whereas VLP titers increased up to the end of the experiment (Figure 2F). Therefore, considering a good compromise between VLP production and cell viability at harvest as an important criterion for production, the harvest time in shake flask cultures was defined as 120 h. In these conditions, a maximum VLP concentration of 1.5 ± 1.4 × 10^6 VLP per mL was achieved, and remarkable amounts of other nanoparticles, mainly extracellular vesicles (EVs), were detected (7.5 ± 0.9 × 10^8 total nanoparticles per mL) as similarly encountered with the BEVS,[22] with the 16.5% of them belonging to the Sf900III medium itself. Thus, considering the presence of these nanoparticles, which are similar in size to Gag VLPs, is of relevance since not contemplating them might lead to an overestimation of the amount of VLPs produced, especially when using high-throughput techniques for nanoparticle quantification.[37] Furthermore, it is here highlighted the need to develop efficient strategies that enable the separation of these different nanoparticle populations. Despite the recent advanced reported in this field,[38,39] more research is still required to achieve a complete separation between these specimens. Measurement of the VLP concentration in the supernatant by ELISA yielded 14.8 ng mL^{-1} of Gag-eGFP, which is in the range of the 11.5 ng mL^{-1} of Gag obtained by clonal High Five cell lines developed by recombinase-mediated cassette exchange.[19] This homologous DNA recombination strategy has also been explored for Gag-Cherry VLP production in clonal Sf9 cell lines, achieving similar production yields.[18] In terms of specific Gag VLP productivity, stable High Five cell pools achieved 0.5 ng 10^{-6}

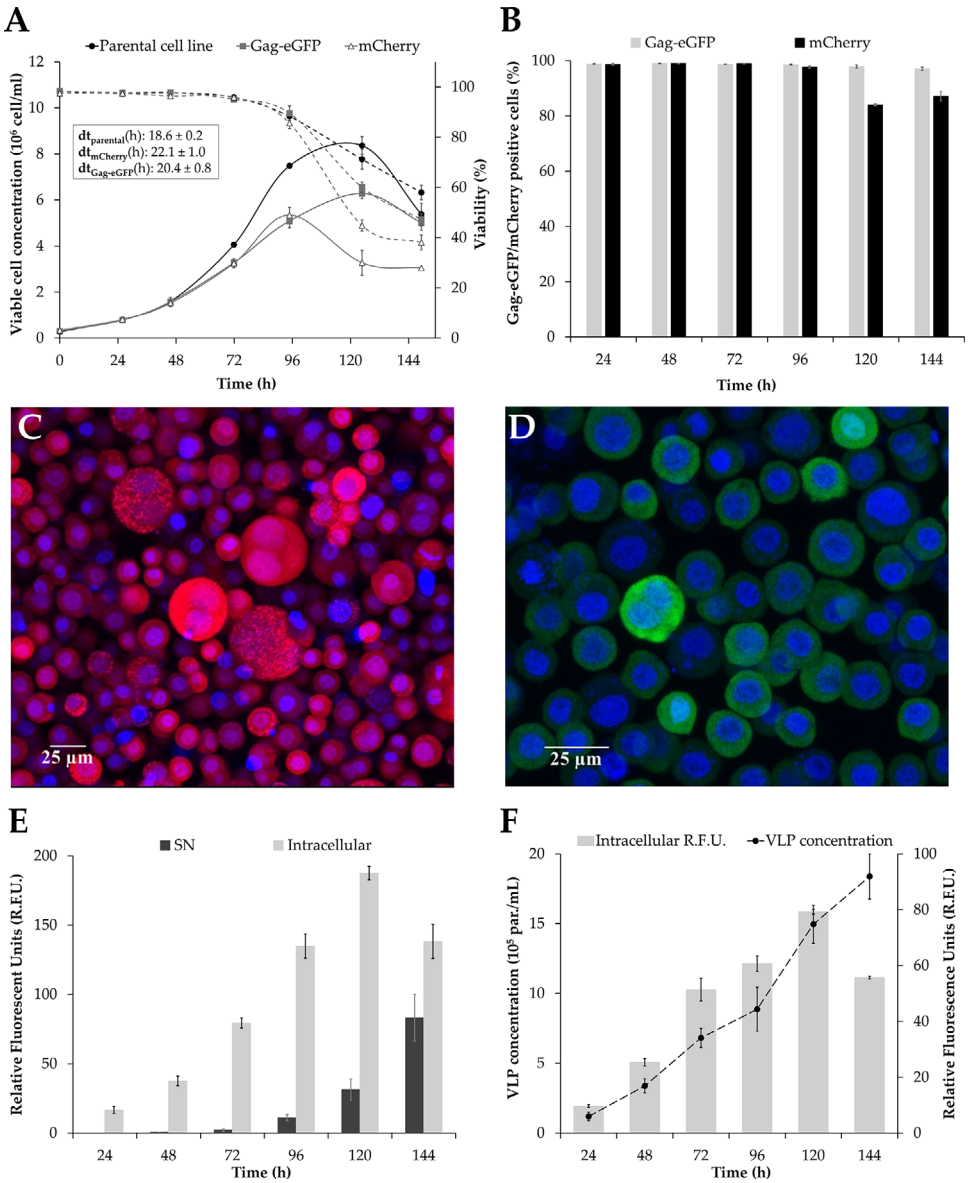

FIGURE 2 Characterization of mCherry and Gag-eGFP stable cell pools cultured in shake flasks in 15 mL of Sf900III medium. (A) Viable cell concentration (straight line) and cell viability (dashed line) profiles and doubling times of parental High Five cells, mCherry and Gag-eGFP stable cell pools. Cells were seeded at a viable cell concentration of 0.3×10^6 cell per mL in all cases. (B) Analysis of the percentage of fluorescent cells by flow cytometry in the mCherry and Gag-eGFP stable cell pools. (C–D) Three-dimensional images of stable cell pools obtained by fluorescence confocal microscopy at 48 h. The nuclei of mCherry (magenta, C) and Gag-eGFP (green, D) stable cell pools were stained with Hoechst (blue). mCherry (E), Gag-eGFP and VLP production profiles (F). Fluorescence levels of mCherry and Gag-eGFP were measured by spectrofluorometry whereas VLP concentration was assessed by flow virometry. The average and standard deviation of triplicate experiments are presented. dt: doubling time

cell·day, resulting in comparable levels to those obtained in clonal High Five cell lines[19] and 1.8-fold higher in comparison to clonal Sf9 cell lines.[18] The VLP production yields shown in this work are still lower than those obtained with the BEVS,[22] but the development of new strategies for the intensified production of recombinant proteins[40] as well as the specific supplementation of cell cultures[41] open a window of opportunity to further increase VLP yields.

Analysis of the Gag-eGFP expression stability in the stable cell pool was also assessed by cell passaging in shake flasks during a month (Figure S2). The specific Gag-eGFP fluorescence levels were maintained, indicating that Gag-eGFP production was stable and not subjected to variations in production during a prolonged time in culture.

3.4 | VLP production in bioreactor

The feasibility of stable High Five cell pools as a system to produce VLPs was evaluated in a stirred tank bioreactor and compared with shake flask and parental cell cultivation in the same conditions (Figure 3A). Cell growth and viability of Gag-eGFP stable cell pools and

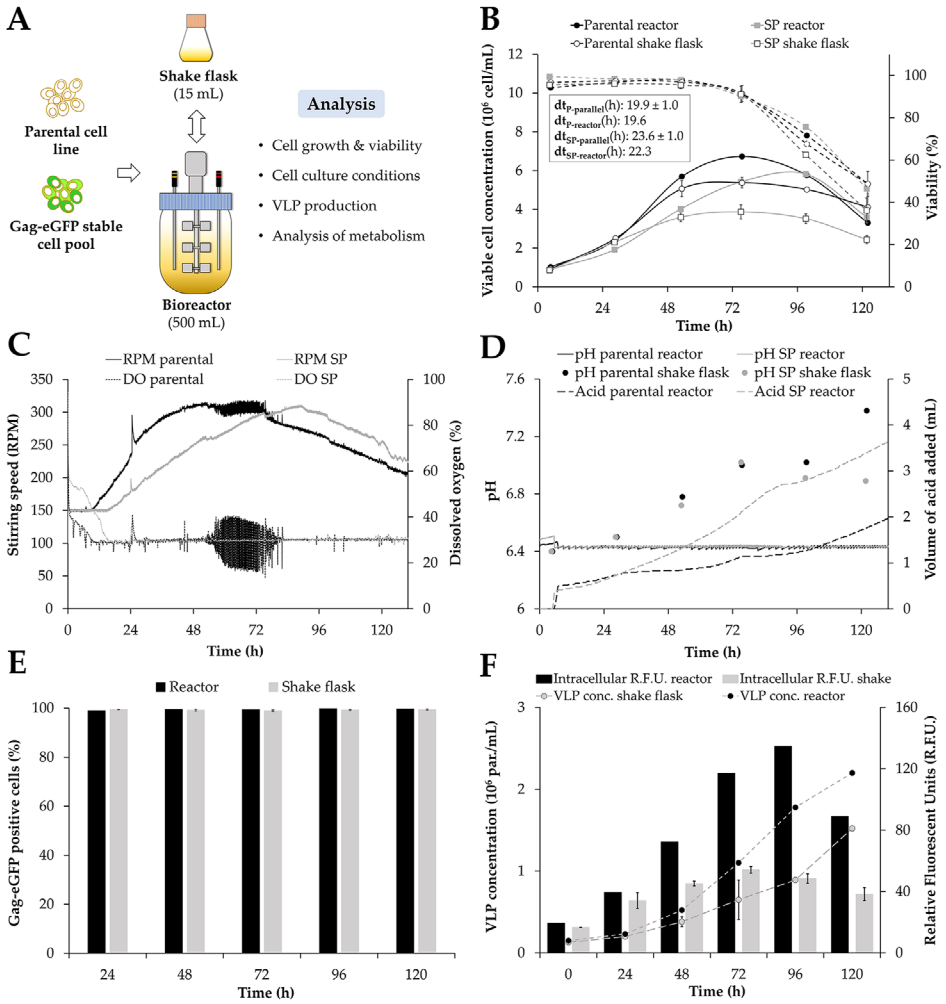

FIGURE 3 Gag-eGFP VLP stable cell pool cultivation at bioreactor scale and comparison to parental High Five cells. (A) Schematic of the bioreactor experiment and comparison to shake flask cell culture. (B) Viable cell concentration (straight line) and viability (dashed line) of Gag-eGFP stable cell pools and parental High Five cells cultured in shake flasks and bioreactor. Cells were seeded at 1.0×10^6 cell per mL in the different conditions evaluated. (C) Stirring speed and dissolved oxygen profiles of the Gag-eGFP stable cell pool and parental cells cultured in a bioreactor. (D) Evolution of pH in the Gag-eGFP stable cell pool and parental cells cultured in bioreactor and shake flasks. The volume of 20% w/w H_3PO_4 acid added for pH maintenance in the bioreactor is also shown. (E) Flow cytometry analysis of the percentage of fluorescent cells in the Gag-eGFP stable cell pool cultured in bioreactor and shake flasks. (F) Gag-eGFP VLP production and intracellular Gag-eGFP fluorescence levels of the stable cell pool cultured in bioreactor and shake flasks. VLP quantification was performed by flow virometry, and intracellular Gag-eGFP fluorescence by spectrofluorometry. DO: dissolved oxygen, dt: doubling time, R.F.U.: relative fluorescence units, RPM: revolutions per minute, SP: stable cell pool

parental High Five cells in bioreactor and shake flasks are shown in Figure 3B. Maximum viable cell concentration was attained at around 72 h of culture, and parental cells achieved higher densities both in bioreactor and in shake flasks, which is in agreement with the results observed in the previous section. The bioreactor culture reached the highest viable cell concentration even though no significant differences were observed in terms of cell doubling times (*dt*). The Gag-eGFP stable cell pool exhibited a larger *dt* in comparison to parental cells, as previously observed (Figure 2A). Nevertheless, *dt* of the Gag-eGFP stable cell pool (23.6 ± 1.0 h) and parental High Five cells (19.9 ± 1.0 h) cultured in shake flasks were higher than those observed in the previous experiments (Figure 2A). This could be a consequence of the higher seeding density used in the bioreactor to avoid a lag phase.[42] In the same line, cell viability started declining 24 h earlier (96 h) and was more pronounced for the shake flask conditions.

Bioreactor cultivation of parental cells and the stable cell pool enabled the detection of differences in culture patterns for both conditions. Parental cell cultures showed faster-dissolved oxygen (DO) consumption and achieved the peak of stirring speed around 36 h earlier than the stable cell pool (Figure 3C), which correlates with the faster cell growth kinetics observed for parental cells. pH was kept at the setpoint of 6.4 in the bioreactor conditions, but 1.8-fold more H_3PO_4 acid addition was required in the Gag-eGFP stable cell pool to maintain the setpoint (Figure 3D). The evolution of pH in shake flasks was similar in both conditions until 72 h, when pH increased in parental cell shake flasks until the end of the experiment (7.4) while achieving a plateau at

6.9–7.0 in the stable cell pool. The uncontrolled pH conditions in shake flasks, leading to significantly exceeding the optimal pH for High Five cell culture (6.2–6.4), as well as the limitation of DO in the medium could explain the differences observed in cell growth with respect to bioreactor conditions. Variations in insect cell performance with the BEVS have been recently reported and attributed to the different cell culture strategies employed.[43]

The number of Gag-eGFP expressing cells in the stable cell pool cultured in bioreactor was kept constant and at the same level observed in shake flasks (Figure 3E). In terms of Gag-eGFP production, higher yields were measured throughout the experiment in the bioreactor condition, with intracellular Gag-eGFP concentration peaking between 72 and 96 h (Figure 3F). Considering a balance between VLP production and cell viability, the harvest time was defined as 96 h for the bioreactor. In these conditions, VLP production increased by 2-fold compared with shake flask cultures, demonstrating that High Five cell pools can be cultured in bioreactors for the stable and rapid production of VLPs. Certainly, these cultures could be further intensified, for example with continuous perfusion systems using alternating tangential flow filtration to increase cell concentration and improve VLP titers.

3.5 | Study of metabolism in shake flasks and bioreactors

Analysis of the main metabolites in the four different conditions tested enabled the detection of specific patterns associated with the culture system, shake flask or bioreactor, and the heterologous production of Gag-eGFP VLPs (Table 2). In general, higher metabolite consumption and production rates were observed at the beginning of the exponential growth phase (0–24 h). Glucose and asparagine were evidenced as the principal energy sources, being the latter completely exhausted after 48 h in all cases (Figure 4), and coinciding with the onset of the stationary phase. Glucose is the main carbon source and responsible for pyruvate formation through the glycolysis pathway, which is incorporated into the tricarboxylic acid (TCA) cycle for energy production. On the other hand, asparagine is the principal nitrogen source in High Five cells, entering the TCA cycle in the form of oxaloacetate (OAA) previous hydrolyzation to aspartate and transamination of α-ketoglutarate to glutamate and OAA. This amino acid is preferentially used in High Five cells in comparison to other insect cells, probably due to a higher activity of the enzymes involved in asparagine metabolism.[44] The utilization of maltose, a two-unit glucose disaccharide, was also observed but at significantly lower levels that were moderately higher in the bioreactor conditions. Despite the fact that the uptake rates of asparagine and glucose decreased over time, glucose consumption augmented in shake flasks by the end of the experiment, substantially increasing by 2.7 and 3.1-fold the final lactate concentrations achieved in parental cells and the stable cell pool, respectively, as compared with the bioreactor. Lactate is formed from pyruvate under glucose excess concentrations, but the higher levels measured in shake flasks could be attributed to limitations in oxygen transfer or the absence of pH control.[29] The production of this by-product has also been previously reported to partially inhibit cell growth in insect cells[45] and aside from pH and DO, could explain the reduction of cell growth in shake flasks. In turn, the lower viable cell concentration attained caused a reduction of phosphate consumption in shake flasks since less biomass was generated (Table 2).

A preference for glutamate over glutamine was observed in all cases at the beginning of the experiment, but glutamine was generally preferred over glutamate from the late exponential phase until the end of the culture. These metabolites are important sources of energy and nitrogen for insect cell metabolism besides asparagine, and their uptake results in the release of ammonia ions, which could be the reason behind the pH increase in shake flasks.[44] Asparagine, glutamine, glutamate, and aspartate consumption were faster in the Gag-eGFP stable cell pool, and leucine exhaustion was measured at 72 h in all conditions. Leucine has been reported to act as an energy source in High Five cells via incorporation into the TCA cycle as acetyl-CoA,[46] but no reports are disclosing its complete depletion in cell culture. This indicates that this amino acid might play an important role in High Five cells cultured in low hydrolysate media, and its consumption could be associated to cell growth since leucine metabolization decreases when the cell growth rate of High Five cells is reduced, as recently observed in the transient gene expression of these cells.[47]

In parallel to lactate formation, the production of increasing amounts of alanine was also detected, achieving a maximum yield of 28 mM in the stable cell pool cultured in shake flasks (Figure 4C and D). In this condition, the highest level of lactate generation was also observed (23 mM). Alanine is formed from pyruvate in glucose excess conditions, acting as a nitrogen sink for the ammonium released from the metabolism of amino acids such as asparagine, aspartate, glutamate, and glutamine. A correlation between the formation of this by-product and the rate of asparagine consumption has been recently described in High Five cells,[48] which could describe the higher levels of alanine formation in the stable cell pool. In either case, alanine has not been shown to inhibit cell growth or recombinant protein production in insect cells.[49]

Overall, the majority of amino acids were consumed at higher rates in the stable cell pool during the exponential phase, which could be an indication of the additional metabolic pressure due to Gag-eGFP VLP production (Table 2). These differences in amino acid consumption rates decreased along the culture but were generally higher for the stable cell pool. As for the bioreactor, a reduction in by-product formation and an increase in VLP production were observed, possibly due to the favorable environment provided by pH and DO controlled conditions.

4 | CONCLUDING REMARKS

This work provides a proof of concept of stable High Five cell pools as a promising approach for rapid and efficient recombinant protein production, with yields comparable to those achieved in stable cell lines, but requiring a shorter development time of less than two months since the clonality and suspension adaptation phases are avoided. Moreover, stable cell pool maintenance in culture for one month had no nega-

TABLE 2 Consumption and production rates of the different metabolites in parental High Five cells and Gag-eGFP stable cell pools cultured in shake flasks and in the bioreactor. Rates are expressed in nmol/(10^6 cell h) and red squares show metabolite consumption (negative values) while the blue ones refer to production. The darker the color, the higher the rate. P-SF: parental – shake flask, P-R: parental – reactor, SP-SF: stable cell pool—shake flask, SP-R: stable cell pool reactor

Consumption **0** **Production**

Metabolite	Time (h)																			
	Exponential phase								Stationary phase								Death phase			
	0–24				24–48				48–72				72–96				96–120			
	P-SF	P-R	SP-SF	SP-R	P-SF	P-R	SP-SF	SP-R	P-SF	P-R	SP-SF	SP-R	P-SF	P-R	SP-SF	SP-R	P-SF	P-R	SP-SF	SP-R
Glucose	−157.6	−118.5	−109.8	−104.8	−114.4	−95.3	−110.1	−108.9	−110.4	−55.4	−133.7	−70.5	−77.4	−85.5	−147.0	−86.2	−105.3	−57.0	−165.4	−55.3
Maltose	−9.7	−3.2	−9.3	−10.5	−15.3	−10.2	−17.5	−17.4	−23.9	−2.3	−34.5	−11.3	−25.5	−31.7	−31.8	−22.9	−4.1	−16.3	−4.6	−17.6
Lactate	−12.5	−17.8	−12.2	−13.0	0.8	−8.5	4.2	−16.0	16.4	0.7	25.6	−6.7	24.3	3.0	74.7	13.7	56.3	7.0	115.7	13.6
Phosphate	−55.3	−137.9	−48.5	−114.3	−16.1	−16.8	−27.9	−58.6	−21.1	−13.6	−21.2	−31.9	−3.7	−14.0	−3.5	−25.6	−1.3	−12.2	−1.5	−29.5
Aspartate	−0.5	14.1	−63.3	−42.5	−12.2	−17.3	−0.8	−44.3	−26.5	−7.1	−51.8	−34.1	−26.6	−24.6	−49.2	−41.1	−19.8	−24.5	−31.9	−8.3
Glutamate	−39.4	−37.0	−102.8	−112.3	−22.3	−23.1	−26.1	−46.9	−14.5	−7.6	−25.1	−16.4	0.5	3.4	−3.3	−6.0	0.5	−1.6	−6.1	−2.2
Asparagine	−117.1	−117.7	−145.4	−169.5	−22.9	−19.7	−45.7	−51.9	–	–	–	−6.6	–	–	–	−0.2	–	–	–	−0.1
Serine	−6.4	−0.1	−17.1	−11.6	−8.1	−5.9	0.5	−7.0	3.5	7.1	−4.7	6.1	8.0	10.1	11.5	5.0	2.5	11.1	−0.2	9.7
Glutamine	−39.5	−23.7	−73.7	−57.8	−36.4	−30.0	−8.5	−33.4	−28.2	−19.8	−42.9	−11.3	−5.6	−9.4	−33.9	−27.7	−6.9	−6.8	−30.1	−14.3
Histidine	−3.6	−2.0	−11.4	−8.4	−3.1	−2.8	0.5	−4.2	−2.3	−0.9	−4.3	0.2	0.4	−0.3	−0.5	−2.2	0.3	0.1	−0.7	−0.5
Glycine	−8.8	−7.7	−20.8	−20.1	−5.0	−5.1	1.0	−8.9	−4.3	−1.4	−7.1	0.4	0.7	−0.1	−1.3	−3.0	2.9	5.1	0.9	0.2
Threonine	−6.6	−5.0	−15.9	−14.8	−12.8	−4.8	−12.1	−15.7	−4.8	−7.9	−9.8	−4.3	−0.5	−0.8	−3.0	−4.1	0.1	−0.2	0.5	0.1
Arginine	−13.2	−9.6	−38.3	−31.2	−9.5	−9.3	−5.8	−15.8	−7.1	0.7	−10.9	1.5	8.1	2.8	15.2	1.8	1.2	−1.8	0.9	−0.6
Alanine	162.9	161.6	116.9	142.0	66.4	41.3	120.3	53.6	−1.9	24.5	42.0	54.5	5.5	−6.8	53.1	−1.2	2.8	−20.0	3.7	−11.0
Tyrosine	−4.4	−1.5	−9.8	−0.1	−3.6	−3.5	−1.3	−4.3	−1.8	−1.1	−2.9	−0.6	1.4	1.0	0.7	−1.4	−4.2	−4.0	1.8	0.9
Valine	−8.2	−3.2	−33.3	−28.2	−6.8	−8.4	1.5	−12.4	−8.5	−1.7	−10.6	−0.1	0.6	−1.3	−1.3	−6.1	1.3	−0.8	−0.4	−0.3
Methionine	−2.8	3.1	−32.7	−21.4	−3.8	−6.4	2.0	−13.1	−9.2	2.7	−18.3	2.2	−7.1	−9.7	−14.0	−11.2	−3.1	−9.9	−9.0	−13.8
Tryptophan	−1.9	−1.6	−3.6	−3.0	−1.7	−1.3	−0.8	−1.4	0.0	−0.5	−1.8	−0.3	0.0	−0.1	−1.4	−0.9	−0.2	−0.4	−0.4	−0.5
Phenylalanine	−2.2	2.6	−32.6	−20.2	−3.3	−6.6	6.4	−11.7	−5.5	4.0	−4.7	6.3	0.3	−1.7	2.1	−5.5	0.7	−4.2	−3.1	−1.0
Isoleucine	−5.6	0.0	−35.1	−25.0	−5.0	−7.5	4.4	−12.9	−6.6	1.7	−8.1	4.0	0.7	−1.4	1.0	−6.1	2.3	−3.4	−1.0	−1.0
Leucine	−12.4	−10.0	−19.7	−17.3	−10.1	−8.3	−7.6	−10.2	–	–	−10.5	−6.6	–	–	–	–	–	–	–	–
Lysine	−13.0	−9.5	−55.7	−29.7	−9.3	−7.9	9.8	−9.3	−5.9	−8.7	−13.4	−1.7	−1.2	3.8	−4.7	−6.6	0.1	−2.6	2.6	−5.0
Proline	−7.3	−1.3	−31.4	−27.3	−6.0	−6.3	1.1	−12.2	−4.7	0.5	−9.4	1.8	0.1	−1.0	−1.0	−6.1	0.3	−0.7	−1.6	−0.4

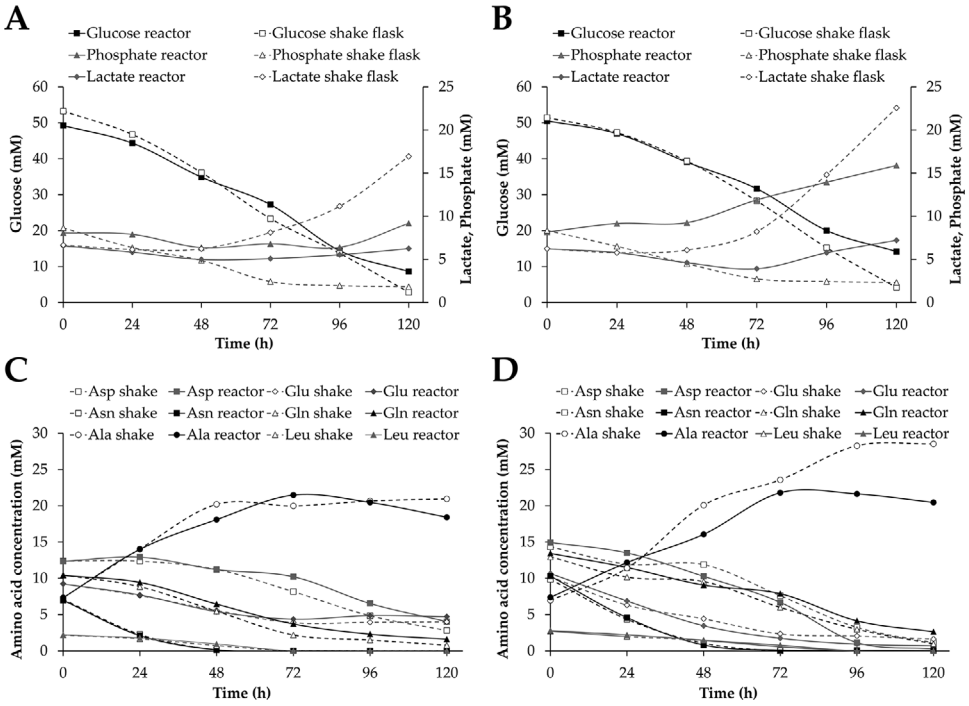

FIGURE 4 Analysis of metabolite consumption and production in Gag-eGFP stable cell pools and parental High Five cells. (A–B) Measurement of glucose, phosphate, and lactate concentrations in parental (A) and Gag-eGFP stable cell pools (B) cultured in shake flasks (dashed lines) and in bioreactor (straight lines). (C–D) Representation of the main amino acids experiencing noticeable variations in their concentration in parental (C) and Gag-eGFP stable cell pools (D) cultured in shake flasks (dashed lines) and in bioreactor (straight lines). Ala: alanine, Asn: asparagine, Asp: aspartate, Gln: glutamine, Glu: glutamate, Leu: leucine

tive impact on protein expression. Culture of the Gag-eGFP VLP stable cell pool at bioreactor scale was successfully achieved, with a 2-fold improvement in VLP production and a reduction in by-product formation and accumulation compared with shake flask cultures. Analysis of High Five cell metabolism revealed a general increase in the uptake of amino acids in the stable cell pool, highlighting a higher metabolic cargo due to VLP production.

Future works will be conducted to determine the conditions for perfusion cultures and design feeding strategies to intensify cell growth and final VLP titers with the aim to establish a baculovirus-free production process for VLP-based vaccines.

ACKNOWLEDGMENTS

The authors would like to thank Dr. Paula Alves (Instituto de Biologia Experimental e Tecnológica, Oeiras, Portugal) for providing the BTI-TN-5B1-4 cell line and the pIZTV5-his plasmid. Ángel Calvache (Beckman Coulter) facilitated the access to the CytoFlex LX flow cytometer. The support of Núria Barba (Servei de Microscòpia, UAB) and Manuela Costa (Servei de Cultius Cel·lulars, Producció d'Anticossos i Citometria, UAB) with confocal microscopy and FACS is appreciated. Irene González-Domínguez (Departament d'Enginyeria Química, Biològica i Ambiental, UAB) developed the mCherry standard curve and Sahar Masoumeh (University of Natural Resources and Life Sciences, Vienna, Austria) provided support in the ELISA quantification. Eduard Puente-Massaguer is a recipient of an FPU grant from Ministerio de Educación, Cultura y Deporte of Spain (FPU15/03577). The research group is recognized as 2017 SGR 898 by Generalitat de Catalunya.

CONFLICT OF INTEREST

The authors declare that they have no competing interests.

AUTHOR CONTRIBUTIONS

Eduard Puente-Massaguer: Conceptualization-Lead, Formal analysis-Lead, Investigation-Lead, Methodology-Lead, Software-Equal, Writing-original draft-Lead; Paula Grau-Garcia: Formal analysis-Equal, Investigation-Lead; Florian Strobl: Methodology-Equal, Software-Equal; Reingard Grabherr: Funding acquisition-Equal, Resources-Equal, Writing-review & editing-Equal; Gerald Striedner: Funding acquisition-Equal, Resources-Equal, Writing-review & editing-Equal; Martí Lecina: Supervision-Equal, Writing-review & editing-Equal; Francesc Godia: Funding acquisition-Equal, Project administration-Lead, Resources-Equal, Supervision-Equal, Writing-review & editing-Equal.

DATA AVAILABILITY STATEMENT

The data that supports the findings of this study are available in the supplementary material of this article.

ORCID

Eduard Puente-Massaguer https://orcid.org/0000-0002-2816-7051

REFERENCES

1. Stolt-Bergner, P., Benda, C., Bergbrede, T., Besir, H., Celie, P. H. N., Chang, C., … Suppmann, S. (2018). Baculovirus-driven protein expression in insect cells: A benchmarking study. *J. Struct. Biol.*, *203*, 71–80.
2. van Oers, M. M., Pijlman, G. P., & Vlak, J. M. (2015). Thirty years of baculovirus–insect cell protein expression: From dark horse to mainstream technology. *J. Gen. Virol.*, *96*, 6–23.
3. Mena, J. A., & Kamen, A. A. (2011). Insect cell technology is a versatile and robust vaccine manufacturing platform. *Expert Rev. Vaccines.*, *10*, 1063–1081.
4. Gutiérrez-Granados, S., Cervera, L., Kamen, A. A., & Gòdia, F. (2018). Advancements in mammalian cell transient gene expression (TGE) technology for accelerated production of biologics. *Crit. Rev. Biotechnol.*, *38*, 918–940.
5. Hacker, D. L., De Jesus, M., & Wurm, F. M. (2009). 25 years of recombinant proteins from reactor-grown cells — Where do we go from here?. *Biotechnol. Adv.*, *27*, 1023–1027.
6. Román, R., Miret, J., Roura, A., Casablancas, A., Lecina, M., & Cairó, J. J. (2019). Enabling HEK293 cells for antibiotic-free media bioprocessing through CRISPR/Cas9 gene editing. *Biochem. Eng. J.*, *151*, 107299.
7. Fernandes, F., Vidigal, J., Dias, M. M., Prather, K. L. J., Coroadinha, A. S., Teixeira, A. P., & Alves, P. M. (2012). Flipase-mediated cassette exchange in Sf9 insect cells for stable gene expression. *Biotechnol. Bioeng.*, *109*, 2836–2844.
8. Gaj, T., Gersbach, C. A., & Barbas, C. F. (2013). ZFN, TALEN, and CRISPR/Cas-based methods for genome engineering. *Trends Biotechnol.*, *31*, 397–405.
9. Phan, Q. V., Contzen, J., Seemann, P., & Gossen, M. (2017). Site-specific chromosomal gene insertion: Flp recombinase versus Cas9 nuclease. *Sci. Rep.*, *7*, 1–12.
10. Hacker, D. L., & Balasubramanian, S. (2016). Recombinant protein production from stable mammalian cell lines and pools. *Curr. Opin. Struct. Biol.*, *38*, 129–136.
11. Pilbrough, W., Munro, T. P., & Gray, P. (2009). Intraclonal protein expression heterogeneity in recombinant CHO cells. *PLoS One*, *4*, 1–11.
12. Tharmalingam, T., Barkhordarian, H., Tejeda, N., Daris, K., Yaghmour, S., Yam, P., … Stevens, J. (2018). Characterization of phenotypic and genotypic diversity in subclones derived from a clonal cell line. *Biotechnol. Prog.*, *34*, 613–623.
13. Scarcelli, J. J., Hone, M., Beal, K., Ortega, A., Figueroa, B., Starkey, J. A., & Anderson, K. (2018). Analytical subcloning of a clonal cell line demonstrates cellular heterogeneity that does not impact process consistency or robustness. *Biotechnol. Prog.*, *34*, 602–612.
14. Vcelar, S., Melcher, M., Auer, N., Hrdina, A., Puklowski, A., Leisch, F., … Borth, N. (2018). Changes in chromosome counts and patterns in CHO cell lines upon generation of recombinant cell lines and subcloning. *Biotechnol. J.*, *13*, 1–9.
15. Balasubramanian, S., Peery, R. B., Minshull, J., Lee, M., White, R., Kelly, R. M., & Barnard, G. C. (2018). Generation of high expressing chinese hamster ovary cell pools using the leap-in transposon system. *Biotechnol. J.*, *13*, 1700748.
16. Poulain, A., Perret, S., Malenfant, F., Mullick, A., Massie, B., & Durocher, Y. (2017) Rapid protein production from stable CHO cell pools using plasmid vector and the cumate gene-switch. *J. Biotechnol.*, *255*, 16–27.
17. Rajendra, Y., Balasubramanian, S., McCracken, N. A., Norris, D. L., Lian, Z., Schmitt, M. G., … Barnard, G. C. (2017). Evaluation of piggyBac-mediated CHO pools to enable material generation to support GLP toxicology studies. *Biotechnol. Prog.*, *33*, 1436–1448.
18. Vidigal, J., Fernandes, B., Dias, M. M., Patrone, M., Roldão, A., Carrondo, M. J. T., … Teixeira, A. P. (2018). RMCE-based insect cell platform to produce membrane proteins captured on HIV-1 Gag virus-like particles. *Appl. Microbiol. Biotechnol.*, *102*, 655–666.
19. Fernandes, B., Vidigal, J., Correia, R., Carrondo, M. J. T., Alves, P. M., Teixeira, A. P., & Roldão, A. (2020). Adaptive laboratory evolution of stable insect cell lines for improved HIV-Gag VLPs production. *J. Biotechnol.*, *307*, 139–147.
20. Puente-Massaguer, E., Lecina, M., & Gòdia, F. (2018). Nanoscale characterization coupled to multi-parametric optimization of Hi5 cell transient gene expression. *Appl. Microbiol. Biotechnol.*, *102*, 10495–10510.
21. Shen, X., Pitol, A. K., Bachmann, V., Hacker, D. L., Baldi, L., & Wurm, F. M. (2015). A simple plasmid-based transient gene expression method using High Five cells. *J. Biotechnol.*, *216*, 67–75.
22. Puente-Massaguer, E., Lecina, M., & Gòdia, F. (2020). Integrating nanoparticle quantification and statistical design of experiments for efficient HIV-1 virus-like particle production in High Five cells. *Appl. Microbiol. Biotechnol.*, *104*, 1569–1582.
23. Krammer, F., Schinko, T., Palmberger, D., Tauer, C., Messner, P., & Grabherr, R. (2010). Trichoplusia ni cells (High Five™) are highly efficient for the production of influenza A virus-like particles: A comparison of two insect cell lines as production platforms for influenza vaccines. *Mol. Biotechnol.*, *45*, 226–234.
24. Hermida-Matsumoto, L., & Resh, M. D. (2000). Localization of human immunodeficiency virus type 1 gag and env at the plasma membrane by confocal imaging. *J. Virol.*, *74*, 8670–8679.
25. Puente-Massaguer, E., Gòdia, F., & Lecina, M. (2020). Development of a non-viral platform for rapid virus-like particle production in Sf9 cells. *J. Biotechnol.*, *322*, 43–53.
26. Berrow, N. S., Alderton, D., Sainsbury, S., Nettleship, J., Assenberg, R., Rahman, N., … Owens, R. J. (2007). A versatile ligation-independent cloning method suitable for high-throughput expression screening applications. *Nucleic Acids Res.*, *35*, 1–12.
27. Bleckmann, M., Schürig, M., Chen, F. F., Yen, Z. Z., Lindemann, N., Meyer, S., … Van Den Heuvel, J. (2016). Identification of essential genetic baculoviral elements for recombinant protein expression by transactivation in Sf21 insect cells. *PLoS One*, *11*, 1–19.
28. Vidigal, J., Dias, M. M., Fernandes, F., Patrone, M., Bispo, C., Andrade, C., … Teixeira, A. P. (2013). A cell sorting protocol for selecting high-producing sub-populations of Sf9 and High Five™ cells. *J. Biotechnol.*, *168*, 436–439.
29. Ikonomou, L., Schneider, Y. J., & Agathos, S. N. (2003). Insect cell culture for industrial production of recombinant proteins. *Appl. Microbiol. Biotechnol.*, *62*, 1–20.
30. Sleiman, R. J., Gray, P. P., McCall, M. N., Codamo, J., & Sunstrom, N. A. S. (2008). Accelerated cell line development using two-color fluorescence activated cell sorting to select highly expressing antibody-producing clones. *Biotechnol. Bioeng.*, *99*, 578–587.
31. Kempf, J., Snook, L. A., Vonesch, J. L., Dahms, T. E. S., Pattus, F., & Massotte, D. (2002) Expression of the human μ opioid receptor in a stable Sf9 cell line. *J. Biotechnol.*, *95*, 181–187.
32. Hernandez, I., Dhiman, H., Klanert, G., Jadhav, V., Auer, N., Hanscho, M., … Borth, N. (2019). Epigenetic regulation of gene expression in Chinese Hamster Ovary cells in response to the changing environment of a batch culture. *Biotechnol. Bioeng.*, *116*, 677–692.
33. Osterlehner, A., Simmeth, S., & Göpfert, U. (2011). Promoter methylation and transgene copy numbers predict unstable protein production in recombinant chinese hamster ovary cell lines. *Biotechnol. Bioeng.*, *108*, 2670–2681.
34. Spencer, S., Gugliotta, A., Koenitzer, J., Hauser, H., & Wirth, D. (2015). Stability of single copy transgene expression in CHOK1 cells is affected by histone modifications but not by DNA methylation. *J. Biotechnol.*, *195*, 15–29.
35. Pichler, J., Galosy, S., Mott, J., & Borth, N. (2011). Selection of CHO host cell subclones with increased specific antibody production rates by repeated cycles of transient transfection and cell sorting. *Biotechnol. Bioeng.*, *108*, 386–394.

36. Monteiro, F., Bernal, V., Saelens, X., Lozano, A. B., Bernal, C., Sevilla, A., … Alves, P. M. (2014). Metabolic profiling of insect cell lines: Unveiling cell line determinants behind system's productivity. *Biotechnol. Bioeng.*, *111*, 816–828.
37. González-Domínguez, I., Puente-Massaguer, E., Cervera, L., & Gòdia, F. (2020). Quality Assessment of Virus-Like Particles at Single Particle Level: A Comparative Study. *Viruses*, *12*, 223.
38. Steppert, P., Burgstaller, D., Klausberger, M., Berger, E., Aguilar, P. P., Schneider, T. A., … Jungbauer, A. (2016). Purification of HIV-1 gag virus-like particles and separation of other extracellular particles. *J. Chromatogr. A.*, *1455*, 93–101.
39. Reiter, K., Aguilar, P. P., Wetter, V., Steppert, P., Tover, A., & Jungbauer, A. (2019). Separation of virus-like particles and extracellular vesicles by flow-through and heparin affinity chromatography. *J. Chromatogr. A.*, *1588*, 77–84.
40. Lavado-García, J., Cervera, L., & Gòdia, F. (2020). An Alternative Perfusion Approach for the Intensification of Virus-Like Particle Production in HEK293 Cultures. *Front. Bioeng. Biotechnol.*, *8*, 617.
41. Monteiro, F., Bernal, V., Chaillet, M., Berger, I., & Alves, P. M. (2016). Targeted supplementation design for improved production and quality of enveloped viral particles in insect cell-baculovirus expression system. *J. Biotechnol.*, *233*, 34–41.
42. Xie, Q., Michel, P. O., Baldi, L., Hacker, D. L., Zhang, X., & Wurm, F. M. (2011). TubeSpin bioreactor 50 for the high-density cultivation of Sf-9 insect cells in suspension. *Biotechnol. Lett.*, *33*, 897–902.
43. Strobl, F., Ghorbanpour, S. M., Palmberger, D., & Striedner, G. (2020). Evaluation of screening platforms for virus-like particle production with the baculovirus expression vector system in insect cells. *Sci. Rep.*, *10*, 1065.
44. Rhiel, M., Mitchell-Logean, C. M., & Murhammer, D. W. (1997). Comparison of trichoplusia ni BTI-Tn-5b1-4 (high five(TM) and spodoptera frugiperda Sf-9 insect cell line metabolism in suspension cultures. *Biotechnol. Bioeng.*, *55*, 909–920.
45. Stavroulakis, D. A., Kalogerakis, N., Behie, L. A., & Latrou, K. (1991). Kinetic data for the BM-5 insect cell line in repeated-batch suspension cultures. *Biotechnol. Bioeng.*, *38*, 116–126.
46. Drugmand, J. C., Schneider, Y. J., & Agathos, S. N. (2012). Insect cells as factories for biomanufacturing. *Biotechnol. Adv.*, *30*, 1140–1157.
47. Puente-Massaguer, E., Strobl, F., Grabherr, R., Striedner, G., Lecina, M., & Gòdia, F. (2020). PEI-mediated transient transfection of high five cells at bioreactor scale for HIV-1 VLP production. *Nanomaterials*, *10*, 1–16.
48. Monteiro, F., Bernal, V., & Alves, P. M. (2017). The role of host cell physiology in the productivity of the baculovirus-insect cell system: Fluxome analysis of Trichoplusia ni and Spodoptera frugiperda cell lines. *Biotechnol. Bioeng.*, *114*, 674–684.
49. Bédard, C., Kamen, A., Tom, R., & Massie, B. (1994). Maximization of recombinant protein yield in the insect cell/baculovirus system by one-time addition of nutrients to high-density batch cultures. *Cytotechnology*, *15*, 129–138.

SUPPORTING INFORMATION

Additional supporting information may be found online in the Supporting Information section at the end of the article.

How to cite this article: Puente-Massaguer, E., Grau-Garcia, P., Strobl, F., Grabherr, R., Striedner, G., Lecina, M., & Gòdia, F. (2021). Accelerating HIV-1 VLP production using stable insect cell pools. *Biotechnol J*, 16, e2000391. https://doi.org/10.1002/biot.202000391

Research article

Title: Accelerating HIV-1 VLP production using stable High Five insect cell pools

Eduard Puente-Massaguer [1]*

Paula Grau-Garcia [1]

Florian Strobl [2, 3]

Reingard Grabherr [3]

Gerald Striedner [3]

Martí Lecina [4]

Francesc Gòdia [1]

[1] Departament d'Enginyeria Química, Biològica i Ambiental, Universitat Autònoma de Barcelona, Cerdanyola del Vallès, Barcelona, 08193, Spain

[2] Austrian Centre of Industrial Biotechnology (acib GmbH), Vienna, 1010, Austria

[3] Department of Biotechnology, University of Natural Resources and Life Sciences, Vienna, 1190, Austria

[4] IQS School of Engineering, Universitat Ramón Llull, Barcelona, 08017, Spain

***Correspondence:** Dr. Eduard Puente-Massaguer, Departament d'Enginyeria Química, Biològica i Ambiental, Universitat Autònoma de Barcelona, carrer de les Sitges, 08193 Cerdanyola del Vallès, Barcelona, Spain

E-mail: eduard.puente-massaguer@mssm.edu

ORCID: 0000-0002-2816-7051

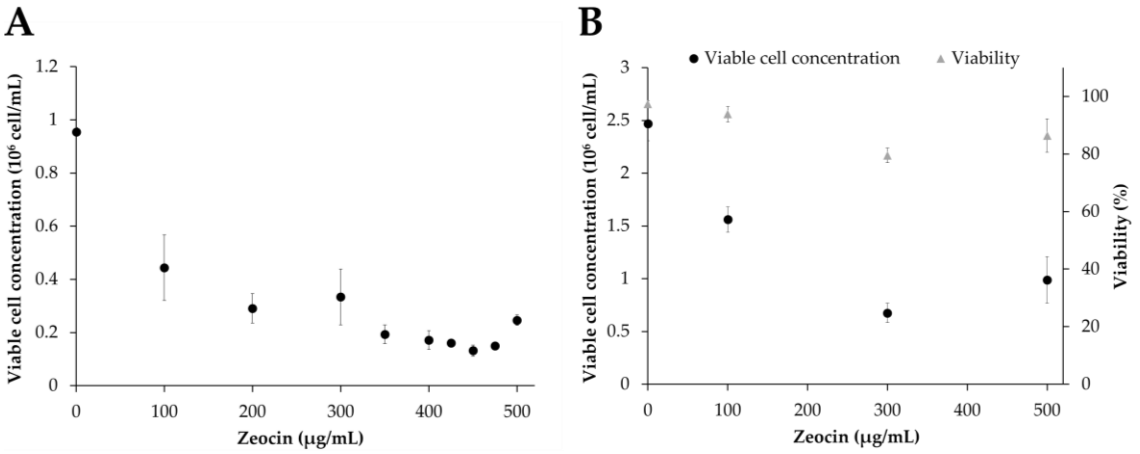

Figure S1. Cytotoxicity assays in parental High Five cells with the antibiotic zeocin. (A) Viable cell concentration with different zeocin concentration in a 96-well plate (Nunc, Thermo Fisher Scientific). The colorimetric CellTiter® 96 AQ_{ueous} One Solution Cell Proliferation Assay (Promega, Madison, WI, USA) was used to measure cell proliferation at 48 h post zeocin addition according to manufacturer's instructions. Cells were seeded at 0.3 × 10^6 cell/mL and maintained at 130 rpm and 27 °C. A calibration curve of known High Five cell concentration (0 - 1.3 × 10^6 cell/mL) was included to transform absorbance measurements to cell concentration. (B) Viable cell concentration and viability of High Five cells cultured in 10 mL of Sf900III medium in Erlenmeyer shake flasks at 48 h post antibiotic addition. Cells were seeded at 0.5 × 10^6 cell/mL. Results from triplicate experiments are represented.

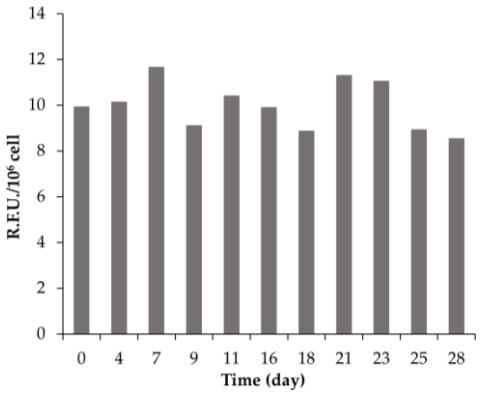

Figure S2. Analysis of the intracellular production levels of the Gag-eGFP stable cell pool. Gag-eGFP fluorescence is measured by spectrofluorometry. Cells were maintained in the exponential phase during the stability experiment.

Publication VI

EBioMedicine 67 (2021) 103348

Contents lists available at ScienceDirect

EBioMedicine

journal homepage: www.elsevier.com/locate/ebiom

Research paper

A comprehensive antigen production and characterisation study for easy-to-implement, specific and quantitative SARS-CoV-2 serotests

Miriam Klausberger[a,1], Mark Duerkop[a,b,1], Helmuth Haslacher[c], Gordana Wozniak-Knopp[a,d], Monika Cserjan-Puschmann[a,e], Thomas Perkmann[c], Nico Lingg[a,e], Patricia Pereira Aguilar[a,e], Elisabeth Laurent[a,f], Jelle De Vos[a,g], Manuela Hofner[h], Barbara Holzer[i], Maria Stadler[j], Gabriele Manhart[k], Klemens Vierlinger[h], Margot Egger[l], Lisa Milchram[h], Elisabeth Gludovacz[a], Nicolas Marx[a], Christoph Köppl[a,e], Christopher Tauer[a], Jürgen Beck[a], Daniel Maresch[m], Clemens Grünwald-Gruber[m,n], Florian Strobl[o], Peter Satzer[a,e], Gerhard Stadlmayr[a,d], Ulrike Vavra[p], Jasmin Huber[h], Markus Wahrmann[q], Farsad Eskandary[q], Marie-Kathrin Breyer[r], Daniela Sieghart[s], Peter Quehenberger[c], Gerda Leitner[t], Robert Strassl[c], Alexander E. Egger[u], Christian Irsara[u], Andrea Griesmacher[u], Gregor Hoermann[u,v], Günter Weiss[w], Rosa Bellmann-Weiler[w], Judith Loeffler-Ragg[w,2], Nicole Borth[a], Richard Strasser[p], Alois Jungbauer[a,e], Rainer Hahn[a,e], Jürgen Mairhofer[o], Boris Hartmann[i], Nikolaus B. Binder[x], Gerald Striedner[a,b,e,o], Lukas Mach[p], Andreas Weinhäusel[h], Benjamin Dieplinger[l], Florian Grebien[k,*], Wilhelm Gerner[j,y,z,1], Christoph J. Binder[c,1,*], Reingard Grabherr[a,1,*]

[a] *Department of Biotechnology, University of Natural Resources and Life Sciences (BOKU) Vienna, Muthgasse 18, 1190 Vienna, Austria*
[b] *Novasign GmbH Vienna, Austria*
[c] *Department of Laboratory Medicine, Medical University of Vienna, Währinger Gürtel 18-20, 1090 Vienna, Austria*
[d] *CD Laboratory for innovative Immunotherapeutics, Vienna, Austria*
[e] *ACIB-Austrian Centre of Industrial Biotechnology, Graz, Austria*
[f] *BOKU Core Facility Biomolecular & Cellular Analysis, University of Natural Resources and Life Sciences (BOKU),Vienna, Austria*
[g] *Department of Chemical Engineering, Vrije Universiteit Brussel (VUB), Brussels, Belgium*
[h] *Competence Unit Molecular Diagnostics, Center for Health and Bioresources, AIT Austrian Institute of Technology GmbH, Vienna, Austria*
[i] *Austrian Agency for Health and Food Safety (AGES), Department for Animal Health, Moedling, Austria*
[j] *Institute of Immunology, University of Veterinary Medicine, Vienna, Austria*
[k] *Institute for Medical Biochemistry, University of Veterinary Medicine, Veterinärplatz 1, 1210 Vienna, Austria*
[l] *Department of Laboratory Medicine, Konventhospital Barmherzige Brueder Linz and Ordensklinikum Linz Barmherzige Schwestern, Linz, Austria*
[m] *BOKU Core Facility Mass Spectrometry, University of Natural Resources and Life Sciences (BOKU), Vienna, Austria*
[n] *Department of Chemistry, University of Natural Resources and Life Sciences (BOKU) Vienna, Austria*
[o] *enGenes Biotech GmbH, Vienna, Austria*
[p] *Department of Applied Genetics and Cell Biology, University of Natural Resources and Life Sciences (BOKU) Vienna, Austria*
[q] *Department of Medicine III, Division of Nephrology and Dialysis, Medical University of Vienna, Austria*
[r] *Department of Respiratory and Critical Care Medicine and Ludwig Boltzmann Institute for Lung Health, Otto Wagner Hospital, Vienna, Austria*
[s] *Division of Rheumatology, Department of Medicine III, Medical University of Vienna, Austria*
[t] *Department of Blood Group Serology and Transfusion Medicine, Medical University of Vienna, Austria*
[u] *Central Institute for Medical and Chemical Laboratory Diagnosis, Innsbruck University Hospital, Innsbruck, Austria*
[v] *MLL Munich Leukemia Laboratory, Munich, Germany*
[w] *Department of Internal Medicine II, Innsbruck Medical University, Innsbruck, Austria*
[x] *Technoclone Herstellung von Diagnostika und Arzneimitteln GmbH, Vienna, Austria*
[y] *Christian Doppler Laboratory for an Optimized Prediction of Vaccination Success in Pigs, University of Veterinary Medicine, Vienna, Austria*
[z] *Present address: The Pirbright Institute, Pirbright, United Kingdom*

* Corresponding authors.
E-mail addresses: florian.grebien@vetmeduni.ac.at (F. Grebien), christoph.binder@meduniwien.ac.at (C.J. Binder), reingard.grabherr@boku.ac.at (R. Grabherr).
[1] These authors contributed equally to this work.
[2] On behalf of the CovILD study group.

https://doi.org/10.1016/j.ebiom.2021.103348

ARTICLE INFO

Article History:
Received 9 February 2021
Revised 15 March 2021
Accepted 2 April 2021
Available online 25 April 2021

Keywords:
COVID-19
Antibody assay validation
Antigen purity
Dual-antigen testing
SARS-CoV-2 neutralisation
Kinetics of primary antibody response

ABSTRACT

Background: Antibody tests are essential tools to investigate humoral immunity following SARS-CoV-2 infection or vaccination. While first-generation antibody tests have primarily provided qualitative results, accurate seroprevalence studies and tracking of antibody levels over time require highly specific, sensitive and quantitative test setups.
Methods: We have developed two quantitative, easy-to-implement SARS-CoV-2 antibody tests, based on the spike receptor binding domain and the nucleocapsid protein. Comprehensive evaluation of antigens from several biotechnological platforms enabled the identification of superior antigen designs for reliable serodiagnostic. Cut-off modelling based on unprecedented large and heterogeneous multicentric validation cohorts allowed us to define optimal thresholds for the tests' broad applications in different aspects of clinical use, such as seroprevalence studies and convalescent plasma donor qualification.
Findings: Both developed serotests individually performed similarly-well as fully-automated CE-marked test systems. Our described sensitivity-improved orthogonal test approach assures highest specificity (99.8%); thereby enabling robust serodiagnosis in low-prevalence settings with simple test formats. The inclusion of a calibrator permits accurate quantitative monitoring of antibody concentrations in samples collected at different time points during the acute and convalescent phase of COVID-19 and disclosed antibody level thresholds that correlate well with robust neutralization of authentic SARS-CoV-2 virus.
Interpretation: We demonstrate that antigen source and purity strongly impact serotest performance. Comprehensive biotechnology-assisted selection of antigens and in-depth characterisation of the assays allowed us to overcome limitations of simple ELISA-based antibody test formats based on chromometric reporters, to yield comparable assay performance as fully-automated platforms.
Funding: WWTF, Project No. COV20−016; BOKU, LBI/LBG

Research in context

Evidence before this study

Highly specific, yet sensitive SARS-CoV-2 serodiagnosis for seroprevalence studies or quantitative serotesting almost exclusively relies on fully-automated test platforms, merely available only in well-equipped diagnostic laboratories. Yet, academic research groups and laboratories with basic equipment require access to high-quality test formats for robust and meaningful SARS-CoV-2 seroanalysis. Of note, quantitative high-quality test formats that are easy-to-implement are gaining additional importance as means to characterise the extent of vaccine-induced immunity and to monitor decline of antibody titres over time.

Added value of this study

The present study describes two extensively validated quantitative and highly specific IgG antibody tests that rely on optimised designs of the SARS-CoV-2 receptor binding domain and nucleocapsid protein. In validation studies with unprecedented large and heterogenous multi-centric specificity and sensitivity cohorts, including samples with an increased propensity for cross-reactivity and convalescent sera from SARS-CoV-2-infected individuals covering the full spectrum of clinical manifestations, the simple ELISA-based antibody tests performed equally well or even better than fully automated CE-marked test platforms. Our study highlights that antibody test performance is already influenced as early as by the choice of the antigen production system and discloses process-related peculiarities and parameters that are often underestimated in terms of an antigen for diagnostic use. Moreover, we disclose that false positive and false negative results are highly antigen-dependent. With strategic cut-off modelling and sensitivity-improved orthogonal testing, we provide optimised approaches for different aspects of clinical utility, ranging from serodiagnosis in low-prevalence settings to monitoring antibody levels after infection.

Implications of all the available evidence

Our findings propose that antigen selection and quality are crucial aspects for assay development and may profoundly influence diagnostic performance. A comprehensive approach supported by biotechnological quality attributes aid in improving selectivity of the tests and thereby test performance. Well-characterised, quantitative and simple test formats are urgently needed to support the thorough characterisation of infection- and vaccine-induced antibody responses and their longevity in any research laboratory with minimal equipment. The comprehensively characterised test systems and highly pure antigen reagents described in this study are available from the authors under disclosed addresses.

1. Introduction

Serological testing of severe acute respiratory syndrome coronavirus 2 (SARS-CoV-2) infections remains an essential tool for seroprevalence studies and complements PCR-based diagnosis in identifying asymptomatic individuals [1]. Antibody tests are gaining additional importance as means to characterise the extent of infection- or vaccine-induced immunity. To cope with the urgent demand for sensitive and reliable test systems, many manual and automated serological tests for coronavirus disease 2019 (COVID-19) became available within a short period of time [2]. Owing to the acuity of a spreading pandemic, many of these early developed test systems lacked adequate validation and thereby fuelled mistrust, while stocks of others were exhausted rapidly due to increased demand [3].

Antigen selection and quality are crucial aspects of assay development and influence diagnostic performance [4], such as sensitivity and specificity as well as assay availability, scalability and their field of application. Ideal candidate antigens for *in-vitro* serodiagnosis are highly immunogenic, support early and robust detection of seroconversion after an infection and result in low false positivity rates. Additionally, production platforms supporting high process yields ensure

sustainable assay supply. To date, biotechnological performance attributes and their influence on serodiagnostics have not been reported during the development of assays for SARS-CoV-2 detection. Likewise, no comprehensive study comparing and validating the same SARS-CoV-2 antigen produced in different expression systems with larger cohorts is available.

In this study, we developed two quantitative, enzyme-linked immunosorbent assay (ELISA)-based serotests relying on the SARS-CoV-2 receptor-binding domain (RBD) and nucleocapsid protein (NP) antigens of superior design and quality. Thus far, quantitative tests usually rely on automated test systems. Yet, also minimally-equipped academic and diagnostic laboratories require affordable and high-quality test formats for robust and meaningful SARS-CoV-2 seroanalysis. Since the developed assays utilise established ELISA technology, they are easy to implement in any minimally-equipped lab worldwide. For a simple chromogenic test format with a narrow dynamic measurement range the quality of the diagnostic antigen is particularly important. We describe a comprehensive approach for the first time assessing biotechnological parameters such as antigen quality attributes and manufacturability for an ideal test setup. For this purpose, we compared several animal cell lines and plant-based expression platforms for their ability to support high-quantity and quality RBD production and assessed whether the employed production host influences antigen performance. We extensively validated the tests for clinical utility featuring sera from individuals covering the full spectrum of disease presentations at different time points post infection and a large specificity cohort including samples with antibodies towards endemic human coronaviruses (hCoVs) and those from individuals with underlying non-infectious diseases. Moreover, we validated the tests with time-resolved acute and early convalescent samples from hospitalised patients and showed that only RBD-specific antibodies demonstrate excellent correlation with neutralization assays already in the early phase of infection. Our extensive validation allowed us to define tailor-made test cut-off criteria for the highly diverse fields of clinical applications, which greatly differ in their demands.

2. Methods

2.1. Production of recombinant SARS-CoV-2 antigens for serodiagnosis

2.1.1. Genetic constructs

pCAGGS mammalian expression vectors encoding the canonical SARS-CoV-2 receptor-binding domain (RBD, pCAGGS-RBD, aa Arg319 – Phe541, residue numbering as in NCBI Reference sequence: YP_009724390.1) sequence from the first human isolate Wuhan-1 [5] with a C-terminal hexa-histidine tag, were a kind gift from Florian Krammer, Icahn School of Medicine at Mount Sinai, NY [4]. Both sequences were codon-optimised for the expression in mammalian cells.

A pTT28 mammalian expression vector (National Research Council, NRC, Ottawa, Canada) encoding a truncated version of the SARS-CoV-2 Spike receptor-binding domain (tRBD, pTT28-tRBD, aa Arg319 - Lys537) with a C-terminal octa-histidine tag was generated.

A pEAQ-HT plant expression vector [6] encoding RBD (pEAQ-HT-RBD, aa Arg319 – Phe541) fused to the barley α-amylase signal peptide and a C-terminal hexa-histidine tag was generated. The RBD sequence was codon-optimised for the expression in plants and synthesized by GeneArt (Thermo Fisher Scientific, Regensburg, DE).

A pET30a*cer E. coli* expression vector [7] encoding the full-length SARS-CoV-2 Wuhan-1 NP sequence (aa Met1–Ala419, GenBank: NC_045512.2) [5] fused to a completely removable N-terminal CASPON tag [8,9], yielding pET30a*cer*-CASPON—NP, was generated as described elsewhere [10]. Briefly, SARS-CoV-2 NP sequence was amplified via PCR using the qPCR positive control plasmid 2019-nCoV_N obtained from Integrated DNA Technologies (Coralville, Iowa, USA) and was fused to the CASPON tag consisting of the negative charged T7AC solubility tag [8], a hexa-histidine tag, a short linker (GSG) and the caspase-2 cleavage site (VDVAD) resulting in the sequence MLEDPERNKERKEAELQAQTAEQHHHHHHGSGVDVAD.

Expression vectors pFUSEss-CHIg-hG1 and pFUSEss2-CLIg-hK, encoding the heavy and light chains of the SARS-CoV/SARS-CoV-2 monoclonal antibody CR3022 [11] were kindly provided by Florian Krammer (Icahn School of Medicine at Mount Sinai, New York, NY).

2.1.2. Large-scale production of transfection-grade plasmid DNA

Plasmid DNA for transient transfection of HEK293–6E cells was produced according to an upstream process described previously [12]. Briefly, the plasmids pCAGGS-RBD and pTT28-tRBD were transformed into *E. coli* JM108 by electroporation and cultivated in 1-L fed-batch mode. Cells were harvested by centrifugation and pDNA was extracted by alkaline lysis at 5 g/L cellular dry mass (CDM) following a protocol of Urthaler and colleagues [13]. pDNA was processed to >95% purity by multiple chromatography steps based on a platform purification protocol (Cytiva, Little Chalfont, UK) [14].

2.1.3. Transient expression of RBD, tRBD and NP in diverse biotechnological platforms

Human embryonic kidney cells: Shake flask cultivation. HEK293–6E cells (licensed from National Research Council, NRC, Ottawa, Canada) were routinely cultivated in suspension in Freestyle™ F17 medium supplemented with 4 mM L-glutamine, 0.1% (v/v) Pluronic F-68 and 25 μg/mL G-418 (all Thermo Fisher Scientific, Waltham, MA) in a humidified atmosphere of 5–8% (v/v) CO_2 at 37 °C shaking at 125 rpm. Polyethylenimine (PEI)-mediated transient transfections with either pCAGGS-RBD, pTT28-tRBD or pFUSEss-CHIg-hG1 and pFUSEss2-CLIg-hK for the expression or RBD, tRBD or mAb CR3022 were performed according to the manufacturer's protocol as previously described [15,16].

Transfections were performed by dropwise addition of a mixture of one μg plasmid DNA and two μg linear 25-kDa or 40-kDa PEI (Polysciences, Inc., Hirschberg, DE) per mL of culture volume ($1.7–2.0 \times 10^6$ cells/mL). Two- and four-days post-transfection, cells were supplemented with 0.5% (w/V) tryptone N1 (Organotechnie, La Courneuve, FR) and 0.25% (w/V) D (+)-glucose (Carl Roth, Karlsruhe, DE). Supernatants were harvested five to six days post-transfection by centrifugation (2000 g, 15 min) and were filtered through 0.45 μm filters before downstream procedures.

Medium-scale cultivation. Stepwise upscaling was performed using a Multi-bioreactor system DASGIP (Eppendorf, Hamburg, DE) followed by a 10-L scale bioreactor System BioFlo320 (Eppendorf, Hamburg, DE). The bioreactors were inoculated at half the final volume (F17 expression medium supplemented with 4 mM L-Glutamine and 0.1% (v/v) Pluronic) with a seeding density of 0.5×10^6 cells/mL. The inoculum was prepared in shake flask cultures as described above. The bioreactors were controlled to a pH of 7.2 using CO_2 and 7.5% (w/V) carbonate base and to 50% (v/v) dissolved oxygen by submerged aeration. Transfection was performed at a cell concentration of 1.7×10^6 cells/mL. PEI and the respective plasmid DNA were diluted in media, mixed and incubated at room temperature for ten minutes prior to addition to the cultures (45 μg PEI and 15 μg of plasmid per 10^6 cells). Twenty-four hours post transfection, cells were expanded and 24 h later were fed TN1 peptone at a concentration of 0.5% (v/v). Each day post-transfection viability, cell density and glucose concentration were measured and a daily bolus feed to a glucose concentration of 2.5 g/L was performed. The cultures were harvested once viability dropped below 60%.

Chinese hamster ovary cells: CHO-K1 and CHO-S cells were routinely propagated in CD-CHO medium (Thermo Fisher Scientific, Waltham, MA) or in Hyclone Actipro medium (Cytiva, Chicago, IL) both supplemented with 0.2% (v/v) Anti-Clumping Agent (Thermo Fisher Scientific, Waltham, MA) and 8 mM L-glutamine (CHO-K1, Sigma

Aldrich, St. Louis, MO) or 8 mM GlutaMAX (CHO-S, Thermo Fisher Scientific, Waltham, MA), respectively. Cells were cultivated in suspension at 37 °C, 7% (v/v) CO_2 and humidified air, shaking at 140 rpm.

For nucleofection, a total of 1×10^7 cells in the exponential growth phase were pelleted for eight minutes at 170 g and were resuspended in 99 μL resuspension buffer R (Thermo Fisher Scientific, Waltham, MA). Cells were mixed with pCAGGS-RBD, which had been pre-diluted with UltraPure™ DNase/RNase-Free distilled water to a concentration of 2 μg/μL in a total volume of 11 μL and were electroporated with a Neon® Nucleofector using a 100 μL Neon® Transfection Kit (all Thermo Fisher Scientific, Waltham, MA) with 1700 V and one pulse of 20 ms. Seven to eight transfections per cell line were performed and subsequently pooled in a 500 mL shake flask with a 200 mL working volume. Supernatants were harvested five days post transfection by centrifugation (170 g, 10 min) and were sterile-filtered before further use.

*Insect cells: Tnms*42, an alphanodavirus-free subclone of the High-Five insect cell line [17,18], were routinely propagated in adherent culture in HyClone SFM4 insect cell medium (Cytiva, Marlborough, MA) at 27 °C and were expanded in suspension culture for recombinant protein expression. A passage one virus seed stock expressing the SARS CoV-2 RBD was amplified in *Sf*9 cells to generate a passage three working stock and was titrated by plaque assay as previously described [19]. *Tnms*42 insect cells at 2×10^6 cells/mL were infected at a multiplicity of infection (MOI) of two, and the supernatant was harvested three days post-infection, clarified (1000 g, 10 min, followed by 10,000 g, 30 min) and was filtered through a 0.45 μm filter before downstream procedures.

Tobacco plants: The pEAQ-HT-RBD expression vector was transformed into *Agrobacterium tumefaciens* strain UIA143 [6]. Syringe-mediated agroinfiltration of leaves from five-week-old *Nicotiana benthamiana* ΔXT/FT plants was used for transient expression [20]. Four days after infiltration, leaves were harvested and intracellular fluid was collected by low-speed centrifugation as described in detail elsewhere [21].

E. coli: The pET30a*cer*-CASPON—NP expression vector was transformed into *E. coli* enGenes-X-press for growth-decoupled recombinant protein production as described elsewhere [7]. Briefly, for cultivation cells were grown in fed-batch mode in a 1.0 L (0.5 L batch volume, 0.5 L feed) DASGIP® Parallel Bioreactor System (Eppendorf AG, Hamburg, DE) equipped with standard probes (pH, dissolved oxygen [pDO]). The pH was maintained at 7.0 ± 0.05, temperature was maintained at 37 ± 0.5 °C during the batch phase and decreased to 30 ± 0.5 °C at the beginning of the feed phase. The dissolved oxygen level was stabilized at > 30% (V/V). Induction of NP production was facilitated at feed hour 19 with the addition of 0.1 mM IPTG and 100 mM arabinose.

2.1.4. Downstream procedures

Purification of SARS-CoV-2 RBD and tRBD from different expression systems: His-tagged RBD and tRBD from filtered HEK supernatants, as well as RBD from *Tnms*42 insect cell supernatants, were concentrated and diafiltrated against 20 mM sodium phosphate buffer supplemented with 500 mM NaCl and 20 mM imidazole (pH 7.4) using a Labscale TFF system equipped with a Pellicon™ XL Ultracel 5 kDa, 0.005 m^2 ultrafiltration module (Merck, Darmstadt, DE). The proteins were captured using a 5-mL HisTrap FF Crude or a 1-mL HisTrap Excel immobilized metal affinity chromatography (IMAC) column connected to an ÄKTA Pure chromatography system (all from Cytiva, Marlborough, MA) and were eluted by applying a linear gradient of 20 to 500 mM imidazole over 5 to 20 column volumes, as appropriate. Intracellular fluid collected from plant material was directly loaded onto a 5-mL HisTrap HP column and was purified as described elsewhere [22]. CHO-K1 and CHO-S expression supernatants were supplemented with 20 mM imidazole and were directly loaded onto a 1-mL HisTrap FF column connected to an ÄKTA Start chromatography system (both Cytiva, Marlborough, MA), equilibrated with 50 mM sodium phosphate buffer supplemented with 300 mM NaCl and 20 mM imidazole (pH 7.4). Proteins were eluted by applying a linear gradient of 20 to 500 mM imidazole over 20 column volumes.

Fractions containing RBD or tRBD were pooled and either diluted with 20 mM sodium phosphate buffer (pH 7.4) to a conductivity of ~10 mS/cm and then loaded onto a Fractogel EMD DEAE column (Merck Millipore, Germany) or loaded onto HiTrap DEAE FF column (Cytiva, Marlborough, MA), both pre-equilibrated with 20 mM sodium phosphate buffer (pH 7.4). A residence time of two minutes was used. The flow-through fractions, containing RBD or tRBD, were collected. Impurities were subsequently eluted using 20 mM sodium phosphate buffer, 1 M NaCl, pH 7.4 and the column was cleaned in place by incubation in 0.5 M NaOH for 30 min. The protein of interest present in the flow-through fraction was buffer-exchanged into PBS using Amicon Ultra-15 Ultracel 10 kDa spin columns (Merck Millipore, Germany) or was dialyzed against PBS. IMAC-captured RBD from insect cell supernatants was ultra- and diafiltrated using Amicon Ultra Centrifugal Filter Units (10 kDa MWCO, Merck Millipore) to change the buffer to PBS and was further purified by size exclusion chromatography using a HiLoad 16/600 Superdex 200 pg column (Cytiva, Marlborough, MA) equilibrated with the same buffer. Fractions containing RBD were concentrated using Amicon Ultra-15 Ultracel 10 kDa spin columns (Merck Millipore, Germany). All purified proteins were quantified by measuring their absorbance at A_{280} with a Nanodrop instrument and stored at −80 °C until further use.

Purification of SARS-CoV-2 NP from E. coli cellular lysates: The purification of NP was optimised and performed as described by De Vos and colleagues [10]. In brief, NP was produced by using the CASPON platform process [9] with modifications. The process consisted of an IMAC capture step (WorkBeads 40 Ni NTA, Bio-Works, Uppsala, SE) of the clarified cell lysate. A nuclease treatment (Salt Active Nuclease High Quality, ArcticZymes Technologies ASA, Tromsø, NO) was required to reduce CASPON—NP nucleic acid binding. Imidazole was removed from the IMAC eluate using a Butyl Sepharose HP hydrophobic interaction chromatography (Cytiva, Uppsala, SE) which also separated full-length from fragmented CASPON—NP. A variant of cpCasp2 [8] was used to remove the affinity fusion-tag. Finally, an IMAC polishing step was used to separate native NP from residual CASPON—NP, the free affinity fusion-tag, the affinity-tagged cpCasp2 variant and metal binding host cell proteins. The polishing fraction was buffer exchanged to PBS using tangential flow filtration on Pellicon 3 Ultracel 10 kDa membrane (Merck Millipore, Darmstadt, DE).

Purification of mAb CR3022: mAb CR3022 was purified by affinity chromatography using a 5-mL HiTrap Protein A HP column connected to an ÄKTA pure chromatography system (both from Cytiva, Marlborough, MA) according to the manufacturer's protocol. The antibody was eluted using 0.1 M glycine-HCl buffer (pH 3.5). Eluate fractions containing CR3022 were immediately neutralized using 1 M Tris−HCl buffer (pH 8.0), pooled and concentrated using Amicon ultrafiltration cartridges with a cut-off of 10 kDa (Merck, Darmstadt, DE) and were further dialyzed against PBS (pH 7.4) at 4 °C overnight using Snake-Skin Dialysis Tubing with a 10 kDa cut-off (Thermo Fisher Scientific, Germering, DE). CR3022 was further purified by size exclusion chromatography using a HiLoad 16/600 Superdex 200 pg column (Cytiva, Marlborough, MA) equilibrated with the same buffer as used for dialysis.

2.2. Commercial antigen and antibody reagents

Recombinant spike proteins of the four common-cold hCoV strains, HKU-1, OC43, NL63 and 229E were purchased from Sino Biological Inc, Beijing, CN (#40,606-V08B, #40,607-V08B, #40,604-V08B and #40,605-V08B, respectively). A recombinant chimeric human/mouse anti-SARS-CoV-2 NP antibody consisting of a mouse scFv

fused to the Fc region of human IgG1 (clone 1A6) was purchased from Abcam, Cambridge, UK (#ab272852).

2.3. Assessment of recombinant protein quality

2.3.1. Analytical size exclusion chromatography (SEC)

High-performance liquid chromatography (HP)-SEC experiments were performed on a Dionex™ UltiMate™ 3000 RSLC system equipped with an LPG-3400SD Standard Quaternary Pump module, a WPS-3000 TSL Analytical Split-Loop Well Plate Autosampler and a DAD-3000 Diode Array Detector equipped with a ten μL analytical flow cell (all from Thermo Fisher Scientific, Germering, DE). RBD, tRBD and NP samples (25−80 μg per sample) were run on a Superdex™ 200 Increase 10/300 GL column (Cytiva, Uppsala, SE) and UV signals were detected at λ = 280 nm. For RBD and tRBD, Dulbecco's PBS buffer (DPBS) supplemented with 200 mM NaCl was used as mobile phase, the flow rate was set to 0.75 mL/min and a 45 min isocratic elution was performed. For NP samples 0.1 M sodium phosphate buffer (pH 7.0) containing 300 mM NaCl was used as mobile phase, the flow rate was set to 0.5 mL/min and a 60 min isocratic elution was performed. HP control, data acquisition and data evaluation were performed using Chromeleon™ 7.2 Chromatography Data System software (Thermo Fisher Scientific, Germering, DE). Sample purity (P), monomer (M), dimer (D) and full-length (FL) content were determined based on the respective peak area of the UV signal at 280 nm. For RBD and tRBD purity was defined as P=(M+D)/total area, monomer and dimer content were respectively defined as M[%]=M/(M+D)*100 and D=100-M[%]. For NP, full-length content was defined as FL[%]=FL/total area.

2.3.2. Bio-layer interferometry (BLI) measurements

Interaction studies of RBD, tRBD and NP with in-house produced anti-RBD mAb CR3022 and a commercial anti-SARS-CoV-2 nucleocapsid protein antibody (ab272852, Abcam, Cambridge, UK) were performed on an Octet RED96e system using high precision streptavidin (SAX) biosensors (both from FortéBio, Fremont, CA). Antibodies were biotinylated using the EZ-Link Sulfo-NHS-LC-Biotin kit (Thermo Fisher Scientific, Waltham, MA). Excess sulfo-NHS-LC-biotin was quenched by adding Tris−HCl buffer (800 mM, pH 7.4) to a final concentration of 3 mM. Biotinylated antibodies were further purified using PD-10 desalting columns (Cytiva, Marlborough, MA) according to the manufacturer's protocol. All binding assays were conducted in PBS supplemented with 0.05% (v/v) Tween 20 and 0.1% (w/V) BSA (PBST-BSA) at 25 °C with the plate shaking at 1000 rpm. SAX biosensors were first equilibrated in PBST-BSA and then loaded with the respective biotinylated capture molecules, either for 180 s (34 nM CR3022 solution) or until a signal threshold of 0.8 nm was reached (50 nM anti-NP mAb solution). Subsequently, antibody-loaded biosensors were dipped into PBST-BSA for 90 s to record a baseline, before they were submerged into different concentrations of their respective analytes. To determine K_D values, biotinylated antibodies loaded onto biosensors were exposed to six concentrations of the binding partners (RBD, tRBD or NP) to cover a broad concentration range around the respective K_D value [23]. For antigen association, mAb CR3022 was exposed to a three-fold serial dilution of RBD or tRBD (range: 300 nM−1.2 nM in PBST-BSA) for 300 s, while anti-NP mAb-was dipped into two-fold serial dilutions of the NP protein (40 nM - 1.3 nM in PBST-BSA) for 600 s. For dissociation, the biosensors were dipped into PBST-BSA. Each experiment included a baseline measurement using PBST-BSA (negative control) as well as a positive control (RBD monomer) where applicable. SAX biosensors loaded with biotinylated CR3022 or anti-NP mAb could be regenerated by dipping them into 100 mM glycine buffer (pH 2.5). RBD or tRBD proteins were measured in triplicates or quadruplicates, while NP proteins were measured in duplicates. No unspecific binding of proteins to SAX biosensors was observed. Data were evaluated under consideration of the lower limit of detection (LLOD) and lower limit of quantification (LLOQ) as reported elsewhere [24,25]. The analysis was performed using the Octet data analysis software version 11.1.1.39 (FortéBio, Fremont, CA) according to the manufacturer's guidelines. For easier comparison of the RBD variants produced in different expression hosts, the K_D values were determined from the measured equilibrium response (steady state analysis). However, the interaction between the CR3022 mAb and the final tRBD batches were also evaluated kinetically by fitting the BLI data to a 2:1 heterogeneous ligand binding model. Note, although the CR3022 mAb has two identical binding sites, the second binding event is dependent on the first binding since allosteric effects or sterical hindrance can ultimately lead to a positive or negative cooperative binding behaviour [16,26,27]. However, in case of the reported interaction, the affinity constant (K_D) values are very close to one other in the low nanomolar range.

The interaction between the NP protein and the anti-NP mAb is difficult to characterise due to avidity effects that arise from the dimeric nature of both interaction partners. Kinetic evaluation of the BLI data is problematic since the dissociation curves are heterogenic. Additionally, if the dissociation phase shows less than 5% decrease in signal during the defined dissociation phase, as observed for the lower concentration range of NP protein, a precise determination of the dissociation rate constants (k_d) is not possible [28,29]. However, it is feasible to calculate an upper limit for the k_d (s^{-1}) which is given by $k_d < -\ln(0.95)/t_d$, where td is the dissociation time in seconds [28,30] Thus, an upper limit for the K_D value, calculated by the ratio of kd/ka, resulted in < 0.7 nM, suggesting a strong interaction in the picomolar range. Moreover, for comparison of single batches the observed binding rate (k_{obs}) was plotted as a function of the NP concentration and used for the comparison of the single batches.

2.3.3. Liquid chromatography electrospray ionization mass spectrometry (LC/ESI-MS)

Purified proteins were S-alkylated with iodoacetamide and digested with endoproteinases LysC (Roche, Basel, CH) and GluC (Promega, Madison, WI) or chymotrypsin (Roche, Basel, CH) in solution. Digested samples were analyzed using a Thermo Ultimate 3000 HP connected to a 150 × 0.32 mm, 5 μm BioBasic C18 column (both Thermo Fisher Scientific, Waltham, MA) and a maXis 4 G QTOF mass spectrometer (Bruker, Billerica, MA). An 80 mM ammonium format buffer was used as the aqueous solvent and a linear gradient from 5% B (B: 80% acetonitrile) to 40% B in 45 min at a flow rate of 6 μL/min was applied, followed by a 15 min gradient from 40% B to 95% B that facilitated elution of large peptides. The MS system was equipped with the standard ESI source and operated in positive ion, DDA mode (= switching to MSMS mode for eluting peaks). MS-scans were recorded (range: 150−2200 Da) and the six highest peaks were selected for fragmentation. Instrument calibration was performed using ESI calibration mixture (Agilent, Santa Clara, CA). The analysis files were converted (using Data Analysis, Bruker) to mgf files, which are suitable for performing a MS/MS ion search with MASCOT. The files were searched against a database containing the target sequences. In addition, manual glycopeptide searches were done. Glycopeptides were identified as sets of peaks consisting of the peptide moiety and the attached N-glycan varying in the number of HexNAc, hexose, deoxyhexose and pentose residues. Theoretical masses of these peptides were determined using the monoisotopic masses for the respective amino acids and monosaccharides.

2.4. Ethics statement

The present study includes work with human sera from three different sites. Acute lithium heparin plasma samples collected from outpatient and hospitalised individuals for routine clinical testing were available at the B&S Central Laboratory Linz, Austria. Left-over

samples were assessed for SARS-CoV-2 antibody levels and neutralizing titers in the early phase of infection. The study protocol and the use of residual material from routine clinical examinations for biomedical research without explicit consent was approved by the ethics committee of Upper Austria (EK1083/2020), in accordance with the Declaration of Helsinki. For ELISA validations, left-over sera from SARS-CoV-2 patients and sera from convalescent donors, as well as historical sera (collected prior to 2020) were taken from the MedUni Wien Biobank, as approved by the ethics committee of the Medical University of Vienna (EK 1424/2020). All individuals whose samples were used provided written informed consent for their samples to be added to a biobank and to be used for biomedical research/methods evaluation. The inclusion of residual material from routine clinical examinations without explicit consent was approved by the Ethics Committee of the Medical University of Vienna. The underlying sample collections were reviewed and approved by the ethics committee of the Medical University of Vienna (EK 595/2005, EK 404/2011, EK 518/2011), or by the ethics committee of the City of Vienna (EK-11−117−0711), respectively. Samples from hospitalised COVID-19 patients at the University Hospital of Innsbruck, reconvalescent COVID-19 patients with persistent cardio-pulmonary damage participating in a prospective observational study (CovILD-study, ClinicalTrials.gov number, NCT04416100, Reference: PMID: 33303539) and reconvalescent persons volunteering as plasma donors were used for test validation in Innsbruck [31]. The underlying sample collections were reviewed and approved by the ethics committee of the Medical University of Innsbruck (EK 1103/2020, EK 1167/2020). Left-over SARS-CoV-2 acute and convalescent sera from blood donors and pre-COVID-19 sera from the Austrian Institute of Technology were taken for SARS-CoV-2 antigen pre-validation. The study protocol and the use of residual material from routine clinical examinations for biomedical research/methods evaluation without explicit consent was approved by the ethics committee of the city of Vienna (EK 20−179−0820).

2.5. Human serum and plasma samples

Careful consideration of samples size is important to ensure that a study has sufficient participants to be meaningful and to also accurately detect small effects. Sample size requirements usually rely on hypothesized values on sensitivity and specificity and their clinically acceptable degree of precision, and an estimated prevalence of disease in the target population [32]. At the time of clinical validation we had data on the estimated 5% seroprevalence in Austria [33] as well as data on specificity and sensitivity estimates from a previous study on SARS-CoV-2 diagnostic tests available [34]. Sample size estimations were based on the following assumptions: Type I error 0.05 (two-sided), type II error 0.20. At the beginning of the pandemic, high specificity was required to ensure a sufficient positive predictive values (PPV) at a low seroprevalence of about 5%. Thus, it was necessary to determine the specificity with high accuracy. To discriminate a specificity of 99.2% (see, e.g. Abbott SARS-CoV-2 IgG, [34]) from one that is 1% below this value (H0=98.2%), a total of 1.126 negative cases would be required, just as many as have been included in the specificity cohort. In a real-life setting, sensitivities of Anti-SARS-CoV-2 immunoassays are usually in the range of 90% [31,34]. To significantly differentiate a sensitivity of 95% from 90%, at least 239 positive samples would need to be included (244 samples were used in the sensitivity cohort).

2.5.1. Sensitivity cohorts

SARS-CoV-2 acute sera from a cohort of outpatient and hospitalised individuals, B&S central laboratory Linz, Austria: A cohort of hospitalised individuals and outpatients included a total number of 64 SARS-CoV-2 RT-PCR-confirmed (from respiratory specimens) COVID-19 patients (median age 65 [14−95, IQR 56−87 years], 17.2% females) who were treated in one of the two tertiary care hospitals Konventhospital Barmherzige Brueder Linz or Ordensklinikum Linz Barmherzige Schwestern in Linz, Austria, between March 15th and April 10th 2020. Of these, ten patients were treated as outpatients and 54 patients were hospitalised; twelve of them were treated at the intensive care unit (ICU). From the 64 patients, a total of 104 serial blood samples were drawn at different time points after symptom onset until April 10th· 2020. Sixty-four patients had at least one, 28 patients had two, nine patients had three and three patients had four blood draws, which were sent to the central laboratory for routine clinical testing. The date of onset of symptoms was retrieved from medical records and was available for all patients. Left-over lithium heparin plasma samples were aliquoted and frozen at −80 °C and had up to two freeze-thaw cycles.

Sera of SARS-CoV-2-positive patients and convalescent donors, Medical University of Vienna and Medical University of Innsbruck: The SARS-CoV-2 positive samples for ELISA validation comprise 70 serum specimens from unique patients or convalescent donors with (previous) SARS-CoV-2 infection from Vienna (either PCR-positive or symptomatic close contacts), as well as 174 SARS-CoV-2 PCR positive patients including hospitalised patients (n = 123) and convalescent blood donors (n = 51) from Innsbruck. All samples were collected >14 days after symptom onset (or positive PCR, in case of asymptomatic infection). A representative serum panel of these samples (n = 28−31) was taken for the pre-validation of SARS-CoV-2 antigens by ELISA and for the assessment of SARS-CoV-2 neutralization titers.

SARS-CoV-2-convalescent and acute sera from a cohort of non-hospitalised blood donors, Austrian Institute of Technology (AIT) and Medical University of Vienna: The sensitivity cohort for antigen pre-validation covered 124 COVID sera. Among these, 96 sera were deidentified excess samples from infected individuals collected for routine SARS-CoV-2 serodiagnosis using a seven-plex bead-based Luminex-FlexMap system-based serotest and were available at the AIT. These serotests had been conducted similar to the analysis procedure outlined below. Seronegativity and/or seropositivity was based on cut-off values and end-point titres defined according to Frey et al. [35] on the basis of 160 pre-COVID-19 sera. Additionally, the study cohort included a set of 28 COVID-19 sera from the Medical University (from the above), covering samples from primarily asymptomatic individuals or those with mild to moderate illness.

2.5.2. Specificity cohorts

Pre-COVID-19 cohort, Meduni Wien Biobank: The pre-COVID-19 cohort covered a total of 1126 samples from healthy, non-SARS-CoV-2-infected individuals collected before 2020 to guarantee seronegativity. Banked human samples including sera from voluntary donors (n = 265, median age 38 [25−52] years, 59.0% females), samples from a large population-based cohort aged 8−80 years, representing a cross-section of the Austrian population (N = 494, collected 2012−2016 from November to March to increase the likelihood of infection with other respiratory viruses, median age 43 [26−56], 50.0% females) [36], samples from patients with rheumatic diseases (N = 359, median age 52 [41-61], 76.0% females), and eight samples from patients with previous seasonal coronavirus infection collected for routine clinical testing at the Regional Hospital Feldkirch. Sera with PCR-confirmed hCoV infection (hCoV 229-E, n = 3; hCoV NL63, n = 2 [one of which with 229E co-infection], hCoV OC43, n = 2; non-typed, n = 2) were drawn between January 2019 and February 2020 and were kindly provided by Andreas Leiherer (Vorarlberg Institute for Vascular Investigation and Treatment VIVIT, Dornbirn, AT). A set of 14 sera of the above (not including hCoV sera) was used for pre-validation of SARS-CoV-2 antigens in an ELISA. Samples (except for those from patients after seasonal .coronavirus infection) were processed and stored according to standard operating procedures within the MedUni Wien Biobank facility in a certified (ISO 9001:2015) environment [37].

Pre-COVID cohort, Austrian Institute of Technology: Control sera from AIT covered 210 samples of blood donors were obtained in 2014 from the Austrian Red Cross blood bank; collected samples have been stored at −80 °C without any freeze thaw cycles.

2.6. Pre-validation of antigens using seroreactivity assays

2.6.1. Luminex assay

In-house produced SARS-CoV-2 RBD, tRBD and NP as well as spike proteins of hCoV HKU-1, OC43, NL63 and 229E (all from Sino Biological Inc, Beijing, CN) were separately coupled to MagPlex carboxylated polystyrene microspheres (Luminex Corporation, Austin, TX) according to the manufacturer's instruction, with the following minor modifications: For coupling, five μg of each antigen was used per one million microspheres. Coupling was performed in a total volume of 500 μL in 96-Well Protein LoBind Deepwell plates (Eppendorf, Hamburg, DE) and plates were incubated at 600 rpm on a Heidolph Titramax 1000 plate shaker (Heidolph, Schwabach, DE). After each incubation step plates were centrifuged at 400 g for one minute. To collect the microspheres at the bottom of the plate, plates were placed on a Magnetic plate separator (Luminex Corporation, Austin, TX) and the supernatant was poured off by inverting the plates. Coupling was performed in 200 μL coupling buffer (50 mM MES, pH 5.0). Microspheres with coupled proteins were stored in Assay buffer (PBS supplemented with 1% (w/V) BSA, 0.05% (w/V) NaN_3, pH 7.4) at a final concentration of 10,000 microspheres per μL at 4 °C in the dark. Sera of patients and controls were five-fold diluted in PBS-Triton X-100 buffer (PBS supplemented with 1% (V/V) Triton X-100, 0.05% (w/V) NaN_3, pH 7.4) and were further diluted 240-fold with Assay buffer. Coupled microspheres (800 beads per sample) were first equilibrated to room temperature for 30 min. Plates were then vortexed for 30 s and sonicated for 20 s using a Transsonic T470/H sonicator (Elma Electronics, Wetzikon, CH). The required amounts (based on multiples of samples to be analysed) of microspheres (+10% excess) were transferred to 1.5 mL Protein LoBind tubes (Eppendorf, Hamburg, DE) and centrifuged for three minutes at 1200 g. Microtubes were then placed on a Magneto Dynal magnetic tube separator (Invitrogen, Carlsbad, CA), supernatants were carefully removed and microspheres were resuspended in 200 μL Assay buffer. Different microspheres were then combined in a 50 mL Falcon tube to yield a total of 800 microspheres per coupled antigen in 30 μL assay buffer per single measurement. Thirty μL of the mixed microsphere suspension was then transferred to wells of a clear 96-well microplate (Corning Inc, Corning, NY). Assay plates were placed on the magnetic plate separator and supernatants were poured off by inverting the plates. Fifty μL of sera (1:1200-diluted) or assay buffer (blank samples) was applied to each well. Assays were incubated for two hours at RT on the plate shaker (600 rpm). Assay plates were placed on the magnetic plate holder and the supernatants were poured off by inverting the plates. Microspheres were washed by removing the magnetic plate holder and the addition of 100 μL Wash buffer (PBS; 0.05% (V/V) Tween-20; 0.05% (w/V) NaN_3; pH 7.4) per well. After two minutes of incubation at room temperature, plates were again placed on the magnetic plate holder and supernatants were poured off. After three wash steps 50 μL of a 1:1 mixture of 2.5 μg/mL goat anti-human R-Phyco AffiniPure $F(ab')_2$, Fcγ-specific (Jackson ImmunoResearch Labs Cat# 109−116−098, RRID:AB_2,337,678)and $F(ab')_2$-specific IgG (Jackson ImmunoResearch Labs Cat# 109−116−097, RRID: AB_2,337,677) in Assay buffer were added. Plates were incubated for one hour at room temperature on the plate shaker (600 rpm) in the dark. Microspheres were then washed again three times and microspheres were resuspended in 100 μL Assay buffer and median fluorescence intensity (MFI) was immediately measured on a Flexmap 3D Suspension Array System (BioRad, Hercules, CA) with a minimal Count of 100 per microsphere type, a DD Gating of 7500−25,000 and the Reporter Gain set to "Enhanced PMT (high)". MFI values were extracted from FM3D result files. A minimum microsphere count of 25 counts was set as cut-off. All samples and single bead types analysed fulfilled the minimum bead count criterium. FM3D results files were compiled in Microsoft Excel and were log2-transformed and blank-corrected by subtracting the mean MFI values of blank samples (assay buffer only) from MFI values of the test samples.

2.6.2. ELISA assay

Initially, ELISA conditions were optimised in terms of antigen coating conditions (0.5−8 μg/mL) and serum-dilutions (1:50−1:3200) to optimise the trade-off between background seroreactivity and sensitivity in samples from individuals with weak antibody responses. The final protocol was as follows: SARS CoV-2 and hCoV antigens (see above) were diluted to 6 μg/mL in phosphate-buffered saline (PAN Biotech #P-04−36,500) and 50 μL were added to each well of MaxiSorp 96-well plates (Thermo #442,404). After incubation at 4 °C overnight, wells were washed 3x with PBS + 0.1% Tween-20 (PBS-T, Merck #8.22184) and blocked for one hour at room temperature with PBS-*T* + 3% (w/V) milk powder (Fluka #70,166). Serum samples were diluted 1:200 in PBS-*T* + 1% (w/V) milk powder. 100 μL were applied to each well and plates were incubated for two hours at RT with shaking (450 rpm). Plates were washed 4x before incubation with goat anti-human IgG (Fc-specific) horseradish peroxidase (HRP) conjugated antibodies (Sigma-Aldrich #A0170, RRID:AB_257,868; 1:50,000 in PBS-*T* + 1% (w/V) milk powder, 50 μL/well) for one hour at RT while shaking. After four washes, freshly prepared substrate solution (substrate buffer [10 mM sodium acetate in dH_2O, pH 5, adjusted with citric acid] + 1:60 TMB-stock [0.4% Tetramethylbenzidine (Fluka #87,748) in DMSO] + 1:300 H_2O_2 [0.6% in dH_2O) was applied (150 μL/well) and plates were incubated for 25 min at RT with shaking. Reactions were stopped by the addition of 1 M sulfuric acid (25 μL/well). Absorbance was measured at 450 nm on a Tecan Sunrise Microplate reader using a reference wavelength of 620 nm and the Magellan V 7.2 SP1 Software.

2.7. TECHNOZYM anti-SARS-CoV-2 RBD and NP IgG ELISAs assays

The above-described methodology was slightly adapted for the development of the TECHNOZYM Anti SARS-CoV-2 NP and RBD IgG ELISA test kits (Technoclone, Vienna, AT). The tests plates were provided with the antigens coated at a concentration of 6 μg/mL and lyophilized according to a proprietary in-house protocol. The RBD test kit employs the described tRBD as coating antigen. To allow for a quantitative measurement of SARS-CoV-2 antibody levels, a calibrator set consisting of five calibrators with assigned values was provided for the creation of a calibration curve and was run in parallel with the patients' samples. The calibrated values were established using the monoclonal antibody CR3022 as a reference material, with 1 U equivalent to 100 ng/mL mAb CR3022 (#Ab01680−10.0, Absolute Antibody, Oxford, UK). The calibrator set covered the concentration range 0 − 100 U/mL and concentrations of anti SARS-CoV-2 IgG antibodies recognizing either tRBD or NP in patient sera could be read directly from the calibration curve.

2.8. Technozym NP and RBD IgG ELISA test validations

The established NP and RBD IgG ELISA assays were either processed manually and analyzed on a Filtermax F5 plate reader (Molecular Devices, San José, USA) or on an Immunomat instrument (Serion Diagnostics, Würzburg, DE) according to the manufacturer's instructions. IgG antibody levels were reported as numeric values in form of arbitrary U/mL derived from the five-point calibration curve. Cut-offs for test validations were determined by ROC-analysis and the non-parametric 99th right-sided percentile method (CLSI C28-A3). Sensitivities, specificities, PPV, and negative predictive values (NPV, both at 5% estimated seroprevalence) were calculated. ROC-analysis data

from automated tests (including Abbott ARCHITECT SARS-CoV-2 IgG, DiaSorin LIAISON® Anti-SARS-CoV-2 S1/S2 IgG) were available for 64 of the positive and 1117 of the negative samples from a previously published study [34].

2.9. SARS-CoV-2 neutralisation assay

A tissue culture infectious dose ($TCID_{50}$) assay for authentic SARS-CoV-2 virus was developed for the determination of neutralizing antibodies. The virus was originally isolated from a clinical specimen, a nasopharyngeal swab taken in mid-March 2020 from a 25-year old male patient in Lower Austria, and was further passaged twice on Vero E6 TMPRSS-2 cells in Dulbecco's modified Eagle's medium (DMEM) with 10% (V/V) foetal bovine serum (FBS). Vero E6 TMPRSS-2 cells, initially described in Hoffmann et al. [38] were kindly provided by Stefan Pöhlmann; Deutsches Primatenzentrum, Göttingen, Germany.

Briefly, assays were performed with Vero 76 clone E6 cells (CCLV-RIE929, Friedrich-Loeffler-Institute, Riems, Germany) cultured in minimum essential medium Eagle (E-MEM) with BioWhittaker Hank's balanced salt solution (HBSS) (Lonza, Basel, CH) supplemented with 10% (V/V) FBS (Corning Inc, Corning, NY). Neutralizing antibody titres in human serum and plasma were determined as previously described [39] with the following alterations: the heat-treated sera were diluted 1:4 in triplicates in serum-free HEPES-buffered DMEM medium. In the case neutralizing antibody titres were determined in human lithium heparin plasma, no heat-treatment was applied and the medium was supplemented with 1x Antibiotic/Antimycotic solution (Thermo Fisher Scientific, Waltham, MA). The heat treatment had no effect on neutralizing titres, as verified in a pre-experiment on SARS-CoV-2 positive and negative plasma samples. In addition, a toxicity control, which was processed the same way as plasma samples, was included. Here, no virus was added, to prevent a false readout of the assay. Cytopathic effect (CPE) was evaluated and scored for each well using an inverted optical microscope. To determine neutralization titres the reciprocal of the highest serum dilution that protected more than 50% of the cells from the CPE was used and was calculated according to Reed and Muench [40].

2.10. Statistical analyses

Raw data were assessed for normality of distribution and homogeneity of variances using the D'Agostino−Pearson omnibus test before statistical procedures. Differences in median seroreactivity between pre-COVID and COVID sera were compared using the Mann-Whitney U tests on blank-corrected log2-transformed median fluorescence intensities (Luminex data) or OD_{450} absorbances (ELISA), respectively. Correlation analyses of nonparametric data were performed by Spearman's rank-order correlation (r_s), otherwise Pearson's' correlation (r) was used. Relative IgG signals of outliers against SARS-CoV-2 and hCoV antigens were compared by One-Way ANOVA followed by a Sidak test to correct for multiple comparisons. ROC-analysis data from automated tests were compared to the established ELISA tests according to DeLong. Sensitivities and specificities were compared by z-tests. Data on the diagnostic performances of antigens and cross-reactivity were analysed using Graphpad Prism Version 8.1.0 (GraphPad Software, San Diego, CA, USA) Validation data were analysed using MedCalc v19 (MedCalc Software, Ostend, Belgium) and analyse-it 5.66 (analyse-it Software, Leeds, UK) and SPSS 23.0 (SPSS Inc.). Data from SARS-CoV-2 acute sera from hospitalised individuals or outpatients obtained by the B&S Central Laboratory Linz were statistically analysed with the MedCalc 13.1.2.0.

2.11. Role of the funding source

The funding sources had no role in the study design, the collection, analysis and interpretation of data, in writing this manuscript and in the decision to submit the paper for publication.

3. Results

3.1. Comparative profiling of expression hosts for SARS CoV-2 RBD and NP production for diagnostic use

Initially, five eukaryotic expression systems were compared for their capacity to support high-quantity and high-quality expression of the glycosylated SARS-CoV-2 spike RBD. Our pre-defined quality attributes covered activity in a functional binding assay using a conformation-dependent RBD-specific antibody (CR3022), protein integrity and glycosylation determined by mass spectrometry, as well as manufacturability (**Fig. 1a**). Biolayer interferometry analysis revealed that RBD obtained from different mammalian and insect expression systems have comparable affinities (range: 21 − 43 nM) for the mAb CR3022 (**Fig. 1a, left panel**). Glycan analysis confirmed host-specific N-glycosylation of the respective proteins, which was of complex-type for the human (HEK-6E) and non-human mammalian cell lines (CHO-K1, CHO-S) as well as for plant (*Nicotiana benthamiana*)-derived RBD. We found paucimannosidic N-glycosylation for the *Trichoplusia ni* insect cell line (*Tnms*42)-derived RBD (**Fig. S1a, b**). Peptide mapping verified the integrity of the protein primary structure (data not shown). Unoptimised and small-scale electroporation of non-human cell lines (CHO-K1 and CHO-S) and baculovirus infection of insect cell lines (*Tnms*42) produced overall yields after purification of less than one mg RBD per litre of culture. Polyethylenimine (PEI) transfection of HEK cells readily provided higher overall volumetric yields (~40 mg/L) without further process optimisation (**Fig. 1a, left panel**). Analytical size-exclusion chromatography (HP-SEC) revealed expression platform and production batch-dependent RBD homodimer contents. (**Fig. S2**). For plant-expressed RBD, dimerisation was particularly pronounced. We identified an unpaired cysteine residue (Cys538) close to the C-terminus of the canonical RBD sequence as a possible cause for RBD dimerisation. A truncated RBD construct (tRBD) lacking this cysteine residue was less prone to homodimer formation, but retained full functionality in the binding assay and similar expression yields (**Fig. 1a right panel, Fig. S3**). From a manufacturing perspective, tRBD thus provided less batch-to-batch variation, which is a pre-requisite for a diagnostic antigen.

To assess the performance of the antigens for discrimination between sera from SARS-CoV-2-exposed (n = 124) and uninfected individuals (n = 210), we applied a high-throughput (HTP) automated bead-based multiplex assay (**Fig. 1b, c**). The performance of diagnostic tests is commonly assessed through receiver operating characteristic (ROC) curves and the analysis of area under the ROC curve (AUC-ROC). ROC curves are simple graphical representations of the relationship between sensitivity and specificity of a test over all possible diagnostic cut-off values and AUCs give the overall ability of a test to discriminate between two populations [41]. We used theses analyses to assess potential differences in the diagnostic performance of the RBD from different expression hosts. Almost all antigens at this high purity demonstrated AUC values of >0.99, demonstrating the high suitability of the RBD from any source as diagnostic antigen. The AUC value of insect-derived RBD was slightly lower (AUC: 0.978 [0.964−0.992]); the differences, however, were not significant (**Fig. 1b**). We then applied antigen-specific cut-offs to compare the performance of the antigens at a pre-defined consensus specificity of 99.1%. At this criterion, we obtained high sensitivities (range 94.4%−96.0%) with all antigens, except for insect-derived RBD. There, seroreactivity with pre-COVID-19 sera was about 2^2- (4)-fold higher than observed for CHO-expressed RBDs. This resulted in 26% of COVID-19 sera to fall below the threshold, increasing the rate of false-negatives **(Fig. 1c)**. The tRBD displayed a comparable seroreactivity profile to the RBD.

During our pre-validation experiments we observed a strong effect of residual host cell proteins on assay performance (**Fig. S4**), even in formulations derived from human cell lines. Therefore, RBD/

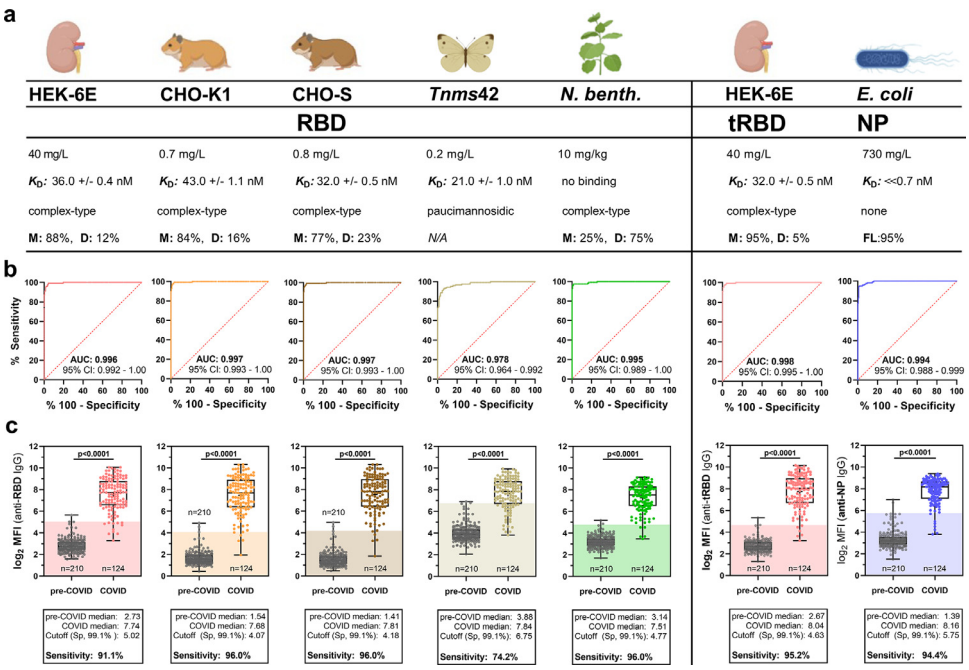

Fig. 1. Comparative profiling of SARS CoV-2 antigens from different expression hosts for serodiagnosis. a-c, the canonical SARS-CoV-2 RBD expressed in five biotechnological platforms (HEK-6E, CHO-K1, CHO-S, *Tnms*42, *N. benthamiana,* **left panel**), an optimised RBD construct expressed in HEK cells (tRBD) as well as the NP produced in *E. coli* (**right panel)** were compared in terms of biotechnological parameters as well as seroreactivity to identify ideal candidates that may be sustainably produced for specific and sensitive SARS-CoV-2 serodiagnosis. (**a)** Pre-defined process and protein quality parameters include overall yield after purification, functional binding to the conformation-dependent mAb CR3022 (RBD) or a commercially available anti-NP antibody as verified by biolayer interferometry, as well as glycosylation analysis. Purified monomer (M), dimer (D), and NP full-length protein (FL)-content was determined by HP-SEC. **b-c,** Pre-validation of antigens for serodiagnosis with sera of healthy blood donors collected prior to 2018 (n = 210) and convalescent sera from a COVID cohort (n = 124; see methods for cohort description) with an automatable bead-based, multiplex Luminex serotest. (**b)** Receiver operating characteristic (ROC) curves of the assayed antigens with an indication of the area under the curve (AUC) and 95% confidence interval (CI), (**c**) Seroreactivity of the two cohorts at a final serum dilution of 1:1200. Blank-corrected values are shown. Shades indicate the calculated cut-off yielding a specificity (Sp) of 99.1% for comparison of antigen performance. P-values were calculated by Mann-Whitney U tests.

tRBDs were purified via an immobilized metal affinity chromatography (IMAC) capture followed by a scalable and fast flow-through anion exchange (AIEX) chromatography step, leading to purities of up to 99%. Owing to reproducible highest production yields of functional protein with adequate diagnostic performance and less batch-to-batch variation, we decided to pursue with HEK-expressed tRBD for our further validations.

As the NP of SARS-CoV-1 has been described to be well produced in bacteria [42], we decided to produce the SARS-CoV-2 NP in *Escherichia coli*. We combined two recently developed generic manufacturing strategies, the CASPON (cpCasp2-based platform fusion protein process) technology [8] and the enGenes-X-press technology [7], allowing for high-level soluble expression of heterologous proteins. NP was expressed as a fusion protein with an N-terminally fused CASPON tag that enables affinity purification and can afterwards be efficiently proteolytically removed, thereby generating the authentic N-terminus. High soluble volumetric titres of 3.7 g/L in a growth-decoupled fed-batch production process yielded 730 mg/L NP after purification with a modified CASPON platform process (**Fig. 1a, right panel**). This strategy delivered untagged NP protein at exceptionally high quality (94.6% purity, defined as protein full-length content) after a multi-step-downstream process. The remaining impurities consisted of NP-related fragments and RNA. Residual host cell protein concentration was 0.9 ng/mg NP and dsDNA concentration was 1 μg/mg NP, as determined by De Vos and colleagues [10]. NP has an intrinsic propensity to oligomerize and displays very slow dissociation from the NP-specific antibody (Abcam, ab272852). Therefore, we provide an upper limit for the K_D value, and calculated k_{obs} values as a surrogate kinetic parameter instead (**Fig. 1a, right panel, Fig. S3**). The nucleocapsid protein also presented with excellent AUC values of 0.994 (0.988−0.999) and comparable performance to HEK-derived tRBD. While the seroreactivity profile of pre-COVID sera appeared to be more heterogenous against the NP than for tRBD, COVID sera demonstrated a more consistent, robust response against the nucleocapsid protein (**Fig 1b, c, right panel**). This comprehensive set of biotechnological and assay performance characteristics prompted us to pursue ELISA test development with HEK-expressed tRBD and bacterially produced NP.

3.2. Assessment of antigen-dependency of false-positive and false-negative results

A set of sera (28−31 convalescence sera from the above tested) that was considered to be particularly challenging since it included 80% of the identified outliers or borderline serum samples, was selected to optimise the conditions for an ELISA with tRBD and NP to maximise sensitivity of the tests. By titration of the coating antigen as well as the seropositive samples we defined our final conditions to be: 6 μg/mL coating antigen and 1:200 serum dilution (data not shown). Using this consensus set of COVID-sera, but different specificity cohorts for both assays, both antigens allowed for highly sensitive antibody detection, yielding 85.7% and 100% sensitivity with the Luminex and ELISA platform, respectively, at the pre-defined consensus specificity criteria (99.1%, Luminex, 92.9% ELISA, **Fig. 2a**). While antigens are covalently coupled to microspheres via their N-terminal and endogenous primary amines, they are passively adsorbed to ELISA plates via hydrophobic as well as electrostatic interaction [43]. With both, physical and chemical immobilization, antigens get immobilized in a randomly oriented manner. Despite previous studies demonstrating good correlation between the results obtained with both methods [44,45], we aimed to verify that the different immobilization mechanisms do not result in major antigenic changes of the tRBD and NP antigens and that we can adopt our learnings from the bead-based antigen pre-validation for the setup of an ELISA.

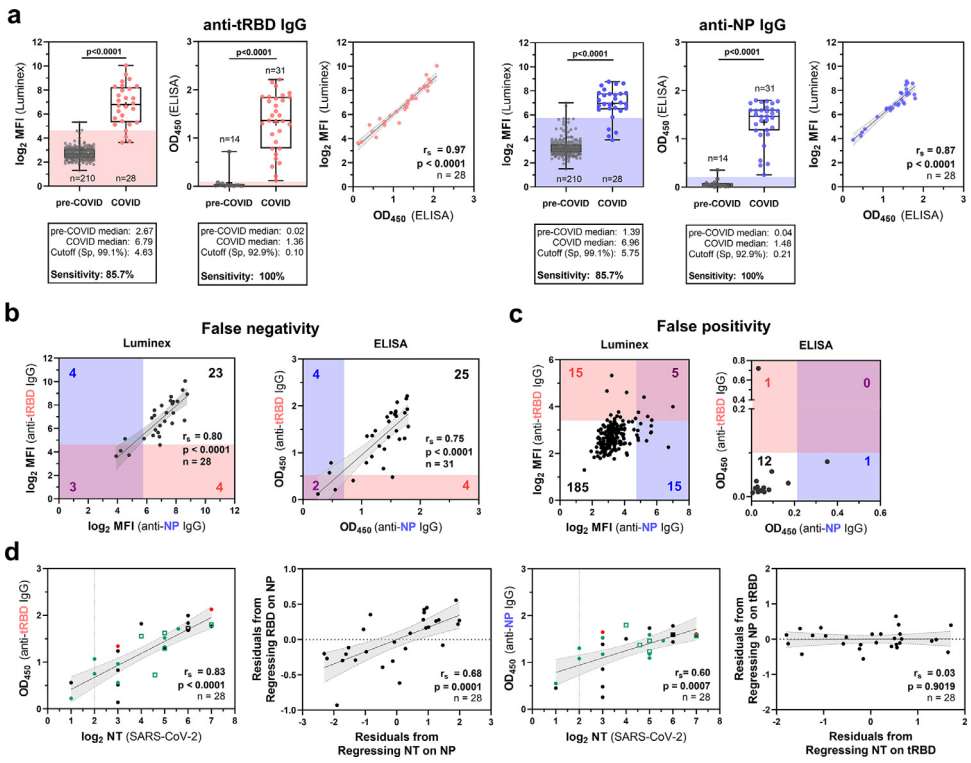

Fig. 2. Convalescent sera from blood donors with mild to moderate courses of disease indicate an advantage of dual-antigen testing and a correlation of tRBD-specific antibodies with SARS-CoV-2 neutralization. a-d, A small set of convalescent sera (n = 28−31, part of the Medical University of Vienna COVID-19-cohort) with described courses of disease was used for in-depth analysis of the ELISA candidate antigens. Pre-COVID-19 sera included blood donor sera (n = 210 and n = 14) collected in pre-COVID-19 times (see methods for detailed cohort description). (**a**) Seroreactivity of HEK-tRBD and *E. coli*-derived NP as assessed by the Luminex platform and ELISA at serum dilutions of 1:1200 and 1:200, respectively, and the cross-platform correlation of the respective readouts. Data give the mean of blank-corrected values from three independent antigen production batches. Sensitivities with the respective test antigens at the indicated pre-defined specificities were calculated by AUC-analysis of ROC curves, P-values were calculated by Mann-Whitney U tests. **b-c,** Assessment of overlaps in (**b**) false-negative and (**c**) false-positive serum samples identified with both the tRBD or NP antigen in the Luminex and ELISA assay. The cut-offs were set to yield low sensitivity (87.1%, ELISA; 85.,7%, Luminex) or specificity (92.9%, both assays), respectively. Shades are coloured according to the respective antigens (NP: blue, tRBD: pink) and indicate the cut-offs. Numbers in blue and red give the total numbers of false-positives/false-negatives for NP or tRBD, respectively, while purple numbers give samples that are classified as false-positives/-negatives with both antigens. (**d**) Correlation and partial correlation analysis of ELISA anti-tRBD as well as anti-NP levels with neutralization titres obtained with authentic SARS-CoV-2 virus. Partial correlations take the effect of antibody levels towards the respective other antigen into account. Individual sera are color-coded according to the course of disease (green: asymptomatic and mild; black: moderate; red: severe). Solid lines indicate the linear regression and shades with dotted borders give the 95% CI. Full circles are for sera from individuals with a PCR-confirmed SARS-CoV-2 infection, open squares indicate asymptomatic close contacts. r_s, Spearman's correlation factor.

Three independently produced tRBD and NP production batches were tested for seroreactivity with the described panel of COVID-sera using ELISA and Luminex assays. The fluorescence (MFI, Luminex) and colorimetric (OD, ELISA) mean readouts obtained with antigens from three independent production batches demonstrated excellent cross-platform correlation (tRBD: r_s=0.97, p<0.0001; NP: r_s=0.87, p <0.0001, both Spearman correlation) and confirmed that results are in good agreement (**Fig. 2a**). While this does not inform us about potential differences at the resolution of a single-epitope level, it still verifies the equivalence of the assay readouts when using polyclonal serum samples, which is most relevant in our case. Next, we aimed to assess whether false-positive or false-negative results are independent of the test antigen. Thereby, we set the assay cut-offs to either yield low sensitivity or low specificity and then compared whether samples above/below the threshold are shared between the diagnostic antigens. With both test formats, up to 50% of the false-negative samples did not simultaneously react with both antigens (**Fig. 2b**). Concurrently, none of the false-positive sera in the ELISA, and only 20% of the false-positive sera (5 out of 25) in the Luminex test simultaneously reacted with both the tRBD and NP (**Fig. 2c**). Levels of tRBD- and NP-specific antibodies correlated well with each other (r_s=0.75−0.80, p<0.0001, Spearman, **Fig. 2b**) and also with the ability of the respective sera to neutralize authentic SARS-CoV-2 virus. Yet, with partial correlation analysis we could demonstrate that only anti-tRBD antibodies do have a causal relation with viral neutralization (r_s=0.68, p = 0.0003, Spearman, **Fig. 2d**).

3.3. Cut-off modelling and diagnostic performance of the tests in a large validation cohort

The above data provided an indication that reactivity of COVID-19 sera is dependent on the test antigen, fostering the idea for combined use in applications requiring high specificity. Test kits for both antigens were generated (termed Technozym NP or RBD IgG Test, Technoclone, Vienna, AT), providing the antigens in lyophilized form at a coating concentration of 6 μg/mL. The kits included a five-point calibrator set, based on the RBD-specific antibody CR3022, to enable quantitative readouts and further expand the tests' fields of application.

Both the tRBD and the NP ELISA were evaluated using 244 samples from patients with active or previous SARS-CoV-2 infection covering the full spectrum of disease presentations (asymptomatic to individuals requiring intensive care). The large specificity cohort (n = 1126) covered a great variety in samples from pre-COVID times including sera from individuals with rheumatic disease, human coronavirus infections and serum samples drawn during winter months to increase the likelihood for respiratory infections. A detailed description of the SARS-CoV-2 positive cohorts can be found in

Table S1. In ROC-analysis, both assays presented with excellent areas under the curve (tRBD: 0.976, NP: 0.974, **Fig. 3a, b**). The Youden index was maximal at a cut-off of >2.549 U/mL for tRBD (Youden index=0.901) and at >3.010 U/mL for NP (Youden index=0.882) yielding high sensitivities (tRBD: 95.8% [91.6–97.4], NP: 93.0% [89.1–95.9] at these cut-offs. Yet, specificities (tRBD 95.3% [93.6–96.2], NP 95.1% [93.7–96.3]) were insufficient to yield satisfactory positive predictive values (PPVs), which give the probabilities that an individual with a positive test result indeed has antibodies for SARS-CoV-2. At a low seroprevalence rate of 5% the PPVs at these cut-offs would be equivalent to a coin toss, with 50.2% (43.8–56.5) for tRBD and 50.1% (43.6–56.5) for NP. To increase assay specificity of each test individually, thereby increasing predictability at low seroprevalences, cut-off criteria based on the 99th percentile method were established. Ninety-nine percent of all negative samples showed results below 7.351 (95% CI: 5.733–10.900) U/mL for the tRBD and 7.748 (5.304–11.157) U/mL for the NP ELISA. When shifting the cut-off to 8.000 U/mL (taking a safety margin into account), specificities increased to 99.2% for the tRBD and 99.1% for the NP ELISA. This is a remarkable result for an ELISA test and qualifies the tests for seroprevalence studies. At the same time, sensitivities slightly dropped to 86.3% and 76.7% for the tRBD and NP assays, respectively. The PPVs increased to 84.8% for tRBD and 82.5% for NP (**Fig. 3a, b**). To monitor of immune responses after infection or vaccination, a cut-off yielding higher sensitivities at acceptable specificities was established. A cut-off between the criteria suggested by the ROC analysis and that calculated by the 99th percentile method, e.g., 5.000 U/mL, yielded a sensitivity of 89.8% and a specificity of 98.0% for the tRBD assay, as well as a sensitivity of 86.5% and a specificity of 98.3% for the NP assay (**Fig. 3a, b**).

3.4. Orthogonal testing approach at very low seroprevalences to approximate 100% specificity

For low seroprevalences, when specificities need to approximate 100% in order to achieve acceptable PPVs, we considered an orthogonal testing approach (OTA). Our previous experiments already provided an indication that false-positives among pre-COVID-19 sera do not necessarily react with both antigens (**Fig. 2c**). As a classical OTA might negatively affect sensitivities an adaptive, sensitivity-improved (SI-OTA) was applied [46]. To this end, the above-described validation cohorts were screened with the tRBD ELISA. All samples with results ranging

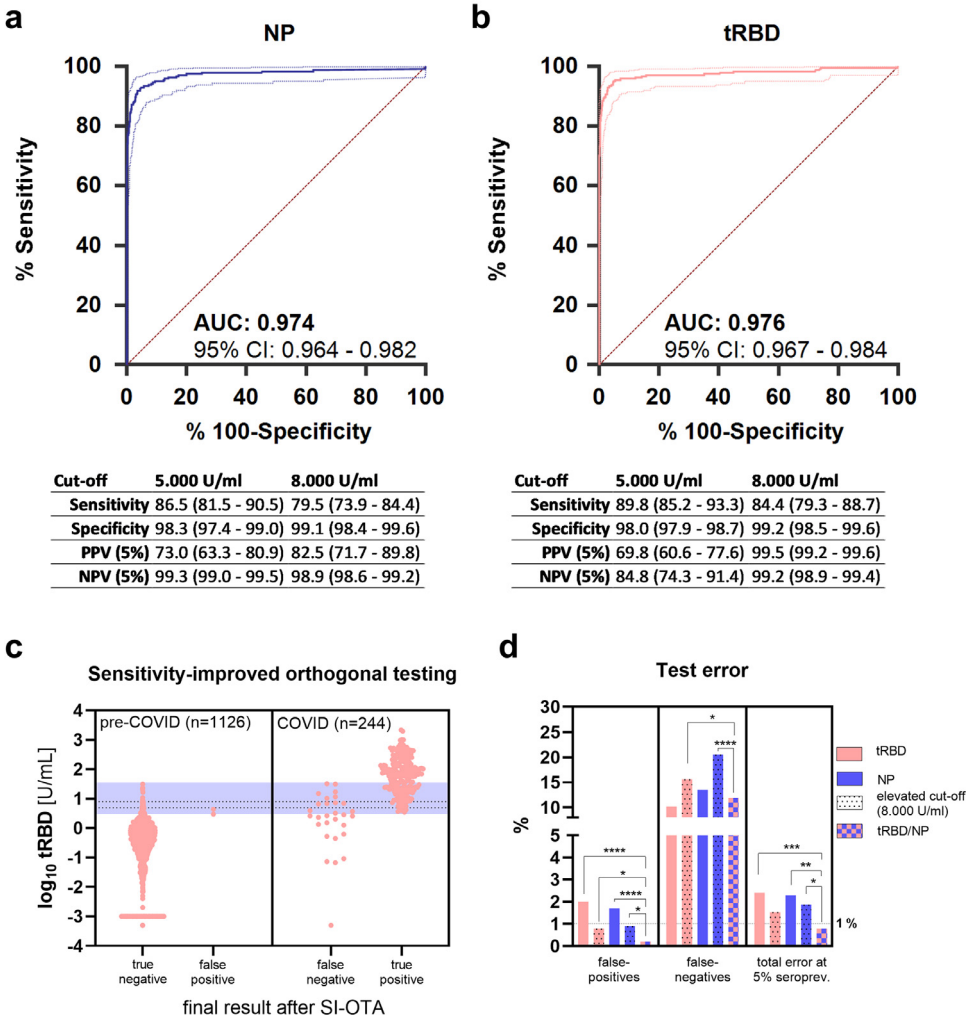

Cut-off	5.000 U/ml	8.000 U/ml
Sensitivity	86.5 (81.5 - 90.5)	79.5 (73.9 - 84.4)
Specificity	98.3 (97.4 - 99.0)	99.1 (98.4 - 99.6)
PPV (5%)	73.0 (63.3 - 80.9)	82.5 (71.7 - 89.8)
NPV (5%)	99.3 (99.0 - 99.5)	98.9 (98.6 - 99.2)

Cut-off	5.000 U/ml	8.000 U/ml
Sensitivity	89.8 (85.2 - 93.3)	84.4 (79.3 - 88.7)
Specificity	98.0 (97.9 - 98.7)	99.2 (98.5 - 99.6)
PPV (5%)	69.8 (60.6 - 77.6)	99.5 (99.2 - 99.6)
NPV (5%)	84.8 (74.3 - 91.4)	99.2 (98.9 - 99.4)

Fig. 3. Performance validation of the Technozym NP and RBD tests. ROC-curve (AUC±95% confidence intervals) of (**a**) the Technozym RBD- and (**b**) the NP-ELISA on basis of a cohort of 1126 pre-COVID-19 and 244 COVID-19 serum samples. (**c**) Results from an adaptive orthogonal testing approach, where all samples yielding <3.000 U/mL in the tRBD ELISA were considered negative and samples with tRBD >35.000 U/mL positive. Samples with tRBD values between those borders were re-tested with the NP ELISA (blue shade). If NP>3.500 U/mL, positivity was confirmed, otherwise it was ruled out. Dashed lines indicate the cut-offs determined by the 99th percentile method (8.000 U/mL) and a reduced cut-off with increased sensitivity (5.000 U/mL, between 99th percentile- and Youden-index criteria) to display the increase in sensitivity gained by the orthogonal test system. (**d**) Differences in false-positive and -negative test results for different individual and combined test setups were compared by z-tests, total errors at an estimated 5% seroprevalence were compared by χ^2-tests for proportions. PPV, positive predictive value, NPV, negative predictive value. * $P<0.05$, ** $P<0.01$, *** $P<0.001$, **** $P<0.0001$.

between the cut-off defined by the Youden index (including a safety margin, i.e., 3.000 U/mL) and 35.000 U/mL (as no false-positives occurred above 31.500 U/mL) were re-tested with the NP ELISA. There, also the Youden index criterion, adding a safety margin, was applied for positivity (>3.500 U/mL). Samples with <3.000 U/mL in the screening test were considered negative; samples with results between 3.000 U/mL and 35.000 U/mL in the screening tests and at the same time >3.500 U/mL in the confirmation test were considered positive; samples >35.000 U/mL in the screening test were considered positive. Applying these criterions 133 of 1370 samples needed to be re-tested. In turn, this approach led to a significantly enhanced specificity (99.8% [99.4–100.0]) when compared to the tRBD test alone both at a cut-off of 5.000 U/mL (+0.019, $P<0.0001$, z-test) and 8.000 U/mL (+0.006, $P = 0.035$, z-test). Compared to the latter, sensitivity (88.1% [83.4–91.9]) was improved (+0.037, $p<0.050$, z-test) and the PPV rose to 96.3% (86.7–99.1), see **Fig. 3c**. To achieve this improvement, only 133 (i.e., those with tRBD levels between 3.000 and 35.000 U/mL) of the overall 1370 samples needed to be re-tested by the NP assay, resulting in less than 10% increase in testing volume.

3.5. Cross-reactivity of SARS-CoV-2 IgG antibodies with endemic and seasonal coronaviruses

To better characterise our specificity cohorts, we explored the prevalence of antibodies towards common cold coronaviruses and possible cross-reactivities with our assays. To do so, outliers among the pre-COVID-19 cohort were defined as sera with readouts higher than the 75th percentile + 1.5x interquartile range (IQR) of the total cohort seroreactivity towards the SARS-CoV-2 NP or tRBD (outlier NP: $n = 17$; tRBD: $n = 4$). Above these cutoffs, all sera from our specificity cohorts reacted strongly with the spike proteins of circulating human coronaviruses (hCoVs) HKU-1, OC43, 229E, and NL63, confirming widespread seroprevalence in the general population (**Fig. 4a, b).** To further characterise the identified outliers among the pre-COVID-19 sera, we calculated their relative IgG signals, set them in relation to a roughly equal number of sera located at the other extreme on the seroreactivity scale (sera with readouts <25th percentile toward the respective antigen) and compared the differences in relative IgG levels to that towards hCoV antigens. Among our pre-validation cohort, sera with highest relative reactivity towards NP (mean difference: 0.88, $p<0.0001$, One-Way ANOVA with Sidak post hoc test) also demonstrated significantly elevated relative median IgG levels towards the spike protein of HKU-1 (mean difference: 0.13, $p = 0.0113$, One-Way ANOVA and Sidak post hoc test, **Fig. 4b**). The specificity cohort we used for clinical validation included eight sera from individuals with PCR-confirmed hCoV infection. None of these yielded false-positive readouts at a cutoff of 5.000 U/mL (**Fig. 4c**) at comparably low specificities of 95.3% (tRBD) and 96.1% (NP) (see **Fig. 3a, b**).

3.6. Clinical evaluation of test performance after symptom onset

Diagnostic accuracy of the Technozym NP or RBD IgG Tests was evaluated at different time points after symptom onset in plasma from hospitalised individuals (general ward and intensive care unit

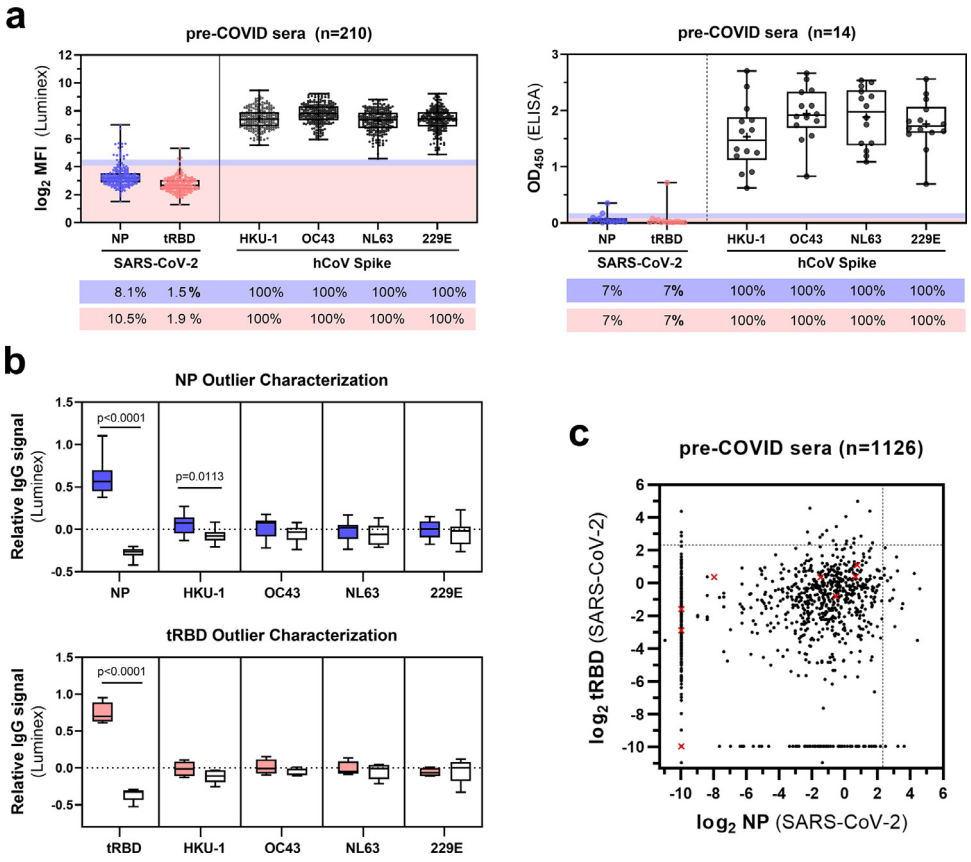

Fig. 4. Characterisation of cross-reactive IgG responses between SARS-CoV-2 and endemic hCoV strains in the specificity cohorts. (a) Seroreactivity of serum samples from the two specificity cohorts (AIT pre-COVID-19 cohort, $n = 210$ and MedUni Wien Biobank pre-COVID-19, $n = 14$) employed for pre-validation of the SARS-CoV-2 tRBD and NP antigens with the Luminex or ELISA assays respectively, was measured with the spike proteins of common-cold hCoVs HKU-1, OC43, 229E and NL63. Outliers were classified as observations that fall above the 75th percentile + 1.5 x IQR. Shades give the respective calculated cut-offs and are color-coded for NP (blue) or tRBD (pink). Values below the box-plots give the measured seropositivity in percent. **(b)** Relative IgG levels of NP ($n = 17$, blue boxes) and tRBD ($n = 4$, pink boxes) outliers towards the spike proteins of hCoV. White boxes give relative IgG levels of sera with readouts <25th percentile ($n = 16$ for NP, $n = 5$ for tRBD) to compare with outliers. Means within groups were compared by One-Way ANOVA followed by a Sidak test to correct for multiple comparisons. **c)** tRBD and NP-specific seroreactivity of the specificity cohort ($n = 1126$ MedUni Wien Biobank) used for clinical validation. Red crosses display sera from individuals with PCR-confirmed hCoV infection. Dashed lines indicate the cut-off of 5 U/mL.

[ICU] patients) and outpatients. A total of 104 plasma samples were drawn during the acute and early convalescent phase of SARS-CoV-2 infection. NP-specific IgG levels correlated well with tRBD-specific IgG levels, even at levels being below the set threshold for seropositivity (1–5 d: r_s=0.67, p<0.0001; 6–10 d: 0.76, <0.0001; 11–15 d: 0.76, 0.0006, Spearman correlation, **Fig. 5**). The positivity rates increased over time, peaking at 100% 15–22 days after symptom onset in both assays. True positivity rates for the NP ELISA were consistently higher than with the tRBD ELISA at all time points (1–5 d: NP vs tRBD: 14.7% vs 5.9%; 6–10 d: 45.7% vs 34.2%; 11–15 d: 76.5% vs 64.7%, **Fig. 5 and Table S2**). Yet, sera displayed a great heterogeneity in antibody levels throughout the observation period (**Table S2**). None of the false-negative results among the samples were obtained with both assays. Astonishingly, 85.7% of the sera already contained neutralizing antibodies (median titre: 1:24; range 1:4 – 1:128, **Table S2**) as soon as by day five after symptom onset. Of these, however, only a total of 18% of the sera demonstrated seroreactivity above the cut-off for either the NP or tRBD antigen (**Fig. 5**). Yet, the quantitative nature of the assay allowed us to correlate antibody levels below the cut-off for seropositivity and we could demonstrate excellent correlation of tRBD-specific antibodies with neutralizing function at all four investigated time points (1–5 d: r_s=0.49, p = 0.0004; 6–10 d: r_s=0.77,p <0.0001; 11–15 d: r_s=0.82, p<0.0001; 16–22: r_s=0.67, p = 0.0003, Spearman, **Fig. 5**).

4. Discussion

Superb assay specificity is of utmost importance for the assessment of antibodies directed against SARS-CoV-2, as a substantial proportion of infected individuals escapes identification due to the frequent asymptomatic course of the disease, thereby distorting the true seroprevalence in any given population [47]. The biological basis for false-positives is multifactorial, but the influence of the production platform- and process-related peculiarities or impurities on performance of a diagnostic protein are factors that are often underestimated. While the viral NP is almost exclusively being produced in bacteria [48,49], we expressed the spike receptor binding domain in HEK cells, CHO cells, insect cells and plants [4,50–52]. To find out which of these systems leads to the highest quality and manufacturability of the RBD diagnostic antigen of potentially high demand, we evaluated these production platforms and pre-validated the proteins based on diagnostic performance with a large set of pre-COVID-19 and COVID-19 sera using the Luminex platform. All five expression platforms demonstrated suitability for the production of

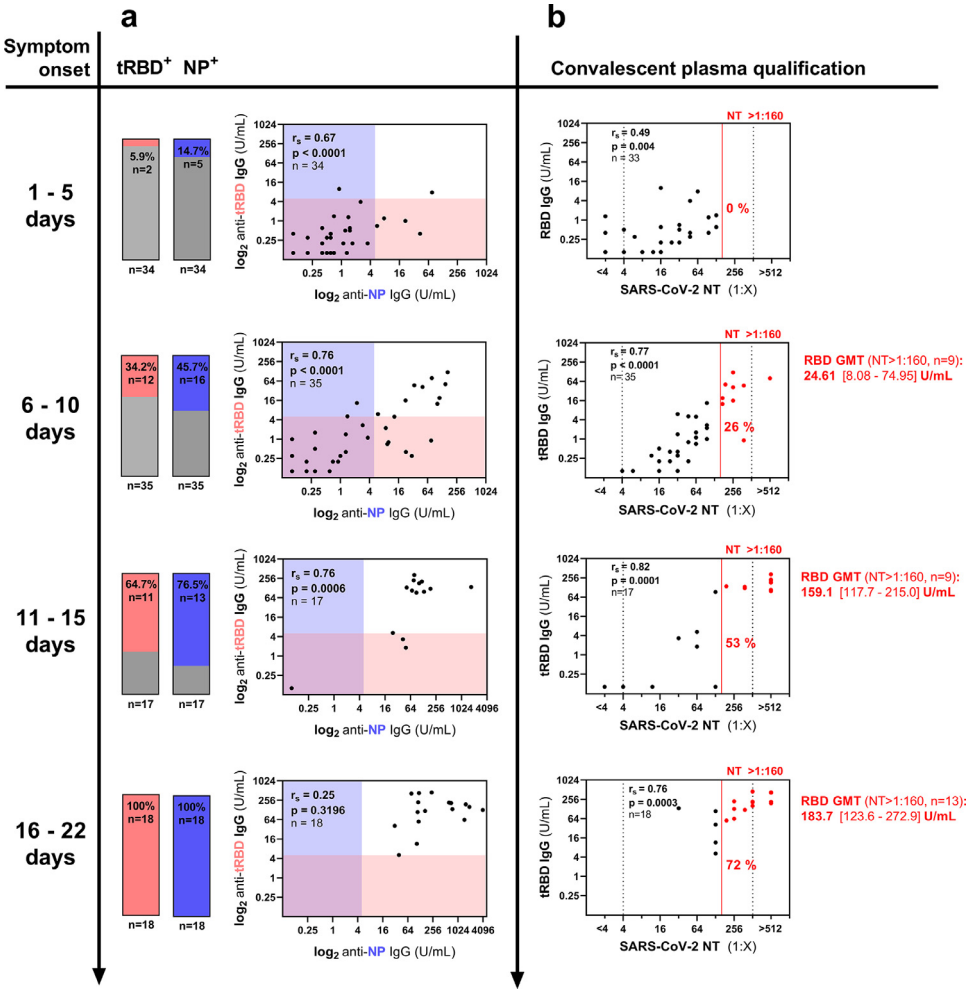

Fig. 5. Time-resolved evaluation of NP, tRBD-specific and neutralizing antibodies in the acute and early convalescent phase after SARS-CoV-2 infection. a-b, A total of 104 plasma samples from 64 outpatients (16%) and hospitalised individuals (65% general ward, ICU 19%) were analyzed for anti-NP and anti-tRBD antibodies and neutralizing antibodies at the indicated time points. (**a**) Antibody levels were assessed with the Technozym ELISAs according to the suggested cut-off of 5.000 U/mL. Bars indicate the fraction of NP, tRBD-positive samples among the tested. Shades give the respective ELISA cut-offs (NP: blue, tRBD: pink). (**b**) Neutralization assays with authentic SARS-CoV-2 virus were performed within a serum dilution range of 1:4 – 1:512 (dashed lines). Values below or above these limits were assigned a titer of 1:2 or 1:1024 for correlation analysis, respectively. The red line indicates a NT of 1:160 that is recommended by the FDA for the screening of recovered COVID-19 patients for convalescent plasma therapy. All sera above this cut-off are color-coded in red. Geometric mean titers and 95% CI in the RBD ELISA are given for sera with a NT >1:160. r_s, Spearman's correlation factor.

functional protein, proven by a binding assay with the SARS-CoV-2-RBD-specific mAb CR3022. Yet, in part due to the different transfection/infection methods used, RBD yields from CHO-K1, CHO-S as well as from *Tnms*42 insect cells and tobacco plants were insufficient for sustainable commercial antigen supply (< 1 mg/L, **Fig. 1**). In contrast, HEK cells readily produced overall yields of 40 mg/L using PEI-transfection. Yields of 30 mg/mL per liter have also been described for CHO-expressed RBD. However, this can be traced back to optimised design of expression constructs and improved production processes for stable RBD-expressing CHO cells together with less extensive purification protocols [53]. We observed higher basal seroreactivity of control sera with insect-derived RBD than with RBD from human and non-human mammalian cell lines; which is in line with other reports [4]. Host-related impurities do not account for that, as insect-cell produced RBD demonstrated the highest purity among all our RBD samples (99%, **Fig. S2**). While there was a common set of false-positive samples shared by RBD from non-human and human mammalian cell lines as well as plants, false-positives reactive with the insect material were entirely insect-RBD-specific (**Fig. S6**). A possible reason may be platform-specific protein modifications, such as glycosylation, that provide the protein with a unique process-derived signature. Indeed, *T. ni*-derived insect cells were demonstrated to generate core α1,3-fucose structures with allergenic potential in humans [54], which might be associated with this peculiar seroreactivity profile.

Based on our observation that RBD tends to form homodimers in an unpredictable manner among different production batches of the same expression host, we used an optimised, truncated version of an RBD as diagnostic antigen (tRBD), enabling the production of large amounts of RBD with consistent quality (**Fig. S2**). For tRBD performance, antigen purity was of utmost importance, even when expressed in human cell lines. A reduction in tRBD purity by 11% (pure: 98.5%, impure: 87.5% purity, **Fig S4a**) resulted in a significant increase in seroreactivity with pre-COVID sera (+0.3, $p<0.0001$, Mann-Whitney test) in the bead-based Luminex assays, while the median fluorescence readouts with COVID sera significantly decreased (−2.5, $p<0.0001$, Mann-Whitney tests). This resulted in a drastic change of the antigens' capability to discriminate the two cohorts and sensitivity decreased by 83.9% (pure: 95.2% versus impure: 11.3% sensitivity, respectively) at a pre-defined consensus specificity of 99.1% (**Fig. S4c**). Since purity after an IMAC capture step was highly batch-dependent and resulted in inconsistent seroreactivity profiles, our standard downstream process included a scalable AIEX chromatography polishing step to account for these inconsistencies and to improve the diagnostic performance of the antigens.

The two test antigens, tRBD from HEK cells and NP from *E. coli*, were further used for ELISA assay development. We configured the assays with a number of sera taken from SARS-CoV-2-infected individuals with weak antibody responses to ensure high assay sensitivity. In contrast to available literature [4,55,56], we used high antigen coating concentrations (6 μg/mL) to yield satisfactory readouts and to achieve a higher dynamic measurement range. A caveat of many assay validation studies is that performance characteristics are skewed by the exclusive inclusion of samples from hospitalised individuals, where robust antibody levels are to be expected [57]. Likewise, the sole consideration of healthy donors in control groups may lead to overestimated assay specificity, as the impact of potential cross-reactive factors present in the general population is largely ignored. In this respect, auto-antibodies commonly found in individuals with inflammatory diseases [58] were already described to cross-react with SARS-CoV-1 antigens [59]. To challenge our tests systems, we biased our large specificity cohort (n = 1126) by including samples with an increased propensity for cross-reactivity, including sera from individuals with inflammatory illnesses (n = 359), sera from PCR-confirmed hCoV infections (n = 8) and sera drawn during winter months to increase the likelihood of respiratory infections (n = 494). Similarly, our sensitivity cohort (n = 244) included convalescent sera from SARS-CoV-2-infected individuals covering the full spectrum of clinical manifestations (from asymptomatic to ICU patients). Among them, 21% of the sera were collected from asymptomatic individuals or from individuals with mild to moderate illness, who may mount less robust and durable antibody responses after an infection [60]. Based on these cohorts, we defined adequate test parameters to enable highly specific detection of SARS-CoV-2-specific antibodies. A cut-off deduced by the 99th percentile method (8.000 U/mL) allowed for high specific serodiagnosis with 99.2% for the Technozym RBD Test and 99.1% for the Technozym NP Test (at sensitivities of 86.3% and 76.7%, respectively). This is a remarkable result for a tetramethylbenzidine-based manual test system, considering the highly diverse nature of our study cohorts. While some automated systems were described to achieve specificities approximating 100% [61,62], assay performance is highly cohort-specific. The use of diverse study cohorts was also associated with performance deteriorations in such test platforms (i.e. Abbot, Specificity: 97.5%) [63]. For the Meduni Wien Biobank cohort we had performance data with CE-marked automated test systems available [46] to directly compare with our ELISAs at the high specificity cut-off criterion (8.000 U/mL). With an AUC of 0.987 [0.979−0.992] and a specificity of 99.1%, the NP ELISA presented with comparable performance to the Abbott SARS-CoV-2 chemiluminescence microparticle assay (AUC: 0.993 [0.987−0.997], **Fig. S5**, Sp 99.2%) [46], that also relies on the NP antigen. The tRBD ELISA even outperformed the DiaSorin LIAISON® SARS-CoV-2 S1/S2 IgG chemiluminescence assay (tRBD ELISA: AUC/Sp/Sen=0.993/99.2%/84.9% vs DiaSorin:0.976/98.2%/82.8%, see **Fig. S5** and Perkmann and colleagues [46]. While we cannot rule out minor cross-reactivity between hCoV-specific antibodies and SARS-CoV-2 antigens, they appeared to have a limited effect on assay performances (**Fig. 4c**).

Yet, for an estimated seroprevalence of 5% in the general European population [33,64], a test with a specificity and sensitivity of 99.2% and 86.3%, respectively, only scores a PPV of 85.0% resulting in 15 false-positive results out of 100, which is still insufficient. In line with previous results from us and others [34,65,66], we demonstrate that false-positive results are largely antigen-dependent (**Figs. 2b**, **4c**). Orthogonal testing is suggested by the Centers of Disease Control and Prevention (CDC) to remedy specificity problems in low transmission settings [67]. Previous studies have used RBD as screening antigen and the trimeric spike protein or the spike S2 domain in second-line tests to confirm initial positive results [4,66]. Such conventional orthogonal test strategies, however, increase specificity often at the expense of sensitivity. We therefore established an adaptive orthogonal test algorithm where positive sera were first identified with the tRBD ELISA allowing for highly sensitive testing (at the expense of specificity) and samples within a predefined area of uncertainty then underwent confirmatory testing with the NP ELISA [46]. This two-test algorithm resulted in a cumulative specificity of 99.8% and an even higher change in sensitivity of 88.1% (+0.037, $p<0.050$, z-test), yielded a PPV of 96.3% [86.7−99.1] (**Fig. 3**). This is an excellent result for a manual test format and its specificity is on par with other orthogonal tests relying on automated systems [46].

As the Technozym NP and RBD ELISAs provide a five-point calibrator set ELISA antibody levels can be quantified, compared and followed over time. For such an application, we chose a cut-off of 5.000 U/mL that allowed for more sensitive analysis of antibody levels at acceptable specificity, adapted from the cut-off given by the Youden index. With convalescent sera taken at median 43−54 days post-symptom onset, the tRBD ELISA allowed for a more sensitive detection of antibodies than the NP ELISA (**Fig. 3a, b**). Yet, time-resolved analysis of seroconversion demonstrated that NP-specific antibodies develop earlier after an infection and true positive rates were consistently higher with the NP ELISA for samples collected within the first 15 days post-symptom onset (**Fig. 5, Table S2**). This

phenomenon has already been described in patients infected with SARS-CoV-1 [68,69] and was associated with higher sensitivities of other SARS-CoV-2 test systems, relying on the NP, in the early phase after an infection [70]. Determining the neutralizing capacity of SARS-CoV-2 anti-RBD antibodies is critical to elucidate possible protective effects of the immune response. Considering all neutralizing activity above background as positive, we observed neutralizing antibodies in 85% of the sera already by day five after symptom onset (**Fig. 5**), which is in line with previous studies [71,72]. Of note, RBD-seroconversion, defined by IgG antibody levels above a threshold of 5.000 U/mL, was observed for only 6% of the sera at this time point. Yet, despite 33 out of 35 samples demonstrating reactivity below our pre-defined cutoff, neutralizing titers correlated well with RBD-specific IgG responses. A recent study demonstrated that the early neutralizing response is dominated by RBD-specific IgA antibodies [73]. As we exclusively measured RBD-specific IgG responses we cannot rule out that part of the early neutralizing activity we observe derive from neutralizing IgA or even earlier IgM responses.

Tests for the screening of reconvalescent COVID-19 patients for the presence of anti-SARS-CoV-2 antibodies are of great interest for identifying suitable donors for convalescent plasma therapy [74]. A retrospective, propensity score–matched case–control study performed at the Mount Sinai hospital (New York, NY) provides evidence for a survival benefit in patients receiving convalescent plasma transfusion as an effective intervention in COVID-19 [74]. In August 2020, the FDA issued a new guidance on the Emergency Use Authorization (EUA) for COVID-19 convalescent plasma, recommending plasma donations to be qualified by either the Mount Sinai COVID-19 ELISA IgG Antibody Test or Ortho VITROS IgG assay [75]. Prior to this guidance, NTs of at least 1:160 were considered acceptable in the absence of high-titer samples [76]. As we did not have the beforementioned tests available, we qualified plasma donors according to the NT 1:160 criterion. The fraction of samples exceeding this threshold gradually increased over time and by day 15 after symptom onset, 53% of the sera and by day 22, 72% of sera had titers higher than 1:160 (**Fig. 5, Table S2**). The geometric mean RBD titers in these sera corresponded to 159.1 U/mL and 183.7 U/mL, respectively. Since correlates of protection from infection remain to be determined we cannot deduce whether these titers are clinically relevant in prophylaxis, at this point.

In conclusion, we have developed two highly specific, quantitative, easy-to-implement and now commercially available SARS-CoV-2 antibody tests and defined optimal thresholds for their application in different aspects of clinical use. We established tailor-made testing algorithms to maximize test performance in a wide range of applications of clinical utility, such as the follow-up of patients after an infection (which demand high sensitivity), but also developed a sensitivity-improved orthogonal testing algorithm for seroprevalence studies (which demand high specificity). Comprehensive test validation with large multi-center cohorts and neutralization assays indicated that our simple, but well-designed tests even outperforms commercially available automated CE-marked test systems with challenging human serum samples. Yet, a dual-testing approach also enables to differentiate between vaccinated and infected individuals, valid for all vaccines not triggering NP responses, or to study the rate of re-infection in people that had been infected or vaccinated. Moreover, the RBD ELISA allows for the identification of donors for convalescent plasma therapy as RBD-specific antibody levels correlate well with the induction of functional neutralization responses. Both tests allow to comprehensively monitor the dynamics of antibody responses after infection. Yet, our data disclose different kinetics for antigen-specific antibody responses, which affect their performance at different time points after an infection. These findings are essential for ongoing efforts to establish serological tests for clinical diagnostics. In this respect, also test performance with convalescent sera collected more than two months after infection and the effect of antigen-specific antibody waning should be carefully addressed in future studies and compared to the comprehensive findings of this study.

Contributors

A.J.,A.W.,C.J.B.,E.L.,F.E.,F.G.,G.S.,G.W.K.,H.H.,J.M.,M.S.,M.D.,M.W.,M.K.,M.C.P.,N.L.,N.Bo.,N.Bi.,P.P.A., R.G.,T.P.,W.G. designed study concepts. A.J.,A.W.,C.J.B,F.E.,F.G.,G.S.,J.M.,M.W.,M.K.,M.C.P.,N.Bi.,R.G.,W.G. acquired financial support for this project. A.W.,B.H.,B.D.,C.J.B,E.G.,E.L.,F.G.,G.M.,G.S.,G.SM.,G.W.K.,H.H.,J.H.,J.B.,J.M.,Li.M.,M.H.,M.E.,M.S.,M.D.,M.W.,M.K.,M.C.P.,N.L.,N.M.,N.Bi.,P.P.A.,P.S.,R.H.,R.G.,Ri.S.,T.P.,W.G. developed and designed methodology . A.E.E.,A.G.,A.W.,B.H.,B.D.,C.I.,C.J.B,C.K.,C.T.,C.G.G,D.M.,D.S.,E.G.,E.L.,F.S.,G.M.,G.L.,G.SM.,G.W.K.,G.H., J.H.,J.D.V.,J.L.R.,J.B.,Lu.M.,M.H.,M.S.,M.K.B.,M.D.,M.W.,M.K.,N.L.,N.M.,N.Bi.,P.P.A.,P.Q.,P.S.,R.H.,R.G.,Ri.S.,Ro.S.,R.B.W.,T.P.,U.V. conducting a research and investigation process, specifically performing the experiments, or data/evidence collection. K.V. developed evaluation software code. A.E.E.,A.G.,B.D.,C.I.,F.G.,G.H.,H.H.,M.D.,M.K.,R.B.W.,T.P. performed data curation. A.W.,F.G.,H.H.,J.H.,M.H.,M.S.,M.K.,W.G. performed data validation and evaluated data reproducibility. B.D.,H.H.,M.D.,M.K. verified the underlying data. A.E.E.,A.G.,A.W.,B.H.,B.D.,C.I.,C.G.G,D.M,E.L.,F.G.,G.M.,G.SM.,G.W.K.,G.H.,H.H.,J.D.V.,K.V.,Lu.M.,M.E., M.D.,M.K.,M.C.P.,N.L.,P.P.A.,Ri.S. applied statistical, mathematical, computational, or other formal techniques to analyze or synthesize study data. H.H.,M.D.,M.K.,R.B.W. performed data visualization. A.E.E., A.J.,A.G.,C.I.,C.J.B,D.S.,E.L.,F.E.,F.G.,G.S.,G.L.,G.H.,G.W.,J.D.V.,J.L.R.,J.M.,Lu.M.,M.K.B.,M.W.,M.C.P.,N.Bo.,N.Bi.,P.Q.,R.H.,R.G.,Ro.S.,R.B.W.,W.G., provided study materials, reagents, laboratory samples, animals, instrumentation, computing resources, or other analysis tools. A.W.,C.J.B,F.G.,G.S.,G.W.,Lu.M.,M.C.P,M.D.,M.K.,N.Bo.,N.Bi.,R.G.,R.B.W.,W.G. were responsible for supervising research activities and for project administration. H.H.,M.D.,M.K.,M.C.P.,R.G.,T.P. wrote the original draft. B.D., C.J.B,E.L.,F.G.,G.W.K.,J.D.V.,J.M.,Lu.M.,M.E.,M.C.P.,N.L.,P.P.A.,P.S.,R.G.,W.G. reviewed and edited the manuscript. All authors read and approved the final version of the manuscript and have had access to the raw data.

Data sharing statement

All data needed to evaluate the conclusions in the paper are present in the manuscript and/or the Supplementary Materials. Further information on the study protocol will be made available to interested researchers. Recombinant SARS-CoV-2 antigens can be requested from interested researchers for research purposes under www.boku-covid19.at (after registration). For commercial purposes antigens can be requested from enGenes Biotech GmbH. Technozym NP and RBD IgG serotests are available from Technoclone (Technoclone Herstellung von Diagnostika und Arzneimitteln GmbH, Vienna, Austria).

Declaration of Competing Interest

Dr. Klausberger has nothing to disclose. Dr. Duerkop has nothing to disclose. Dr. Haslacher has nothing to disclose. Dr. Wozniak-Knopp has nothing to disclose. Dr. Cserjan-Puschmann has nothing to disclose. Dr. Perkmann has nothing to disclose. Dr. Lingg has nothing to disclose. Dr. Pereira Aguilar has nothing to disclose. Dr. Laurent has nothing to disclose. Dr. De Vos has nothing to disclose. Mag.rer.nat. Hofner has nothing to disclose. Dr. Holzer has nothing to disclose. Mrs. Stadler has nothing to disclose. Dipl.-Ing. Manhart has nothing to disclose. DI Vierlinger has nothing to disclose. Dr. Egger has nothing to disclose. Dipl. Ing. Milchram has nothing to disclose. Dr. Gludovacz has nothing to disclose. Dr. Marx has nothing to disclose. Dipl.-Ing. Köppl has nothing to disclose. Christopher Tauer, BSc has nothing to disclose. Jürgen Beck, MSc reports nothing to disclose. Daniel

Maresch has nothing to disclose. Dr. Grünwald-Gruber has nothing to disclose. Mr. Strobl has nothing to disclose. Dr. Satzer has nothing to disclose. Dr. Stadlmayr has nothing to disclose. Ing. Vavra has nothing to disclose. Ms. Huber BSc has nothing to disclose. Dr. Wahrmann has nothing to disclose. Dr. Eskandary has nothing to disclose. Dr. Breyer has nothing to disclose. Dr. Sieghart has nothing to disclose. Dr. Quehenberger reports other from Roche Austria, personal fees from Takeda, outside the submitted work; . Dr. Leitner has nothing to disclose. Dr. Strassl has nothing to disclose. Dr. Egger has nothing to disclose. Dr. IRSARA has nothing to disclose. Dr. Griesmacher has nothing to disclose. Dr. Hoermann has nothing to disclose. Dr. Weiss has nothing to disclose. Dr. Bellmann-Weiler has nothing to disclose. Dr. Löffler-Ragg has nothing to disclose. Dr. Borth has nothing to disclose. Dr. Strasser has nothing to disclose. Dr. Jungbauer has nothing to disclose. Dr. Hahn has nothing to disclose. Dr. Mairhofer reports other from enGenes Biotech GmbH, outside the submitted work; In addition, Dr. Mairhofer has a patent PCT/EP2016/059597-Uncoupling growth and protein production issued. Dr. Hartmann has nothing to disclose. Dr. Binder reports grants from Vienna Business Agency, during the conduct of the study; and Employee of Technoclone Herstellung von Diagnostika und Arzneimitteln GmbH. Dr. Striedner reports other from enGenes GmbH, outside the submitted work; In addition, Dr. Striedner has a patent. US20180282737A1 issued to enGenes GmbH. Dr. Mach has nothing to disclose. Dr. Weinhaeusel has nothing to disclose. Dr. Dieplinger has nothing to disclose. Dr. Grebien has nothing to disclose. Dr. Gerner has nothing to disclose. Dr. Christoph Binder is board member of Technoclone GmbH. Dr. Grabherr has nothing to disclose.

Acknowledgments

We thank the Vienna Science and Technology Fund (WWTF) for partial funding of this project (Project No. COV20−016). We thank the University of Natural Resources and Life Sciences (BOKU) Vienna, the Ludwig Boltzmann Institute (LBI) for Experimental and Clinical Traumatology and the Ludwig Boltzmann Gesellschaft (LBG) for financial support of the project. Jelle De Vos acknowledges the Research Foundation Flanders (FWO) for support by grants 12J6520N and V443719N, and the OEAD (Austria) for scholarship ICM-2019−14929. We thank Florian Krammer (Icahn School of Medicine at Mount Sinai, New York, NY) for providing the constructs used for the production of RBD and CR3022. We thank George Lomonossoff (John Innes Centre, Norwich, UK) and Plant Bioscience Limited (PBL) (Norwich, UK) for supplying the pEAQ-HT expression vector. The authors thank Naila Avdic, Kristina Jagersberger, Christina Hausjell, Viktoria Mayer, Anna-Carina Frank, Sophie Vazulka, Florian Mayer, Matthias Müller, Andreas Dietrich, Mathias Fink, Florian Weiss, Giulia Borsi, Mohammed Hussein, Patrick Mayrhofer, Andreas Fischer, Alexander Doleschal (all Department of Biotechnology, University of Natural Resources and Life Sciences (BOKU) Vienna or and/or ACIB GmbH affiliated) for their tremendous dedication and support in the framework of the inter-department BOKU-COVID-19 Initiative, which included lab-work for the cloning, production and analysis of SARS-CoV-2 antigens described in this work. The BLI and mass spectrometry equipment was kindly provided by the EQ-BOKU VIBT GmbH and the BOKU Core Facilities *Biomolecular & Cellular Analysis* (BOKU BmCA) and *Mass Spectrometry* (BOKU CFMS). The authors thank Irene Schaffner and Jakob Wallner (BOKU BmCA) for assisting in BLI measurements and ForteBio for providing SAX biosensors. Boehringer Ingelheim RCV GmbH & Co KG fully supported the endeavour and granted access to manufacturing technologies for process development and manufacturing. Icons in Figure 1 were generated with BioRender.com. The authors want to thank Maria Ozsvar-Kozma, Patrick Mucher, Manuela Repl and Astrid Radakovics (Department of Laboratory Medicine, Medical University Vienna) for outstanding technical assistance. The authors thank the following collaborators for providing biomaterial and data for ELISA evaluation: Manfred Nairz, Sabina Sahanic, Thomas Sonnweber, Alex Pizzini, Ivan Tancevski (Department of Internal Medicine II, Medical University of Innsbruck), Markus Anliker, Lorin Loacker, Wolfgang Prokop (Central Institute for Medical and Chemical Laboratory Diagnosis, Innsbruck University Hospital), Wolfgang Mayer, Harald Schennach (Central Institute for Blood Transfusion & Immunological Department, University Hospital of Innsbruck), Daniel Aletaha (Department of Internal Medicine III, Medical University of Vienna), Robab Breyer-Kohansal, Otto C Burghuber, and Sylvia Hartl (LEAD-Study - Ludwig Boltzmann Institute for Lung Health, Vienna, Austria), Andreas Leiherer (Vorarlberg Institute for Vascular Investigation and Treatment [VIVIT], Dornbirn, Austria). The BOKU Spin-off Novasign GmbH supported the sustainability concept of BOKU by creating and hosting the BOKU-COVID19 Portal (portal.boku-covid19.at) that enables researchers worldwide to obtain free samples of the SARS-CoV-2 antigens described within this work. Roger Dalmau Díaz and Armin Khodaei have implemented the portal application and its dependencies.

Supplementary materials

Supplementary material associated with this article can be found in the online version at doi:10.1016/j.ebiom.2021.103348.

References

[1] Long Q-X, Liu B-Z, Deng H-J, Wu G-C, Deng K, Chen Y-K, et al. Antibody responses to SARS-CoV-2 in patients with COVID-19. Nat Med 2020;26(6):845–8 Jun.
[2] Foundation for Innovative New Diagnostics (FIND). SARS-CoV-2 diagnostic pipeline. [cited 2021 Mar 11]; Available from: https://www.finddx.org/covid-19/pipeline/?avance=Commercialized&type=Manual+or+automated+immunoassays&test_target=Antibody&status=all&section=immunoassays&action=default#diag_tab
[3] Lisboa Bastos M, Tavaziva G, Abidi SK, Campbell JR, Haraoui L-P, Johnston JC, et al. Diagnostic accuracy of serological tests for covid-19: systematic review and meta-analysis. BMJ 2020;1:m2516. Jul.
[4] Amanat F, Stadlbauer D, Strohmeier S, Nguyen THO, Chromikova V, McMahon M, et al. A serological assay to detect SARS-CoV-2 seroconversion in humans. Nat Med 2020;26(7):1033–6 Jul.
[5] Wu F, Zhao S, Yu B, Chen Y-M, Wang W, Song Z-G, et al. A new coronavirus associated with human respiratory disease in China. Nature 2020;579(7798):265–9 Mar.
[6] Sainsbury F, Thuenemann EC, Lomonossoff GP. pEAQ: versatile expression vectors for easy and quick transient expression of heterologous proteins in plants. Plant Biotechnol J 2009;7(7):682–93 Sep.
[7] Stargardt P, Feuchtenhofer L, Cserjan-Puschmann M, Striedner G, Mairhofer J. Bacteriophage inspired growth-decoupled recombinant protein production in Escherichia coli. ACS Synth Biol 2020;9(6):1336–48 Jun 19.
[8] Cserjan-Puschmann M, Lingg N, Engele P, Kröß C, Loibl J, Fischer A, et al. Production of circularly permuted caspase-2 for affinity fusion-tag removal: cloning, expression in Escherichia coli, purification, and characterization. Biomolecules 2020;10(12):1592. Nov 24.
[9] Lingg N., Cserjan-Puschmann M., Fischer A., Engele P., Kröß C., Schneider R., et al. Advanced purification platform using circularly permuted caspase-2 for affinity fusion-tag removal to produce native fibroblast growth factor 2. J Chem Technol Biotechnol [Internet]. 2021 Jan 27 [cited 2021 Mar 11]; Available from: https://onlinelibrary.wiley.com/ 10.1002/jctb.6666
[10] DeVos J., Pereira Aguilar P., Köppl C., Fischer A., Grünwald-Gruber C., Dürkop M., et al. Native hydrophobic interaction chromatography hyphenated to multi-angle light scattering detection for in-process control of SARS-CoV-2 nucleocapsid protein produced in Escherichia Coli. 2021 Mar 11 [cited 2021 Mar 11]; Available from: 10.26434/chemrxiv.14195318.v1
[11] Tian X, Li C, Huang A, Xia S, Lu S, Shi Z, et al. Potent binding of 2019 novel coronavirus spike protein by a SARS coronavirus-specific human monoclonal antibody. Emerg Microbes Infect 2020;9(1):382–5 Jan 1.
[12] Mairhofer J, Cserjan-Puschmann M, Striedner G, Nöbauer K, Razzazi-Fazeli E, Grabherr R. Marker-free plasmids for gene therapeutic applications—Lack of antibiotic resistance gene substantially improves the manufacturing process. J Biotechnol 2010;146(3):130–7 Apr 1.
[13] Urthaler J, Ascher C, Wöhrer H, Necina R. Automated alkaline lysis for industrial scale cGMP production of pharmaceutical grade plasmid-DNA. J Biotechnol 2007;128(1):132–49 Jan.
[14] Cytiva. Application Note 28-4094-85 AA: PlasmidSelect Xtra for downstream processing of supercoiled plasmid DNA. 2020 Jul.
[15] Durocher Y. High-level and high-throughput recombinant protein production by transient transfection of suspension-growing human 293-EBNA1 cells. Nucl Acids Res 2002;30(2):9e–9 Jan 15.

[16] Lobner E, Humm A-S, Göritzer K, Mlynek G, Puchinger MG, Hasenhindl C, et al. Fcab-HER2 interaction: a Ménage à Trois. Lessons from X-Ray and solution studies. Structure 2017;25(6):878–89 June5.

[17] Chen Y-R, Zhong S, Fei Z, Hashimoto Y, Xiang JZ, Zhang S, et al. The transcriptome of the Baculovirus Autographa Californica Multiple Nucleopolyhedrovirus in Trichoplusia ni cells. J Virol 2013;87(11):6391–405 Jun 1.

[18] Koczka K, Peters P, Ernst W, Himmelbauer H, Nika L, Grabherr R. Comparative transcriptome analysis of a Trichoplusia ni cell line reveals distinct host responses to intracellular and secreted protein products expressed by recombinant baculoviruses. J Biotechnol 2018;270:61–9 Mar.

[19] Klausberger M, Wilde M, Palmberger D, Hai R, Albrecht RA, Margine I, et al. One-shot vaccination with an insect cell-derived low-dose influenza A H7 virus-like particle preparation protects mice against H7N9 challenge. Vaccine 2014;32(3):355–62 Jan.

[20] Strasser R, Stadlmann J, Schähs M, Stiegler G, Quendler H, Mach L, et al. Generation of glyco-engineered Nicotiana benthamiana for the production of monoclonal antibodies with a homogeneous human-like N-glycan structure: XylT and FucT down-regulation in N. benthamiana. Plant Biotechnol J 2008;6(4):392–402 May.

[21] Castilho A, Gattinger P, Grass J, Jez J, Pabst M, Altmann F, et al. N-Glycosylation engineering of plants for the biosynthesis of glycoproteins with bisected and branched complex N-glycans. Glycobiology 2011;21(6):813–23 Jun.

[22] Göritzer K, Turupcu A, Maresch D, Novak J, Altmann F, Oostenbrink C, et al. Distinct Fcα receptor N -glycans modulate the binding affinity to immunoglobulin A (IgA) antibodies. J Biol Chem 2019;294(38):13995–4008 Sep 20.

[23] Hulme EC, Trevethick MA. Ligand binding assays at equilibrium: validation and interpretation: equilibrium binding assays. Br J Pharmacol 2010;161(6):1219–37 Nov.

[24] Armbruster DA, Pry T. Limit of blank, limit of detection and limit of quantitation. Clin Biochem Rev 2008;29(Suppl 1):S49–52 Aug.

[25] Carvalho SB, Moreira AS, Gomes J, Carrondo MJT, Thornton DJ, Alves PM, et al. A detection and quantification label-free tool to speed up downstream processing of model mucins editor D'Auria S, editor. A detection and quantification label-free tool to speed up downstream processing of model mucins. PLoS One 2018;13(1):e0190974 Jan 9.

[26] Klein JS, Bjorkman PJ. Few and far between: how HIV may be evading antibody avidity editor Rall GF, editor. Few and far between: how HIV may be evading antibody avidity. PLoS Pathog 2010;6(5):e1000908 May 27.

[27] Hattori T, Lai D, Dementieva IS, Montaño SP, Kurosawa K, Zheng Y, et al. Antigen clasping by two antigen-binding sites of an exceptionally specific antibody for histone methylation. Proc Natl Acad Sci 2016;113(8):2092–7 Feb 23.

[28] Wallner J, Lhota G, Schosserer M, Vorauer-Uhl K. An approach for liposome immobilization using sterically stabilized micelles (SSMs) as a precursor for biolayer interferometry-based interaction studies. Colloids Surf B 2017;154:186–94 Jun.

[29] Katsamba PS, Navratilova I, Calderon-Cacia M, Fan L, Thornton K, Zhu M, et al. Kinetic analysis of a high-affinity antibody/antigen interaction performed by multiple biacore users. Anal Biochem 2006;352(2):208–21 May.

[30] Abdiche YN, Malashock DS, Pons J. Probing the binding mechanism and affinity of tanezumab, a recombinant humanized anti-NGF monoclonal antibody, using a repertoire of biosensors. Protein Sci 2008;17(8):1326–35 Aug.

[31] Irsara C., Egger A.E., Prokop W., Nairz M., Loacker L., Sahanic S., et al. Evaluation of four commercial, fully automated SARS-CoV-2 antibody tests suggests a revision of the Siemens SARS-CoV-2 IgG assay. Clin Chem Lab Med (CCLM) [Internet]. [cited 2021 Mar 11];0(0). Available from: https://www.degruyter.com/view/journals/cclm/ahead-of-print/article-10.1515-cclm-2020-1758/article-10.1515-cclm-2020-1758.xml

[32] Buderer NMF. Statistical methodology: I. Incorporating the prevalence of disease into the sample size calculation for sensitivity and specificity. Acad Emerg Med 1996;3(9):895–900 Sep.

[33] Statistik Austria, Medical University of Vienna. In the middle/end of October 2020, 4.7% of the Austrian population had antibodies to SARS-CoV-2. Extrapolation of Austria-wide COVID 19 prevalence study [Internet]. [cited 2021 Mar 11]. Available from: https://www.meduniwien.ac.at/web/en/ueber-uns/news/detailseite/2020/news-im-dezember-2020/47-der-oesterreichischen-bevoelkerung-hatten-mitte/ende-oktober-2020-antikoerper-gegen-sars-cov-2/

[34] Perkmann T, Perkmann-Nagele N, Breyer M-K, Breyer-Kohansal R, Burghuber OC, Hartl S, et al. Side-by-side comparison of three fully automated SARS-CoV-2 antibody assays with a focus on specificity. Clin Chem 2020;66(11):1405–13 Nov 1.

[35] Frey A, Di Canzio J, Zurakowski D. A statistically defined endpoint titer determination method for immunoassays. J Immunol Methods 1998;221(1−2):35–41 Dec.

[36] Breyer-Kohansal R, Hartl S, Burghuber OC, Urban M, Schrott A, Agusti A, et al. The LEAD (Lung, Heart, Social, Body) study: objectives, methodology, and external validity of the population-based cohort study. J Epidemiol 2019;29(8):315–24 Aug 5.

[37] Haslacher H, Gerner M, Hofer P, Jurkowitsch A, Hainfellner J, Kain R, et al. Usage data and scientific impact of the prospectively established fluid bioresources at the hospital-based MedUni Wien Biobank. Biopreserv Biobanking 2018;16(6):477–82 Dec.

[38] Hoffmann M, Kleine-Weber H, Schroeder S, Krüger N, Herrler T, Erichsen S, et al. SARS-CoV-2 cell entry depends on ACE2 and TMPRSS2 and is blocked by a clinically proven protease inhibitor. Cell 2020;181(2):271–80 Apre8.

[39] Laferl H., Kelani H., Seitz T., Holzer B., Zimpernik I., Steinrigl A., et al. An approach to lifting self-isolation for health care workers with prolonged shedding of SARS-CoV-2 RNA. Infection. 2020 Oct 6;

[40] Reed LJ, Muench H. A simple method of estimating fifty per cent endpoints12. Am J Epidemiol 1938;27(3):493–7 May.

[41] Beck JR, Shultz EK. The use of relative operating characteristic (ROC) curves in test performance evaluation. Arch Pathol Lab Med 1986;110(1):13–20 Jan.

[42] Pei H, Liu J, Cheng Y, Sun C, Wang C, Lu Y, et al. Expression of SARS-coronavirus nucleocapsid protein in Escherichia coli and Lactococcus lactis for serodiagnosis and mucosal vaccination. Appl Microbiol Biotechnol 2005;68(2):220–7 Aug.

[43] Welch NG, Scoble JA, Muir BW, Pigram PJ. Orientation and characterization of immobilized antibodies for improved immunoassays (Review). Biointerphases 2017;12(2):02D301. Jun.

[44] Elshal MF, McCoy JP. Multiplex bead array assays: performance evaluation and comparison of sensitivity to ELISA. Methods 2006;38(4):317–23 Apr.

[45] Tyson J, Tsai W-Y, Tsai J-J, Mässgård L, Stramer SL, Lehrer AT, et al. A high-throughput and multiplex microsphere immunoassay based on non-structural protein 1 can discriminate three flavivirus infections editor Gubler DJ, editor. A high-throughput and multiplex microsphere immunoassay based on non-structural protein 1 can discriminate three flavivirus infections. PLoS NeglTrop Dis 2019;13(8):e0007649 Aug 23.

[46] Perkmann T., Perkmann-Nagele N., Oszvar-Kozma M., Koller T., Breyer M.-.K., Breyer-Kohansal R., et al. Increasing both specificity and sensitivity of SARS-CoV-2 antibody tests by using an adaptive orthogonal testing approach [Internet]. [cited 2021 Mar 11]. Available from: http://medrxiv.org/lookup/ 10.1101/2020.11.05.20226449

[47] Yong SEF, Anderson DE, Wei WE, Pang J, Chia WN, Tan CW, et al. Connecting clusters of COVID-19: an epidemiological and serological investigation. Lancet Infect Dis 2020;20(7):809–15 Jul.

[48] Yue L, Cao H, Xie T, Long R, Li H, Yang T, et al. N-terminally truncated nucleocapsid protein of SARS-CoV-2 as a better serological marker than whole nucleocapsid protein in evaluating the immunogenicity of inactivated SARS-CoV-2. J Med Virol 2021;93(3):1732–8 Mar.

[49] Rump A, Risti R, Kristal M-L, Reut J, Syritski V, Lookene A, et al. Dual ELISA using SARS-CoV-2 nucleocapsid protein produced in E. coli and CHO cells reveals epitope masking by N-glycosylation. Biochem Biophys Res Commun 2021;534:457–60 Jan 1.

[50] Das D, Suresh MR. Copious production of SARS-CoV nucleocapsid protein employing codon optimized synthetic gene. J Virol Methods 2006;137(2):343–6 Nov.

[51] Pino P, Kint J, Kiseljak D, Agnolon V, Corradin G, Kajava AV, et al. Trimeric SARS-CoV-2 spike proteins produced from CHO cells in bioreactors are high-quality antigens. Processes 2020;8(12):1539. Nov 25.

[52] Rattanapisit K, Shanmugaraj B, Manopwisedjaroen S, Purwono PB, Siriwattananon K, Khorattanakulchai N, et al. Rapid production of SARS-CoV-2 receptor binding domain (RBD) and spike specific monoclonal antibody CR3022 in Nicotiana benthamiana. Sci Rep 2020;10(1) [Internet]Dec [cited 2021 Mar 11]Available from: http://www.nature.com/articles/s41598-020-74904-1.

[53] Sinegubova MV, Orlova NA, Kovnir SV, Dayanova LK, Vorobiev II. High-level expression of the monomeric SARS-CoV-2 S protein RBD 320-537 in stably transfected CHO cells by the EEF1A1-based plasmid vector editor Ho PL, editor. High-level expression of the monomeric SARS-CoV-2 S protein RBD 320-537 in stably transfected CHO cells by the EEF1A1-based plasmid vector. PLoS One 2021;16(2):e0242890 Feb 2.

[54] Palmberger D, Ashjaei K, Strell S, Hoffmann-Sommergruber K, Grabherr R. Minimizing fucosylation in insect cell-derived glycoproteins reduces binding to IgE antibodies from the sera of patients with allergy. Biotechnol J 2014;9(9):1206–14 Sep.

[55] Roy V, Fischinger S, Atyeo C, Slein M, Loos C, Balazs A, et al. SARS-CoV-2-specific ELISA development. J Immunol Methods 2020;484−485:112832 Sep.

[56] Alandijany TA, El-Kafrawy SA, Tolah AM, Sohrab SS, Faizo AA, Hassan AM, et al. Development and optimization of in-house ELISA for detection of human IgG antibody to SARS-CoV-2 full length spike protein. Pathogens 2020;9(10):803. Sep 28.

[57] Marklund E, Leach S, Axelsson H, Nyström K, Norder H, Bemark M, et al. Serum-IgG responses to SARS-CoV-2 after mild and severe COVID-19 infection and analysis of IgG non-responders editor Walsh SR, editor. Serum-IgG responses to SARS-CoV-2 after mild and severe COVID-19 infection and analysis of IgG non-responders. PLoS One 2020;15(10):e0241104 Oct 21.

[58] Kang EH, Ha Y-J, Lee YJ. Autoantibody biomarkers in rheumatic diseases. Int J Mol Sci 2020;21(4):1382. Feb 18.

[59] Wang Y, Sun S, Shen H, Jiang L, Zhang M, Xiao D, et al. Cross-reaction of SARS-CoV antigen with autoantibodies in autoimmune diseases. Cell Mol Immunol 2004;1(4):304–7 Aug.

[60] Long Q-X, Tang X-J, Shi Q-L, Li Q, Deng H-J, Yuan J, et al. Clinical and immunological assessment of asymptomatic SARS-CoV-2 infections. Nat Med 2020;26(8):1200–4 Aug.

[61] Bryan A, Pepper G, Wener MH, Fink SL, Morishima C, Chaudhary A, et al. Performance characteristics of the Abbott architect SARS-CoV-2 IgG assay and Seroprevalence in Boise, Idaho editor McAdam AJ, editor. Performance characteristics of the Abbott architect SARS-CoV-2 IgG assay and Seroprevalence in Boise, Idaho. J Clin Microbiol 2021;58(8).

[62] Harley K, Gunsolus IL. Comparison of the clinical performances of the Abbott alinity IgG, Abbott architect IgM, and Roche Elecsys total SARS-CoV-2 antibody assays editor Tang Y-W, editor. Comparison of the clinical performances of the Abbott alinity IgG, Abbott architect IgM, and Roche Elecsys total SARS-CoV-2 antibody assays. J Clin Microbiol 2020;59(1):e02104–20 Dec 17.

[63] Jääskeläinen A, Kuivanen S, Kekäläinen E, Ahava M, Loginov R, Kallio-Kokko H, et al. Performance of six SARS-CoV-2 immunoassays in comparison with microneutralisation. J Clin Virol 2020;129:104512 Aug.

[64] Rostami A, Sepidarkish M, Leeflang MMG, Riahi SM, Nourollahpour Shiadeh M, Esfandyari S, et al. SARS-CoV-2 seroprevalence worldwide: a systematic review and meta-analysis. Clin Microbiol Infect 2021;27(3):331–40 Mar.
[65] Pflüger LS, Bannasch JH, Brehm TT, Pfefferle S, Hoffmann A, Nörz D, et al. Clinical evaluation of five different automated SARS-CoV-2 serology assays in a cohort of hospitalized COVID-19 patients. J Clin Virol 2020;130:104549 Sep.
[66] Ripperger TJ, Uhrlaub JL, Watanabe M, Wong R, Castaneda Y, Pizzato HA, et al. Orthogonal SARS-CoV-2 serological assays enable surveillance of low-prevalence communities and reveal durable humoral immunity. Immunity 2020;53(5):925–33 Nove4.
[67] CDC Centers for Disease Control and Prevention. Interim guidelines for COVID-19 antibody testing in clinical and public health settings [Internet]. 2020 Jan [cited 2021 Mar 11]. Available from: https://www.cdc.gov/coronavirus/2019-ncov/lab/resources/antibody-tests-guidelines.html
[68] Woo PCY, Lau SKP, Wong BHL, Tsoi H -w, Fung AMY, Kao RYT, et al. Differential sensitivities of severe acute respiratory syndrome (SARS) coronavirus spike polypeptide enzyme-linked immunosorbent assay (ELISA) and SARS coronavirus nucleocapsid protein ELISA for serodiagnosis of SARS coronavirus pneumonia. J Clin Microbiol 2005;43(7):3054–8 Jul 1.
[69] Tan Y-J, Goh P-Y, Fielding BC, Shen S, Chou C-F, Fu J-L, et al. Profiles of antibody responses against severe acute respiratory syndrome coronavirus recombinant proteins and their potential use as diagnostic markers. Clin Diagn Lab Immunol 2004;11(2):362–71 Mar.
[70] Turbett SE, Anahtar M, Dighe AS, Garcia Beltran W, Miller T, Scott H, et al. Evaluation of three commercial SARS-CoV-2 serologic assays and their performance in two-test algorithms Editors Caliendo AM, editor. Evaluation of three commercial SARS-CoV-2 serologic assays and their performance in two-test algorithms. J Clin Microbiol 2020;59(1) Oct 5.
[71] Suthar MS, Zimmerman MG, Kauffman RC, Mantus G, Linderman SL, Hudson WH, et al. Rapid generation of neutralizing antibody responses in COVID-19 patients. Cell Rep Med 2020;1(3):100040 Jun.
[72] Wu F, Liu M, Wang A, Lu L, Wang Q, Gu C, et al. Evaluating the association of clinical characteristics with neutralizing antibody levels in patients who have recovered from mild COVID-19 in Shanghai, China. JAMA Intern Med 2020;180(10):1356. Oct 1.
[73] Sterlin D, Mathian A, Miyara M, Mohr A, Anna F, Claër L, et al. IgA dominates the early neutralizing antibody response to SARS-CoV-2. Sci Transl Med 2020;7:eabd2223. Dec.
[74] Liu STH, Lin H-M, Baine I, Wajnberg A, Gumprecht JP, Rahman F, et al. Convalescent plasma treatment of severe COVID-19: a propensity score–matched control study. Nat Med 2020;26(11):1708–13 Nov.
[75] Food and Drug Administration (FDA). Recommendations for investigational COVID-19 convalescent plasma [Internet]. 2020 [cited 2021 Mar 11]. Available from: https://www.fda.gov/vaccines-blood-biologics/investigational-new-drug-ind-or-device-exemption-ide-process-cber/recommendations-investigational-covid-19-convalescent-plasma#compliance
[76] Lee WT, Girardin RC, Dupuis AP, Kulas KE, Payne AF, Wong SJ, et al. Neutralizing antibody responses in COVID-19 convalescent sera. J Infect Dis 2021;223(1):47–55 Jan 4.

Supplementary Materials for

A comprehensive antigen production and characterisation study for easy-to-implement, highly specific and quantitative SARS-CoV-2 antibody assays

Miriam Klausberger, Mark Dürkop, Helmuth Haslacher, Gordana Wozniak-Knopp, Monika Cserjan-Puschmann, Thomas Perkmann, Nico Lingg, Patricia Pereira Aguilar, Elisabeth Laurent, Jelle De Vos, Manuela Hofer, Barbara Holzer, Maria Stadler, Gabriele Manhart, Klemens Vierlinger, Margot Egger, Lisa Milchram, Elisabeth Gludovacz, Nicolas Marx, Christoph Köppl, Christopher Tauer, Jürgen Beck, Daniel Maresch, Clemens Grünwald-Gruber, Florian Strobl, Peter Satzer, Gerhard Stadlmayr, Ulrike Vavra, Jasmin Huber, Markus Wahrmann, Farsad Eskandary, Marie-Kathrin Breyer, Daniela Sieghart, Peter Quehenberger, Gerda Leitner, Robert Strassl, Alexander E. Egger, Christian Irsara, Andrea Griesmacher, Gregor Hoermann, Günter Weiss, Rosa Bellmann-Weiler, Judith Loeffler-Ragg, Nicole Borth, Richard Strasser, Alois Jungbauer, Rainer Hahn, Jürgen Mairhofer, Boris Hartmann, Nikolaus B. Binder, Gerald Striedner, Lukas Mach, Andreas Weinhäusl, Benjamin Dieplinger, Florian Grebien*, Wilhelm Gerner and Christoph J. Binder* and Reingard Grabherr*

*Corresponding authors. Email: FG: florian.grebien@vetmeduni.ac.at
CJB: christoph.binder@medunivie.ac.at
RG: reingard.grabherr@boku.ac.at

The Supplementary File includes:

Fig. S1. **MS spectra of the two RBD glycosites a) SIVRFPNITNLCPFGE and b) VFNATRFASVYAWNRK.**
Fig. S2. **HP-SEC elution profiles of RBD produced in different expression systems.**
Fig. S3. **Biolayer-Interferometry analysis of SARS-CoV-2 antigens with specific antibodies.**
Fig. S4. **Purity of HEK-expressed tRBD is of utmost importance for sensitive anti-RBD IgG detection.**
Table S1. **Characteristics of SARS-CoV-2 positive samples used for test evaluation.**
Fig. S5. **ROC curve analysis of the Technozym NP and RBD ELISA in comparison with CE-marked automated Abbott and DiaSorin test systems.**
Table S2. **Time-resolved monitoring of SARS-CoV-2 NP- and tRBD-specific antibody levels and neutralization titres**
Fig. S6. **Specificity control testing with RBD variants derived from different expression systems.**

peptide: SIVRFPNITNLCPFGE
mass: 1863.9421
range: 1000-2000

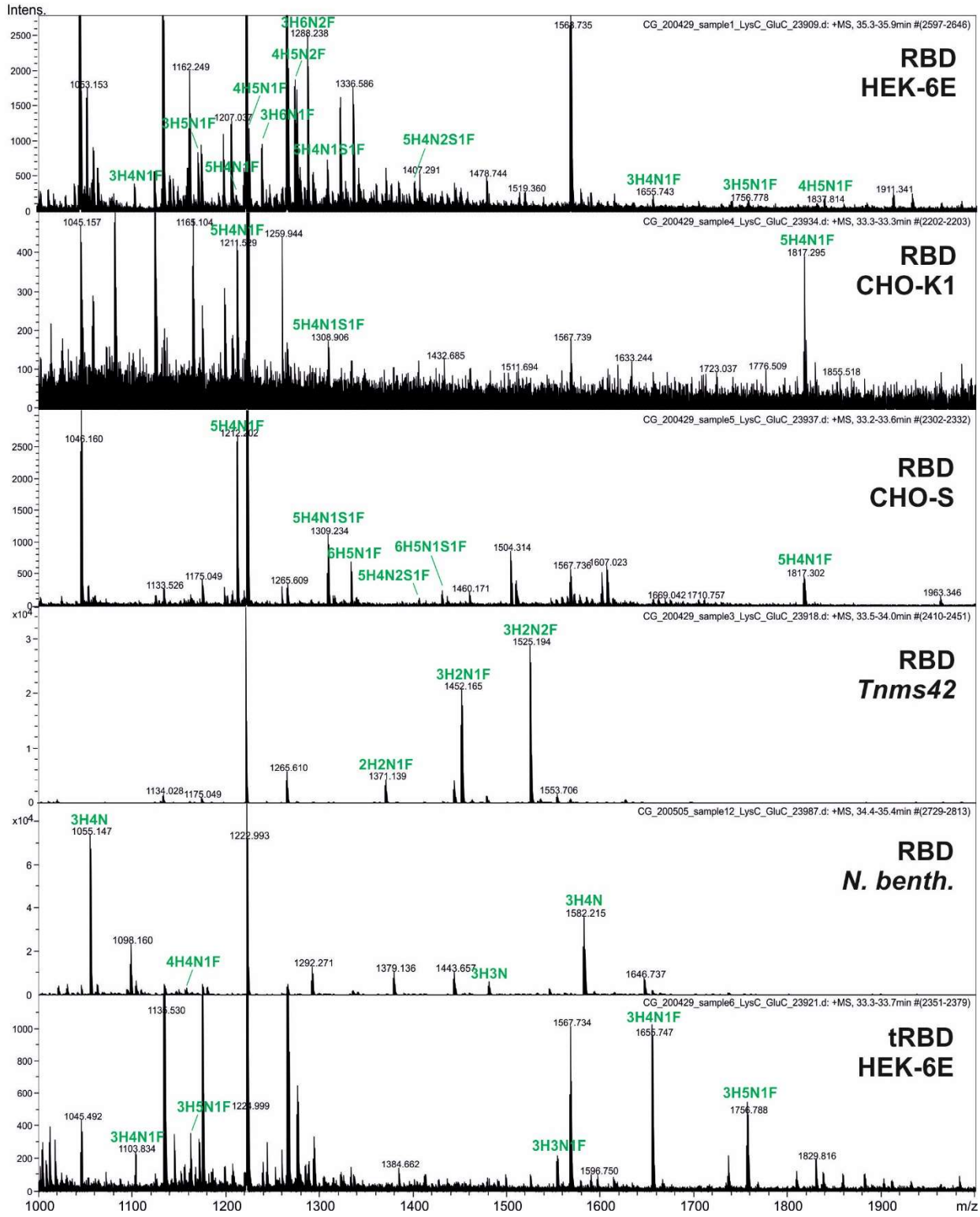

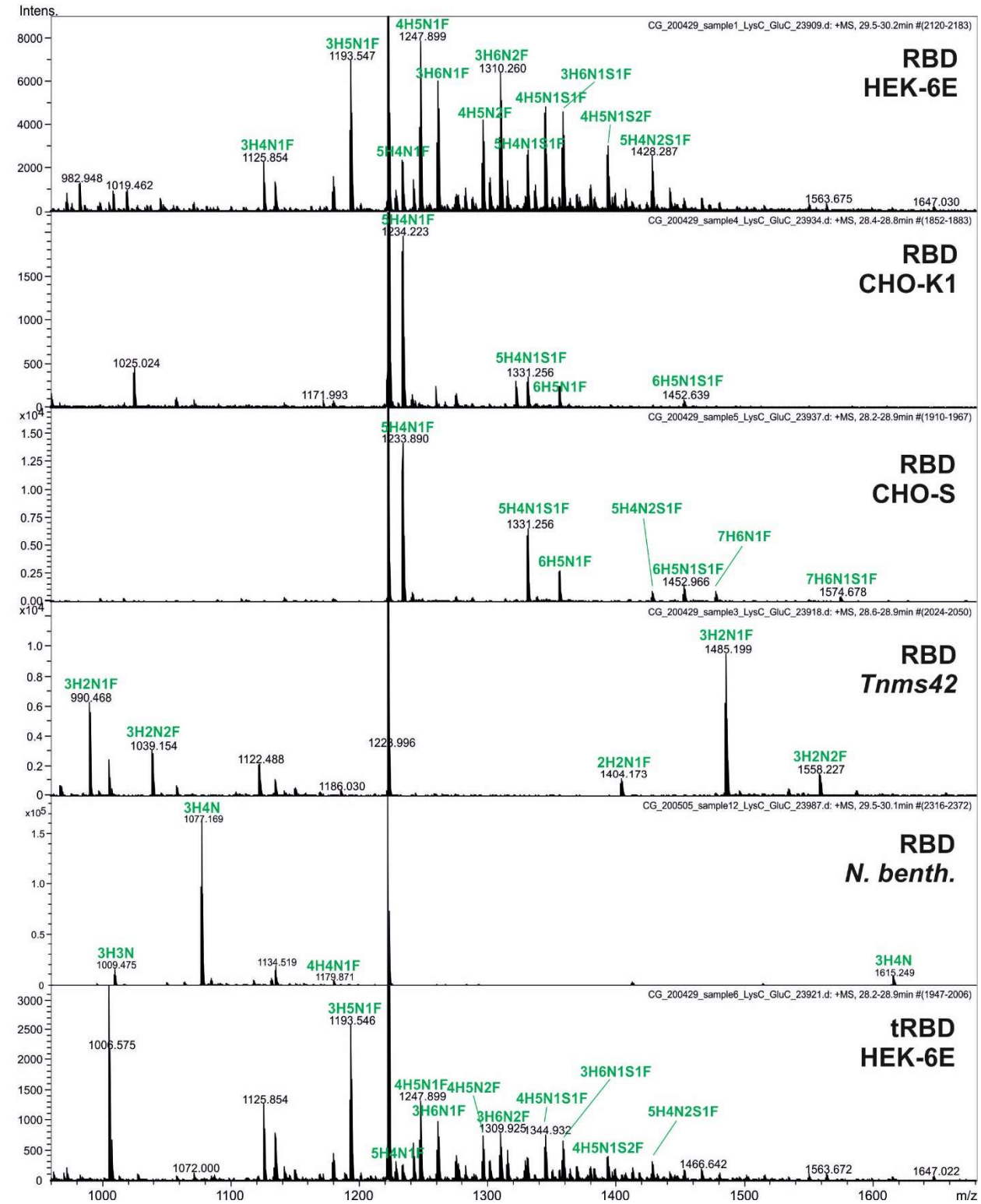

Fig. S1. MS spectra of the two RBD glycosites a) SIVRFPNITNLCPFGE and b) VFNATRFASVYAWNRK.

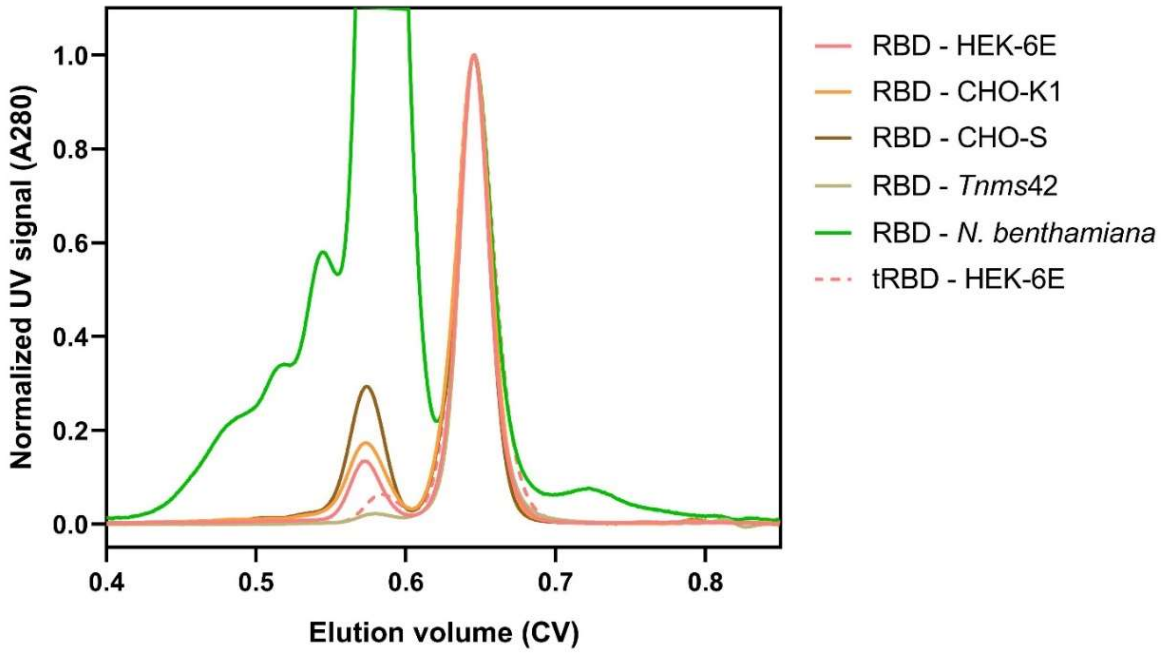

Fig. S2. HP-SEC elution profiles of RBD produced in different expression systems. Content of monomer was normalized in order to allow for dimer comparison. All proteins where purified with IMAC and AIEX, except for *Tnms*42 RBD which was purified with IMAC and preparative SEC resulting in dimer removal.

a

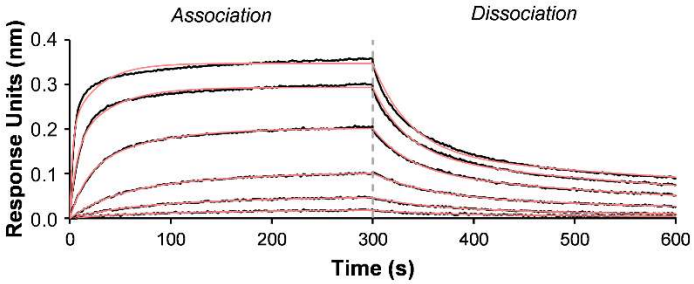

	K_D1 (nM)	K_D2 (nM)	k_a1 (M^{-1} s^{-1})	k_a2 (M^{-1} s^{-1})	k_d1 (s^{-1})	k_d2 (s^{-1})
Batch 1	25	8	1.1E+06	2.7E+05	2.7E-02	1.8E-03
SEM	1.4	0.7	5.8E+04	2.1E+04	5.3E-04	8.4E-05
Batch 2	28	8	9.2E+05	3.7E+05	2.5E-02	2.4E-03
SEM	1.6	0.9	3.1E+04	1.7E+04	6.6E-04	2.7E-04

b

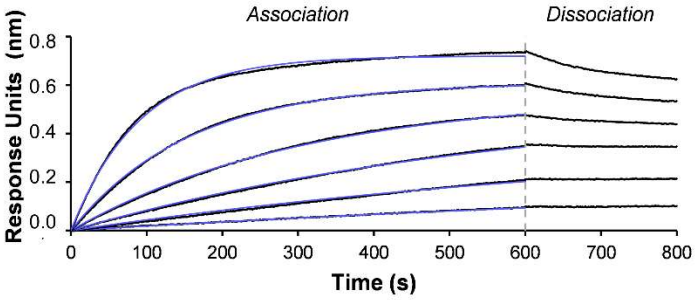

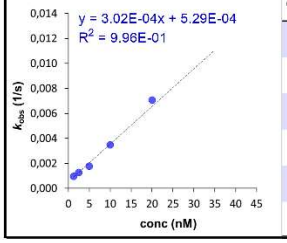

Conc. (nM)	k_{obs}(1/s)	SEM
1.25	5.1E-04	2.1E-04
2.5	6.5E-04	1.2E-04
5	1.5E-03	7.8E-05
10	3.4E-03	9.6E-05
20	6.9E-03	2.1E-04
40	1.2E-02	5.0E-04

Fig. S3. Biolayer-Interferometry analysis of SARS-CoV-2 antigens with specific antibodies. **a)** Binding kinetics of the interaction between biotinylated mAb CR3022 loaded on SAX biosensors and tRBD at a concentration range of 1.2 - 300 nM. Representative real-time association and dissociation curves are shown. The lower panel gives the mean kinetic parameters of a quadruplicate measurement from two independent tRBD production batches. **b)** Representative binding curves of the interaction of a biotinylated commercially available anti-NP mAb (ab272852, Abcam) and NP (1.25 – 40 nM). As kinetic parameters could not be calculated, a surrogate kinetic parameter, k_{obs}, is given as a mean of two duplicate measurements of two independently produced NP batches in the lower panel. Black lines represent the response curves of the association and dissociation. Fitted curves are shown as red and blue lines, respectively, dashed vertical lines indicate the transition between association and disassociation phases. K_D, equilibrium dissociation constant; k_a, association rate constant; k_d, dissociation rate constant, k_{obs}, observed binding rate constant, SEM, standard error of the mean, Conc., concentration

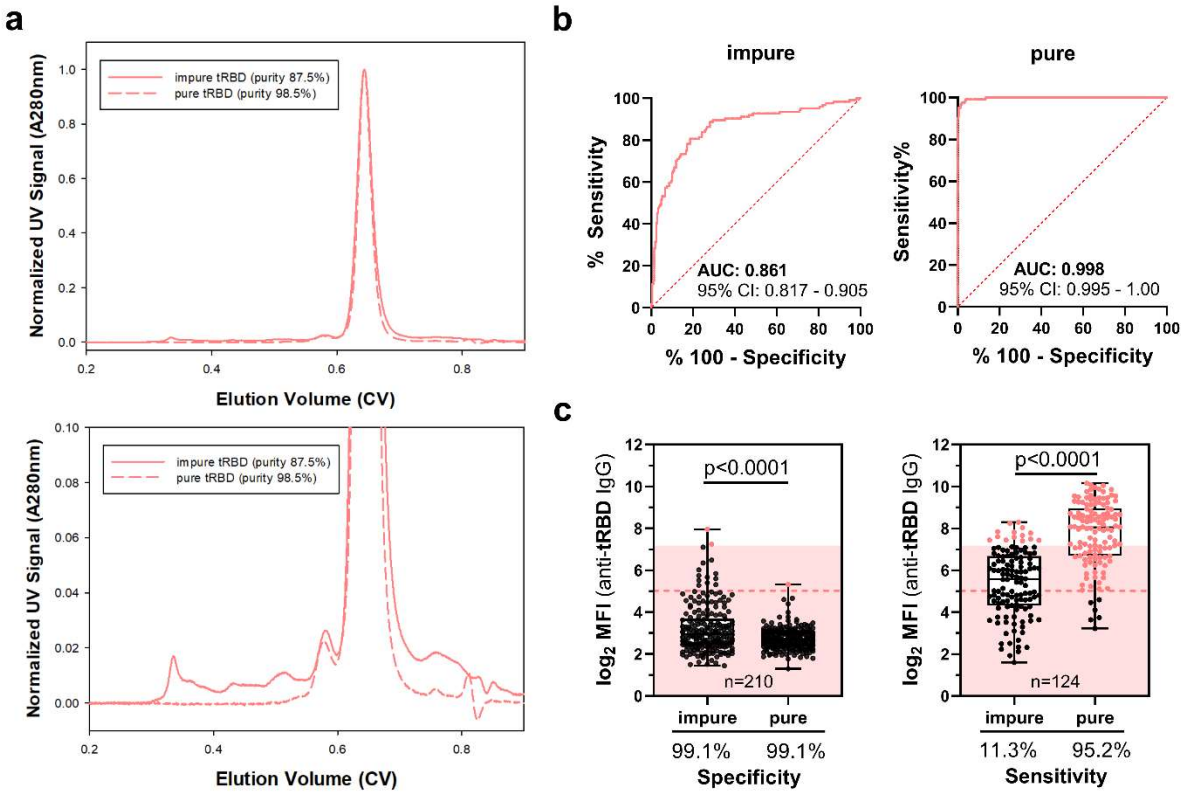

Fig. S4. Purity of HEK-expressed tRBD is of utmost importance for sensitive anti-RBD IgG detection. a) HP-SEC profiles of HEK-expressed tRBD that was either only IMAC-purified (impure, 87.5% purity) or was additionally polished using anion-exchange chromatography (pure, 98.5% purity).**b)** ROC curves with AUC-analysis for both proteins, also indicating the 95% confidence intervals. Seroreactivity with convalescent COVID-sera (n=124) and 210 pre-COVID sera was assessed by a Luminex assay. Pure tRBD gives the blank-corrected mean of three individual production batches, while data from impure tRBD are from a single batch. **c)** Seroreactivity of individual sera at a serum dilution of 1:1,200. Cut-offs were pre-defined to ensure a specificity of 99.1%. Shades indicate the cut-off for impure tRBD, dashed lines indicate the cut-off for pure tRBD (both calculated from the ROC curve). Pink circles among the pre-COVID sera indicate sera that are above the cut-off, while black circles among the COVID-sera indicate sera that fall below the cut-off. Group medians were compared by a Mann-Whitney test.

Table. S1. Characteristics of SARS-CoV-2 positive samples used for test evaluation. *symptom onset for symptomatic patients/donors from Vienna, first positive PCR for asymptomatic donors from Vienna and patients/donors from Innsbruck.

Collection site	**N**	**Age [y]**	**Female sex**	**Median days after PCR/ symptom onset***	**Severity**
Vienna	70	49 (37 – 56)	34 (49%)	43 (IQR 28 – 51)	asymptomatic=5 (7%) mild=29 (41%) moderate=18 (26%) severe=4 (6%) hospitalised=14 (20%)
Innsbruck	174	54 (39 – 62)	113 (65%)	54 (IQR 45 – 65)	outpatient=71 (41%) hospitalised, general ward= 75 (43%) Hospitalised, intensive care = 28 (16%)

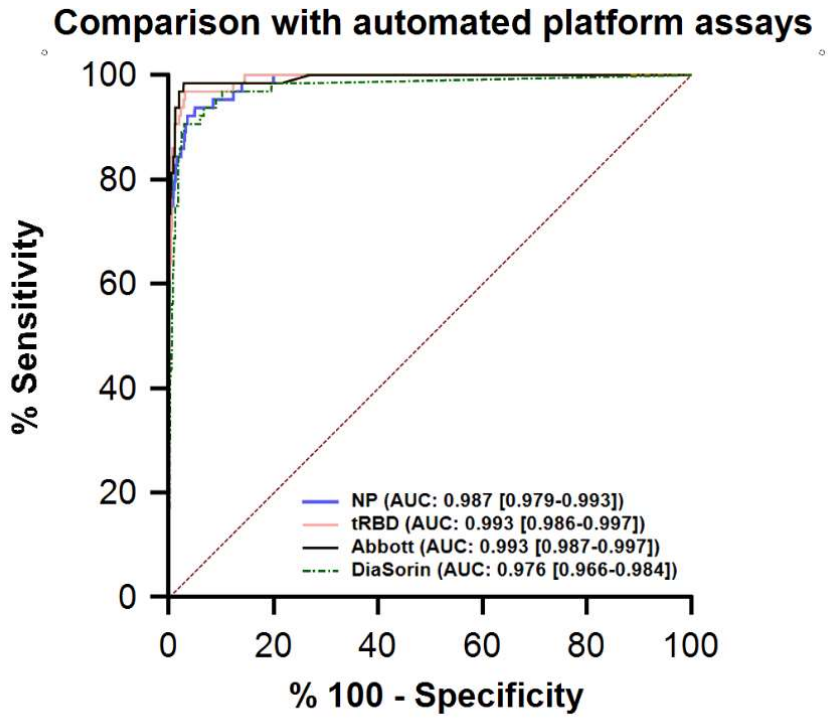

Fig. S5. **ROC curve analysis of the Technozym NP and RBD ELISA in comparison with CE-marked automated Abbott and DiaSorin test systems**. Test performance was validated with the MedUni Wien Biobank pre-COVID cohorts (N=1,117, excluding the described 8 hCoV samples) and COVID cohorts (N=64).

Table S2. **Time-resolved monitoring of SARS-CoV-2 NP- and tRBD-specific antibody levels and neutralization titres**. Titres for the SARS-CoV-2 NT assay, and Units/mL (U/mL) for the TC NP and RBD IgG ELISAs in 64 patients with SARS-CoV-2 RT-PCR confirmed COVID-19 with serial blood samples (n=104) collected at different time points from symptom onset. For descriptive statistics and statistical analyses, a neutralization titre below 1:4 was assigned a value of 1:2 and a titre above 1:512 was assigned 1:1,024. Likewise, RBD and NP ELISA titres of 0 U/mL were assigned a value of 0.1 U/mL.

Symptom onset (days)	**n (%)**	**NT assay (titre)**	**TC NP IgG (U/mL)** n negative (%) n positive (%)	**TC RBD IgG (U/mL)** n negative (%) n positive (%)
1-5 (days)	**34 (100%)**		**29 neg. (85.3%)**	**32 neg. (94.1)**
median		N/A	0.6	0.3
range		N/A	(0.0-3.5)	(0.0-3.9)
IQR		N/A	(0.2-1.3)	(0.1-0.6)
			5 pos. (14.7%)	**2 pos. (5.9%)**
median		1:16	21.3	8.8
range		(<1:4-1:128)	(5.5-76.0)	(7.7-9.9)
IQR		(1:5-1:48)	(6.6-59.5)	N/A
6-10 (days)	**35 (100%)**		**19 neg. (54.3%)**	**23 neg. (65.7%)**
median		N/A	0.6	0.4
range		N/A	(0.0-3.7)	(0.0-2.7)
IQR		N/A	(0.2-1.3)	(0.2-1.0)
			16 pos. (45.7%)	**12 pos. (34.2%)**
median		1:48	32.0	17.6
range		(1:4->1:512)	(6.0-166)	(5.0-121.0)
IQR		(1:32-1:172)	(10.7-95.8)	(7.6-50.0)
11-15 (days)	**17 (100%)**		**4 neg. (23.5%)**	**6 neg. (35.3%)**
median		N/A	0.0	0.1
range		N/A	(0.0-0.1)	(0.0-3.3)
IQR		N/A	(0.0-0.1)	(0.0-2.2)
			13 pos. (76.5%)	**11 pos. (64.7%)**
median		1:192	78.6	133.8
range		(<1:4->1:512)	(24.6-1732.4)	(5.2-328.8)
IQR		(1:48-1:1,024)	(51.0-126.4)	(98.3-206.4)
16-22 (days)	**18 (100%)**		**0 neg. (0%)**	**0 neg. (0%)**
median		N/A	N/A	N/A
range		N/A	N/A	N/A
IQR		N/A	N/A	N/A
			18 pos. (100%)	**18 pos. (100%)**
median		1:320	202.6	146.6
range		(1:32->1:512)	(30.9-4064.0)	(5.1-447.6)
IQR		(1:128-1:1,024)	(109.0-933.8)	(61.3-217.5)

[a] NT assay: negative (titer <1:4); positive (titer ≥1:4)

[b]TC NP IgG ELISA: negative (<5.000 U/mL); positive (≥5.000 U/mL)

[c]TC RBD IgG ELISA: negative (<5.000 U/mL); positive (≥5.000 U/mL)

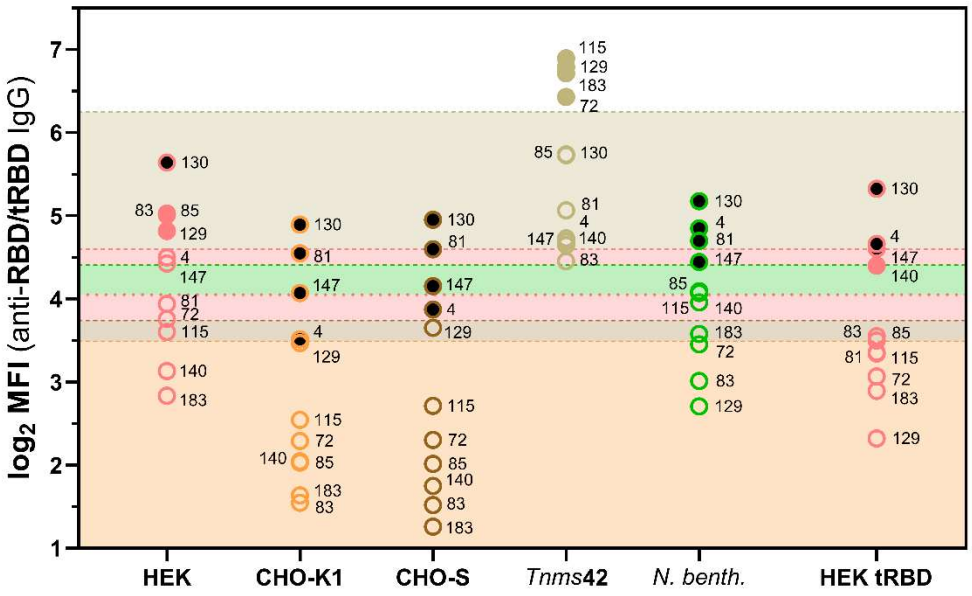

Fig. S6. Specificity control testing with RBD variants derived from different expression systems. Sera (serum dilution: 1:1,200) were from a pre-COVID cohort (n=210) and were identified as false-negative using the Luminex platform with a pre-specified specificity of 99.1%. Numbers represent the identification codes of the respective sera. Shades and dashed lines indicate the respective cut-offs color-coded according to the different expression systems. Open circles indicate sera that fall below the cut-off. Full circles indicate outlier sera that fall above the cut-off and are considered as false-positive; black-filled circles indicate sera that are identified as false-positive with antigens from at least three expression platforms.

Publication VII

Research Article

Received: 21 June 2021 Revised: 22 August 2021 Accepted article published: 28 August 2021 Published online in Wiley Online Library: 19 September 2021

(wileyonlinelibrary.com) DOI 10.1002/jctb.6895

Stable Sf9 cell pools as a system for rapid HIV-1 virus-like particle production

Eduard Puente-Massaguer,[a*†] Paula Grau-Garcia,[a] Florian Strobl,[b,c] Reingard Grabherr,[c] Gerald Striedner,[c] Martí Lecina[d] and Francesc Gòdia[a]

Abstract

BACKGROUND: The emergence of infectious diseases is accelerating the intensification of bioprocess strategies to support the increasing demand for the manufacture of higher quantities of vaccines in short timeframes. Here, the development of stable Sf9 cell pools producing human immunodeficiency virus serotype 1 (HIV-1) Gag-eGFP virus-like particles (VLPs) is assessed.

RESULTS: Fluorescence-activated cell sorting (FACS) was employed to select high producing cells, achieving an 8.1-fold increase in fluorescence intensity compared to unsorted cell pools after three rounds of cell sorting. The transferability of this system to bioreactor scale was also successfully achieved, attaining a 1.4-fold increase in VLP production and maintaining a higher cell viability than shake flask controls. Analysis of the metabolism of stable cell pools and parental Sf9 cells did not show significant differences regarding metabolite consumption and production, even though a better performance and more efficient metabolism were observed in bioreactor compared with shake flask cultures, highlighting the flexibility of these cells to adapt to different culture conditions and heterologous recombinant protein production.

CONCLUSIONS: Stable Sf9 cell pools represent a suitable system for shortening bioprocess development times and accelerating vaccine production.

Supporting information may be found in the online version of this article.

Keywords: stable Sf9 cell pools; virus-like particle (VLP); fluorescence-activated cell sorting (FACS); DASGIP Parallel Bioreactor System; metabolism

ABBREVIATIONS

BEVS	baculovirus expression vector system
CQA	critical quality attributes
eGFP	enhanced green fluorescent protein
EV	extracellular vesicle
FACS	fluorescence-activated cell sorting
FBS	foetal bovine serum
GOI	gene of interest
HIV-1	human immunodeficiency virus serotype 1
hpt	hours post-transfection
R.F.U.	relative fluorescence units
SGE	stable gene expression
TGE	transient gene expression
VLP	virus-like particle

INTRODUCTION

Virus-like particles (VLPs) are a new generation of vaccines formed by the highly ordered repetitive assembly of viral proteins that resemble the natural virus configuration.[1] This property renders them immunogenic since they retain comparable cell uptake mechanisms and trigger immune processing pathways in a similar way to native viruses.[2] Despite the fact that VLPs can incorporate random nucleic acids,[3] they are not infective as well as replication-incompetent, which makes them safer in comparison with classical live-attenuated and inactivated vaccines.[4] Human immunodeficiency virus serotype 1 (HIV-1) VLPs are a class of enveloped VLPs formed by the multimerization of the Gag polyprotein via the C-terminal domain,[5] a phenomenon that takes place in the inner plasma membrane of the host cell. After a certain number of monomers are recruited, they are able to leave the cell through a budding process forming the

* *Correspondence to: Eduard Puente-Massaguer, Department of Chemical, Biological and Environmental Engineering, Universitat Autònoma de Barcelona, Barcelona, Spain. E-mail: eduard.puente-massaguer@mssm.edu*

† *Present address: Department of Microbiology, Icahn School of Medicine at Mount Sinai, New York, USA*

a *Department of Chemical, Biological and Environmental Engineering, Universitat Autònoma de Barcelona, Barcelona, Spain*

b *Austrian Centre of Industrial Biotechnology (acib GmbH), Vienna, Austria*

c *Department of Biotechnology, University of Natural Resources and Life Sciences, Vienna, Austria*

d *IQS School of Engineering, Universitat Ramón Llull, Barcelona, Spain*

enveloped VLPs.[6] The properties of Gag VLPs make them an interesting platform for multiple applications.[7] Their use goes beyond the HIV field since the robust structure is an attractive scaffold for multivalent vaccines.[8]

Stable cell pools are emerging as an efficient system for the production of recombinant products in a short period of time. The initial purpose of stable cell pools is centred on the production of sufficient amounts of representative material to screen different recombinant products in the early phases of preclinical development.[9] Using this strategy, issues related with transient gene expression (TGE) approaches can be mitigated, including the need to produce large amounts of plasmid DNA and production in large-scale volumes.[10] Advances in the methodology of developing stable gene expression (SGE) systems, for instance the incorporation of fluorescence-activated cell sorting (FACS) to select high producing cells possibly displaying a favourable genomic environment for the expression of the gene of interest (GOI),[11] have substantially improved production titers achieved by stable cell pools to the levels offered by clonal cell lines.[12,13] In comparison to conventional SGE strategies, stable cell pools eliminate the need for single cell cloning and screening, which represent two of the most time-consuming steps in cell line development. Furthermore, it is not necessary to add a fluorescent reporter tag to the GOI during cell sorting since specific staining methods that correlate with cell productivity have been proposed recently.[14]

Cell heterogeneity is viewed as the main drawback of stable cell pools since they are formed by different cells with varied cell growth rates and recombinant production titers.[15] Nevertheless, recent studies indicate that cell-to-cell heterogeneity can also be encountered after several generations in clonally derived cell lines, as it occurs in production processes, and that stable cell pools are able to produce recombinant products matching similar critical quality attributes (CQA).[16] So far, most of the work with stable cell pools has been conducted in mammalian cells. However, insect cell lines have a higher biosafety profile due to the absence of known human pathogens,[17] and offer a highly suitable environment for the production of complex nanoparticles such as VLPs.[18] Indeed, there is growing interest in the production of VLPs in insect cells by means of SGE to overcome some of the limitations associated with the baculovirus expression vector system (BEVS), but development timelines are generally long.

In this study, the use of stable Sf9 cell pools was assessed as a system for the rapid production of HIV-1 Gag VLPs. The *gag* gene was fused in-frame to the enhanced green fluorescent protein (*eGFP*) gene with the aim to facilitate the detection of Gag expressing cells, and for VLP quantification. Cell sorting was applied to select high-producing cells with the GOI stably integrated. Initially, the production of the simple mCherry protein was evaluated and the workflow developed was employed for the generation of VLPs. As a proof-of-concept, the transferability of the system was appraised in a bioreactor for the production of Gag-eGFP VLPs, and the metabolism of stable cell pools and parental cells in distinct culture strategies was analyzed to detect differences between conditions.

MATERIALS AND METHODS

Cell line

Sf9 cells (cat. no. 71104, Merck, Darmstadt, Germany) were cultured in 20 mL of serum-free Sf900III medium (Thermo Fisher Scientific, Grand Island, NY, USA) and maintained in the exponential phase by cell passaging at 0.4–0.6 × 10^6 cell mL^{-1} in polycarbonate Erlenmeyer flasks (Corning, Steuben, NY, USA) every 2–3 days.[19] Cells were maintained in suspension conditions by agitation at 130 rpm in a Stuart SSL1 orbital shaker (Stuart, Stone, UK) placed in HERAcell 150 incubator at 27 °C (Thermo Fisher Scientific).

Cell count and viability were routinely performed in the automatic cell counters Nucleocounter NC-3000 (Chemometec, Allerød, Denmark) and LUNA-II (Logos biosystems, Anyang-si, South Korea) according to the manufacturer's instructions.

DNA plasmid constructs

The pIZTV5-mCherry plasmid encoding the intracellular mCherry fluorescent reporter protein was generated by PCR cloning of the *mCherry* gene in the pPEU3 plasmid developed as described elsewhere.[20] The following pair of primers was used: forward 5′-CGTAAAGCTTATTTACAATCAAAGGAGATATACCA-3′ and reverse 5′-CGTAGCGGCCGCCTACTTGTACAGCTCGTCCATGC-3′, and the PCR-amplified mCherry insert was ligated into the pIZTV5 vector (Thermo Fisher Scientific) by previous digestion with *Hin*dIII and *Not*I, resulting in the pIZTV5-mCherry plasmid. The pIZTV5-Gag-eGFP plasmid was obtained by digestion of the plasmid construct containing the *eGFP* gene fused in frame to the C-terminal domain of the *gag* gene (cat no. 11468, NIH AIDS Reagent Program), as described previously.[21] The *mCherry* and *gag-eGFP* genes were under the control of the *Op*IE2 (*Orgia pseudotsugata* immediate-early 2) promoter in the pIZTV5 plasmid, with the *bleomycin* gene that confers resistance to zeocin under the control of the *Op*IE1 promoter (Fig. 1).

Transfection and stable cell pool generation

Introduction of the plasmids encoding mCherry and Gag-eGFP into Sf9 cells was conducted as described previously.[22] First 1.0 μg of circular pIZTV5-mCherry or pIZTV5-Gag-eGFP DNA plasmid per 10^{-6} cell, and 2.0 μg of PEI per 10^{-6} cell were added sequentially to ultrapure water in a final volume of 0.8 mL, vortexed for 3 s three times and added to 8 mL of cells at 17.6 × 10^6 cell mL^{-1}. After 1 h incubation, cells were diluted to 4.0 × 10^6 cell mL^{-1}. Zeocin (InvivoGen, San Diego, CA, USA) was used to select cells that had incorporated the GOI, and was added to the culture at a concentration of 300 μg mL^{-1} after 3 days post-transfection [Fig. 2(A)]. Sf9 cells were kept in the exponential phase by cell passaging at 0.5 × 10^6 cell mL^{-1} during zeocin selection, which was maintained until the cell viability of the culture was recovered completely.

Three rounds of FACS were performed to enrich stable cell pools with high producer cells when cell viability was restored. Cells were sorted in suspension conditions using a BD FACSJazz cell sorter (BD Biosciences, San Jose, CA, USA) at a constant pressure of 27 psi and a sorting rate in the range of 700 to 1400 cell s^{-1}. Before FACS, cells were grown to 3 × 10^6 cell mL^{-1} and Pluronic F-68 and antibiotic-antimycotic (Thermo Fisher Scientific) were added at a final concentration of 1% v/v and 1×, respectively. For each stable cell pool, 2 × 10^6 cells were collected in fresh Sf900III medium containing 2% v/v foetal bovine serum (FBS; Sigma Aldrich, St Louis, MO, USA) and 1× antibiotic-antimycotic solution. The 30% most fluorescent cells of the stable cell pool were selected in the different rounds of sorting. After FACS, cells were centrifuged at 300×*g* for 5 min and resuspended at a final concentration of 1 × 10^6 cell mL^{-1} in fresh Sf900III medium with 5% v/v FBS and 1× antibiotic-antimycotic solution. Sorted cell pools were grown in six-well plates (Nunc, Thermo Fisher Scientific) maintained in the incubator at 150 rpm and, when the viable cell density increased (~4 × 10^6 cell mL^{-1}), transferred to a 125-mL Erlenmeyer flask with 8 mL serum-free Sf900III medium

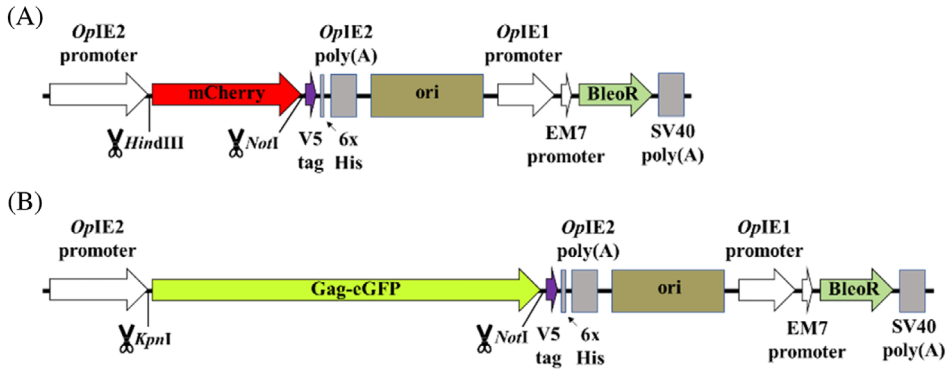

Figure 1. The pIZTV5-mCherry (3351 bp, A) and pIZTV5-Gag-eGFP (4873 bp, B) insect cell expression plasmids. mCherry and Gag-eGFP expression is under the control of the *Orgia pseudotsugata* immediate-early 2 (*Op*IE2) promoter. *Sh ble* expression (BleoR) confers resistance to zeocin and its production is driven by the *Op*IE1 promoter in insect cells and by the EM7 promoter in *E. coli*. Poly(A), polyadenylation sequence; ori, pUC origin of replication; V5 tag, epitope tag from simian virus 5; 6×His, polyhistidine tag. (✂) Restriction enzymes employed to clone the GOI into the pIZTV5 vector.

at a concentration of 0.5×10^6 cell mL^{-1}. One week was required between FACS rounds for cell amplification from six-well plate to shake flask. Zeocin was removed from cell culture after the FACS rounds were completed.

Flow cytometry

The percentage of mCherry and Gag-eGFP positive cells was analyzed in a BD FACS Canto II flow cytometer (BD Biosciences) equipped with blue and red lasers. First, 0.3 mL of cells were collected by centrifugation at 300×*g* for 5 min and fixed using 4% v/v *p*-formaldehyde. After 10 min, *p*-formaldehyde was removed by centrifugation at 500×*g* for 5 min and cells were resuspended in fresh Dulbecco's phosphate-buffered saline solution (DPBS, Thermo Fisher Scientific) and kept at 4 °C until analysis. 2×10^4 cells were analysed for each sample at a rate of 60 μL min^{-1}. Side (SSC-H) *versus* forward scatter (FSC-A) dot plots, and PerCP-Cy5-5-A (mCherry) or GFP FITC-A (Gag-eGFP) histograms were used to gate the individual cell populations and assess the percentage of fluorescent cells, respectively. A negative control consisting of parental Sf9 cells was included as a reference. All analyses were performed with the BD FACSDIVA software (BD Biosciences).

Confocal fluorescence microscopy

Stable cell pools were observed under a TCS SP5 confocal microscope (Leica, Wetzlar, Germany) to detect the expression of mCherry (red) and Gag-eGFP (green). Cell nuclei were stained with 0.1% v/v Hoechst and cell plasma membrane with 0.1% v/v CellMask (Thermo Fisher Scientific). After staining, cells were carefully centrifuged at 300×*g* for 5 min to remove dye excess and resuspended in fresh DPBS. For visualization, samples were placed in 14-mm microwell Petri dishes (MatTek Corporation, Ashland, MA, USA). Confocal microscopy images were obtained and processed with the LAS X software (Leica).

DASGIP Parallel Bioreactor System

A four-unit 2-L glass bioreactor system (DASGIP Parallel Bioreactor System, Eppendorf, Hamburg, Germany) was used to culture the Gag-eGFP stable cell pool and parental Sf9 cells simultaneously. In each case, 0.5 L exponentially growing cells were inoculated at $\sim 1 \times 10^6$ cell mL^{-1}, and the temperature was held at 27 °C throughout the experiment. A cascade control was defined in the DASware software (Eppendorf) to maintain the dissolved oxygen (DO) setpoint at 30% air saturation with 1 L h^{-1} air flow rate, and an initial stirring speed of 150 rpm without upper speed limit. The pH setpoint was fixed at 6.2 and maintained in these conditions by the addition of 20% w/w phosphoric acid (H_3PO_4) and 7.5% w/w sodium bicarbonate ($NaHCO_3$) base.

Metabolite analysis

Metabolite concentrations were analyzed by high-performance liquid chromatography (HPLC). Glucose, maltose, lactate and phosphate concentrations were assessed with an Aminex HPX-87H ion exclusion liquid chromatography (Bio-Rad, Hercules, CA, USA) in an Agilent 1200 series HPLC system (Agilent, Santa Clara, CA, USA). Maltose and sucrose could not be fully separated using this strategy but maltose consumption was only considered since sucrose is not metabolized at detectable concentrations in uninfected Sf9 cells.[23] Phosphate consumption was calculated taking into consideration the quantity of remaining phosphate available in the medium and compared to the amount of H_3PO_4 added previously. The concentration of amino acids was measured in a reversed-phase Eclipse Plus C18 column (Agilent Technologies) by a post-column derivatization method according to manufacturer's instructions, and detected at 266/305 and 450 nm.

Correlation of the consumption and production of the main metabolites was performed by linear regression of the calculated metabolic fluxes with the coefficient of determination R^2. All regression analyses were conducted with Excel 2016 (Microsoft, Redmond, WA, USA).

Spectrofluorometry

The concentrations of mCherry and Gag-eGFP produced intracellularly and in the supernatant were assessed in a Cary Eclipse spectrophotometer (Agilent Technologies). Intracellular mCherry and Gag-eGFP fluorescence intensities were analyzed by disrupting cell pellets with three freeze–thaw cycles (2.5 h at −20 °C and 0.5 h at 37 °C), vortexed for 5 s three times between cycles, and resuspended in tris/magnesium/saline (TMS) buffer.[24] mCherry fluorescence intensities were measured with a $\lambda_{ex} = 587$ nm (slit = 5), $\lambda_{em} = 600$–630 nm (slit = 10), whereas for Gag-eGFP the equipment settings were adjusted to $\lambda_{ex} = 488$ nm (slit = 5), $\lambda_{em} = 500$–530 nm (slit = 10). For the calculation of mCherry protein concentration, a standard curve based on the linear correlation between known mCherry concentrations (BioVision, Milpitas, CA, USA) and their corresponding fluorescence values in relative fluorescence units (R.F.U.) was established:

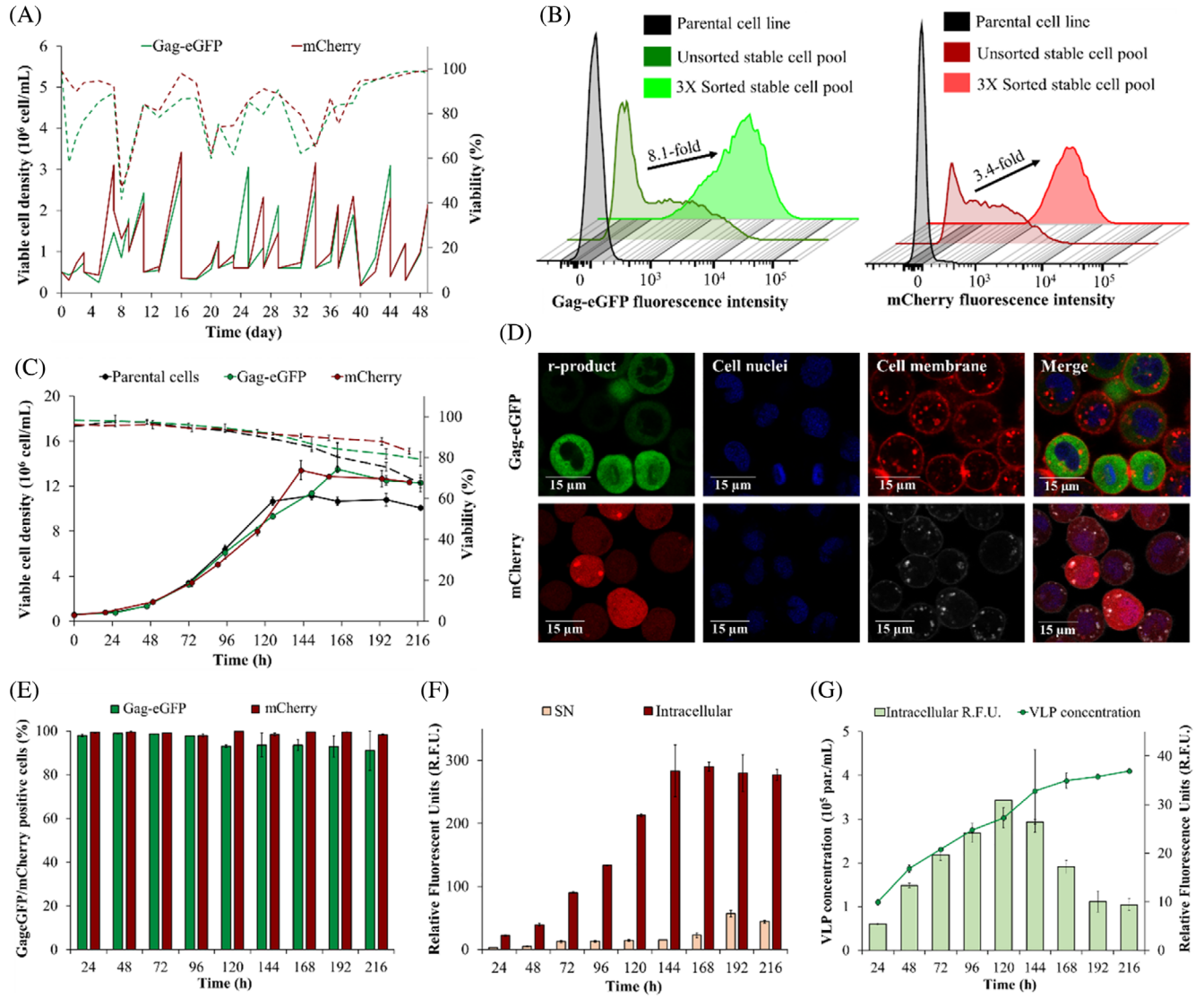

Figure 2. Development of mCherry and Gag-eGFP stable cell pools, sorting of high producer cells and evaluation at shake flask level. (A) Viable cell density (straight line) and viability (dashed line) during the process of developing the stable cell pools after transfection. Zeocin was added at day 3 post-transfection. (B) Average fluorescence intensity of parental cells (black), unsorted stable cell pools (dark) and enriched stable cell pools by three rounds of FACS (light). (C) Viable cell density (straight line) and viability (dashed line) of cultured parental cells, mCherry and Gag-eGFP stable cell pools in Erlenmeyer shake flasks. Sf9 cells were seeded at 0.5×10^6 cell mL^{-1} in 20 mL Sf900III medium. (D) Confocal fluorescence microscopy images of mCherry (red) and Gag-eGFP (green) stable cell pools with cell nuclei (blue) stained with Hoechst and plasma membranes (red or grey) with CellMask. (E) Percentage of Gag-eGFP and mCherry positive cells in stable cell pools cultured in shake flasks. (F) Intracellular mCherry production and in the supernatant (SN) during the shake flask experiment. (G) VLP and intracellular Gag-eGFP production.

$$\text{mCherry}\left(\text{mgL}^{-1}\right) = (\text{R.F.U} - 55.008)/9.0401 \qquad (1)$$

R.F.U. were assessed by subtracting the fluorescence intensities of parental cells from those of stable cell pools. A 0.1 mg mL^{-1} quinine sulphate solution was used as an internal control to normalize fluorescence yields between experiments.

Enzyme-linked immunosorbent assay (ELISA)

Gag-eGFP production was quantified using an HIV-1 p24 ELISA (Sino Biological, Wayne, NJ, USA). The Gag-eGFP present in the supernatant was obtained by cell culture centrifugation at 3000×*g* for 5 min and Gag-eGFP quantification was conducted as described previously.[22] An HIV-1 p24 standard of known concentration was included to measure Gag-eGFP concentrations (cat. no. ab9071; Abcam, Cambridge, UK). p24 concentrations were converted to Gag-eGFP concentration according to the Gag-eGFP molecular weight (87.7 kDa).

Flow virometry

Gag-eGFP VLPs and total nanoparticles were measured in a CytoFlex LX (Beckman Coulter, Brea, CA, USA) equipped with a 488 nm blue laser and a 405 nm violet laser.[25] A 1:50 sample dilution in 0.22 µm-filtered DPBS was performed to adjust the nanoparticle concentration before injection, and 3×10^5 events were acquired for each sample with an abort rate of ~1% and a sampling speed of 10 µL min^{-1}. Assessment of the sampling volume required to calculate VLP and total nanoparticle concentrations was measured with the weight volume tool of the CytExpert v2.3 software (Beckman Coulter).

RESULTS

Development and enrichment of stable cell pools

Sf9 cells were transfected with the pIZTV5-mCherry and pIZTV5-Gag-eGFP plasmids [Fig. 1(A),(B)] to produce the intracellular mCherry fluorescent protein and the Gag-eGFP polyprotein, respectively, the latter being responsible for HIV-1 VLP formation. After 72 h post-transfection (hpt), zeocin was added at 300 μg mL^{-1} to the cell culture to select cells stably expressing the GOI. The zeocin concentration employed was selected based on preliminary experiments with Sf9 cells and varying concentrations of this antibiotic (Appendix S1, Fig. S1). Cell viability increased ≤90% in both cell pools after 40 days of culture, and completely recovered after 50 days, when cell pools were considered stable [Fig. 2(A)]. No remarkable differences were observed during the generation of the stable cell pools, but the percentage of stably expressing cells differed for Gag-eGFP (53.1%) and mCherry stable cell pools (74.1%) at the end of the process.

After stable cell pool generation, FACS was applied to remove nonproducing cells and enrich the stable cell pools with high producing cells [Fig. 2(B)]. After three rounds of cell sorting, 3.4- and 8.1-fold increases in the average fluorescence intensity of sorted *versus* unsorted mCherry and Gag-eGFP (respectively) stable cell pools were achieved. In these conditions, the 4.9% and 7.8% of most fluorescent cells from the initial Gag-eGFP and mCherry unsorted stable pools, respectively, comprised the new sorted stable pools.

Assessment of stable cell pools to produce different recombinant proteins

An initial small-scale evaluation of stable cell pools in shake flasks was performed before assessing their performance in a stirred tank bioreactor [Fig. 2(C)]. Stable mCherry and Gag-eGFP production did not affect the maximum cell density attained by the stable cell pools in comparison to parental Sf9 cells. Both stable cell pools peaked between 144 h (mCherry, $13.4 \pm 0.8 \times 10^6$ cell mL^{-1}) and 168 h (Gag-eGFP, $13.5 \pm 0.3 \times 10^6$ cell mL^{-1}), whereas parental cells did so at 120 h ($11.1 \pm 0.4 \times 10^6$ cell mL^{-1}). In addition, no differences were observed in the doubling times of the Gag-eGFP stable cell pool and parental cells in the exponential phase, but there was an increase for the mCherry stable pool (Table 1). Confocal fluorescence microscopy analysis confirmed the expression of Gag-eGFP (green) and mCherry (red), and the percentage of fluorescent cells was maintained for up to 96 h in both cases [Fig. 2(D),(E)]. A decline in the number of fluorescent cells was observed afterwards for the Gag-eGFP stable cell pool in parallel with a decrease in cell viability.

Intracellular mCherry production increased up to 144 h (283.4 ± 41.0 R.F.U.), corresponding to a concentration of 37.4 ± 4.5 mg L^{-1}. mCherry was also detected in the supernatant at the end of the production phase, possibly related to protein release by dead cells. For the Gag-eGFP stable cell pool, VLP production measured by ELISA reached a plateau at 144 h (12.5 ng mL^{-1}), whereas intracellular Gag-eGFP production peaked 24 h earlier. The time of harvest was defined as 144 h since extending the production phase might not provide additional advantages and would impact cell culture viability. Under these conditions, an intracellular mCherry specific productivity of 0.5 ± 0.1 μg 10^{-6} cell·day was calculated, whereas 0.2 ng 10^{-6} cell·day was determined for Gag-eGFP stable cell pools. VLP quantification by flow virometry yielded a maximum concentration of $3.6 \pm 0.9 \times 10^5$ VLP mL^{-1}, and important amounts of extracellular vesicles (EV) were also encountered ($4.4 \pm 0.6 \times 10^8$ EV mL^{-1}). Interestingly, overall EV production levels did not increase in the Gag-eGFP stable cell pool compared to parental Sf9 cells because a similar EV concentration of $3.2 \pm 1.1 \times 10^8$ EV mL^{-1} was measured. Furthermore, nanoparticles were also detected in fresh Sf900III medium (1.2×10^8 particles mL^{-1}).

The stability of expression was assessed in the Gag-eGFP stable cell pool by cell passaging in the exponential phase every 3–5 days for one month (Appendix S1, Fig. S2). The stable cell pool was divided into two cultures, one maintained under zeocin selection and the other without selective pressure. No significant differences were observed between conditions in terms of the number of Gag-eGFP positive cells and production for at least one month in the absence of the antibiotic.

HIV-1 VLP production in the DASGIP bioreactor system

A proof-of-concept for VLP production using stable cell pools at bioreactor scale was conducted in a stirred tank DASGIP Parallel Bioreactor System. The Gag-eGFP stable cell pool was cultured in parallel to parental Sf9 cells, and triplicate shake flask experiments were also included as controls (Fig. 3). Cell viability was maintained at >80% in all conditions, with cells peaking at 96–120 h, except parental Sf9 cells cultured in shake flasks that attained the maximum viable cell density 24 h later [Fig. 3(A)]. Doubling times were reduced in the bioreactor conditions compared to shake flasks, especially for parental cells, but increased in comparison to previous shake flask experiments, probably as a consequence of the different seeding cell densities (Table 1). No oxygen limitation was detected in bioreactor cultures (DO ≥30% of air saturation) but parental Sf9 cells required higher stirring speeds over the Gag-eGFP stable cell pool to maintain the setpoint [Fig. 3(B)]. The peak of stirring speed was attained at 96 h in both conditions, close to the maximum viable cell density, with no impact on cell viability in comparison to shake flask cultures [Fig. 3(A)].[26] Similar trends were observed for pH values between the different conditions, with an initial decrease of pH up to 120 h followed by an increase until the end of the experiment [Fig. 3(C)]. This could also be found in bioreactor cultures, requiring the initial addition of comparable volumes of $NaHCO_3$ (2.6–2.7 mL) and later of H_3PO_4 (0.6–0.8 mL) to counterbalance pH changes.

Analysis of the number of Gag-eGFP positive cells in the stable cell pool revealed that the percentage decreased faster in shake flasks compared to the bioreactor, which could be attributed to the more rapid decline of cell viability in the former [Fig. 3(D)]. Regarding the production of VLPs, the bioreactor achieved higher Gag-eGFP fluorescence yields, which could explain the higher VLP concentration observed in this condition throughout the culture [Fig. 3(E)]. The harvest time for the bioreactor was defined as 120 h to maximize specific productivity, representing a 1.4-fold increase in VLP production and 1.3-fold increase in specific VLP productivity compared to shake flasks.

Comparative analysis of cell metabolism in different cultivation systems

The analysis of the main metabolites of the Gag-eGFP stable cell pool and parental Sf9 cells was performed in order to identify differential metabolic patterns when culturing these cells in bioreactors and shake flasks. Glutamine was the amino acid consumed at the highest rate in all conditions during the exponential phase (96 h), and at a larger level in the bioreactor over shake flasks [Fig. 4(A),(B)]. It was exhausted at 120 h and 144 h in the stable cell pool cultured in bioreactor and shake flasks, respectively, and 24 h earlier in parental Sf9 cells. Glucose consumption was

Table 1. Doubling times of stable Sf9 cell pools and parental cells cultured in shake flasks and stirred tank bioreactors

Experiment	Condition	Culture mode	VCD at seeding (10^6 cell mL^{-1})	Doubling time (h)
Characterization (Fig. 2)	Parental cell line	Shake flask	0.5	23.0 ± 0.2
	Gag-eGFP stable cell pool			22.7 ± 0.3
	mCherry stable cell pool			26.5 ± 2.0
Comparison (Fig. 3)	Parental cell line	Shake flask	1.0	28.9 ± 1.0
	Gag-eGFP stable cell pool			29.0 ± 0.7
	Parental cell line	Bioreactor	1.0	22.7
	Gag-eGFP stable cell pool			27.9

maintained until the end of the culture, although it decreased by approximately 2-fold in the stationary phase (Appendix S1, Tables S1–S4). Interestingly, glucose uptake by the stable cell pool was generally reduced by 2- to 5-fold in the exponential phase in shake flask cultures compared to the bioreactor (Appendix S1, Tables S3, S4). The use of alternative sugar sources such as maltose was also detected but kept at a lower level in comparison to glucose. Analysis of phosphate concentrations showed a higher consumption rate in bioreactor cultures, probably related to the faster cell growth kinetics in this cell culture system, reaching a plateau at the end of the exponential phase [96–120 h; Fig. 4(C), (D)]. Thereafter, an increase in phosphate concentration was measured in bioreactor cultures, which coincided with the addition of H_3PO_4 from 144 h to maintain the pH setpoint at 6.2 [Fig. 3(C)].

Besides glutamine, serine was also depleted at 96 h in bioreactor cultures and at 120 h in shake flasks. Similarly, leucine concentrations decreased to very low levels at the end of the exponential phase in all cases (Fig. 4(A)–(C)). Alanine was the main by-product generated by Sf9 cells and its production rate decreased steadily until the end of the culture, reaching a plateau at 20 mmol L^{-1} in the bioreactors, whereas it continued to increase in shake flasks. A correlation between alanine production and glutamine and glucose consumption could be established in the majority of the conditions evaluated [Appendix S1, Fig. S3(A)–(D)]. No lactate formation was measured in any of the conditions tested.

DISCUSSION

The need to shorten production timelines in vaccine development bioprocesses is crucial to combat disease outbreaks. In this work, insect cell pools stably producing HIV-1 Gag-eGFP VLPs were assessed as a system to accelerate vaccine production. The complete generation process from transfection to stable production, including the enrichment rounds with high producer cells, took 2.5 months. This represents a substantial reduction in time compared to classical SGE approaches requiring single cell cloning and screening of high producer insect cells, which can take several months.

Initial evaluation of stable insect cell pools for the production of different recombinant proteins revealed distinct features. The Gag-eGFP polyprotein was produced at lower levels compared to mCherry, highlighting the higher complexity associated with VLP production, and had a greater impact on cell viability at the end of cell culture [from 144 h; Fig. 2(C)]. Similar results have recently been described with stable High Five cell pools.[27] Continuous Gag VLP production in Sf9 cells has not been shown to be cytotoxic,[28] but a slight effect on cell viability was observed here. Differences between both recombinant products were also detected after achieving expression stability in the unsorted stable cell pools. A higher level of production was obtained in the mCherry stable cell pool, possibly as a consequence of the smaller size of the pIZTV5-mCherry plasmid, thus increasing the likelihood of a complete cassette integration. However, a negative impact on VLP expression due to the slight cytotoxicity observed could not be discarded, likely making some cells in the unsorted Gag-eGFP pool more prone to gene silencing.[29] In both cases, the heterologous production of mCherry and Gag-eGFP exerted an additional pressure on cells by increasing the cell doubling time compared to parental Sf9 cells.[30] This phenomenon was more pronounced in the mCherry pool from the mid-exponential phase, but also noticeable for VLP expression in the late exponential phase, when the peak of Gag-eGFP production was attained. The production of HIV-1 VLPs was also tested in bioreactor, resulting in higher viable cell densities and cell viability profiles compared to shake flask experiments. Moreover, the doubling times were reduced in bioreactors, indicating a more suitable environment for cell growth due to the controlled culture conditions. This could also be appreciated in the higher phosphate consumption rates of bioreactor cultures observed until the end of the exponential phase, coinciding with cell growth stabilization. The maintenance of DO and pH setpoints in the cell culture might also explain that cell viabilities remained at >95% for a longer period of time.[31] pH fluctuations in shake flasks did not exceed the 5.9–6.4 range, showing that Sf9 cells maintain a more stable pH in culture than other insect cell lines such as High Five cells.[27,32] In terms of production, VLP titers achieved in bioreactor were 1.4-fold higher than those obtained in shake flasks, illustrating the scalability of stable cell pools and also reinforcing the necessity of controlling culture parameters to improve the production of recombinant proteins.

Cell heterogeneity has been one of the major arguments against recombinant protein production using stable cell pools. However, it has been reported that heterogeneity is also present in cells derived from an individual clone to a large extent.[33,34] Recently, greater emphasis has been placed on the productivity of the system and the quality of the product produced, rather than the clonality of producing cells.[35] Therefore, the development of stable cell pools is shown to be an attractive approach for the stable production of both simple and more complex recombinant products. The time and effort needed to generate a stable cell line originating from an individual clone might not be worthwhile if a substantial difference with stable cell pools is not achieved. In this work, similar production levels to those achieved in stable insect cell lines with significantly shorter development timelines are reported (Table 2).

The titers shown here are in the range of those obtained with stable High Five cell pools,[27] but lower than those reported in insect cells with the baculovirus expression vector system

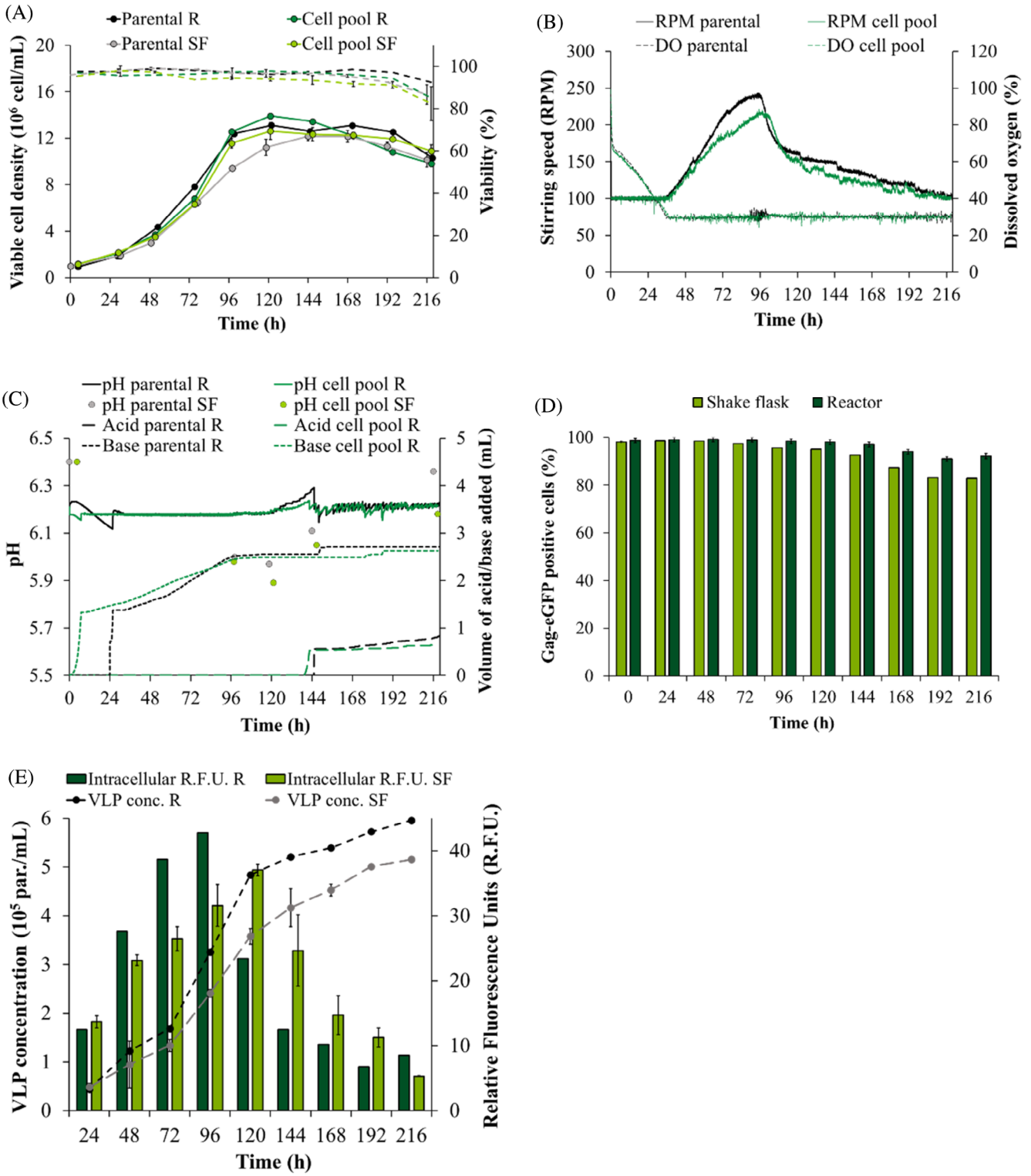

Figure 3. Proof-of-concept of Gag-eGFP stable cell pool culture in bioreactor and comparison to parental Sf9 cells. (A) Cell growth (straight line) and viability (dashed line) profiles of the Gag-eGFP stable cell pool and parental cells cultured in shake flasks (SF) and in the DASGIP Parallel Bioreactor System (R). Cells were seeded in 20 and 500 mL of fresh Sf900III medium at 1×10^6 cell mL^{-1} in Erlenmeyer shake flasks and in bioreactor, respectively. (B) Dissolved oxygen (DO) and stirring speed profiles of the Gag-eGFP stable cell pool and parental cells cultured in bioreactor. (C) pH profile during cultivation of the Gag-eGFP stable cell pool and parental cells in shake flasks (dot) and in bioreactor (line), and volume of H_3PO_4 (long-dashed line) and $NaHCO_3$ (short-dashed line) added in the bioreactor. (D) Percentage of Gag-eGFP positive cells in the stable cell pool cultured in shake flasks and in bioreactor. (E) VLP and intracellular Gag-eGFP production in shake flasks and in bioreactor.

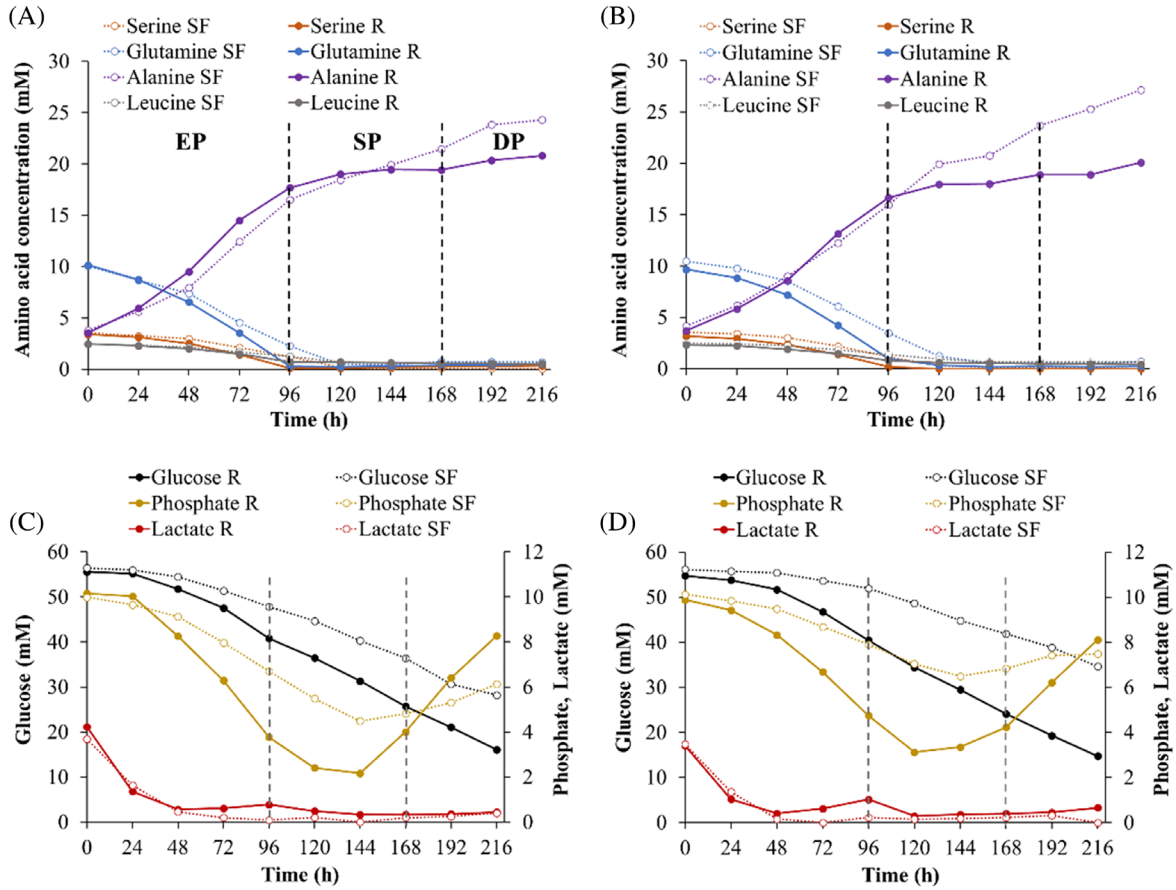

Figure 4. Representation of the main metabolites produced and consumed in parental cells and Gag-eGFP stable cell pools. Glucose, phosphate, and lactate concentrations in parental cells (A) and the Gag-eGFP stable cell pool (B) cultured in shake flasks (SF) and in bioreactor (R). Amino acids with substantial changes in their concentrations in parental cells (C) and the Gag-eGFP stable cell pool (D) cultured in shake flasks and in bioreactor. EP, exponential phase; SP, stationary phase; DP, death phase.

(BEVS)[19,39] and TGE,[21,22] probably reflecting the lower amount of Gag-eGFP produced in the stable cell pool. However, the possibility of having a continuous platform to produce VLPs devoid of baculoviruses and baculovirus-derived proteins makes the use of this system appealing, especially in combination with production techniques enabling increased cell concentrations, such as continuous perfusion, and subsequently the final VLP titers.[40] This study is a first proof-of-concept and there is an opportunity to increase VLP yields by tailored supplementation strategies[41] or adaptive laboratory evolution techniques.[37]

The implementation of flow virometry for VLP quantification enabled the detection of the co-expression of EVs. Recent studies indicate that these nanoparticles not only impact mammalian cell cultures, but are also important to consider in insect cells,[24] particularly in continuous operation processes aiming to achieve reproducible and constant culture conditions. EVs facilitate the intercellular communication by transporting functional molecules[42]; however, the influence of EVs in insect cell bioprocesses is still not well understood. In this sense, it is important to consider that these nanoparticles are also present in the insect cell

Table 2. Comparison of production levels of HIV-1 Gag VLPs in lepidopteran insect cell lines by stable gene expression. p24 concentration values were normalized according to the Gag (55 kDa), Gag-eGFP (87.7 kDa) and Gag-Cherry (83 kDa) polyprotein molecular weight

VLP	Cell line	Method	Production (ng Gag mL^{-1})	Specific productivity (ng Gag 10^{-6} cell·day)	Development time (months)	Reference
Gag-eGFP	Sf21, Sf9	RI - Pool	12.5	0.2	2.5	This work
Gag			1.4	n.a.	n.a.	37
		RMCE – Clonal	<1|25.2*	0.4	7–9.5**	38,39
Gag-Cherry		cell line	20.8	0.3	4–6.5	29,39
Gag	High Five		1.1|11.5*	0.2	n.a.	38
Gag-eGFP		RI - Pool	14.8	0.5	2	28

RI, random integration; RMCE, recombinase-mediated cassette exchange; n.a., not available.
*Gag concentration before and after employingadaptation to hypothermic culture conditions for 3 months.
**Development time considering the 3 months of adaptationto hypothermic culture conditions.

platform, especially when the product of interest is a nanoparticle, since not taking them into consideration might cause product overestimation.

Analysis of the main metabolites in cell culture showed that consumption and production rates were markedly higher during the exponential phase, and maintained at lower levels during the stationary and death phases. In general, no specific signatures were observed between the stable cell pool and parental Sf9 cells, highlighting the ability of this cell line to adapt to continuous heterologous recombinant protein production. Analysis of metabolite concentrations in shake flasks and bioreactor showed that glucose and glutamine were the primary energy sources. These results differ from studies with High Five cells cultured in the same cell culture medium showing a higher dependency on asparagine.[21,27] Glucose is mainly consumed via the glycolysis pathway, being converted to pyruvate before entrance into the Krebs cycle (KC), whereas glutamine is incorporated into the KC after conversion to α-ketoglutarate.[43] Previous studies with Sf9 cells indicate that glucose consumption is around 3-fold higher than that of glutamine.[37,44] However, this difference was not observed here, which could be associated with a more balanced metabolism of Sf9 cells in low hydrolysate cell culture media. The excess glucose and glutamine conditions detected in the exponential phase could explain alanine production in all of the conditions tested, being slightly higher in bioreactor possibly due to the higher glucose and glutamine consumption rates. Alanine production ceased once glutamine was exhausted, as reported previously.[45] No lactate formation was observed, suggesting that there was no oxygen limitation in any of the cell cultures.[32] Of note, lactate concentrations of $\leq$28 mmol L^{-1} were measured in High Five cell pools in the same culture conditions,[27] which highlights a more efficient metabolism in Sf9 cells. Serine, despite being consumed at lower rates than glucose and glutamine, was completely exhausted by the end of the exponential phase; this amino acid has been shown to be very important for Sf9 cell culture and involved in the generation of biomass and energy production.[46] Likewise, leucine concentrations decreased to very low levels by the end of the exponential phase; Sf9 cells typically do not consume much leucine[47,48] and its use is generally associated with biomass generation.[49] However, most of the studies reported so far do not analyze cell metabolism at such high cell densities since Sf9 cells are generally used in combination with the BEVS which prevents cell growth, or are cultured in low-performing cell culture media. Thus, leucine may be an important amino acid to consider to further improve Sf9 cell growth, particularly in perfusion culture systems aiming to increase viable cell concentrations.

In conclusion, this study shows the suitability of stable Sf9 cell pools as a rapid system for VLP production and brings the prospect of development of large-scale bioprocesses for vaccine manufacture. This approach can also be implemented for the flexible production of other VLP candidates and vaccines by incorporating variable surface antigens to target different diseases, including the SARS-CoV-2 spike or the influenza haemagglutinin, among others. Future work will focus on the study of continuous perfusion processes to exploit the full potential of stable Sf9 cell pools and assess their impact on VLP production.

ACKNOWLEDGEMENTS

We thank Nick Berrow (Institute for Research in Biomedicine, Barcelona, Spain) for providing the Sf9 cell line and the pPEU3 plasmid, and Paula Alves (Experimental and Technological Biology Institute, Oeiras, Portugal) for the pIZTV5-His plasmid. The support of Manuela Costa (Cell Culture Service, Antibody Production and Cytometry, UAB) and Núria Barba (Microscopy Research Unit, UAB) with fluorescence-activated cell sorting and confocal microscopy is acknowledged. Sahar Masoumeh (University of Natural Resources and Life Sciences, Vienna, Austria) provided support in ELISA quantification and Irene González-Domínguez (Department of Chemical, Biological and Environmental Engineering, UAB) developed the mCherry standard curve. Ángel Calvache (Beckman Coulter) facilitated the access to the CytoFlex LX flow cytometer. Eduard Puente-Massaguer is a recipient of an FPU grant from the Ministry of Education, Culture and Sport of Spain (FPU15/03577). The research group is recognized as 2017 SGR 898 by the Government of Catalonia.

CONFLICT OF INTEREST

None.

SUPPORTING INFORMATION

Supporting information may be found in the online version of this article.

REFERENCES

1 Gonelli CA, Khoury G, Center RJ and Purcell DFJ, HIV-1-based virus-like particles that morphologically resemble mature, infectious HIV-1 Virions. *Viruses* **11**:507 (2019).
2 Al-Barwani F, Donaldson B, Pelham SJ, Young SL and Ward VK, Antigen delivery by virus-like particles for immunotherapeutic vaccination. *Ther Deliv* **5**:1223–1240 (2014).
3 Valley-Omar Z, Meyers AE, Shephard EG, Williamson A-L and Rybicki EP, Abrogation of contaminating RNA activity in HIV-1 Gag VLPs. *Virol J* **8**:462 (2011).
4 Noad R and Roy P, Virus-like particles as immunogens. *Trends Microbiol* **11**:438–444 (2003).
5 Jowett JBM, Hockley DJ, Nermut MV and Jones IM, Distinct signals in human immunodeficiency virus type 1 Pr55 necessary for RNA binding and particle formation. *J Gen Virol* **73**:3079–3086 (1992).
6 González-Domínguez I, Puente-Massaguer E, Cervera L and Gòdia F, Quantification of the HIV-1 virus-like particle production process by super-resolution imaging: from VLP budding to nanoparticle analysis. *Biotechnol Bioeng* **117**:1929–1945 (2020).
7 Ding X, Liu D, Booth G, Gao W and Lu Y, Virus-like particle engineering: from rational design to versatile applications. *Biotechnol J* **13**:1–7 (2018).
8 Venereo-Sanchez A, Gilbert R, Simoneau M, Caron A, Chahal P, Chen W *et al.*, Hemagglutinin and neuraminidase containing virus-like particles produced in HEK-293 suspension culture: an effective influenza vaccine candidate. *Vaccine* **34**:3371–3380 (2016).
9 Ye J, Alvin K, Latif H, Hsu A, Parikh V, Whitmer T *et al.*, Rapid protein production using CHO stable transfection pools. *Biotechnol Prog* **26**: 1431–1437 (2010).
10 González-Domínguez I, Grimaldi N, Cervera L, Ventosa N and Gòdia F, Impact of physicochemical properties of DNA/PEI complexes on transient transfection of mammalian cells. *N Biotechnol* **49**:88–97 (2019).
11 Sleiman RJ, Gray PP, McCall MN, Codamo J and Sunstrom NAS, Accelerated cell line development using two-color fluorescence activated cell sorting to select highly expressing antibody-producing clones. *Biotechnol Bioeng* **99**:578–587 (2008).
12 Fan L, Rizzi G, Bierilo K, Tian J, Yee JC, Russell R *et al.*, Comparative study of therapeutic antibody candidates derived from mini-pool and clonal cell lines. *Biotechnol Prog* **33**:1456–1462 (2017).
13 Balasubramanian S, Rajendra Y, Baldi L, Hacker DL and Wurm FM, Comparison of three transposons for the generation of highly productive recombinant CHO cell pools and cell lines. *Biotechnol Bioeng* **113**: 1234–1243 (2016).

14 Chakrabarti L, Mathew A, Li L, Han S, Klover J, Albanetti T *et al*., Mitochondrial membrane potential identifies cells with high recombinant protein productivity. *J Immunol Methods* **464**:31–39 (2019). https://doi.org/10.1016/j.jim.2018.10.007.
15 Balasubramanian S, Matasci M, Kadlecova Z, Baldi L, Hacker DL and Wurm FM, Rapid recombinant protein production from piggyBac transposon-mediated stable CHO cell pools. *J Biotechnol* **200**:61–69 (2015).
16 Welch JT and Arden NS, Considering "clonality": a regulatory perspective on the importance of the clonal derivation of mammalian cell banks in biopharmaceutical development. *Biologicals* **62**:16–21 (2019).
17 Geisler C and Jarvis DL, Adventitious viruses in insect cell lines used for recombinant protein expression. *Protein Expr Purif* **144**:25–32 (2018).
18 Fernandes F, Teixeira AP, Carinhas N, Carrondo MJT and Alves PM, Insect cells as a production platform of complex virus-like particles. *Expert Rev Vaccines* **12**:225–236 (2013).
19 Puente-Massaguer E, Lecina M and Gòdia F, Application of advanced quantification techniques in nanoparticle-based vaccine development with the Sf9 cell baculovirus expression system. *Vaccine* **38**:1849–1859 (2020).
20 Berrow NS, Alderton D, Sainsbury S, Nettleship J, Assenberg R, Rahman N *et al*., A versatile ligation-independent cloning method suitable for high-throughput expression screening applications. *Nucleic Acids Res* **35**:1–12 (2007).
21 Puente-Massaguer E, Strobl F, Grabherr R, Striedner G, Lecina M and Gòdia F, PEI-mediated transient transfection of high five cells at bioreactor scale for HIV-1 VLP production. *Nanomaterials* **10**:1–16 (2020).
22 Puente-Massaguer E, Gòdia F and Lecina M, Development of a non-viral platform for rapid virus-like particle production in Sf9 cells. *J Biotechnol* **322**:43–53 (2020).
23 Ikonomou L, Schneider YJ and Agathos SN, Insect cell culture for industrial production of recombinant proteins. *Appl Microbiol Biotechnol* **62**:1–20 (2003).
24 Puente-Massaguer E, Saccardo P, Ferrer-Miralles N, Lecina M and Gòdia F, Coupling microscopy and flow cytometry for a comprehensive characterization of nanoparticle production in insect cells. *Cytom Part A* **97**:921–932 (2020).
25 González-Domínguez I, Puente-Massaguer E, Cervera L and Gòdia F, Quality assessment of virus-like particles at single particle level: a comparative study. *Viruses* **12**:223–235 (2020).
26 Strobl F, Duerkop M, Palmberger D and Striedner G, High shear resistance of insect cells: the basis for substantial improvements in cell culture process design. *Sci Rep* **11**:9413 (2021).
27 Puente-Massaguer E, Grau-Garcia P, Strobl F, Grabherr R, Striedner G, Lecina M *et al*., Accelerating HIV-1 VLP production using stable high five insect cell pools. *Biotechnol J* **16**:1–12 (2021).
28 Vidigal J, Fernandes B, Dias MM, Patrone M, Roldão A, Carrondo MJT *et al*., RMCE-based insect cell platform to produce membrane proteins captured on HIV-1 Gag virus-like particles. *Appl Microbiol Biotechnol* **102**:655–666 (2018).
29 Zhu J, Mammalian cell protein expression for biopharmaceutical production. *Biotechnol Adv* **30**:1158–1170 (2012).
30 Bergametti F, Prigent S, Luber B, Benoit A, Tiollais P, Sarasin A *et al*., The proapoptotic effect of hepatitis B virus HBx protein correlates with its transactivation activity in stably transfected cell lines. *Oncogene* **18**:2860–2871 (1999).
31 Strobl F, Ghorbanpour SM, Palmberger D and Striedner G, Evaluation of screening platforms for virus-like particle production with the baculovirus expression vector system in insect cells. *Sci Rep* **10**:1065 (2020).
32 Rhiel M, Mitchell-Logean CM and Murhammer DW, Comparison of *Trichoplusia ni* BTI-Tn-5b1-4 high five (TM) and *Spodoptera frugiperda* Sf-9 insect cell line metabolism in suspension cultures. *Biotechnol Bioeng* **55**:909–920 (1997).
33 Vcelar S, Melcher M, Auer N, Hrdina A, Puklowski A, Leisch F *et al*., Changes in chromosome counts and patterns in CHO cell lines upon generation of recombinant cell lines and subcloning. *Biotechnol J* **13**:1–9 (2018).
34 Vcelar S, Jadhav V, Melcher M, Auer N, Hrdina A, Sagmeister R *et al*., Karyotype variation of CHO host cell lines over time in culture characterized by chromosome counting and chromosome painting. *Biotechnol Bioeng* **115**:165–173 (2018).
35 Frye C, Deshpande R, Estes S, Francissen K, Joly J, Lubiniecki A *et al*., Industry view on the relative importance of "clonality" of biopharmaceutical-producing cell lines. *Biologicals* **44**:117–122 (2016).
36 Lynch AG, Tanzer F, Fraser MJ, Shephard EG, Williamson AL and Rybicki EP, Use of the piggyBac transposon to create HIV-1 gag transgenic insect cell lines for continuous VLP production. *BMC Biotechnol* **10**:1–13 (2010).
37 Fernandes B, Vidigal J, Correia R, Carrondo MJT, Alves PM, Teixeira AP *et al*., Adaptive laboratory evolution of stable insect cell lines for improved HIV-Gag VLPs production. *J Biotechnol* **307**:139–147 (2020).
38 Vidigal J, Fernandes F, Coroadinha AS, Teixeira AP and Alves PM, Insect cell line development using flp-mediated cassette exchange technology. *Methods Mol Biol* **1104**:15–27 (2014).
39 Puente-Massaguer E, Lecina M and Gòdia F, Integrating nanoparticle quantification and statistical design of experiments for efficient HIV-1 virus-like particle production in high five cells. *Appl Microbiol Biotechnol* **104**:1569–1582 (2020).
40 Alvim RGF, Lima TM, Silva JL, Oliveira GAP and Castilho LR, Process intensification for the production of yellow fever virus-like particles as potential recombinant vaccine antigen. *Biotechnol Bioeng* **118**:3581–3592 (2021).
41 Monteiro F, Bernal V, Chaillet M, Berger I and Alves PM, Targeted supplementation design for improved production and quality of enveloped viral particles in insect cell-baculovirus expression system. *J Biotechnol* **233**:34–41 (2016).
42 Ishikawa R, Yoshida S, Sawada S-i, Sasaki Y and Akiyoshi K, Preparation of engineered extracellular vesicles with full-length functional PD-1 membrane proteins by baculovirus expression system. *Biochem Biophys Res Commun* **526**:967–972 (2020).
43 Benslimane C, Elias CB, Hawari J and Kamen A, Insights into the central metabolism of *Spodoptera frugiperda* (Sf-9) and *Trichoplusia ni* BTI-Tn-5B1-4 (Tn-5) insect cells by radiolabeling studies. *Biotechnol Prog* **21**:78–86 (2005).
44 Drews M, Doverskog M, Öhman L, Chapman BE, Jacobsson U, Kuchel PW *et al*., Pathways of glutamine metabolism in *Spodoptera frugiperda* (Sf9) insect cells: evidence for the presence of the nitrogen assimilation system, and a metabolic switch by 1H/15N NMR. *J Biotechnol* **78**:23–37 (2000).
45 Doverskog M, Ljunggren J, Öhman L and Häggström L, Physiology of cultured animal cells. *J Biotechnol* **59**:103–115 (1997).
46 Brüggert M, Rehm T, Shanker S, Georgescu J and Holak TA, A novel medium for expression of proteins selectively labeled with 15N-amino acids in *Spodoptera frugiperda* (Sf9) insect cells. *J Biomol NMR* **25**:335–348 (2003).
47 Ferrance JP, Goel A and Ataai MM, Utilization of glucose and amino acids in insect cell cultures: quantifying the metabolic flows within the primary pathways and medium development. *Biotechnol Bioeng* **42**:697–707 (1993).
48 Palomares LA and Ramírez OT, The effect of dissolved oxygen tension and the utility of oxygen uptake rate in insect cell culture. *Cytotechnology* **22**:225–237 (1996).
49 Drews M, Paalme T and Vilu R, The growth and nutrient utilization of the insect cell line *Spodoptera frugiperda* Sf9 in batch and continuous culture. *J Biotechnol* **40**:187–198 (1995).

Research paper

Title: Stable Sf9 cell pools as a system for rapid HIV-1 virus-like particle production

Author names and affiliations: Eduard Puente-Massaguer [1,5]*, Paula Grau-Garcia [1], Florian Strobl [2, 3], Reingard Grabherr [3], Gerald Striedner [3], Martí Lecina [4], Francesc Gòdia [1]

[1] Department of Chemical, Biological and Environmental Engineering, Universitat Autònoma de Barcelona, Barcelona, Spain

[2] Austrian Centre of Industrial Biotechnology (acib GmbH), Vienna, Austria

[3] Department of Biotechnology, University of Natural Resources and Life Sciences, Vienna, Austria

[4] IQS School of Engineering, Universitat Ramón Llull, Barcelona, Spain

[5] Department of Microbiology, Icahn School of Medicine at Mount Sinai, New York, USA

***Corresponding author:** Eduard Puente-Massaguer

E-mail: eduard.puente-massaguer@mssm.edu

Present address: [5] Department of Microbiology, Icahn School of Medicine at Mount Sinai, New York, USA

ORCID: 0000-0002-2816-7051

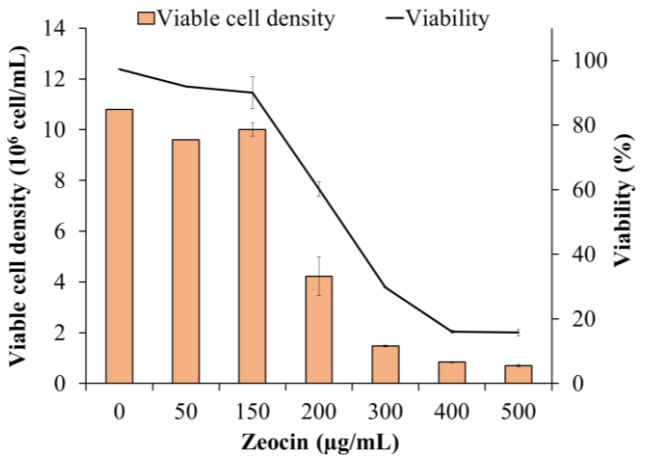

Figure S1. Viable cell density and viability of parental Sf9 cells with different zeocin concentrations ranging from 50 to 500 µg/mL at 48 hpt. A negative control (0 µg/mL) was included for comparison. The average of triplicate experiments is represented.

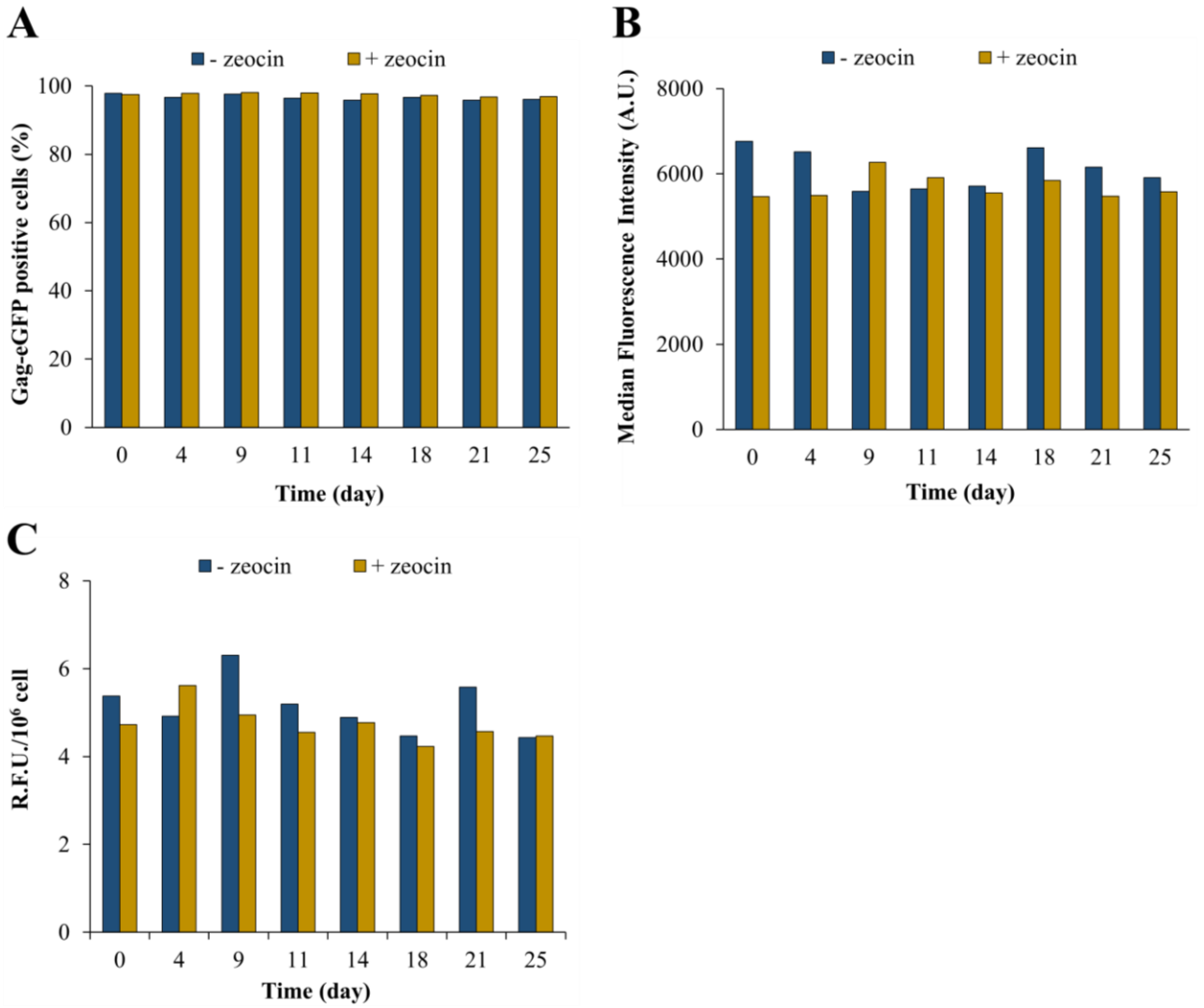
A
- zeocin
+ zeocin
Gag-eGFP positive cells (%)
100
80
60
40
20
0
0
4
9
11
14
18
21
25
Time (day)
B
- zeocin
+ zeocin
Median Fluorescence Intensity (A.U.)
8000
6000
4000
2000
0
0
4
9
11
14
18
21
25
Time (day)
C
- zeocin
+ zeocin
R.F.U./10^6 cell
8
6
4
2
0
0
4
9
11
14
18
21
25
Time (day)

Figure S2. Stability analysis of Gag-eGFP production in the stable cell pool cultured in shake flasks and passaged every 2 – 3 days during one month with and without zeocin addition. (A) Percentage of Gag-eGFP positive cells. (B) Median fluorescence intensity of Gag-eGFP positive cells in arbitrary units (A.U.). (C) Specific intracellular Gag-eGFP production in relative fluorescence units (R.F.U.). Cells were maintained in the exponential phase and intracellular Gag-eGFP production was measured by spectrofluorometry.

.

Table S1. Consumption and production fluxes of the main metabolites in parental Sf9 cells cultured in 125 mL shake flasks. Graph bars are represented for each individual metabolite over 0 – 216 h for a better comprehension of the data. Consumption is represented with red bars (negative values) and production with green bars (positive values). Fluxes are expressed in nmol/(10^6 cell·h).

Metabolite	Exponential phase				Stationary phase			Death phase	
	0 – 24	24 – 48	48 – 72	72 – 96	96 – 120	120 – 144	144 – 168	168 – 192	192 – 216
Glucose	-9.5	-33.5	-23	-21.4	-14.9	-14.8	-13.3	-20.5	-9.3
Maltose	-4.9	-9.7	-9.6	-10.4	-11.1	-2.6	-2.9	-0.7	0.8
Lactate	-46.6	-26	-2	-0.6	0.5	-	-	0.2	0.6
Phosphate	-7.4	-11.8	-8.6	-7.6	-5.8	-3.3	1.1	1.8	3.2
Aspartic acid	-4.4	5.4	-0.2	1.9	-3.6	-0.3	-1.9	-0.6	-1.9
Glutamic acid	-0.7	6.9	0.6	1.1	-5.3	-0.4	1.3	3.7	0.4
Asparagine	-3.7	3.8	-0.7	1.7	-3.5	0.5	0.6	1.6	-0.8
Serine	-7	-6.2	-6.5	-5.4	-4.9	-0.3	0.1	-0.1	0
Glutamine	-31.4	-28.4	-21.2	-13.7	-8.4	-0.2	1.1	0	-0.2
Histidine	-1.6	-0.8	-1.1	-0.5	-0.9	-0.2	0.3	0.1	-0.2
Glycine	-3	-1.3	-1.1	-0.3	-1.6	-0.6	-0.2	-0.2	-0.3
Threonine	-2.9	-1.2	-2.4	-1.1	-1.9	-0.4	0.2	0.1	-0.1
Arginine	-3.4	0.2	-1.9	-0.5	-2.1	-0.1	1.2	1.3	0.5
Alanine	41.4	51.3	33.5	24.4	9.2	4.9	5.3	8.4	1.8
Tyrosine	-1.5	-1.3	-0.9	-0.8	-1	0	0.1	0.1	-0.1
Valine	-4	-1.1	-3.3	-1.1	-2.9	1.6	0.1	1.1	0
Methionine	-0.6	0.3	-0.2	1	-1.3	0	0.2	1.3	-0.3
Tryptophan	-0.4	-0.7	-0.4	-0.2	-0.4	0.2	0	0.1	-0.1
Phenylalanine	-1.5	-1	-1	0	-2.7	2.6	0.2	1.6	-0.3
Isoleucine	-1.6	0.3	-1.1	0.6	-2.1	-0.5	0.2	1.5	-0.2
Leucine	-3.5	-4.1	-3.3	-2.6	-2.6	-0.4	-0.1	0	-0.1
Lysine	-1.2	-2.7	-3.8	-1.2	-3.1	-1.6	1.4	0.2	-1.7
Proline	-2.7	3.3	-4.9	-0.7	-2.4	0.9	0.1	0.7	-0.3

Table S2. Consumption and production fluxes of the main metabolites in parental Sf9 cells cultured in bioreactor. Graph bars are represented for each individual metabolite over 0 – 216 h. Consumption is represented with red bars (negative values) and production with green bars (positive values). Fluxes are expressed in nmol/(10^6 cell·h).

Metabolite	Exponential phase				Stationary phase			Death phase	
	0 – 24	24 – 48	48 – 72	72 – 96	96 – 120	120 – 144	144 – 168	168 – 192	192 – 216
Glucose	-11.4	-45.2	-31	-27.7	-15.2	-17	-17	-14.7	-18.2
Maltose	-4.3	-12.3	-11.5	-12.7	-7.2	-1.3	-0.3	0.1	-0.5
Lactate	-85.5	-10.4	0.4	0.7	-1	-0.5	0	0.1	0.3
Phosphate	-3.5	-23.3	-14.5	-10.4	-4.7	-0.8	-9	4.6	3.2
Aspartic acid	8.9	2.3	4.1	-2.2	-1.8	-2.6	-3.1	-0.7	-2
Glutamic acid	8.3	4.2	4.9	-0.8	3.1	2	-1.1	0.1	-1.6
Asparagine	3.6	0.4	2.8	-3	0.9	-0.1	-1.5	0	-0.9
Serine	-8.6	-7.8	-8	-5.4	0	0.4	0.2	0	0.2
Glutamine	-42.1	-28.9	-22.1	-13.4	-0.2	0.3	0.3	0	0.3
Histidine	-1.2	-1	-0.6	-1.1	0.1	0.4	0.2	0	0.3
Glycine	0.8	-1	-0.2	-1.9	-0.6	-0.3	-0.5	-0.3	-0.3
Threonine	-2.6	-2.1	-1.9	-2.2	0.1	0.2	0	-0.1	0
Arginine	2.6	-1.5	-1	-2.7	-2.1	-0.6	0.3	1	2.4
Alanine	71.1	46.9	36.8	13.1	4.7	1.5	-0.1	3	1.6
Tyrosine	-1.8	-1.1	-0.8	-1.2	0.1	-0.1	-0.2	0	-0.1
Valine	-1.5	-2	-1.3	-2.9	0.4	-0.2	-0.6	0.3	-0.8
Methionine	2	0.4	1	-1.4	0.5	-0.6	-0.9	0.3	-1.1
Tryptophan	-0.6	-0.4	-0.4	-0.4	0	0	-0.1	0	-0.1
Phenylalanine	1.7	0.2	0.7	-1.8	0.6	-0.5	-0.9	0.5	-1.1
Isoleucine	-0.4	-1	0	-2.5	0.6	-0.3	-0.8	0.4	-1.1
Leucine	-4.9	-4	-3.6	-3.3	-0.1	-0.1	-0.2	0	-0.4
Lysine	-21.5	-3.8	4.7	-3.3	0.4	-0.2	-0.8	-2	0.9
Proline	1.8	-1.5	-1.4	-2.6	0.1	-0.3	-0.5	0.2	-0.9

Table S3. Consumption and production fluxes of the main metabolites in the Gag-eGFP stable cell pool cultured in 125 mL shake flasks. Graph bars are represented for each individual metabolite over 0 – 216 h. Consumption is represented with red bars (negative values) and production with green bars (positive values). Fluxes are expressed in nmol/(10^6 cell·h).

Metabolite	Exponential phase				Stationary phase			Death phase	
	0 – 24	24 – 48	48 – 72	72 – 96	96 – 120	120 – 144	144 – 168	168 – 192	192 – 216
Glucose	-10.3	-5.2	-14.8	-8.7	-11.6	-12	-9.6	-10.5	-15.8
Maltose	-8	-6.9	-12.2	-7.2	-5.7	-3.7	-2	-0.6	0.2
Lactate	-51.9	-19.1	-	-	-0.3	0.1	0.1	0.3	-
Phosphate	-7	-5.7	-6.7	-3.9	-3	-1.7	1.1	2.1	0.2
Aspartic acid	10.2	5.9	-5.2	-1.6	1.1	-3.9	1.2	-0.9	0
Glutamic acid	11.9	6	-4.1	-1.3	0.5	-1.6	4.6	2.3	2.3
Asparagine	9.5	4.6	-5.6	-1.3	0.9	-2.5	2.6	-0.2	0.3
Serine	-4	-5.9	-6.9	-5.2	-3.1	-0.5	0	0	-
Glutamine	-17.1	-19.7	-20.9	-12.8	-7.9	-2.3	0.1	-0.1	0.8
Histidine	0.7	-0.5	-1.4	-0.7	-0.3	-0.1	0.2	0.1	0.5
Glycine	0.4	0.6	-1.9	-0.8	-0.1	-1.8	0.2	0	0.3
Threonine	0.6	-1.8	-2.5	-1.5	-0.8	-1.1	0.4	0	0.6
Arginine	2.6	1.8	-3.6	-1.3	-0.2	-1.7	1.4	1.4	0.8
Alanine	49.3	44.9	27.4	18.4	14	2.6	9.7	5.6	7
Tyrosine	-1.1	0.3	-1.7	-0.8	-0.3	-0.4	0.2	0.1	0.1
Valine	3	0.7	-3.8	-1.6	-0.8	-2.2	1.6	0.1	0.8
Methionine	5.2	3.1	-2.4	-0.5	0.8	-2.1	2.3	0.5	1.1
Tryptophan	-0.5	0	-0.5	-0.3	-0.1	-0.1	0.1	0	0.1
Phenylalanine	3.8	2.6	-2.9	-0.5	0.7	-1	2	0.5	1.1
Isoleucine	4	1.6	-3.3	-1.1	0.2	-1.2	1.7	0.3	1.1
Leucine	-1.8	-2.8	-3.5	-2.2	-1.6	-0.9	0	-0.1	0
Lysine	3.3	-4	-4.4	-1.6	-1.2	-1	0.2	0.1	1.3
Proline	-1.1	0.5	-4.2	-2.2	-0.3	0	1	0.3	1.1

Table S4. Consumption and production fluxes of the main metabolites in the Gag-eGFP stable cell pool cultured in bioreactor. Graph bars are represented for each individual metabolite over 0 – 216 h. Consumption is represented with red bars (negative values) and production with green bars (positive values). Fluxes are expressed in nmol/(10^6 cell·h).

Metabolite	Exponential phase				Stationary phase			Death phase	
	0 – 24	24 – 48	48 – 72	72 – 96	96 – 120	120 – 144	144 – 168	168 – 192	192 – 216
Glucose	-25	-31.9	-39.6	-28.8	-19.3	-14.2	-16.9	-17.6	-18.8
Maltose	-10.3	-13.1	-16.3	-9.9	-5.9	-1.6	-0.2	-0.4	-0.3
Lactate	-59	-9.8	1.7	1.9	-2.4	0.2	0.1	0.2	0.9
Phosphate	-11.3	-17	-13.1	-8.8	-5.2	0.7	-9.9	3.9	7.3
Aspartic acid	9.4	-1.6	1.5	-1.4	-1.5	-3.7	-1.7	-2.6	-0.9
Glutamic acid	10.9	-1.5	3.1	0.9	2.8	1	2.5	-1.4	1.1
Asparagine	8.1	-3.7	0.4	-1.8	-0.1	-1.9	0.3	-2.7	-0.4
Serine	-5.6	-8.9	-7.7	-5.5	-	-	-	-	-
Glutamine	-20.5	-25.4	-23.5	-14.9	-2.1	-0.3	0.1	-0.1	0.1
Histidine	0.2	-1.4	-1	-1.1	0.1	-0.2	0.5	-0.7	-0.1
Glycine	0.5	-1.9	-0.6	-1.5	-0.8	-0.6	-0.1	-0.8	-0.2
Threonine	-0.4	-3	-2	-2	-0.2	-0.2	0.3	-1	0.2
Arginine	1.7	-2.5	-1.9	-2.4	-1.8	-1	0.8	0.9	2.5
Alanine	52.5	42.9	36.2	16.1	4.2	0.1	2.9	0	4.9
Tyrosine	-1	-1	-1.2	-1.1	-0.1	-0.1	-0.1	-0.2	0.1
Valine	2.1	-4.3	-1.6	-3.1	0.2	-0.6	0	-0.4	0.1
Methionine	4.2	-3.2	0.6	-1	-0.4	-0.7	-0.1	-0.9	0.3
Tryptophan	0	-0.9	-0.3	-0.6	-0.1	0	-0.1	0	0
Phenylalanine	4.8	-4.4	0.4	-1.2	-0.2	-0.8	0	-0.9	0.5
Isoleucine	4	-4.3	-0.6	-1.7	-0.3	-0.6	0.1	-0.7	0.3
Leucine	-2.2	-5.1	-3.4	-3.1	-0.6	-0.1	-0.2	-0.1	-0.2
Lysine	0.1	-5.2	-3.5	-4.2	0	-1.5	2.1	-2.6	1.2
Proline	2.2	-5.5	-2.4	-0.7	-0.7	-0.5	-0.3	-0.5	-0.4

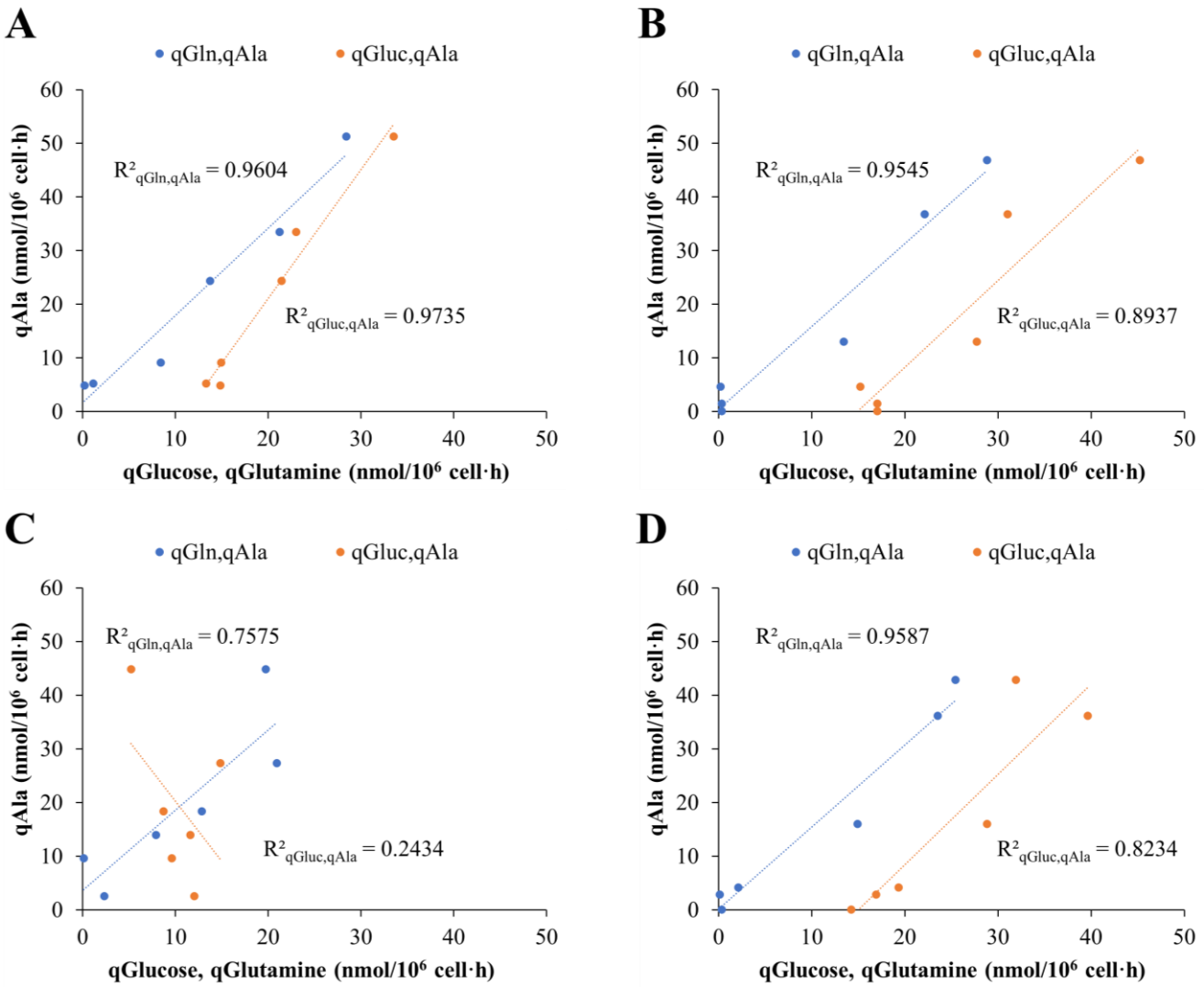
A
qGln,qAla
qGluc,qAla
$R^2_{qGln,qAla}$ = 0.9604
$R^2_{qGluc,qAla}$ = 0.9735
qAla (nmol/10⁶ cell·h)
qGlucose, qGlutamine (nmol/10⁶ cell·h)
B
qGln,qAla
qGluc,qAla
$R^2_{qGln,qAla}$ = 0.9545
$R^2_{qGluc,qAla}$ = 0.8937
qAla (nmol/10⁶ cell·h)
qGlucose, qGlutamine (nmol/10⁶ cell·h)
C
qGln,qAla
qGluc,qAla
$R^2_{qGln,qAla}$ = 0.7575
$R^2_{qGluc,qAla}$ = 0.2434
qAla (nmol/10⁶ cell·h)
qGlucose, qGlutamine (nmol/10⁶ cell·h)
D
qGln,qAla
qGluc,qAla
$R^2_{qGln,qAla}$ = 0.9587
$R^2_{qGluc,qAla}$ = 0.8234
qAla (nmol/10⁶ cell·h)
qGlucose, qGlutamine (nmol/10⁶ cell·h)

Figure S3. Correlation analysis of glutamine and glucose consumption versus alanine production in parental Sf9 cells and the Gag-eGFP stable cell poll cultured in shake flasks and in bioreactor. Parental cells cultured in shake flasks (A) and in bioreactor (B). Gag-eGFP stable cell pool cultured in shake flasks (C) and in bioreactor (D). The correlation analysis is conducted with the fluxes from the exponential and stationary phases (24 – 168 h) in absolute values. Linear regression based on the coefficient of determination (R^2) is employed to evaluate the degree of correlation between fluxes at different time points.